

# GRAVITY GRADIENT STABILIZATION SYSTEM for the

DOCUMENT NO. 65SD4266

20 APRIL 1965

APPLICATIONS  
TECHNOLOGY  
SATELLITE

FACILITY FORM 10-2

N66 24497

(ACCESSION NO. PER)

(AFRO)

343

(PAGES)

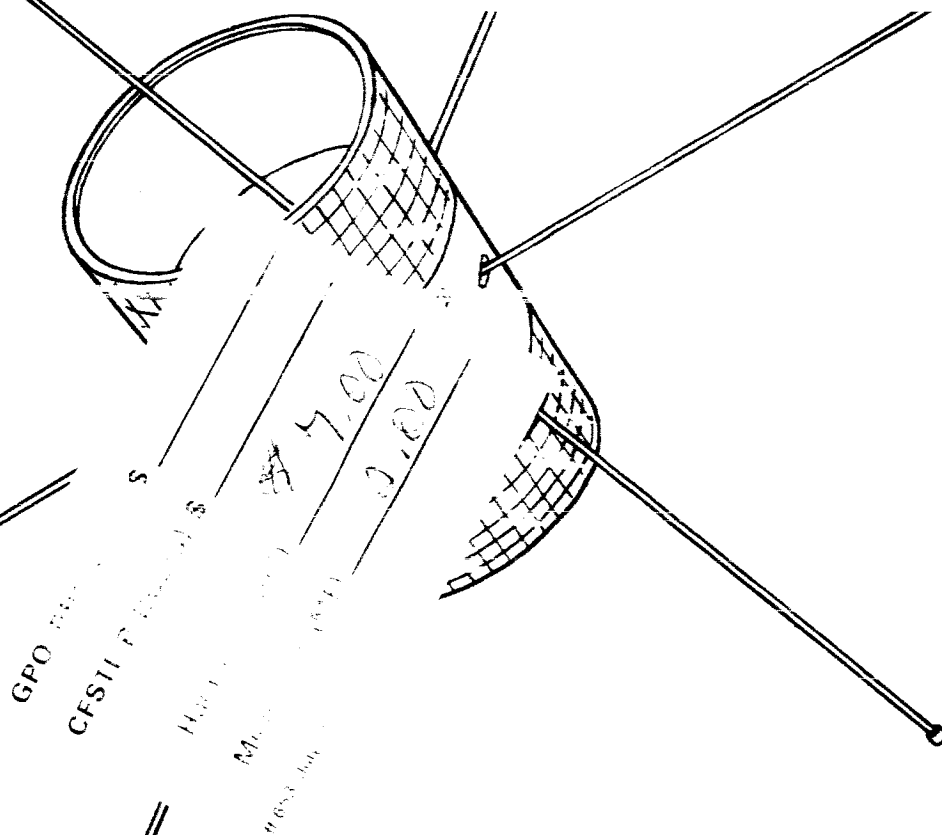
(CODE)

CR-74541

(NASA CR OR TMX OR AD NUMBER)

31

(CATEGORY)



## THIRD QUARTERLY PROGRESS REPORT

NASA CONTRACT NAS 5-9042

GENERAL  ELECTRIC  
SPACECRAFT DEPARTMENT

DOCUMENT NO. 65SD 4266  
20 APRIL 1965

**GRAVITY GRADIENT STABILIZATION SYSTEM  
FOR THE  
APPLICATIONS TECHNOLOGY SATELLITE  
THIRD QUARTERLY PROGRESS REPORT**

1 January through 31 March, 1965

**CONTRACT NO. NAS 5-9042**

**FOR THE  
National Aeronautics and Space Administration**

**JOHN M. THOLE  
ATS TECHNICAL OFFICER**

APPROVED BY



**R. J. Katucki, Manager  
Passive Attitude Control Programs**

**GENERAL  ELECTRIC**  
**SPACECRAFT DEPARTMENT**  
*A Department of the Missile and Space Division*  
**Valley Forge Space Technology Center**  
**P. O. Box 8555 • Philadelphia, Penna. 19101**

## TABLE OF CONTENTS

Section	Page
Abstract . . . . .	vii
1. INTRODUCTION . . . . .	1-1
1.1 Purpose . . . . .	1-1
1.2 Program Contact Scope . . . . .	1-1
1.3 Progress Summary . . . . .	1-1
2. WORK PERFORMED . . . . .	2.1-1
2.1 Systems Analysis and Integration . . . . .	2.1-1
2.2 Boom Subsystem . . . . .	2.2-1
2.3 Combination Passive Damper . . . . .	2.3-1
2.4 Attitude Sensor Subsystem . . . . .	2.4-1
2.5 Quality Control . . . . .	2.5-1
2.6 Manufacturing . . . . .	2.6-1
2.7 Reliability and Parts & Standards . . . . .	2.7-1
3. NEW TECHNOLOGIES . . . . .	3-1
4. GLOSSARY . . . . .	4-1
APPENDIX A . . . . .	A-1
APPENDIX B . . . . .	B-1
APPENDIX C . . . . .	C-1
APPENDIX D . . . . .	D-1
APPENDIX E . . . . .	E-1
APPENDIX F . . . . .	F-1

# LIST OF ILLUSTRATIONS

Figure		Page
2.1-1	Flow Diagram of ATS Mathematical Model . . . . .	2.1-7
2.1-2	ATS Data/Information Flow . . . . .	2.1-15
2.1-3	Flight Evaluation Data/Information Flow and Task Definition at General Electric . . . . .	2.1-19
2.1-4	Performance Comparison Chart, GSFC Configuration, ATS-A . . . . .	2.1-30
2.1-5	Performance Comparison Chart, TM-1 Configuration, ATS-A . . . . .	2.1-31
2.1-6	Performance Comparison Chart, GE-1 Configuration, ATS-A . . . . .	2.1-32
2.1-7	Performance Comparison Chart, TM-2 Configuration, ATS-A . . . . .	2.1-33
2.1-8	Performance Comparison Chart, MF-1 Configuration, ATS-A . . . . .	2.1-34
2.1-9	Performance Comparison Chart, GSFC Configuration, ATS-D . . . . .	2.1-35
2.1-10	Performance Comparison Chart, TM-1 Configuration, ATS-D . . . . .	2.1-36
2.1-11	Performance Comparison Chart, GE-1 Configuration, ATS-D . . . . .	2.-137
2.1-12	Performance Comparison Chart, TM-2 Configuration, ATS-D . . . . .	2.1-38
2.1-13	Performance Comparison Chart, MF-1 Configuration, ATS-D . . . . .	2.1-39
2.1-14	Vehicle Configuration . . . . .	2.1-42
2.1-15	Effect of Primary Rod Length and Tip Mass Weight on ATS-A Pitch Error Caused by 1000 Pole-Cm Dipole Along the Roll Axis (TM-2 Configuration) . . . . .	2.1-43
2.1-16	Effect of Primary Rod Length and Tip Mass Weight on ATS-A Yaw Error Caused by 1000 Pole-Cm Dipole Along the Roll Axis (TM-2 Configuration) . . . . .	2.1-44
2.1-17	Effect of Primary Rod Length and Tip Mass Weight on ATS-A Pitch Error Caused by Rod Thermal Bending and Solar Pressure Torque (TM-2 Configuration) . . . . .	2.1-45
2.1-18	Effect of Primary Rod Length and Tip Mass Weight on ATS-A Yaw Error Caused by Rod Thermal Bending and Solar Pressure Torque (TM-2 Configuration) . . . . .	2.1-46
2.1-19	Effect of Primary Rod Length and Tip Mass Weight on ATS-A Pitch Error Caused by Magnetic and Solar Effects (TM-2 Con- figuration). . . . .	2.1-47
2.1-20	Effect on Primary Rod Length and Tip Mass Weight on ATS-A Yaw Error Caused by Magnetic and Solar Effects (TM-2 Configuration) . . . .	2.1-48
2.1-21	Variation of Damper Characteristics with Pitch Moment of Inertia for TM-2 . . . . .	2.1-62
2.1-22	$I_p$ vs Rod Length . . . . .	2.1-63
2.1-23	Performance of ATS-A Vehicle with 100-Foot Primary Rods and 2.5-Pound Tip Weights . . . . .	2.1-65
2.1-24	Performance of ATS-A Vehicle with 1.33, 75-Foot Primary Rods and 2.5-Pound Tip Weights . . . . .	2.1-66
2.1-25	Effect of Primary Rod Length on Yaw Error Caused by 1000 Pole-Cm Dipole Along the Roll Axis (ATS-D/E TM-2 Parameters) . . . . .	2.1-69



# LIST OF ILLUSTRATIONS (Cont'd)

Figure		Page
2.1-26	Effect of Primary Rod Length on Yaw Error Caused by Rod Thermal Bending and Solar Pressure Torque (ATS-D/E TM-2 Parameters) . . . . .	2.1-70
2.1-27	Effect of Primary Rod Length on Yaw Error Caused by Rod Thermal Bending and Solar Pressure Torque (ATS-D/E, TM-2 Parameters) . . . . .	2.1-71
2.1-28	Effect of Primary Rod Length on Pitch Error Caused by Rod Thermal Bending and Solar Pressure Torque (ATS-D/E, TM-2 Parameters) . . . . .	2.1-72
2.1-29	Effect of Primary Rod Length on Pitch Error Caused by Rod Thermal Bending and Solar Pressure Torque (ATS-D/E, TM-2 Parameters) . . . . .	2.1-73
2.1-30	Coordinate System . . . . .	2.1-76
2.1-31	Thruster Induced Yaw Errors . . . . .	2.1-82
2.1-32	Variation of Pitch Moment of Inertia with Primary Rod Length and Tip Mass Weight . . . . .	2.1-83
2.1-33	Variation of Damper Characteristics with Pitch Moment of Inertia for TM-2 Parameters . . . . .	2.1-84
2.1-34	Rod Length vs $\Theta_y$ . . . . .	2.1-85
2.1-35	Performance of ATS-D Vehicle with 100-Foot Primary Rods and 10-Pound Tip Weights . . . . .	2.1-88
2.1-36	Performance of ATS-D Vehicle with 124.33-Foot Primary Rods and 8-Pound Tip Weights . . . . .	2.1-89
2.1-37	Performance of ATS-D Vehicle with 100-Foot Primary Rods and 10-Pound Tip Weights . . . . .	2.1-92
2.1-38	Performance of ATS-D Vehicle with 124.33-Foot Primary Rods and 8-Pound Tip Weights . . . . .	2.1-93
2.1-39	ATS-A Inversion with 133.75-Foot Rods (Total Maneuver Time = 2.5 Hrs.) . . . . .	2.1-95
2.1-40	ATS-A Inversion with 133.75-Foot Rods (Total Maneuver Time = 3.8 Hrs.) . . . . .	2.1-96
2.1-41	ATS-A Inversion with 100-Foot Rods (Total Maneuver Time = 2.5 Hrs.) . . . . .	2.1-97
2.3-1	Combination Passive Damper Stage III Arrangement (GE Dwg. SK 56130-808-41) . . . . .	2.3-5
2.3-2	Current Boom Caging Mechanism (GE Dwg. SK 56130-808-42) . . . . .	2.3-7
2.3-3 / 4	New CPD Concept . . . . .	2.3-10
2.3-5	CPD Baseplate Taper Pin Caging . . . . .	2.3-13
2.3-6	GE Hysteresis Damper Model . . . . .	2.3-18
2.3-7	Square Fluted Diaphragm . . . . .	2.3-24
2.3-8	Fluted Diaphragm Assembled for Test . . . . .	2.3-25

## LIST OF ILLUSTRATIONS (Cont'd)

Figure		Page
2.3-9	Force vs. Displacement for Square Fluted Diaphragm (.014 in. beryllium copper) .....	2.3-26
2.3-10	Force vs. Displacement for Corrugated Belleville Spring (.012 in. beryllium copper) .....	2.3-27
2.3-11	Force vs. Displacement for Corrugated Belleville Spring with Increased Stroke, First Sample .....	2.3-28
2.3-12	Force vs. Displacement for Corrugated Belleville Spring with Increased Stroke, Second Sample .....	2.3-29
2.3-13	Layout of the GE Hysteresis Damper Design .....	2.3-33
2.3-14	Load Carrying Capability Measurement Test Setup on the Low-Orbit Force Fixture .....	2.3-38
2.4-1	Block Diagram, Electrical, ATS Gravity Gradient Stabilization System (GE Dwg. PR 47E207151, Rev. A) .....	2.4-3
2.4-2	Geometry of a TV Picture Tube .....	2.4-6
2.4-3	Automatic Video Switch .....	2.4-10
2.4-4	Telemetry Power Supply .....	2.4-11
2.4-5	Damper Clutch Solenoid Driver .....	2.4-13
2.4-6	Separation Timer .....	2.4-14
2.4-7	Rod Extension Motor Control Logic Diagram .....	2.4-16
2.4-8	Rod Extension Motor Control Waveforms .....	2.4-17
2.4-9	Solar Aspect Sensor Package .....	2.4-21
2.4-10	Solar Detection Location on ATS Vehicle .....	2.4-22
2.4-11	Solar Aspect Sensor Logic Diagram .....	2.4-25

## ABSTRACT

A preliminary flow diagram was derived for the computer program of the ATS Mathematical Model as part of the System Analysis activity during the quarter. The program is to be written in Fortran IV language and prepared in modular form to correspond with the derivation of the Math Model.

A preliminary Orbit Test Plan for the ATS-A flight is included in the report. The plan up-dates the information presented in the First Quarterly Report, and includes the time for specific events from vehicle steady state to exercise of specific functions in the Gravity Gradient Stabilization System. The initial publication of the ATS Flight Evaluation Plan is presented. It is an integrated plan for the coordinated handling and analysis of flight data from the time of launch until the completion of the prescribed orbit test plan.

Error budgets that were derived by GE for five representative configurations in the Optimization Program are presented together with an analysis of the TM-2 configuration selected by NASA/GSFC.

Development of the Combination Passive Damper has been affected by the results of two decisions. The first was a directive from NASA/GSFC to purchase the Passive Hysteresis Damper portion of the CPD from TRW/Space Technology Laboratories. The second decision was the establishment of the TM-2 configuration which resulted in changes to the CPD mounting interface and critical angle data. GE continued engineering evaluation of its hysteresis damper during negotiations with STL. Their proposals had been evaluated by the close of the reporting quarter and it is anticipated that negotiations will soon be completed.

An in-house design review was conducted on February 12th to determine the adequacy of the CPD concept and acquaint manufacturing and test personnel with the details of the design. The meeting was attended by consultants in several specialties, including representatives from the GE Advanced Technology Laboratories.

Details of several tests in support of the CPD are reported. Tests conducted during the period included evaluation of the diaphragm clutch, measurement of the eddy current damping coefficients, torsional restraint tests, and diamagnetic repulsion force measurements.

The theory and operation of the GE boom angle detector is presented. This design features a digital output and simplified circuitry.

The requirements of the Boom Subsystem for the Thermal Model (T-2) and the Dynamic Model (T-3) were established and transmitted to de Havilland. A survey of lubricants is reported as possible replacements for the silicone-based grease that was planned for use in the high-speed and highly loaded elements of the boom drive system. Appendix E presents the results of a dynamic analysis of the effect of primary rod extension and contraction rates.

The electrical configuration and interface is presented for the Attitude Sensor Subsystem. The method is described for simulating the earth as seen from the TV camera as a test for measuring repeatability of reading the TV target deflection. Design of the Power Control Unit was influenced during the quarter by changes within the Gravity Gradient Stabilization System. A review is presented of the circuits that were designed for inclusion in the PCU to accommodate these changes. Logic and functioning of the Solar Aspect Sensor is discussed. Arrangement of the five sensor detectors is shown relative to the new ATS vehicle configuration.

Emphasis in the area of Reliability and Parts & Standards was directed toward an analysis of the Boom Subsystem since this design has been completed to the point of permitting reliability investigations. Three test plans were evaluated for the primary boom sealed drive unit with the objective of selecting the plan which would provide the most information relative to the capability of the parts that comprise the unit.

Sampling rates of pyrotechnical devices were investigated based on historical data and the Spacecraft Department experience.

The Parts Qualification Program recommended for ATS components is based on tradeoff of risk factor, need and cost.

## SECTION 1.

### INTRODUCTION

#### 1.1 PURPOSE

This report documents the technical progress made during the period from January 1, 1965, to March 31, 1965, toward the design and development of Gravity Gradient Stabilization Systems for the Application Technology Satellites.

#### 1.2 PROGRAM CONTRACT SCOPE

Under Contract NASA 5-9042, the Spacecraft Department of the General Electric Company has been contracted to provide gravity gradient stabilization systems for three Applications Technology Satellites: one to be orbited at 6000 nautical miles (ATS-A), and two to be orbited at synchronous altitude (ATS-D and ATS-E). Each system will consist of primary booms, damper boom, dampers, attitude sensors, power conditioning unit and interface electronics. In addition to the flight systems, GE will provide a thermal model, a dynamic model, engineering unit and two prototype units. GE will also supply two sets of aerospace ground equipment.

#### 1.3 PROGRESS SUMMARY

NASA/GSFC has directed the use of the TM-2 Configuration; the design will be used for the ATS-A and ATS-D/E. This decision followed presentation of results of independent studies that were undertaken by NASA/Ames and GE toward optimization of the original ATS Configuration. These studies were based on a standard set of disturbance torques which had been established by NASA/GSFC. Both studies utilized computer programs to solve the characteristic equations for each of the configurations that were studied and provide natural frequencies and damping characteristics. GE presented error budgets for five configurations (designated: GSFC, TM-1, TM-2, GE-1 and MF-1) to NASA/GSFC on March 22nd. Direction to use the TM-2 configuration was received on March 26, 1965.

The Work Statement describing the effort by General Electric Company to design and fabricate the ATS Gravity Gradient Stabilization System was negotiated at NASA/GSFC during the week of March 22nd. GE Project personnel met with NASA/GSFC personnel in a series of fact-finding sessions and each of the work packages that comprise the Work Statement was reviewed. Recommended changes were incorporated into a preliminary issue of the Work Statement. The final document will be published by GE in April under Document No. 65SD4293.

## WORK PERFORMED

### 2.1 SYSTEMS ANALYSIS AND INTEGRATION

#### 2.1.1 INTRODUCTION

The most significant systems activity during the past quarter has been that associated with the parametric optimization of the basic ATS configuration and the final resolution of systems work scope in the form of 14 negotiated systems work packages. Since the events of the past quarter have had a significant effect on progress and results in the systems area, it is appropriate to briefly summarize the chronology of events leading up to the configuration specifications of paragraph 2.1.6.1, this report.

5 January 1965: GE presentation to Dr. Goett, NASA/GSFC, reviewing the basic ATS gravity gradient program objections. Progress and problems in meeting those objectives were summarized and qualitative configuration recommendations were made for the improvement of system performance.

5 - 25 January 1965: GE initiated work on the development of a computer program for use in the performance of system optimization studies; meetings were held with V. Merrick of NASA/Ames to coordinate mutual efforts; Hughes Aircraft Company modified the basic central body configuration to improve thermal design parameters and reduce solar torques due to external configuration and surface property effects; GE initiated efforts on the generation of error budgets ( system response to isolated disturbance torques).

25 January 1965: Capture and inversion studies were halted because of significant changes in basic spacecraft parameters; these studies are quite sensitive to variations in basic parameters.

27 January 1965: GE was given an informal preview of the new HAC configuration.



1 February 1965: Informal interface meeting in D. Mazur's office, NASA/GSFC, to discuss new HAC configuration. GE was requested to provide error budgets comparing "old" and "new" configurations (GSFC parameters).

6 February 1965: Error budgets were transmitted to NASA/GSFC.

6 - 11 February 1965: GAPS III modified to account for effects due to offset damper rods and station keeping thrusters; progress on optimization studies hampered by lack of a standard set of disturbance parameters (disturbances are a function of the configuration which is being optimized) and technical problems with computer facilities.

11 March 1965: Standard set of disturbance torques, for use in optimization studies, established at GSFC/Ames/GE joint meeting at NASA/Ames.

12 - 15 March 1965: Performance estimates, using standardized disturbance torque profile and GAPS III computer program, generated for 3 configurations: (1) the GSFC "original" (2) the TM-1 (1st set of Ames parameters) and (3) the GE-1 (a compromise set of parameters to meet ATS-A and ATS-D/E commonality requirements).

16 March 1965: Results of GSFC, TM-1, and GE-1 studies presented at ATS interface meeting, NASA/GSFC.

17 - 19 March 1965: GE/HAC joint design effort at GE/VFSTC to resolve configuration interface problems associated with new configuration; GE evaluated a second input from Ames (designated TM-2).

22 March 1965: Interface meeting at NASA/GSFC to choose final set of configuration parameters; 5 configurations were considered: (1) GSFC (2) GE-1 (3) TM-1 (4) TM-2 (5) MF-1. The TM-2 configuration was recommended by GE as a commonality compromise; if commonality requirements removed, GE recommended TM-2 for ATS-A and TM-1 for ATS-D/E.

26 March 1965: NASA/GSFC directed use of TM-2 configuration for both ATS-A and ATS-D/E (TWX from R. Darcy, NASA/GSFC).

26 March - 9 April 1965: Completion of optimization studies at GE using TM-2 non-dimensional parameters. Results are included in this quarterly report (paragraph 2.1.6.1).

## 2.1.2 G<sup>2</sup>S/ATS MATHEMATICAL MODEL

### 2.1.2.1 Introduction

The mathematical model of the ATS configuration will be a digital computer program which integrates (with respect to time) the large amplitude dynamical equations of motion of a semi-rigid body. Included in the model will be all the known external and internal torques which affect the steady state performance of the vehicle. In doubtful areas, such as the earth's albedo, gravity gradient bending of the rods (gravity sag), etc., peripheral studies will be performed to insure that the torques which have been neglected are indeed negligible. In anticipation of the results, provisions are not being made to include these error sources in the mathematical model. Math model coordinate frames to be utilized were reported in the first quarterly report (Section 2.1.5). Sections of the math model that were completed include: the dynamical equations, the spacecraft shadowing effect, and the incorporation of the earth oblateness effects. Techniques were considered for simulation of the ATS math model hysteresis damper.

### 2.1.2.2 Discussion

The mathematical model will be written in Fortran IV computer language. This language is replacing the more common Fortran II and should be widespread by the completion of the model. The basic Fortran IV is a standard IBM machine language which is (or can be made) intelligible to the most large computers.

The mathematical model will be composed of modules, each of which performs a specific function. The modular concept was selected for this application because of the inherent advantages in construction and utilization of the program. With this concept, three modules can be in progress simultaneously, one being derived, one being programmed and one being checked out. The compressed time scale in which the program must be constructed has necessitated the arrangement whereby the analytical and programming efforts are done in parallel.

A great advantage of the modular concept is the flexibility which can be built into the program. Past experience with programs of this nature indicates that the mathematical model must be quite large to incorporate the required analytical refinements and the running time will be slow ("slow" is undefined at the moment) if all the disturbance torques are included simultaneously. Since the mathematical model is an engineering tool, as well as a "performance predictor", it is expected that a large number of runs will not require all the disturbance torques. By a careful arrangement of the logic within the program, it is possible to bypass those modules which are not wanted for any specific run, thereby reducing the number of calculations performed. Hence, "simple cases" will run more rapidly than "complex cases". Since specific modules can be selected, the effect of individual disturbances can be isolated and design studies and configuration optimization (of a limited nature) can be performed.

Since the mathematical model is to be as general a program as possible, the "universal constants", etc., will be inputs and any set of units consistent with these constants can be used for the remaining inputs. One exception to this rule is the magnetic field and magnetic torque modules. In the magnetic field subroutine, the magnetic field is calculated in oersteds, based upon earth latitude, longitude, and attitude in kilometers. Appropriate conversion factors are therefore necessary to maintain consistency within the program. These conversion factors will be inputs or fixed constants within the program.

Aerodynamic torques will not be included in the model and this effectively places a lower limit on the altitude at which the results of the program are indicative of the system performance. The rod length will also be limited since it is not expected that the mathematical

representation of thermal bending will be exact for all rod lengths. The absence of gravity sag also places a limitation on the validity of the results for long rods. For rod lengths on the order of those encountered for ATS, however, the accuracy should be consistent with accuracy of the rest of the program.

#### 2.1.2.3 Flow Diagram

The modules to be included within the program are shown in the flow diagram, Figure 2.1-1. This is a preliminary diagram and it is expected that additional modules or subdivision of the proposed modules will occur at some future time. However, the basic arrangement of the modules and the functions performed within the program will be unchanged.

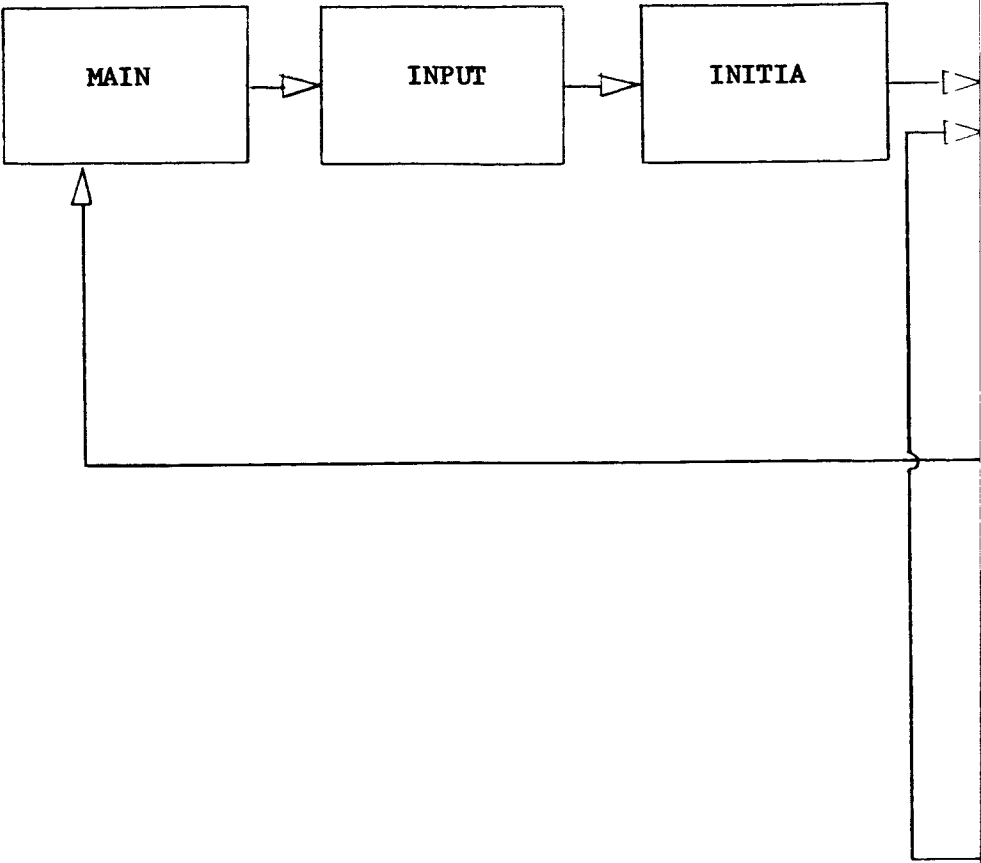
The modules to be included in the program have been divided into three classes:

Class 1 Modules which the program always enters and to which inputs are always required.

Class 2 Modules which the program will enter if required and to which the inputs are always required.

Class 3 Modules which are not entered unless requested and to which inputs are not required unless entered.

The Class 1 modules are shown as blocks (Figure 2.1-1). These modules are basic to the program and will be derived first. By combining these modules and using "dummies" for the uncompleted modules, a working program can be generated quickly. This will permit check-out of the basic program, integration scheme, and the logic. Preliminary checks can be made to insure that singularities do not exist. Because of the analytical complexity and need for experimental data, the hysteresis damping torque (Hystor), will be the last Class 1 module programmed. The rate damping torque will be available immediately and can be used in the interim. The input module and the initialization modules will be updated as the program progresses, and will not be in final form until the program is completed.



LEGEND



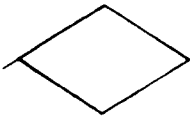
Routines always used

CLASS 1



Routines controlled by  
Input Indicators

CLASS 2



Routines controlled by  
Input Data

CLASS 3

$Q_o$

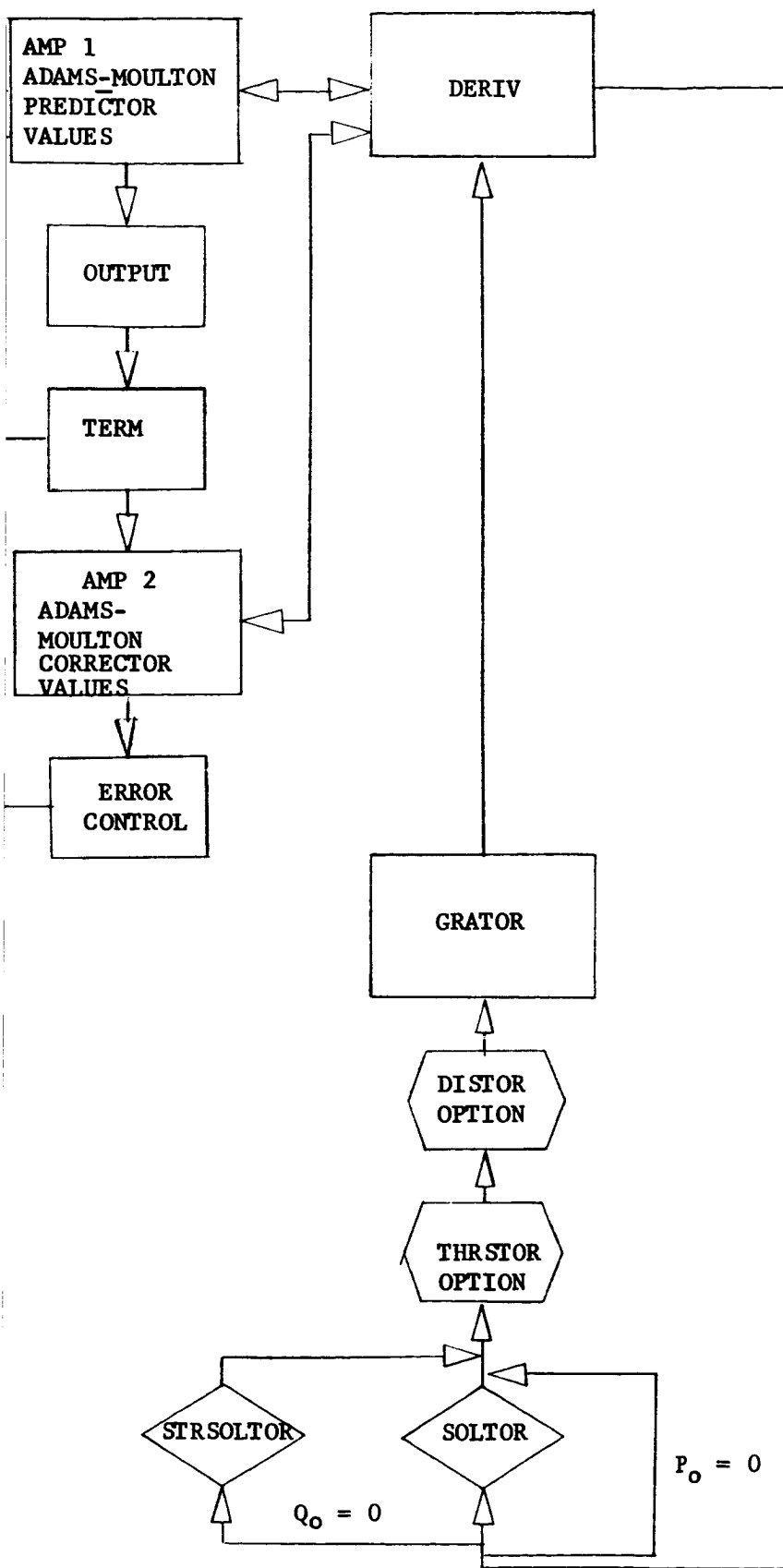
Solar Heat Flux

$P_o$

Solar Pressure Constant

$H_{x,y,z}$

Residual Magnetic Dipole of Vehicle



2

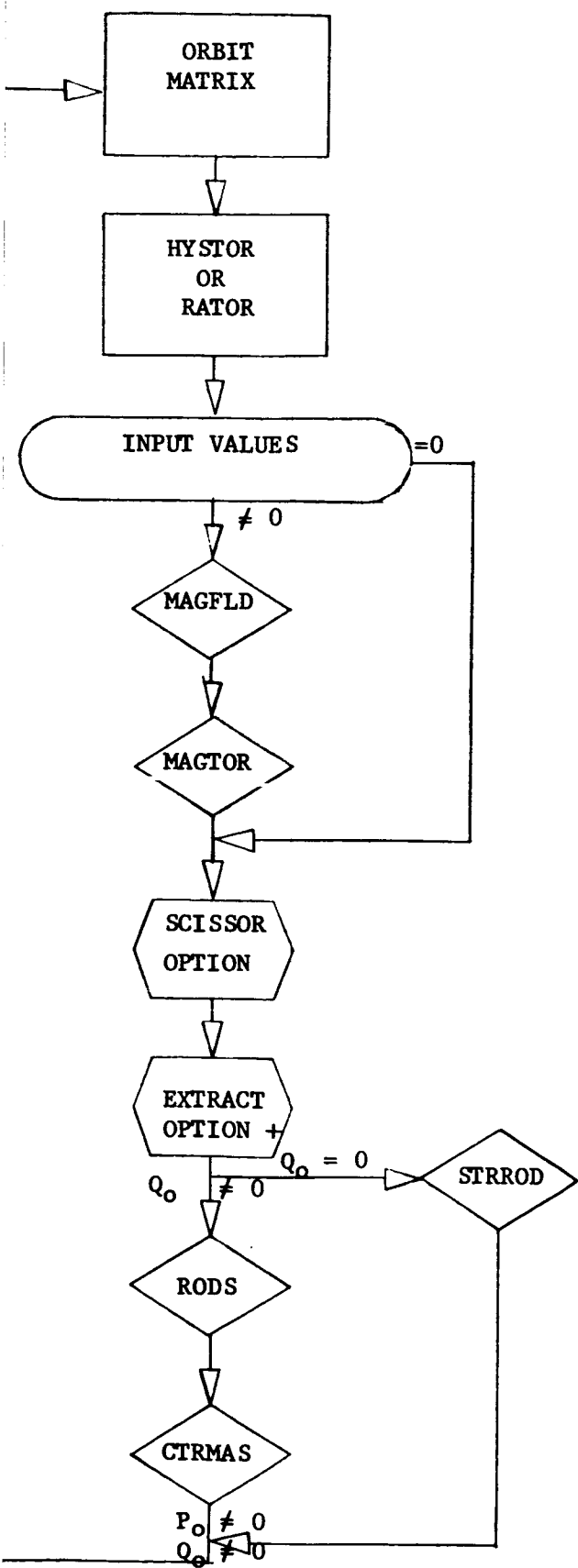


Figure 2.1-1. Flow Diagram of ATS Mathematical Model

3

Following construction of the basic program, the Class 2 modules (shown as diamonds) will be constructed and these will be added to the program at the appropriate locations. Note that the modules can be added directly since the logic for their operation has already been programmed.

These modules are controlled by input variables. In the case of Magtor, for example, the inputs are checked and if magnetic torques are not wanted, both the magnetic field and the magnetic torque module are by-passed. Similarly, the rod geometry module is by-passed if the solar heat flux ( $Q_o$ ) is set to zero. Following this, if the solar energy constant ( $P_o$ ) is not equal to zero, the solar torques on the rods and vehicle body are calculated. If  $P_o$  is equal to zero, no solar torques are calculated. These provisions for by-passing particular modules should result in a significant improvement in running time for simple runs not involving solar torque and thermal bending. Note that thermal bending of the rods with no resultant solar torque is possible. The rod module will be programmed late in the schedule because of need for experimental data.

There remains only the Class 3 routines. These routines are entered and have inputs only if they are specifically selected. Of these, thruster requires definite information from the main program. The scissor routine may or may not require information depending upon the limitations placed upon the module. The same restriction is true of the scissor routine. The Distor routine requires no information from the main program but simply adds its disturbance torque. Most of the subroutines are straightforward and can be done with little difficulty. Several of these, notably scissor and extract, need to be defined prior to their construction. This will be presented in a subsequent report. Brief descriptions of the tasks performed by the modules are given below.

### CLASS 1

<u>Main</u>	"Sets Up" the program in the computer, terminates, etc. It does not perform calculations.
-------------	---



<u>Input</u>	Reads the input into the program. It is entered only once at the start of the program.
<u>Initia</u>	Calculates initial and constant factors for the entire program. It is entered only once at the start of the program.
<u>Deriv</u>	Calculates the vehicle accelerations and Euler parameter accelerations prior to integration. It will control the flow of the program to the modules.
<u>Rods</u>	The rod shape, center of mass, moments of inertia, etc. are calculated for thermally bent rods.
<u>Strrod</u>	The moments of inertia, center of mass, etc., of the straight rods will be calculated in this module if there is no thermal bending.
<u>Ctrmas</u>	Calculates the center of mass of the entire system.
<u>Grator</u>	Calculates the gravity gradient torques.
<u>Orbit/ Matrix</u>	The matrix elements of the rod geometry, sun position, satellite orientation, etc., are calculated in the module. The orbit position, earth position, etc., from orbit are calculated here as a convenience.
<u>Hystor/ Rator</u>	Hystor calculates the hysteresis damping torque. Rator calculates the rate damping torque.
<u>Strsoltor</u>	Calculates the solar torque on straight rods if thermal bending is not required.
<u>Output</u>	Prints the output.

### CLASS 3

<u>Thruster</u>	Calculates the disturbance torque due to a thruster. C. M. wander due to thermal bending is included.
<u>Distor</u>	Calculates miscellaneous disturbance torques (constant plus two sine waves per axis).
<u>Scissor</u>	Calculates moments of inertia, rod position, etc., during the scissoring operation.
<u>Extract</u>	Calculates moments of inertia and their derivatives during rod extension and retraction.

Amp 1 and Amp 2 are part of the integration technique as are term and error control.

#### 2.1.3 ATTITUDE DETERMINATION PROGRAM

The effect of orbit parameter uncertainties on the spacecraft attitude (Appendix A), an analysis of TV attitude errors (Appendix B) and two studies (one comparing on-board R-F measurements with radar polarization angle measurement, and the second comparing on-board earth oriented IF sensor measurements with ground-based polarization angle measurements) form the basis of work completed in the attitude determination program. Still to be documented are the results of the solar aspect sensor/antenna polarization measurement analysis and the solar aspect sensor/ earth sensor analysis. Remaining analyses include the earth sensor and/or solar aspect sensor working in conjunction with two ground station antenna polarization measurements. All work on attitude measurement errors is planned for completion by the end of the next fiscal quarter (25 June 1965). Also by the end of the next fiscal quarter, it is planned to have a preliminary Attitude Determination Program design specification for negotiation with NASA/GSFC and NASA's tracking and data processing group. Specification will include agreements reached at the 9 February 1965 meeting with Marc Selig (NASA Tracking and Data Processing group) at GE/VFSTC.

#### 2.1.4 ORBIT TEST AND FLIGHT EVALUATION PLAN

The scope of work previously included under the general heading of "Orbit Test Plan" has been subdivided for this and future reports into 2 parts: (a) the ATS Orbit Test Plan (b) the ATS Flight Evaluation Plan. Both plans are still tentative in nature but portions of each are included in the following paragraphs to indicate the current status of efforts.

##### 2.1.4.1 ATS Orbit Test Plan

The ATS Orbit Test Plan, as discussed in the First Quarterly Report of 16 October 1964, is fundamentally a detailed statement of the operational plan for accomplishing the basic objectives of the ATS Program. Since publication of that report, the program objectives have been updated and modified to be more compatible with program constraints due to overall cost and schedule limitations. Table 2.1-1 summarizes current program objectives and the tests and data requirements associated with each objective. The ATS Mathematical Model is still planned for the generation of performance predictions; however, it is no longer anticipated that the ATS attitude sensing subsystem will be adequate for the sophisticated data correlation procedures originally conceived. Hence, the Mathematical Model verification objective has been de-emphasized and the requirement for an automated Data Correlation Program has been eliminated. The requirement for "missing link" data has also been deleted. (NASA/GSFC direction on 12/1/64). This simplifies the role of the GE-developed Attitude Determination Program to one of pure data reduction.

Table 2.1-2 summarizes the current status of thinking as to the nature, sequence and duration of gravity gradient orbital tests for the medium altitude (6,000 nautical miles) flight. Most significant changes, from the plan shown in the First Quarterly Report, are:

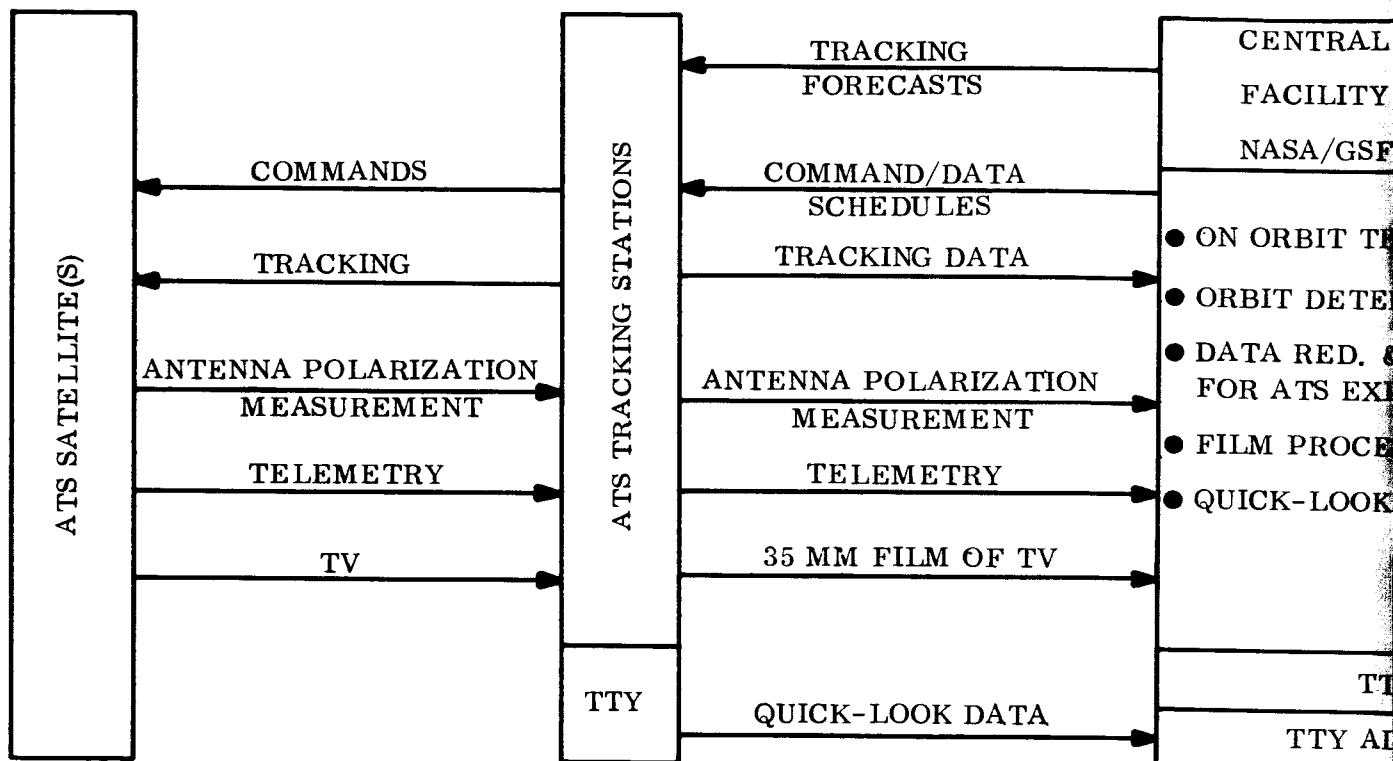
1. Elimination of the orbit eccentricity change
2. Elimination of the CP boom for shifting the spacecraft's center of pressure

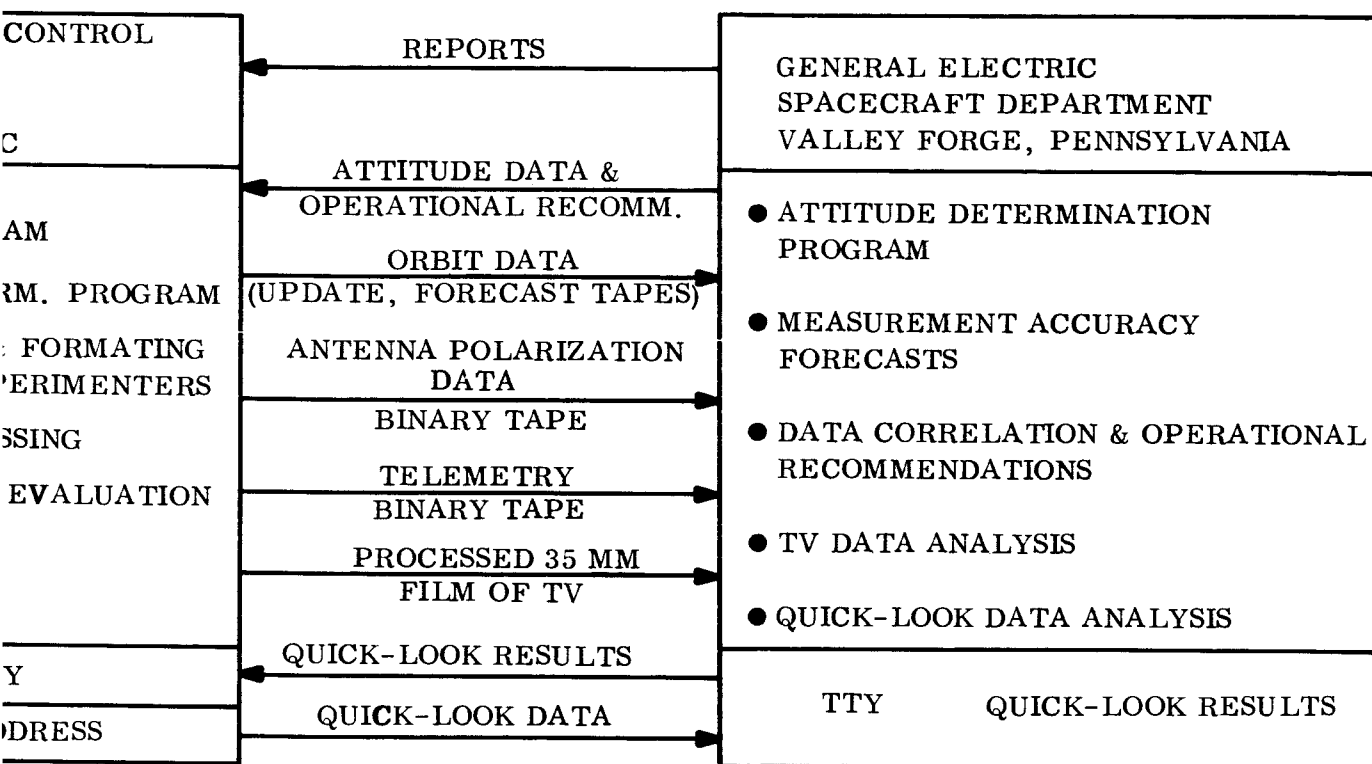
**TABLE 2.1-1. ATS GRAVITY GRADIENT PROGRAM OBJECTIVES**

- I. Demonstrate operational feasibility of gravity gradient systems at medium (6,000 nautical miles) and synchronous altitudes.**
  - A. Upright Capture**
  - B. Spacecraft Inversion**
  - C. Station Keeping Compatibility  
(synchronous orbits only)**
  - D. Eddy Current Damping  
(with diamagnetic suspension)**
  - E. Hysteresis Damping  
(with torsion wire suspension)**
- II. Obtain parametric flight data for application to the other programs**
  - A. Performance Sensitivity to Configuration Parameters (X-boom scissoring to vary spacecraft inertia ratios; retraction and extension of X-booms to vary spacecraft inertia magnitudes).**
  - B. Relative performance (transient and steady state) of eddy current and hysteresis dampers.**
  - C. Damper boom libration data.**
  - D. Boom thermal bending data.**
  - E. Boom dynamics data (eclipse entry and exit, inversion, station keeping, etc.).**
- III. Demonstrate Compatibility with Mission Requirements of Applications Satellites.**
  - A. Tolerances to Internal Disturbances.**
  - B. Communications Experiments.**
  - C. Meteorological Experiments.**

Table 2.1-2. Orbit Test Plan for the ATS-A Gravity Gradient Flight (Preliminary)

TEST NO.	TEST OBJECTIVE	TEST MECHANICS	ALLOWED TEST TIME (Days)	COMMENTS
0 (TIME = $T_0$ )	Spacecraft Separation	--	--	Apogee rate and attitude at separation are critical to successful accomplishment of Test No. 1; requirements and tolerances, based on revised configuration parameters (3/26/65), are being evaluated. (Separation occurs at $T_0 + 7412$ seconds.)
1 ( $T_0 + 2$ days)	Capture in upright orientation without uncaging damper(s) or deploying the damper boom (required as "set up" for test No. 2)	Deploy X-booms 3.96 seconds after separation (deploy to 133.75-foot nominal length at 25.7-degree nominal half-angle). Leave dampers caged and damper boom undeployed.	2	Monitor deployment of booms with TV cameras; monitor attitude dynamics via telemetry data from attitude sensors; in the event of an inverted capture, complete tests 1 through 6, then skip test 7.
2 ( $T_0 + 4$ days)	Establish presence or absence of measurable structural damping	Extend time allowance for initial capture phase; analyze telemetered attitude data.	2	This test is being tentatively retained until the contributions of structural damping have been more thoroughly examined.
3 ( $T_0 + 9$ days)	Determine "settling time" and steady state attitude dynamics with No. 1 Damper	Deploy damper boom, uncage Combination Passive Damper with No. 1 Damper in "clutched" position.	5	3 days allowed for transients to settle out; 2 days allowed for monitoring of steady state performance.
4 ( $T_0 + 11$ days)	Determine steady state attitude dynamics with No. 2 Damper	Clutch CPD to No. 2 Damper; analyze telemetered attitude data.	2	-----
5 ( $T_0 + 14$ days)	Determine settling time with No. 2 Damper	Displace satellite attitude approximately 30 degrees in pitch using inversion rockets; analyze telemetered attitude data.	3	-----
6 ( $T_0 + 20$ days)	Inversion test using subliming rockets	Retract X-booms to 100-foot length; invert spacecraft using subliming rockets (clutch to No. 1 Damper at end of 6 day period).	6	3 days allowed for boom retraction to 100 feet inversion with the subliming rockets ( $7.0 \times 10^{-4}$ foot-pounds torque) must be done at the 100-foot inertia levels to accomplish the desired 2.5-hour inversion time; inversion at the 133.75-foot inertia levels requires 3.8 hours. 3 days allowed for transients following inversion to settle out.
7 ( $T_0 + 23$ days)	Re-invert using subliming rockets	Subliming rocket inversion (No. 1 Damper).	3	If initial capture is inverted, omit this test.
8 ( $T_0 + 27$ days)	Steady state dynamics	Re-extend booms to 133.75 feet; alternate clutching between No. 1 and No. 2 Dampers; clutch to No. 1 Damper at time of first eclipse encounter.	4	This is essentially a delaying action to account for tolerances on timing of first eclipse encounter (Test 9); nominal requirements for a 27-day initial period of continuous sunlight have been established but the actual period obtained is extremely sensitive to launch time ( $\pm 1/2$ hour on launch shifts time of first eclipse encounter by approximately $\pm 8$ days).
9 ( $T_0 + 37$ days)	Isolate effect of eclipse disturbances due to thermal transients in booms	Enter eclipse period, in steady state, with No. 1 Damper in clutched position; alternate dampers each orbit until eclipse-induced transients become repetitive with each damper; observe behavior of booms, with TV camera away from earth, at time of eclipse exit.	10	The time in eclipse increases from zero to about 46 minutes maximum - at some point short of 46 minutes, the thermal transient effects should become repetitive.
10 ( $T_0 + 85$ days)	Obtain parametric performance data at off-nominal inertia ratios	With No. 1 Damper in clutched position, open X-boom half angle to 31 degrees; allow transients to settle and displace satellite approximately 30 degrees in pitch using inversion rockets; allow to settle to steady state; clutch to No. 2 Damper and repeat. Change X-boom half-angles to 19°, 13° and 11°, in that order, repeating displacement sequence for each damper at each X-boom half angle; return to 25.7° nominal in steps compatible with boom dynamics limitations.	48	3 days allowed for each 4-6 degree change of angle; 3 days allowed for each displacement and each damper (9 days for 31° data, 12 days for 19° data, 9 days for 13° data, 9 days for 11° data, and 9 days to return to 25.7°).
11 ( $T_0 + 136$ days)	Obtain parametric performance data at off-nominal inertia magnitudes	Retract X-booms to 100 feet; repeat Test No. 10; return booms to 133.75-foot nominal.	51	3 additional days allowed for boom retraction.
12 ( $T_0 + 141$ days)	Inversion test using rod retraction and re-extension	--	5	-----
13 ( $T_0 + 365$ days)	Misc. GG tests for remainder of orbit test period	--	224	Major portion of time will be spent in steady state for conduct of other ATS experiments.





2

Figure 2.1-2. ATS Data/Information Flow

3. Elimination of the magnetic torquing coil for changing the magnitude and orientation of the spacecraft's residual magnetic dipole.

These tests were designed, primarily, to support requirements for data to verify the ATS Mathematical Model. As discussed previously, this aspect of the program has been de-emphasized due to overall program cost and schedule constraints.

#### 2.1.4.2 ATS Flight Evaluation Plan

The objective of current flight data analysis activity is to insure the development of an integrated and comprehensive plan for the coordinated handling and analysis of flight data from the time of launch till the completion of the prescribed Orbit Test Plan. To ensure responsiveness to the overall post-launch ATS Program requirements, consideration will be given to the following activities: timing and sequencing of events; an unambiguous assignment of personnel and organizational responsibilities; definitive data content; format, reduction and processing requirements; data correlation and empirical evaluation procedures and techniques. The culmination of efforts in this area will be embodied in the ATS Flight Evaluation Plan to be published as a separate document from the ATS Orbit Test Plan. An outline of the proposed document is presented in Table 2.1-3. Preliminary portions of this plan are published herein for comment. A complete and integrated separate document will be published in June, 1965. The ATS Flight Evaluation Plan and Orbit Test Plan are complementary in nature. The Flight Evaluation Plan must be designed to correctly evaluate the results of experiments outlined in the Orbit Test Plan. Specific telemetry, television and antenna polarization measurement periods defined in the Orbit Test Plan must conform with the data requirements specified in the Flight Evaluation Plan. Furthermore, both plans must be flexible enough to account for unexpected deviations from expected performance which cause changes in the operational and/or flight data analysis procedures.



#### 2.1.4.2.1 General Evaluation Plan Description (Paragraph 2.1 of Table 2.1-3)

The information system for the ATS program will consist of a tracking station network (NASA/GSFC ATS control center, and GE/SD). (Figure 2.1-2) The data flow interface between the vehicle and ATS tracking stations will include ground-to-vehicle command links, and vehicle-to-ground data flow links. Between the tracking station network and NASA/GSFC there will exist an information flow interface consisting of received vehicle data (to GSFC, including quick-look capabilities) and tracking forecast (from GSFC) links; and a command/scheduling interface from GSFC to the respective tracking stations. Functions of the NASA control center are expected to include orbit determination, on-orbit program direction, and preliminary data processing. The NASA/GSFC - GE/SD information flow interface will consist of processed-data/information inputs to GE/SD, and flight evaluation results/ reports to GSFC (both to include quick-look capability).

Data and information applicable to the task of evaluating the gravity gradient system performance will be supplied to GE by NASA for reduction and analysis. Two types of reduction and analysis efforts (Figure 2.1-3) will take place during the flight evaluation period of each satellite.

##### 2.1.4.2.1.1 Quick-Look Attitude Determination

This effort involves expedited telemetry and information flow from the tracking stations through NASA-GSFC direct to an automated GE "ATTITUDE DETERMINATION PROGRAM" via teletype where calculation of vehicle attitude information is completed and results transmitted to NASA-GSFC via automated teletype output. Predicted orbit information will be used in this effort.

##### 2.1.4.2.1.2 Long Term Gravity Gradient System Analysis

This effort involves shipment of taped telemetry data to NASA-GSFC from the tracking stations, preselection and conversion of applicable GE telemetry measurement and

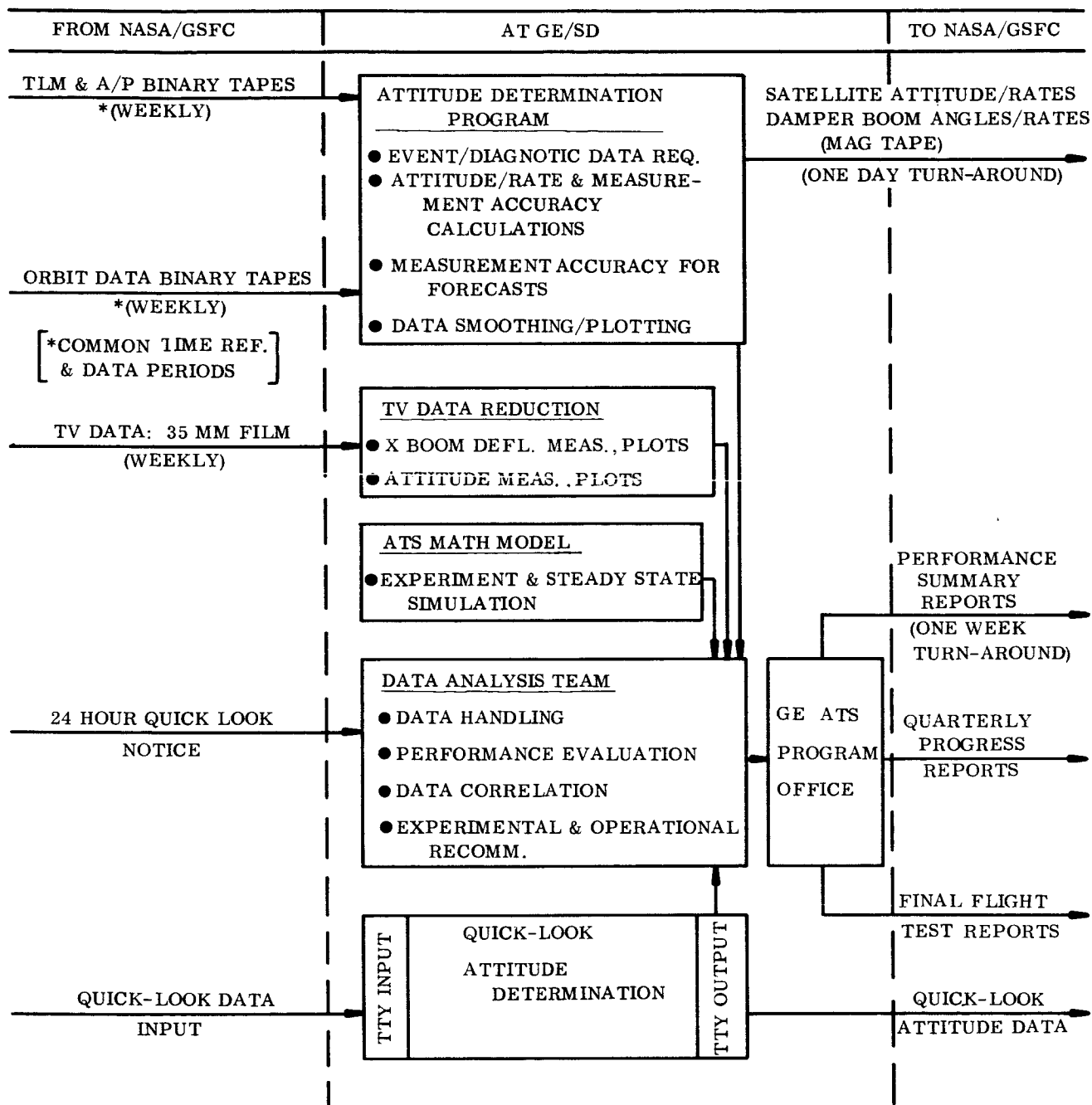


Figure 2.1-3. Flight Evaluation Data/Information Flow and Task Definition at General Electric

updated orbit information into digital format magnetic tapes for each week's worth of data, and shipment to GE for reduction/analysis. The same ATTITUDE DETERMINATION PROGRAM (with expanded capability) will be used for long-term analysis as for QUICK-LOOK data in computing vehicle attitude. In addition, all other telemetry information such as environmental and events monitoring data will be reduced and analyzed; TV data will be analyzed manually to provide X-BOOM deflections data. Results of attitude calculations will be forwarded in the form of a digital tape as soon as possible to NASA with the objective being a 24-hour turn-around time. All analysis results and plots of various vehicle parameters will be returned to NASA/GSFC within one week of receipt of data, on a weekly schedule. Correlation of data/analysis results with the ATS Mathematical Model will be accomplished as required to the extent possible, and results forwarded with the weekly results, or in quarterly, special and final reports according to predetermined requirements and priorities.

#### 2.1.4.2.2 Organization of Flight Evaluation Effort (Paragraph 2.2 of Table 2.1-3)

##### 2.1.4.2.2.1 Central Control Facility NASA/GSFC

Decisions affecting ATS control and data acquisition will be made by the on-orbit team, located at the Central Control Facility, NASA/GSFC, under NASA direction. The decisions involving the Gravity Gradient experiment will be based on the following criteria:

1. Overall Satellite Performance
2. GG System Performance
3. GG Experiment Orbit Test Plan
4. Other Experimenter Requirements
5. Other Satellite/Program Priorities.

Table 2.1-3. ATS Flight Evaluation Plan Outline

1. INTRODUCTION
  - 1.1 Program Description
  - 1.2 Program Objectives
  - 1.3 Gravity Gradient System Description
  - 1.4 Flight Evaluation Objectives and Scope
2. GENERAL EVALUATION PLAN DESCRIPTION AND ORGANIZATION
  - 2.1 Plan Description
  - 2.2 Organization of Flight Evaluation Effort
3. MEASUREMENT SYSTEM DEFINITION
  - 3.1 Satellite-Mounted Measurement/Telemetry System
  - 3.2 TV System Measurements
  - 3.3 Antenna Polarization Measurements
  - 3.4 Orbit Determination Parameters
4. INFORMATION SYSTEM DESCRIPTION
  - 4.1 Long Term Data Flow, Schedule
  - 4.2 Quick-Look Data Flow Schedule
  - 4.3 Operational Requirements Summary
  - 4.4 Data Selection Criteria, Schedule
  - 4.5 Orbit Information Flow, Format
  - 4.6 Supplementary Data Flow, Format
5. DATA REDUCTION AND PROCESSING
  - 5.1 Automated Data Reduction, Plotting
  - 5.2 Quick-Look Data Reduction
  - 5.3 TV Data Reduction
  - 5.4 Computer Facilities/Applications Summary
  - 5.5 Extended Capabilities
6. DATA ANALYSIS/CORRELATION
  - 6.1 Operational Assurance Analysis
  - 6.2 GG Capability Analysis/Math Model Correlation
  - 6.3 Statistical Approach to Correlation
  - 6.4 Interface with On-Orbit Team
7. REPORTING
  - 7.1 Preliminary Flight Test Reports
  - 7.2 Weekly Performance Summary Reports
  - 7.3 Quarterly Progress Reports
  - 7.4 Final Flight Test Reports

The on-orbit team includes both NASA personnel and experimenter consultants in varying numbers for applicable periods of time. GE consultants are tentatively scheduled and charged with the tasks shown in Table 2.1-4.

#### 2.1.4.2.2.2 General Electric Co. - Spacecraft Department

All decisions, transactions, analysis results and operational recommendations affecting each ATS flight will be conducted/transmitted through the GE-ATS Program Office to NASA.

A three-man team will be established to perform the tasks of analyzing the GG system performance, manually correlating results with the ATS Mathematical Model, recommending courses of action to the on-orbit team based on analysis results and supervision of data handling and reduction priorities at GE. One member of the team will be a controls engineer from the GG Engineering Technology Group, experienced in GG theory and the ATS Mathematical Model. The second will be an engineer from the Flight Analysis group thoroughly familiar with the operational plan, measurement system and data flow, and primarily responsible for integration and maintenance of incoming and reduced data and plots.

The third member of the analysis team will be a representative of the Data Reduction group, experienced in the data reduction and computer efforts involved, primarily the Attitude Determination Program.

Data reduction personnel and additional supporting personnel from all contributing engineering design, technology, and operational groups will be available to whatever degree is necessary to support the analysis team.

#### 2.1.4.2.3 TV Data Reduction (Paragraph 5.3 of Table 2.1-3)

TV data reduction will entail the manual reading of 35 millimeter strip films on a reader (Gerber Model) which will convert X-boom disc locations and earth configuration location

to digital scale of the film face and then automatically convert these digital readouts to a form and format for the data evaluation team. The definitization of the film readings will be restricted to a prescribed, fixed procedure and number of data points in order to comply with the turn-around requirements and the continuous work load. The film to be read will have been previously edited by the data evaluation team to enhance the speed of film reading. The sequence of individual manual readings will consist of the following:

1. Locate individual plan square in center of viewing surface and align film along the X- and Y- axes.
2. Read time code displayed on inactive film surface and manually punch into hollerith card.
3. Calibrate the X- and Y- encoders to present zero to 1000 counts across film in both axes.
4. Read the reticule display along X- and Y- axes by aligning head crosshairs over reticules and depressing digitizing button. Approximately ten readings will be made along each coordinate at equal reticule increments.
5. Read the boom disc location by aligning head crosshairs over disc illuminations and depressing digitizing button. When boom disc is unreadable, zero counts in both axes will be placed on hollerith card.
6. Locate earth template fixed to reader head over earth configuration, visually obtaining best representation by the template of the earth outline. Read the earth center by depressing digitizing button.
7. Lay straight edge across shadow line of earth such that the straight edge touches across the tips of the illuminated crescent. The points of intersection of the straight edge and the earth perimeter (two points) will be digitized.

Table 2.1-4. GE Consultant Schedule; On Orbit Support

Flight	Location	Estimated Total (1) Applied Time - Man Weeks			Tasks Required (See List Below)
		Before Launch	Immediately After Launch	(2) Scheduled Experiments	
ATS-A	Central Control Facility-GSFC	0.5	(2 wk period) 3.0	3.0	A, B, C, D, F
	T/S #1	0.5	2.0	2.0	C, D, E
	T/S #2	0.5	2.0	1.0	C, D, E
	T/S #3	0.5	1.0		C, D, E
ATS-D/E	Central Control Facility-GSFC	0.5	(1 mo period) 4.0	5.0	A, B, C, D, F
	T/S #1	0.5	2.0	2.0	C, D, E
	T/S #2		2.0		C, D, E

**TASK DESCRIPTIONS:**

- A. Program direction interface GSFC-GE
- B. Telemetry and orbit data selection/integration/liaison
- C. Quick-look interpretation of flight data
- D. Malfunction identification/action required
- E. TV measurements for attitude, boom data (quick-look measurements)
- F. Assist NASA in interpretation of long-term performance analysis results.

- NOTES:**
- 1. The applied time allocated is based on negotiations with NASA-GSFC on 3/24/65 (16 man-weeks consultant time/launch).
  - 2. Time applied, for scheduled GG experiment evaluation, in conjunction with events specified in orbit test plan, assuming predicted performance.

#### 2.1.4.2.4 Gravity Gradient Capability Analysis/Mathematical Model Correlation (Paragraph 6.2 of Table 2.1-3)

This section of the Flight Evaluation Plan has not yet been completed. However, various studies in smoothing techniques, weighting of the various sensor system combinations for improved confidence, and studies of extended correlation capability beyond the present program scope may affect the final plan. Results of a preliminary study of possible approaches to automated smoothing/correlation techniques are presented in Appendix I.

#### 2.1.5 GE DATA SYSTEM CHECKOUT

The concept and scope of the Orbit Test Simulation Exercise, as discussed in the First Quarterly Report (Section 2.1.2), was considerably reduced during the past quarter by NASA/GSFC direction. The negotiated work scope now includes only an internal checkout of the GE portion of the data system. This will be done briefly as follows:

1. Options in the ATS Mathematical Model will allow, for any performance prediction run, the printout of solar aspect data, earth aspect data and geometrical "polang" data.
2. Data from (1), used as an input to programmed individual sensor equations, will provide computed sensor output voltage data as a function of the spacecraft's attitude-time history.
3. The resultant voltage data will be PCM formatted using available equipment at GE Re-entry Systems Department. Diagnostic and other data will be added to fill out the tape format to be used by NASA on data tapes to be forwarded to GE for processing.
4. The orbit data tape will be generated according to NASA format using orbit data from the Mathematical Model run of Step (1).



5. TV data will be simulated by punched cards generated in the process of checking out the TV data reduction system.
6. The resultant tapes, when processed through the Attitude Determination Program should produce exactly the same results as the Mathematical Model output of Step (1).
7. Intentional deviations from the optional printouts of Step (1) can be artificially introduced to cause a divergence of results in Step (6). The intent here would be to isolate the cause of the deviations through use of data correlation techniques developed for flight test analysis.

Implementation of this plan will require a special computer routine for Step (2). Further definitization of plans for the checkout will be accomplished in the forthcoming quarter.

#### 2.1.6 ANALYTICAL STUDIES AND RESULTS

##### 2.1.6.1 ATS Optimization Studies

For the past several months, NASA/GSFC has expressed concern with the performance of ATS-A and D/E. The large yaw errors were of particular concern and even led to the suggestion of employing a yaw stiffening flywheel to correct the difficulty. Conversations with GE and NASA/Ames, however, convinced NASA/GSFC that the configuration originally specified was not optimum for steady state performance. As a consequence, an optimization study was undertaken by NASA/Ames and GE, both independently and cooperatively. Both studies utilize computer programs which solve the characteristic equation of the configuration (the GE Octic Program) and provide natural frequencies and damping characteristics.

At GE, the roots of the characteristic equation were obtained from the Octic program (which was originally constructed to locate the NASA/GSFC parameters with regard to the

optimum parameters) and the evaluation of the results was performed by engineering personnel. At NASA/Ames, the computer program contains additional routines which find the configuration with the best damping for a specific set of input parameters. In addition, frequency response information is generated.

For these particular studies, GAPS III could not be employed for reasons of economy, computer scheduling, and time.

Discussions with B. E. Tinling and V. K. Merrick of NASA/Ames, who have conducted extensive studies of this system for the past several years, led to the selection of several possible configurations. The GE configurations began to approach those of Tinling and Merrick (Note GE-1 and TM-2 configurations in the Ames Budgets of Figures 2.1-6 and 2.1-7) and it was felt that the Ames program would locate the optimum more rapidly than the Octic program. Consequently GE reduced its efforts in optimizing the configuration by root locus techniques and concentrated on determining the test of the configurations suggested by Ames.

Complete evaluation of the pointing accuracy of a particular configuration requires the use of GAPS III, since the magnitude and phasing of the external disturbances determine the performance capability of the system. All the external disturbances are functions of the vehicle size, shape, dipole, etc., and to provide a common basis for comparison, as well as permit accurate optimization, it is necessary to identify the nature and magnitude of the disturbances. On March 11, a meeting was held with Ames, GSFC, and GE to provide the required "standard conditions" for the GAPS III computer runs. The values, factors, etc., selected were felt to be a reasonable estimate of the real case.

In summary they are:

1. The magnetic dipole of the spacecraft is assumed to be 1,000 pole centimeters located along the system roll axis.

2. The center of pressure/center of mass offset of the entire spacecraft assuming the basic rod straightness tolerances (due to manufacturing only) will be within a one-inch radius circle of uncertainty. (Assume rigid body).
3. The center of mass/center of thrust misalignment will be assumed to be 1/2-inch. (Assume rigid body). A continuous thrust of  $1/2 \times 10^{-5}$  pounds will be used.
4. NASA will use a thermally bent X-rod radius of curvature of 1,825 feet. GE will continue to input basic rod parameters into their computer program. Absorptivity ( $\alpha$ ) of .15 will be used.
5. The present nominal ATS configuration will be used with the 100 foot X-booms and 2.5 pound tip weights for the ATS-A and 10.0 pound tip weights for ATS-D/E. The diameter of the X-booms is  $.500 \pm .020$  inch.
6. The present nominal damper boom length is 45 feet root to tip with 1.9 pound tip weights for ATS-A and 7.15 pound tip weights for ATS-D/E. For the optimization study the 45-foot length will be considered as fixed, and the minimum tip weight will be 1.1 each pound. If the damper boom inertia must be reduced further than the above minimums, the boom length will be changed. The nominal damper boom diameter is  $.560 \pm .020$ -inch. All of the booms weigh .01565 pounds/foot. The radius of curvature of the damper boom is 1630 feet. The damping axis will be assumed to pass through the center of mass of the spacecraft. The distance from the damper boom center line to the spacecraft CM is 30.2 inches.
7. The orbit eccentricity for the ATS-A satellite is considered to be .01.

With this selection of parameters, a series of runs was made to determine the pointing capability of each of the configurations. Performance Comparison Charts (i.e., response

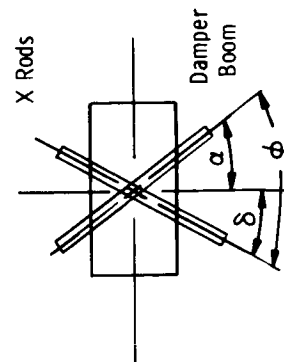
of each system to individual and combined disturbance sources) were constructed in whole and in part, and were presented at the GSFC/HAC/GE Interface Meeting of March 16th. These charts are shown in Figures 2.1-4 through 2.1-13. The error estimates shown on all these charts were determined from GAPS III, with the exception of Rod Alignment and Curved Boom estimates which are included only for reference. The total performance was also determined from GAPS III and the phasing was adjusted to cause as many of the disturbances to add as possible. This should produce pessimistic results. Since the interface meeting, several changes have been made to the charts. The phasings of the error sources were inappropriate in several instances and a dimensional error in the magnetic field routine of GAPS III was corrected).

The results of the runs indicate that the TM-2 Configuration exhibits considerably better yaw response than the original GSFC at a slight decrease in pitch performance. The TM-1 Configuration provides better yaw response than the TM-2, but at a pitch sacrifice which for ATS-A could be unacceptable. As a consequence, at the Optimization Meeting of March 22 at GSFC, GE recommended the TM-2 Configuration for ATS-A, and the TM-1 Configuration for ATS-D. With commonality as a requirement, the TM-2 Configuration was recommended. It should be noted that a pulsed thruster with the pulsing period specified (seven days on and seven days off) causes significant yaw errors, and it is felt that a more rapid pulsing (six cycles per orbit for example) would significantly improve the performance. As a consequence, the selection of the optimum system was predicted on the response of the vehicle to a constant thrust equal to  $5 \times 10^{-5}$  pounds, 1/2 the value specified by HAC on September 24, 1964. (ATS Systems Memo 010).

An additional configuration, MF-1, was devised by GE following the Interface Meeting (3/16/65) to assist in relieving the internal packaging problem of ATS-D. The error budgets for this configuration were not available for the March 22 meeting, but are shown on Figure 2.1-8 and 2.1-13.

## APPLICATIONS TECHNOLOGY SATELLITE

GSFC CONFIGURATION ATS - A	SUN 28° TO ORBIT PLANE						Sun in Orbit Plane					
	Pitch		Roll		Yaw		Pitch		Roll		Yaw	
	Bias	Osc	Bias	Osc	Bias	Osc	Bias	Osc	Bias	Osc	Bias	Osc
Thermal Bending and Rod Solar Torque	0	0.3	0	0.4	0.4	0.4	0	0.3	0	0.3	0.4	0.3
Magnetics	0	0.3	0	0	1.9	0.7	0	0.3	0	0	1.9	0.7
Central Body Solar Torque	0	1.1	0	0.1	0.5	2.3	0	1.1	0	0.1	0.5	2.3
Eccentricity	0.2	0	0.2	0	0.4	0	0.2	0	0.2	0	0.4	0
Rod Alignment												
Curved Booms												
Principal Axis Shift	0.2	0	0.2	0	0.5	0	0.2	0	0.2	0	0.5	0
Solar Torque	0	0	0	0	0	0.1	0	0	0	0	0	0.1
Total Performance	0.1	1.0	0	0.4	3.1	2.4	0.2	1.2	0	0.2	3.1	3.0



$$\frac{b/I_D \omega_0^2}{1.5455} \quad \frac{k/I_D \omega_0^2}{4.5379} \quad \frac{I_Y/I_R}{.12} \quad \frac{I_D/I_R}{.08} \quad \frac{\phi}{62.62} \quad \frac{\alpha}{41.87} \quad \frac{\delta}{20.75} \quad \frac{\xi}{19}$$

Figure 2.1-4. Performance Comparison Chart, GSFC Configuration, ATS-A

# APPLICATIONS TECHNOLOGY SATELLITE

TM - 1 CONFIGURATION ATS - A	SUN 28° TO ORBIT PLANE						Sun in Orbit Plane					
	Pitch		Roll		Yaw		Pitch		Roll		Yaw	
	Bias	Osc	Bias	Osc	Bias	Osc	Bias	Osc	Bias	Osc	Bias	Osc
Thermal Bending and Rod Solar Torque	0.1	0.5	0	0.3	1.1	0.8	0	0.3	0	0.2	1.0	0.3
Magnetics	0	0.5	0	0	0.5	0.7	0	0.5	0	0	0.5	0.7
Central Body Solar Torque	0	2.7	0	0.3	1.3	3.5	0	2.7	0	0.3	1.3	3.5
Eccentricity	0.2	0	0.2	0	0.4	0	0.2	0	0.2	0	0.4	0
Rod Alignment	0.2	0	0.2	0	0.5	0	0.2	0	0.2	0	0.5	0
Curved Booms	0.2	0	0.2	0	0.5	0	0.2	0	0.2	0	0.5	0
Principal Axis Shift	0	0	0	0	0	0.1	0	0	0	0	0	0.1
Solar Torque	0	2.6	0.2	0.4	2.5	3.7	0.2	2.4	0	0.1	2.3	3.8
Total Performance												

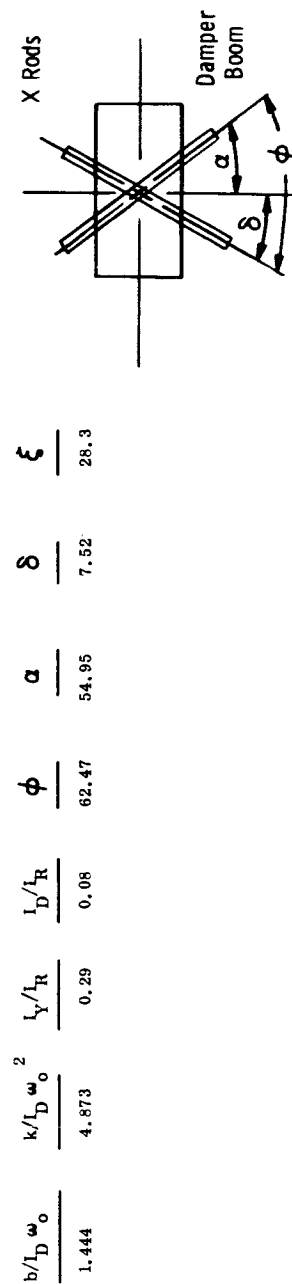
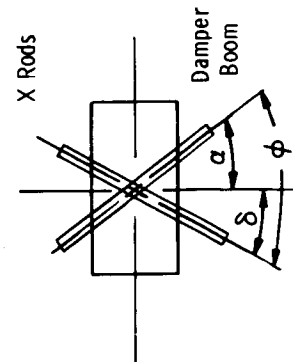


Figure 2.1-5. Performance Comparison Chart, TM-1 Configuration, ATS-A

## APPLICATIONS TECHNOLOGY SATELLITE

GE - 1 CONFIGURATION ATS - A	SUN 28° TO ORBIT PLANE						Sun in Orbit Plane					
	Pitch		Roll		Yaw		Pitch		Roll		Yaw	
	Bias	Osc	Bias	Osc	Bias	Osc	Bias	Osc	Bias	Osc	Bias	Osc
Thermal Bending and Rod Solar Torque	0	0.3	0	0.4	0.9	0.7						
Magnetics	0	0.3	0	0	1.4	0.6	0	0.3	0	0	1.4	0.6
Central Body Solar Torque												
Eccentricity	0	1.5	0	0.1	0.8	2.2	0	1.5	0	0.1	0.8	2.2
Rod Alignment	0.2	0	0.2	0	0.4	0	0.2	0	0.2	0	0.4	0
Curved Booms												
Principal Axis Shift	0.2	0	0.2	0	0.5	0	0.2	0	0.2	0	0.5	0
Solar Torque	0	0	0	0	0	0.1	0	0	0	0	0	0.1
Total Performance	0	2.0	0	0.4	1.9	2.7	0	2.4	0	0.5	1.5	3.9

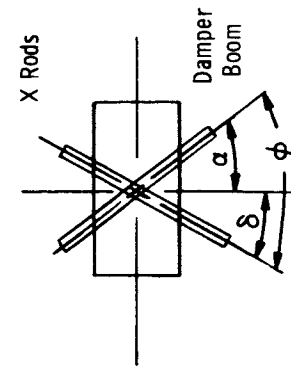


$$\frac{b/I_D \omega_0}{1.300} \quad \frac{k/I_D \omega_0^2}{5.200} \quad \frac{I_Y/I_R}{0.1325} \quad \frac{I_D/I_R}{0.0453} \quad \frac{\phi}{55} \quad \frac{\alpha}{46.3} \quad \frac{\delta}{8.70} \quad \frac{\xi}{25}$$

Figure 2.1-6. Performance Comparison Chart, GE-1 Configuration, ATS-A

# APPLICATIONS TECHNOLOGY SATELLITE

TM-2 CONFIGURATION ATS-A	SUN 28° TO ORBIT PLANE						Sun in Orbit Plane					
	Pitch		Roll		Yaw		Pitch		Roll		Yaw	
	Bias	Osc	Bias	Osc	Bias	Osc	Bias	Osc	Bias	Osc	Bias	Osc
Thermal Bending and Rod Solar Torque	0	0.3	0	0	1.0	0.7	0	0.4	0	0.2	0.1	0.7
Magnetics											1.0	0.7
Central Body Solar Torque	0	1.5	0	0.1	0	2.0	0	1.5	0	0.1	0	2.0
Eccentricity	0.2	0	0.2	0	0.4	0	0.2	0	0.2	0	0.4	0
Rod Alignment												
Curved Booms	0.2	0	0.2	0	0.5	0	0.2	0	0.2	0	0.5	0
Principal Axis Shift	0	0	0	0	0	0.1	0	0	0	0	0	0.1
Solar Torque	0	2.0	0	0.2	1.0	2.5	0.1	1.9	0	0.4	1.1	3.3
Total Performance												



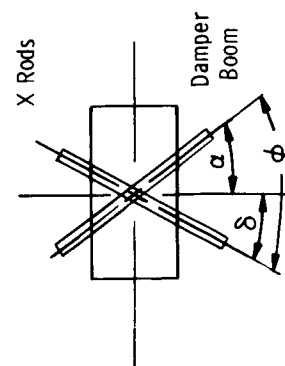
$$\frac{b/I_D \omega_o}{1.0588} \quad \frac{K/I_D \omega_o}{5.1504} \quad \frac{I_Y/I_R}{0.2308} \quad \frac{I_D/I_R}{0.04} \quad \frac{\phi}{58.2} \quad \frac{\alpha}{53.4} \quad \frac{\delta}{4.8} \quad \frac{\xi}{25.65}$$

Figure 2.1-7. Performance Comparison Chart, TM-2 Configuration, ATS-A



## APPLICATIONS TECHNOLOGY SATELLITE

MF-1 CONFIGURATION ATS-A	SUN 28° TO ORBIT PLANE						Sun in Orbit Plane					
	Pitch		Roll		Yaw		Pitch		Roll		Yaw	
	Bias	Osc	Bias	Osc	Bias	Osc	Bias	Osc	Bias	Osc	Bias	Osc
Thermal Bending and Rod Solar Torque												
Magnetics												
Central Body Solar Torque												
Eccentricity												
Rod Alignment	0	0.2	0	0.2	0	0.4	0	0.2	0	0.2	0	0.4
Curved Booms												
Principal Axis Shift	0.2	0	0.2	0	0.5	0	0.2	0	0.2	0	0.5	0
Solar Torque	0	0	0	0	0	0.1	0	0	0	0	0	0.1
Total Performance							0	1.9	0	0.3	1.7	2.3

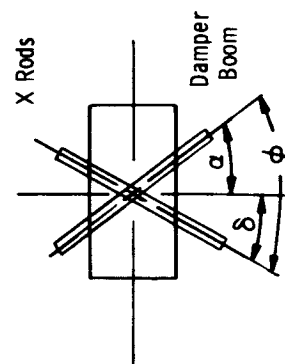


$b/I_D \omega_o$	$K/I_D \omega_o$	$I_Y/I_R$	$I_D/I_R$	$\phi$	$\alpha$	$\delta$	$\xi$
1.5455	4.5379	0.215	0.0846	62.5	51.0	11.5	24.88

Figure 2.1-8. Performance Comparison Chart, MF-1 Configuration, ATS-A

# APPLICATIONS TECHNOLOGY SATELLITE

GSFC CONFIGURATION ATS-D	SUM 23.45° TO ORBIT PLANE						Sun in Orbit Plane					
	Pitch		Roll		Yaw		Pitch		Roll		Yaw	
	Bias	Osc	Bias	Osc	Bias	Osc	Bias	Osc	Bias	Osc	Bias	Osc
Thermal Bending and Rod Solar Torque												
Magnetics	0	0	0	0	0.3	0	0	0	0	0	0.3	0
Central Body Solar Torque	0	0	0	0.1	0.1	0.2						
Rod Alignment	0.2	0	0.2	0	0.4	0	0.2	0	0.2	0	0.4	0
Curved Booms												
Principal Axis Shift	0.2	0	0.2	0	0.5	0	0.2	0	0.2	0	0.5	0
Solar Torque	0	0.1	0	0.1	0.6	0.2	0	0.1	0	0.1	0	0.4
Total Performance												
Without Thruster	0.2	0.9	0	1.0	0.7	2.5	0.2	1.1	0	1.1	0.6	3.8
With Pulsed Thruster	0.3	1.8	0.2	1.6	7.2	12.6	0	1.5	0.2	1.1	4.3	2.0
With Constant Thruster	0.1	1.1	0	0.9	6.9	1.2	0.1	1.2	0	1.1	2.3	2.8

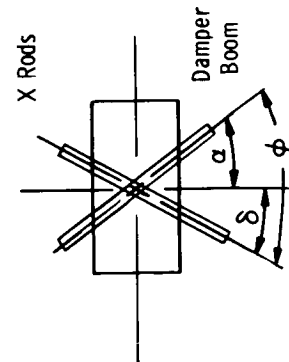


$b/I_D \omega$	$K/I_D \omega$	$I_Y/I_R$	$I_D/I_R$	$\phi$	$\alpha$	$\delta$	$\xi$
1.5455	4.5379	0.08	0.12	62.62	41.87	20.75	19

Figure 2.1-9. Performance Comparison Chart, GSFC Configuration, ATS-D

## APPLICATIONS TECHNOLOGY SATELLITE

TM-1 CONFIGURATION ATS-D	SUN 23.45° TO ORBIT PLANE						Sun in Orbit Plane					
	Pitch		Roll		Yaw		Pitch		Roll		Yaw	
	Bias	Osc	Bias	Osc	Bias	Osc	Bias	Osc	Bias	Osc	Bias	Osc
Thermal Bending and Rod Solar Torque												
Magnetics	0	0	0	0	0.3	0	0	0	0	0	0.3	0
Central Body Solar Torque	0	0	0	0.1	0.1	0.2						
Rod Alignment	0.2	0	0.2	0	0.4	0	0.2	0	0.2	0	0.4	0
Curved Booms												
Principal Axis Shift	0.2	0	0.2	0	0.5	0	0.2	0	0.2	0	0.5	0
Solar Torque	0	0.1	0	0.1	0.3	0.3	0	0.1	0	0.1	0	0.5
Total Performance												
Without Thruster	0	1.4	0	0.5	0.5	1.1	0.1	1.4	0	0.8	0.5	2.4
With Pulsed Thruster	0	2.6	0.1	0.9	4.0	6.2	0.1	2.3	0	0.8	1.4	3.3
With Constant Thruster	0	1.9	0	0.4	3.1	1.1	0.1	1.8	0	0.8	1.2	2.3



$b/I_D \omega_0$	$k/I_D \omega_0^2$	$I_Y/I_R$	$I_D/I_R$	$\phi$	$\alpha$	$\delta$	$\xi$
1.444	4.873	0.29	0.08	62.47	54.95	7.52	28.3

Figure 2.1-10. Performance Comparison Chart, TM-1 Configuration, ATS-D

# APPLICATIONS TECHNOLOGY SATELLITE

GE-1 CONFIGURATION ATS-D	SUN 23.43° TO ORBIT PLANE										Sun in Orbit Plane			
	Pitch		Roll		Yaw		Pitch		Roll		Yaw		Bias	Osc
	Bias	Osc	Bias	Osc	Bias	Osc	Bias	Osc	Bias	Osc	Bias	Osc		
Thermal Bending and Rod Solar Torque														
Magnetics														
Central Body Solar Torque														
Rod Alignment	0.2	0	0.2	0	0.4	0	0.2	0	0.2	0	0.4	0		
Curved Booms														
Principal Axis Shift	0.2	0	0.2	0	0.5	0	0.2	0	0.2	0	0.5	0		
Solar Torque	0	0.1	0	0.1	0.6	0.2	0	0.1	0	0.1	0	0.4		
Total Performance														
Without Thruster	0.1	0.9	0	1.0	0.7	1.8	0.1	1.0	0	1.1	0.7	4.0		
With Pulsed Thruster														
With Constant Thruster	0.1	1.2	0	1.0	5.0	2.8	0.1	1.1	0	1.3	1.0	4.2		

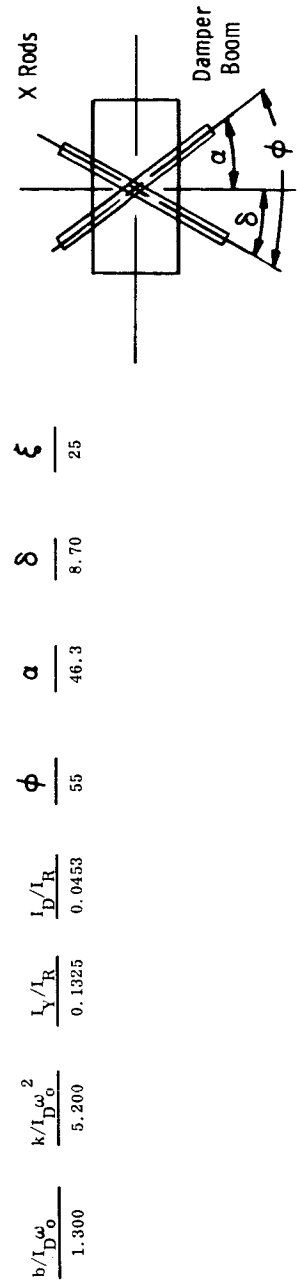
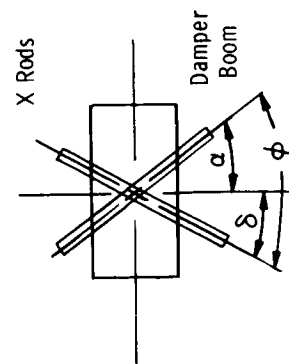


Figure 2.1-11. Performance Comparison Chart, GE-1 Configuration, ATS-D

## APPLICATIONS TECHNOLOGY SATELLITE

TM-2 CONFIGURATION ATS-D	SUN 23.45° TO ORBIT PLANE						Sun in Orbit Plane					
	Pitch		Roll		Yaw		Pitch		Roll		Yaw	
	Bias	Osc	Bias	Osc	Bias	Osc	Bias	Osc	Bias	Osc	Bias	Osc
Thermal Bending and Rod Solar Torque	0	1.0	0	0.7	0.3	1.6	0.1	1.0	0	1.1	0.4	3.6
Magnetics	0	0	0	0	0.4	0	0	0	0	0	0.4	0
Central Body Solar Torque												
Rod Alignment	0.2	0	0.2	0	0.4	0	0.2	0	0.2	0	0.4	0
Curved Booms												
Principal Axis Shift	0.2	0	0.2	0	0.5	0	0.2	0	0.2	0	0.5	0
Solar Torque	0	0.1	0	0.1	0.3	0.3	0	0.1	0	0.1	0	0.4
Total Performance												
Without Thruster	0	1.4	0	0.5	0.4	1.1	0.1	1.4	0	0.8	0.4	2.5
With Pulsed Thruster												
With Constant Thruster	0	1.3	0	0.7	3.7	1.2	0	1.3	0	0.9	1.7	2.9



$$\frac{b/I_D \omega_0}{1.0588} \quad \frac{K/I_D \omega_0^2}{5.1504} \quad \frac{I_Y/I_R}{0.04} \quad \frac{I_D/I_R}{0.2308} \quad \frac{\phi}{58.2} \quad \frac{\alpha}{53.4} \quad \frac{\delta}{4.8} \quad \frac{\xi}{25.65}$$

Figure 2.1-12. Performance Comparison Chart, TM-2 Configuration, ATS-D

# APPLICATIONS TECHNOLOGY SATELLITE

MF-1 CONFIGURATION ATS-D	SUN 23.45° TO ORBIT PLANE						Sun in Orbit Plane					
	Pitch		Roll		Yaw		Pitch		Roll		Yaw	
	Bias	Osc	Bias	Osc	Bias	Osc	Bias	Osc	Bias	Osc	Bias	Osc
Thermal Bending and Rod Solar Torque												
Magnetics												
Central Body Solar Torque												
Rod Alignment												
Curved Booms												
Principal Axis Shift												
Solar Torque												
Total Performance												
Without Thruster												
With Pulsed Thruster												
With Constant Thruster	0.1	1.3	0	0.6	4.4	1.1	0.2	1.5	0	0.9	1.7	2.8

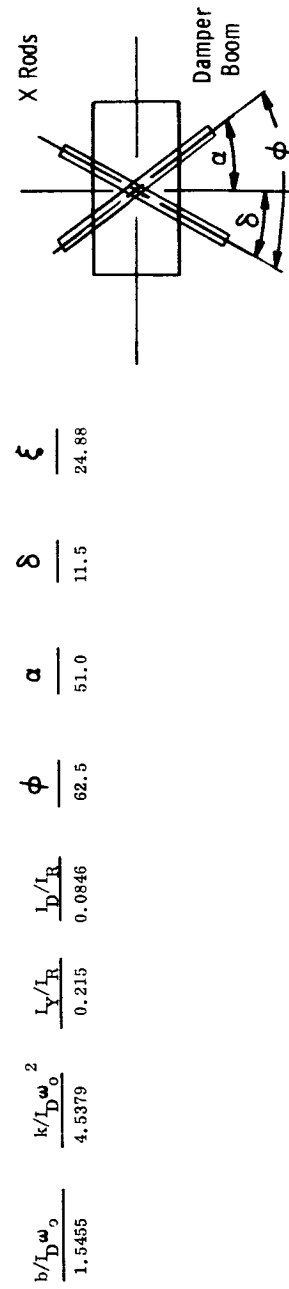


Figure 2.1-13. Performance Comparison Chart, MF-1 Configuration, ATS-D

On March 26th, the TM-2 Configuration was confirmed (by TWX) by GSFC for both ATS-A and ATS-D/E. Following this confirmation, GE embarked upon an optimization study directed towards determining the appropriate rod lengths and tip weights for ATS-A and ATS-D/E. The TM-2 Configuration, as defined by Ames, is not a physical configuration, but a set of non-dimensional parameters which specify the damping and moment of inertia characteristics of the system. To convert these non-dimensional parameters into a vehicle design, it is necessary to select (from analytical studies) moments of inertia, rod lengths, and tip weights. The rod lengths and tip weights used in the performance comparison charts were arbitrary (but identical) and not necessarily the optimum, but are used in the optimization studies as a basis of comparison.

In determining the rod lengths and tip weights, it is necessary to evaluate the effect of these parameters on external disturbances. Long rod lengths, for example, provide large moments of inertia which reduce the effect of the magnetic dipole on pointing accuracy. However, long rods also increase the torques due to thermal bending. Heavy tip weights alleviate both difficulties but may not be acceptable from the weight standpoint. Optimization, therefore, requires evaluation of all disturbances and tradeoff among performance, weight, and engineering capability.

Paragraphs 2.1.6.1.1 and 2.1.6.1.2, contain the optimization studies for both ATS-A and ATS-D/E and the results of these studies. The analytical technique used is a simple scaling procedure devised from a knowledge of the external disturbances and a reference point obtained from GAPS III. This technique is not the type normally employed for optimization, but is equally rated, although not as comprehensive as the standard technique. It has the advantage of speed, and can be completed within a short period of time.

The results of the optimization studies are shown in Table 2.1-5. There are three estimates given for ATS-A, the original TM-2 Configuration (the tradeoff configuration using 100-foot rods), the optimum TM-2 Configuration (as determined from the study), and the TM-2 Configuration finally selected. The optimum configuration was not selected because of

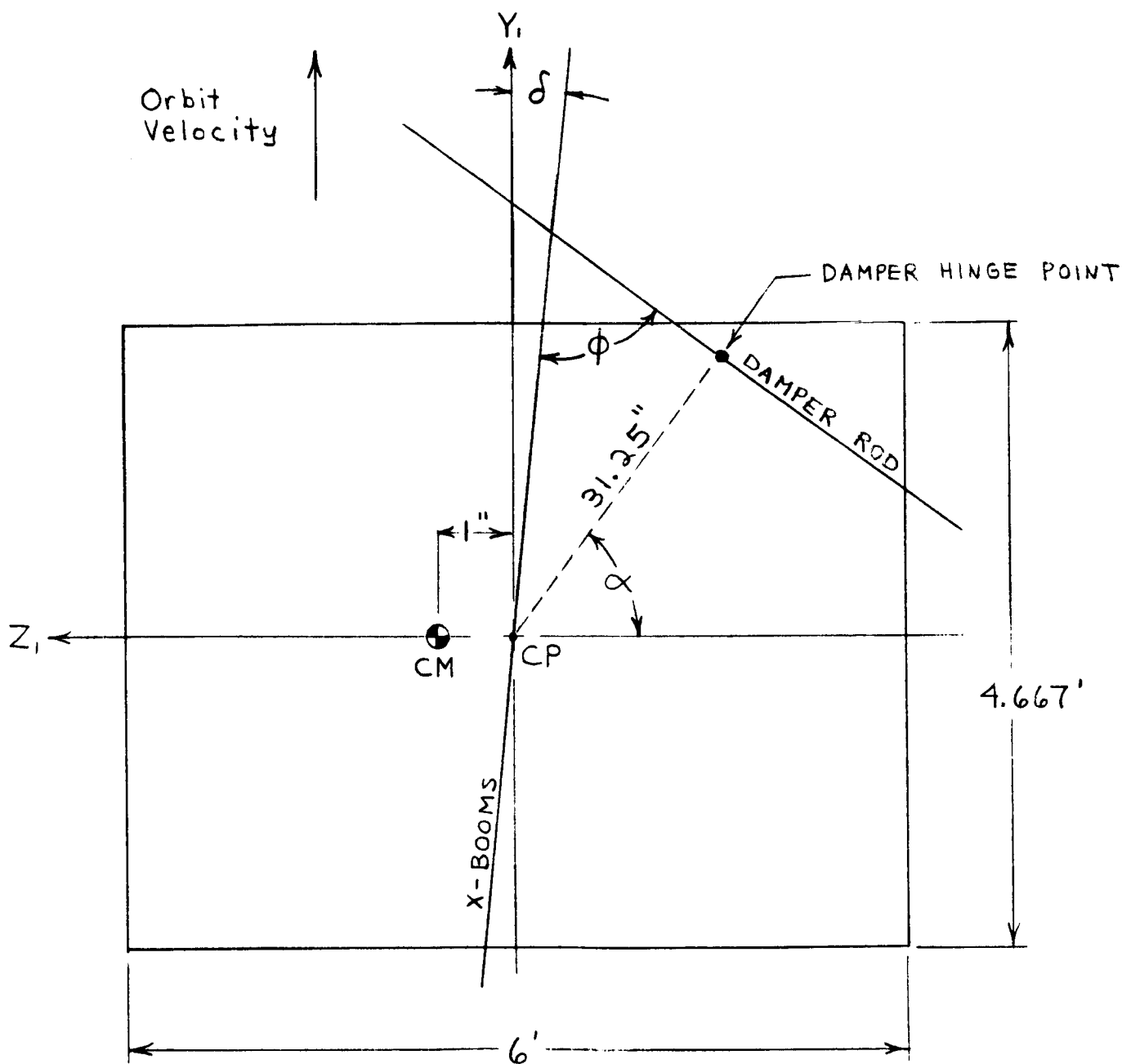
hardware limitations. In the case of ATS-A, the limiting item was the available spring constant. As indicated in Figure 2.1-20, a rod length of 150 feet with heaviest available tip weight would be best. The spring constant, however, cannot be made large enough to match this system without major revision.

The parameters selected for ATS-A are shown in Table 2.1-6 along with the original values as specified by GSFC. The angles are as shown on Figure 2.1-14. The long rod length (150 feet) was selected in order to make better use of the available rod length. The tip masses of 2.5 pounds were retained and, with this tip mass, the rod length had to be reduced to 133.75 feet in order to match the spring capability. Figure 2.1-20 indicates that a heavier tip mass and shorter rod length would give better performance, but the weight increase was felt to be unwarranted.

In the selection of the ATS-D/E system, emphasis was placed on the selection of a light-weight system. As with ATS-A, the heavy tip masses produce better performance than the light tip masses, but the tip masses on ATS-D/E are already heavy (10 pounds) and it was felt that a reduction could be made in this weight without a significant decrease in performance. The results of the optimization (Paragraph 2.1.6.1.2.3) indicated that rod lengths in excess of 125 feet were not very beneficial in yaw. Since there is some degradation in pitch with increasing rod length (the primary error source in pitch is thermal bending), long rod lengths should be avoided.

The limiting hardware item for ATS-D/E is the torsion wire of the hysteresis damper. The originally specified 5 dyne-cm/deg requires a large inertia system and virtually eliminates the possibility of reducing the attitude control weight. Discussions with STL indicate a probable lower limit of 3.5 dyne-cm/deg. This was used for the optimum spring constant and the system was sized accordingly. At a small sacrifice in performance, a weight savings of approximately 14 pounds (over the original GSFC Configuration) was accomplished. The resultant configuration utilizes 8-pound tip masses and 124.33-foot rods. Parameters selected are shown in Table 2.1-7 along with parameters originally specified by GSFC. Angles are shown in Figure 2.1-14.





$$\begin{aligned}\delta &= 4.8^\circ \\ \alpha &= 53.4^\circ \\ \phi &= 58.2^\circ\end{aligned}$$

Figure 2.1-14. Vehicle Configuration

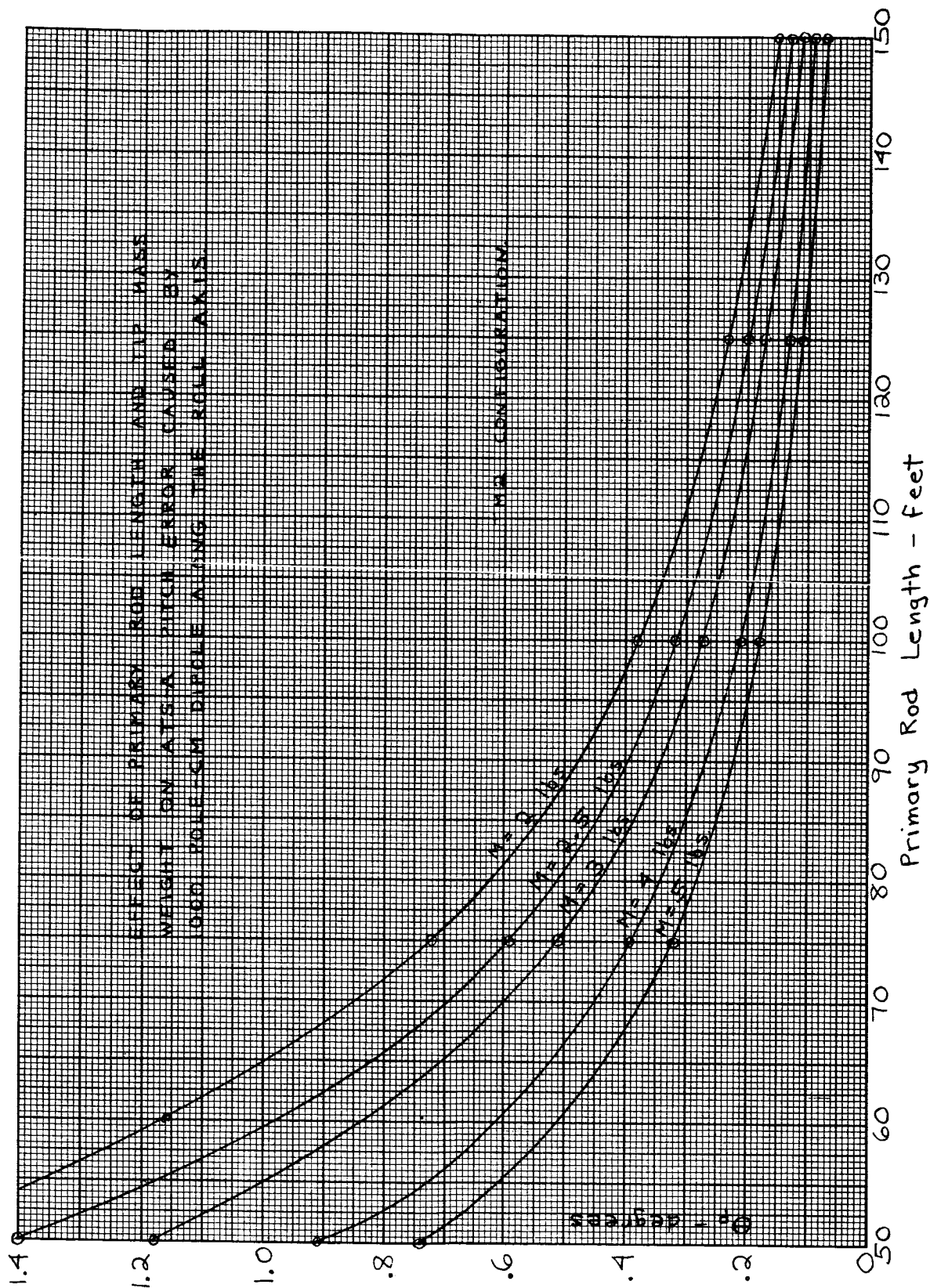


Figure 2.1-15. Effect of Primary Rod Length and Tip Mass Weight on ATS-A Pitch Error Caused By 1000 Pole-CM Dipole Along The Roll Axis

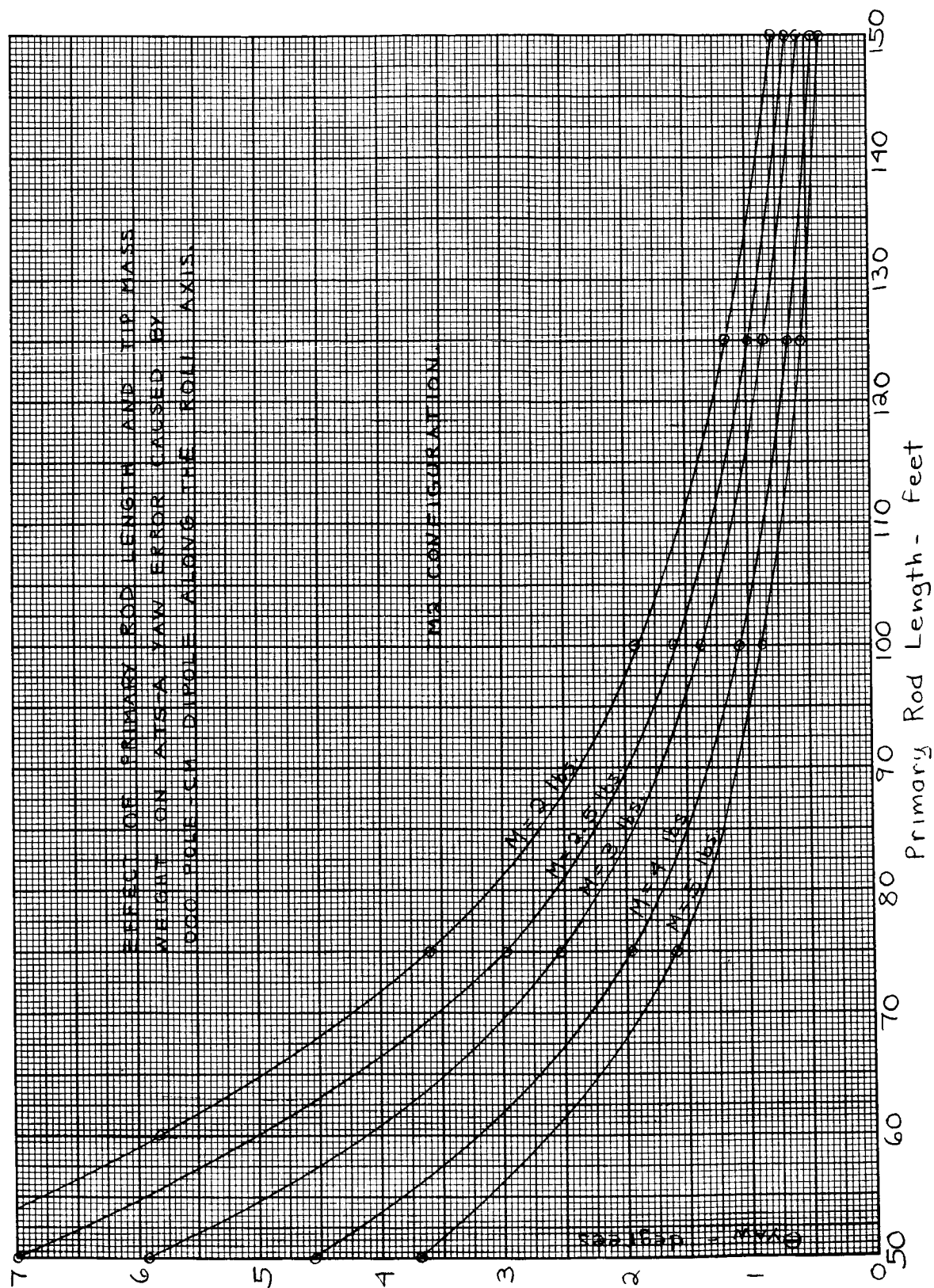


Figure 2.1-16. Effect of Primary Rod Length and Tip Mass Weight on ATS-A Yaw Error Caused By 1000 Pole-CM Dipole Along the Roll Axis

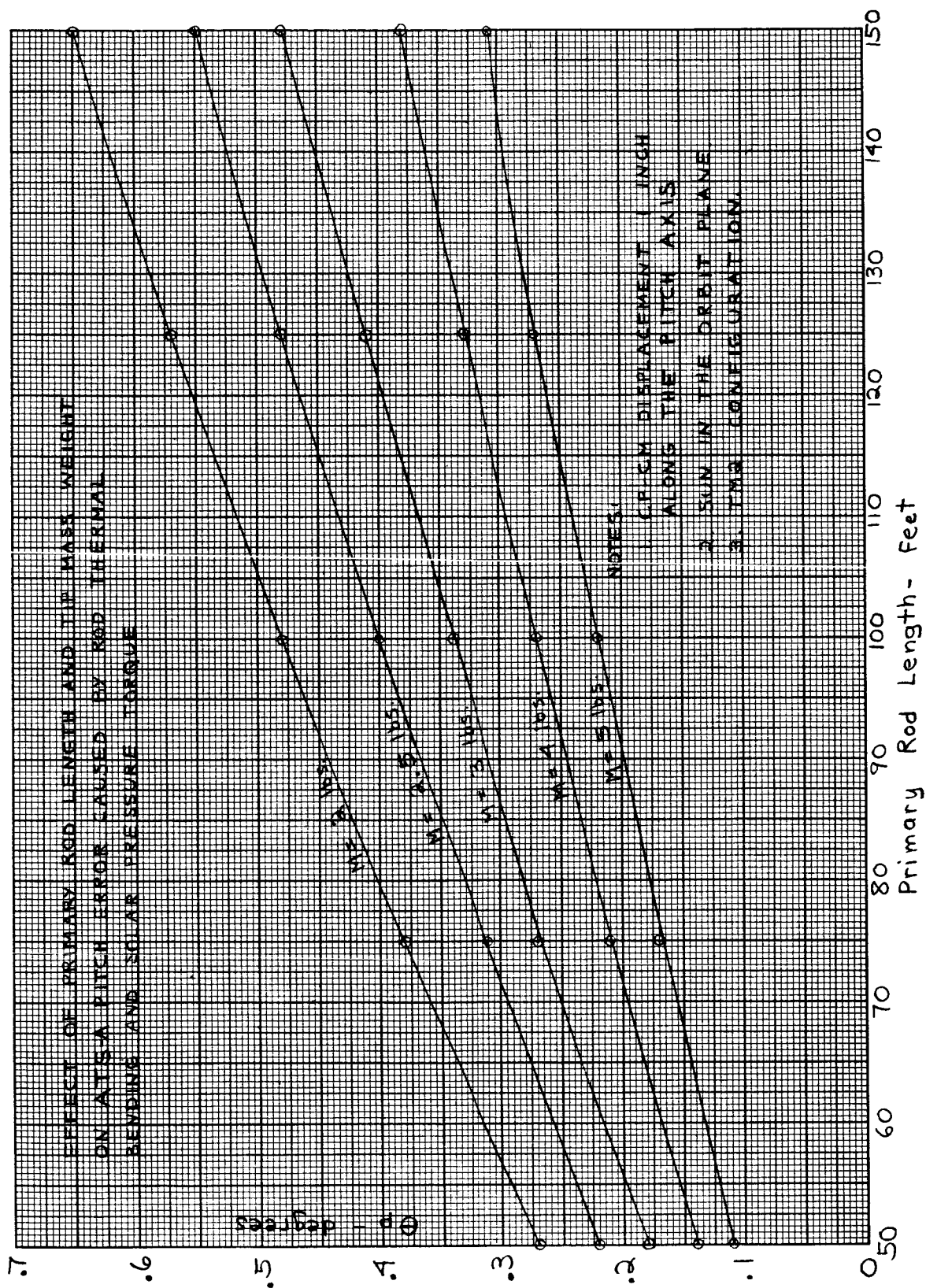


Figure 2.1-17. Effect of Primary Rod Length and Tip Mass Weight on ATS-A Pitch Error Caused By Rod Thermal Bending and Solar Pressure Torque

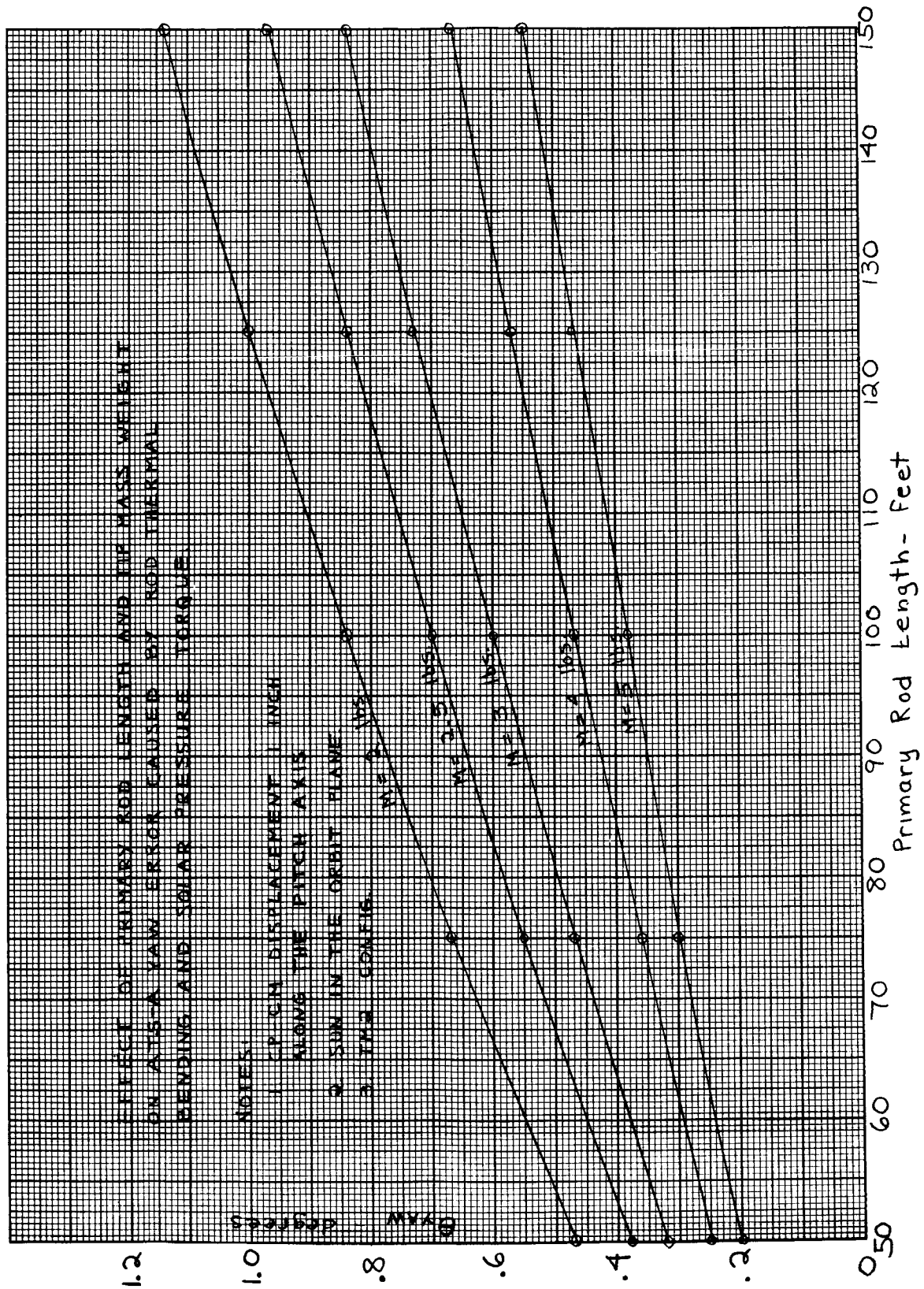


Figure 2.1-18. Effect of Primary Rod Length and Tip Mass Weight on ATS-A Yaw Error Caused By Rod Thermal Bending and Solar Pressure Torque



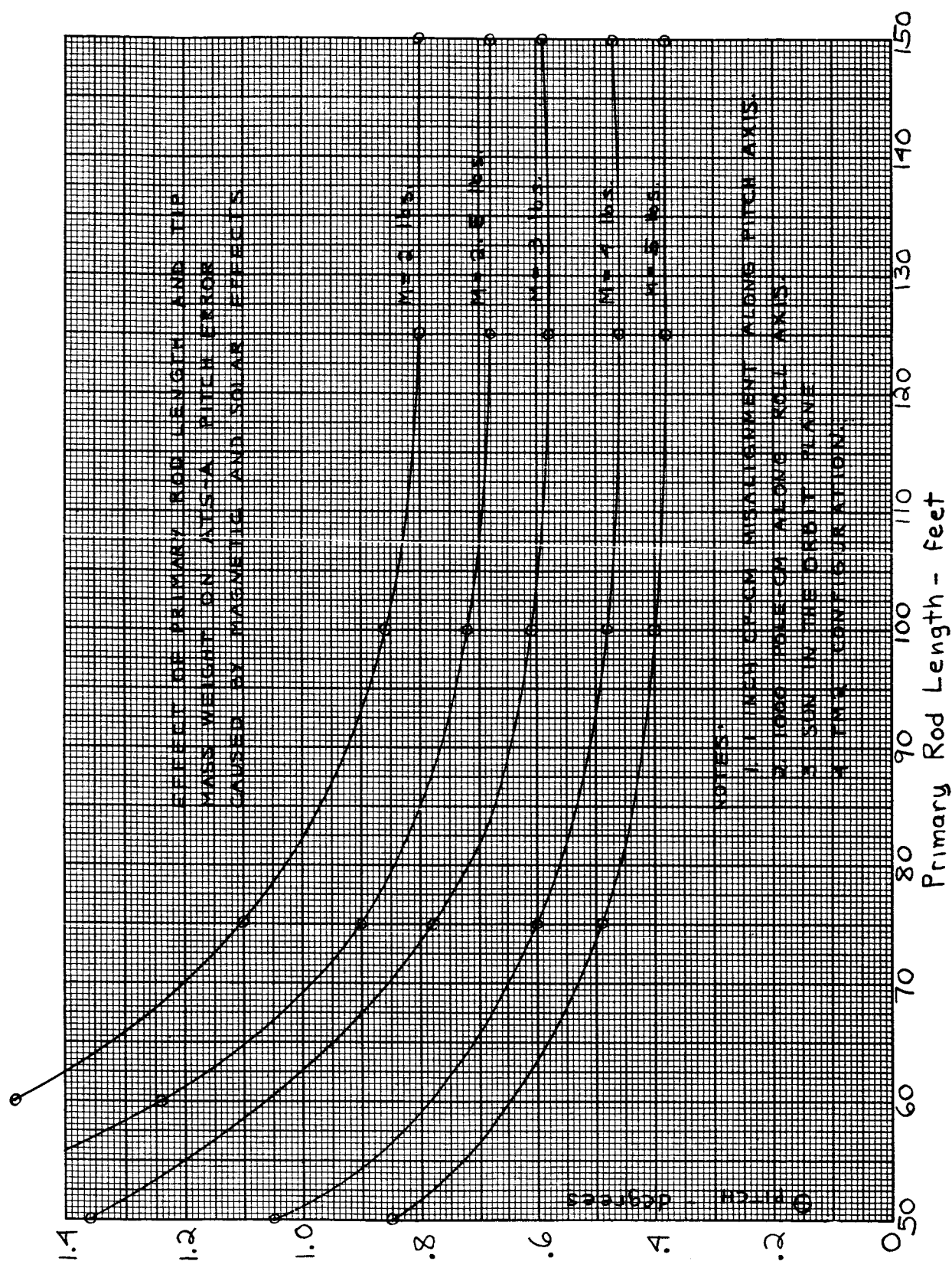


Figure 2.1-19. Effect of Primary Rod Length and Tip Mass Weight on ATS-A Pitch Error Caused By Magnetic And Solar Effects

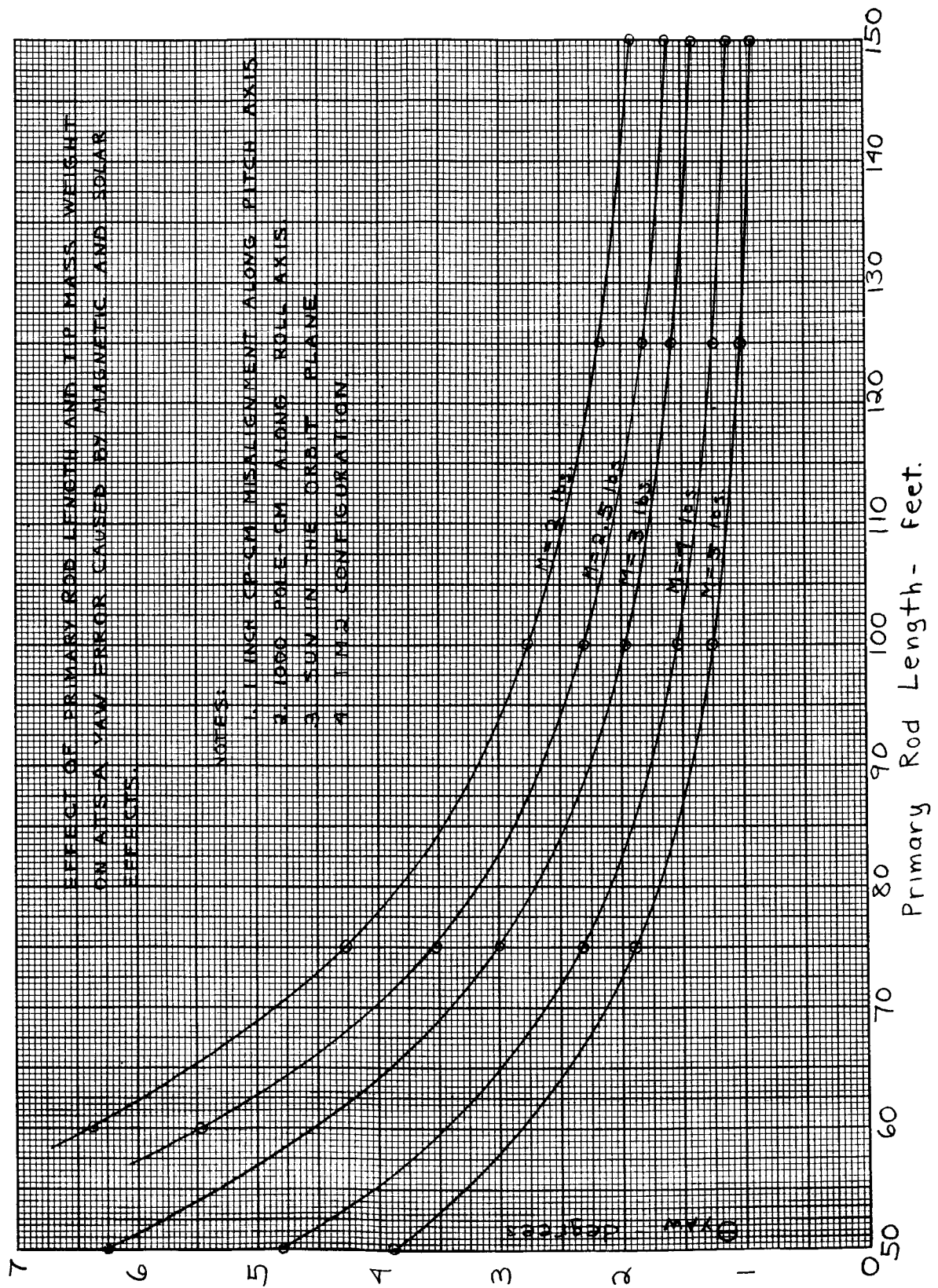


Figure 2.1-20. Effect of Primary Rod Length and Tip Mass Weight on ATS-A Yaw Error Caused By Magnetic And Solar Effects

Table 2.1-5. Peak Pointing Errors for TM-2 Configuration

ATS-A  
(Sum in Orbit Plane)

Configuration	Pitch Error (degrees)	Roll Error (degrees)	Yaw Error (degrees)
Tradeoff Configuration (GAPS III Results)	1.9	0.3	4.3
Optimum Configuration (Study Results)	1.5	0.3	2.4
Selected Configuration (GAPS III Results)	1.8	0.3	3.3

ATS-D/E  
(Sun out of Orbit Plane)

Configuration	Pitch Error (degrees)	Roll Error (degrees)	Yaw Error (degrees)
Tradeoff Configuration (Study Results)	1.0	≈ 0.8	8.3
Optimum Configuration (Study Results)	1.4	≈ 0.8	7.5
Selected Configuration (Study Results)	1.5	≈ 0.8	8.6
Tradeoff Configuration (GAPS III Results)	1.2	0.7	9.4
Selected Configuration (GAPS III Results)	1.5	0.8	6.8



Table 2.1-6 ATS-A Parameters

Parameter	Optimum Configuration	GSFC Configuration
X Rod Length (ft)	133.75	100.0
Damper Rod Length (ft)	45.0	45.0
X Rod Tip Mass (lb)	2.50	2.50
Damper Rod Tip Mass (lb)	1.60	1.91
X Rod Half Angle (deg)	$\approx 26.0$	19.0
Angle Between X Rod Plane and Roll Axis (deg)	4.8	20.8
Angle Between Damping Axis and Pitch Axis (deg)	53.4	41.9
Spring Constant $\frac{(\text{dyne-cm})}{\text{deg}}$	21.0	21.0
Damping Constant $\frac{(\text{dyne-cm})}{\text{deg/sec}}$	15,800.0	27,100.0
Moments of Inertia ( $\text{slug-ft}^2$ )		
Pitch	7,107.0	3,715.0
Roll	5,774.0	3,317.0
Yaw	1,333.0	398.0
Damper	231.0	265.0

Table 2.1-7. ATS-D/E Parameters

Parameter	Optimum Configuration	GSFC Configuration
X-Rod Length (ft)	124.33	100.0
Damper Rod Length (ft)	45.0	45.0
X-Rod Tip Mass (lbs)	8.0	10.0
Damper Rod Tip Mass (lbs)	4.06	7.15
X-Rod Half Angle (deg)	$\approx 26.0$	19.0
Angle Between X-Rod Plane and Roll Axis (deg)	4.8	20.8
Angle Between Damping Axis and Pitch Axis (deg)	53.4	41.9
Spring Constant ( $\frac{\text{dyne-cm}}{\text{deg}}$ )	3.5	5.0
Damping Constant ( $\frac{\text{dyne-cm}}{\text{deg/sec}}$ )	986.7	27,100.0
Moments of Inertia ( $\text{slug-ft}^2$ )		
Pitch	16,617.8	13,078.8
Roll	13,498.7	11,677.5
Yaw	3,115.5	1,401.3
Damper	540.2	934.2

The results of the optimization study in ATS-D/E are shown in Table 2.1-5. There are five error estimates for ATS-D/E based upon the optimization study and GAPS III which yield different results. As explained in Paragraph 2.1.6.1.2.2, there is a peculiar phasing of the oscillations in the new configuration which was not predicated by the optimization. It is uncertain whether this oscillation phasing is a permanent characteristic of the configuration or just an accident in the particular computer run. Work is continuing in this problem, but it is apparent from both GAPS III and the optimization study that the selected configuration provides performance at least comparable to the tradeoff configuration at a considerable weight saving. For this reason, it is being retained as the nominal ATS -D/E configuration.

#### 2.1.6.1.1 Optimization of ATS-A

The control system parameters recommended for use in the ATS-A (medium altitude) gravity gradient control system are shown on Table 2.1-6. These values represent a compromise between maximum pointing accuracy and a minimum change in the present damper design. This compromise is necessary to meet the present schedule and cost estimate.

The predicted steady-state errors for this system for an orbit eccentricity of .01, a CP-CM displacement of 1 inch along the pitch axis, a magnetic dipole moment of 1000 pole-cm along the roll axis, and with the sun in the orbit plane, are shown in Table 2.1-5.

##### 2.1.6.1.1.1 Discussion:

##### A. TM2 Parameters:

The system optimization is based upon a new set of dimensionless parameters provided by B.E. Tinling and V.K. Merrick of NASA/Ames. This set is designated TM-2. Its purpose was to provide a system with a substantially higher yaw restoring torque consistent with satisfactory accuracy in pitch and roll, and good damping. The most serious accuracy

problems in the previous configuration were caused by low yaw restoring torque, and the optimization concentrated on improving yaw response.

The TM2 non-dimensional parameters (as given in Figure 2.1-7) are:

$$\frac{I_P}{I_R} = 1.2308$$

$$\frac{I_Y}{I_R} = .2308$$

$$\frac{I_D}{I_R} = .04$$

$$\frac{b}{I_D \omega_o} = 1.0588$$

$$\frac{k}{I_D \omega_o^2} = 5.1504$$

$$\phi = 58.2^\circ$$

where:

$I_P, I_R, I_Y$  = Pitch, roll and yaw moments of inertia of the X-booms about their own coordinate system

$I_D$  = Damper boom moment of inertia about the damper axis

$b$  = Damping constant

$k$  = Damper spring constant

$\phi$  = Angle between the nominal damper boom position and the plane of the X-booms

$\omega_o$  = Orbital rate

The TM2 parameters determine the crab angle  $\delta$ , and the X-boom half angle  $\zeta$ . Their values are (Figure 2.1-7):

$\delta$  =  $4.8^\circ$

$\zeta$  =  $25.65^\circ$  (Reference only)

The TM-2 parameters do not specify absolute values of moments of inertia. The purpose of the system optimization is to determine the optimum rod lengths and tip masses which provide the required moments of inertia.

#### B. Error Sources

There are three primary sources of attitude error for the ATS-A system. These are:

1. Satellite magnetic dipole moment
2. Orbit eccentricity
3. Solar pressure torques caused by rod thermal bending and displacement between the vehicle center of pressure and center of mass.

The errors caused by these torques were determined individually from GAPS III computer runs for a system based upon the TM-2 parameters, and employing 100-foot

primary rods with 2.5-pound tip weights. The magnitude of the steady-state, zero-to-peak errors obtained are given in Table 2.1-8.

Table 2.1-8. Magnitude of Steady-State (Zero-to-Peak) Errors, Based on TM-2 Configuration

	$\theta_P$ (deg)	$\theta_R$ (deg)	$\theta_Y$ (deg)
Magnetic dipole moment. 1000 pole-cm along the roll axis.	0.32	0.04	1.6
Orbit eccentricity = .01	1.5	0.1	2.1
Thermal bending and solar pressure torques. CP-CM displacement = 1 inch along pitch axis. Sun in the orbit plane.	0.4	0.2	0.7

Both the magnetic dipole moment and the CP-CM displacement were pessimistically assumed to be in a direction which would result in maximum yaw error.

These runs were made for a vehicle with a cylindrical body 6 feet long by 4.667 feet in diameter. The hinge point was offset from the vehicle CP by 31.25 inches. The damper axis passed through the CP. Solar absorptivity of the central body curved surface and ends was 0.7. Total vehicle weight was 697.6 pounds. (Refer to HAC Interdepartmental Correspondence 2225/123, dated January 8, 1965) Some of these characteristics are shown in Figure 2.1-14.

### C. Restoring Torques

The primary tools for system optimization are plots of attitude errors versus X-boom rod lengths for several values of tip weights. These can be constructed by scaling the errors

obtained in the GAPS III runs. This will be done for pitch and yaw errors. Roll error is small comparable to pitch and has been ignored.

The first step in scaling the errors is to determine the pitch and yaw restoring torques,  $T_{pitch}$  and  $T_{roll}$ . This is done assuming the entire vehicle including the damper is a rigid body.

$$T_{PITCH} = 3 \omega^2 (I_{YY_1} - I_{XX_1}) \theta_P$$

$$I_{YY_1} = I_P \sin^2 \delta + I_R \cos^2 \delta + I_D \cos^2 \alpha$$

$$I_{XX_1} = I_Y + I_D$$

For an X-shape with a half angle  $\zeta$ ,

$$I_R = I_P \cos^2 \zeta$$

$$I_Y = I_P \sin^2 \zeta$$

From the TM parameters

$$I_D = .04 I_R \quad I_D = \frac{.04}{1.2308} \quad I_P = .0325 I_P$$

Combining the moment of inertia equations there results

$$I_{YY_1} = I_P (\sin^2 \delta + \cos^2 \delta \cos^2 \zeta + .0325 \sin^2 \alpha)$$

$$I_{XX_1} = I_P (\sin^2 \zeta + .0325)$$

For  $\delta = -4.8^\circ$ ,  $\zeta = 25.66^\circ$ ,  $\alpha = 53.4^\circ$

$$I_{YY_1} = .83474 I_P$$

$$I_{XX_1} = .22002 I_P$$

The ATS-A vehicle is designed for an orbit 6000 n. mi above the earth's surface (geocentric radius of 57,358,820 feet). At this altitude the orbital rate is  $\omega = 2.7313 \times 10^{-4}$  rad/sec.

The linearized pitch restoring torque gradient can now be determined.

$$\frac{T_{\text{PITCH}}}{\theta_P} = 3 (2.7313 \times 10^{-4})^2 (.83474 I_P - .22002 I_P)$$

$$\frac{T_{\text{PITCH}}}{\theta_P} = 1.3988 \times 10^{-7} I_P \quad \frac{\text{lb} - \text{ft}}{\text{rad}}$$

$$= 0.331 I_P \quad \frac{\text{dyne} - \text{cm}}{\text{deg}}$$

The linearized yaw restoring torque is found in a similar manner.

$$T_{\text{YAW}} \approx \omega^2 (I_{ZZ_1} - I_{YY_1}) \theta_Y$$

$$I_{ZZ_1} = I_P \cos^2 \delta + I_R \sin^2 \delta + I_D \cos^2 \alpha$$

$$= I_P (\cos^2 \delta + \cos^2 \delta \sin^2 \delta + .0325 \cos^2 \alpha)$$

$$= 1.0102 I_P$$

$$\frac{T_{\text{YAW}}}{\theta_Y} = (2.7313 \times 10^{-4})^2 (1.0102 I_P - .83474 I_P)$$

$$= 0.13312 \times 10^{-7} I_P \quad \frac{\text{lb} - \text{ft}}{\text{rad}}$$

$$= 0.00315 I_P \quad \frac{\text{dyne} - \text{cm}}{\text{deg}}$$



Both yaw and pitch restoring torques are directly proportional to  $I_P$ . (This is also true for roll restoring torque.)

$$I_P = 4(M \ell^2 + \frac{1}{3} \rho \ell^3)$$

where

$M$  = mass of the primary rod tip weights

$\ell$  = primary rod length

$\rho$  = rod mass per unit length = .000485 slugs/ft.

Therefore, all restoring torque gradients can be expressed as:

$$\frac{T}{\theta} = K_1 M \ell^2 + K_2 \ell^3$$

#### D. Error Scaling

The torque experienced by the vehicle because of its magnetic dipole moment being located in the earth's magnetic field is  $\overline{T} = \overline{B} \times \overline{H}$ .

This torque is independent of the vehicle parameters. Therefore, the error is inversely proportional to the restoring torque.

Torques caused by solar pressure can be divided into those caused by displacement between the the CP and CM, and those caused by rod bending. For this vehicle the torques caused by rod bending are predominant. They constitute approximately 80% and 100% of the total yaw and pitch solar torques respectively. Torque caused by rod bending is proportional to the cube of rod length. Therefore, the error is proportional to the cube of the rod length, and inversely proportional to the restoring torque.

Error caused by orbit eccentricity for a given vehicle in a particular orbit is independent of vehicle moment of inertia. This occurs because the error is inversely proportional to the restoring torque, but directly proportional to  $I_p$  which in turn is directly proportional to restoring torque.

These effects can be summarized as follows:

1. Magnetic dipole moment error.

$$\theta = \frac{K_3}{K_1 M \ell^2 + K_2 \ell^3}$$

2. Rod thermal bending error

$$\theta = \frac{K_3 \ell^3}{K_1 M \ell^2 + K_2 \ell^3}$$

3. Orbit eccentricity error

$$\theta = K$$

Using the errors from the GAPS III runs allows the  $K_3$ 's to be determined. The following equations can then be written.

1. Magnetic dipole moment error.

$$\theta_{\text{YAW}} = \frac{18.9}{.0126 M \ell^2 + 2.037 \times 10^{-6} \ell^3}$$

$$\theta_{\text{PITCH}} = \frac{39.8}{.1324 M \ell^2 + 2.14 \times 10^{-5} \ell^3}$$

## 2. Rod thermal bending error.

$$\theta_{\text{YAW}} = \frac{8.28 \times 10^{-6} \ell^3}{.0126 M \ell^2 + 2.037 \times 10^{-6} \ell^3}$$

$$\theta_{\text{PITCH}} = \frac{49.7 \times 10^{-6} \ell^3}{.1324 M \ell^2 + 2.14 \times 10^{-5} \ell^3}$$

Where  $\theta_{\text{YAW}}$  and  $\theta_{\text{PITCH}}$  are in degrees,  $M$  is the primary rod tip mass in slugs, and  $\ell$  is the primary rod length in feet. Figures 2.1-15 through 2.1-18 show plots of these error functions for  $\ell$  between 50 and 150 feet and  $M$  between 2 and 5 pounds. The maximum rod length available with the present hardware design is 150 feet.

There is an assumption hidden in the thermal bending scaling factor that the length of the damper rod increases directly with the X-rod length. For the shorter X-rod lengths of Figure 2.1-15 through 2.1-18, this would be the case, since the moment of inertia level of the damper would be lower than could be achieved with two 45-foot rods (the nominal rod length) and their extension mechanisms. At high X-rod lengths, however, the tip weights are more likely to change than the rod length. The effect of this difference in the optimization is slight, however, and merely reduces (slightly) the optimum rod length from that shown in Figures 2.1-19 and 2.1-20.

Magnetic dipole error decreases as rod length increases. Thermal bending error increases as rod length increases. The sum of these errors plotted as a function of rod length will reach a minimum value at a particular value of rod length. These plots are shown in Figures 2.1-19 and 2.1-20. It is apparent that minimum yaw errors will be obtained at a rod length greater than 150 feet. Also the larger the tip mass the smaller the errors will be.

### E. Choice of System Parameters

The choice of system parameters was strongly influenced by present hardware designs, the program schedules, and budgets. The primary limiting item was the spring constant of 21 dyne-cm/deg designed for the original ATS Configuration. Increasing this constant would require a complete redesign of the damper component. Figure 2.1-21 shows the variation of damper characteristics with  $I_p$  for the TM-2 parameters. The previous values of spring constant and damper coefficient are shown on the plot. This spring limit fixes  $I_p$  at 7107 slug-ft<sup>2</sup> and damper coefficient at 15,800  $\frac{\text{dyne-cm}}{\text{deg/sec}}$ . The change in damping coefficient can be effected with only minor changes in damper design.

Figure 2.1-22 is a plot of pitch moment of inertia as a function of rod length and tip mass. It is apparent that several combinations of rod length and tip weight can be selected to provide 7107 slug-ft<sup>2</sup>. Figures 2.1-19 and 2.1-20 show that the best rod length is 150 feet and the best performance is obtained from the heaviest tip mass. It is a basic fact of gravity gradient satellites that heavy tip masses almost invariably provide better performance. In general, a limit to the size of the mass must be specified because of weight limitations of the satellite. While ATS-A does not have a weight problem, it was felt to be more profitable to utilize as much of the 150 feet of available rod as possible. Since it was undesirable to reduce the tip masses below the level currently anticipated, the recommended system is X-rod lengths of 133.75 feet with 2.5 pound tip masses. The damper rod is 45 feet with a 1.60-pound tip mass.

#### 2.1.6.1.1.2 Predicted Performance

Two GAPS III computer runs were made to compare the recommended system with the previous configuration, both systems based upon TM-2 parameters. For each run the orbit eccentricity was .01, the CP-CM displacement was 1 inch along the pitch axis, the magnetic dipole moment was 1000 pole-cm along the roll axis, and the sun was in the orbit plane. (The other factors are as defined in ATS System memo 036 and outlined earlier in the report.) The improvement in performance Table 2.1-9 agrees well with the values predicted by Figures 2.1-19 and 2.1-20.

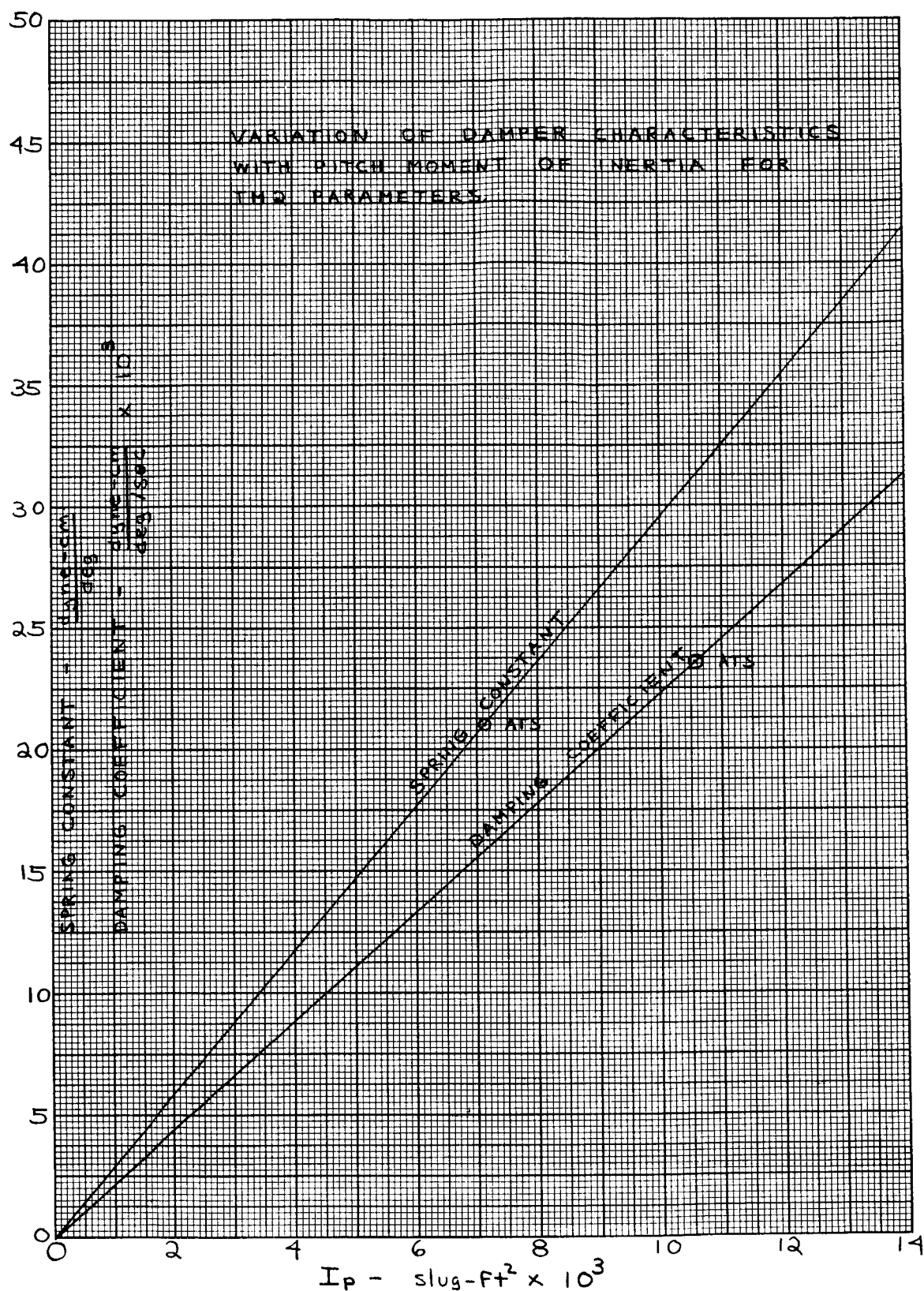


Figure 2.1-21. Variation of Damper Characteristics With Pitch Moment of Inertia For TM2 Parameters

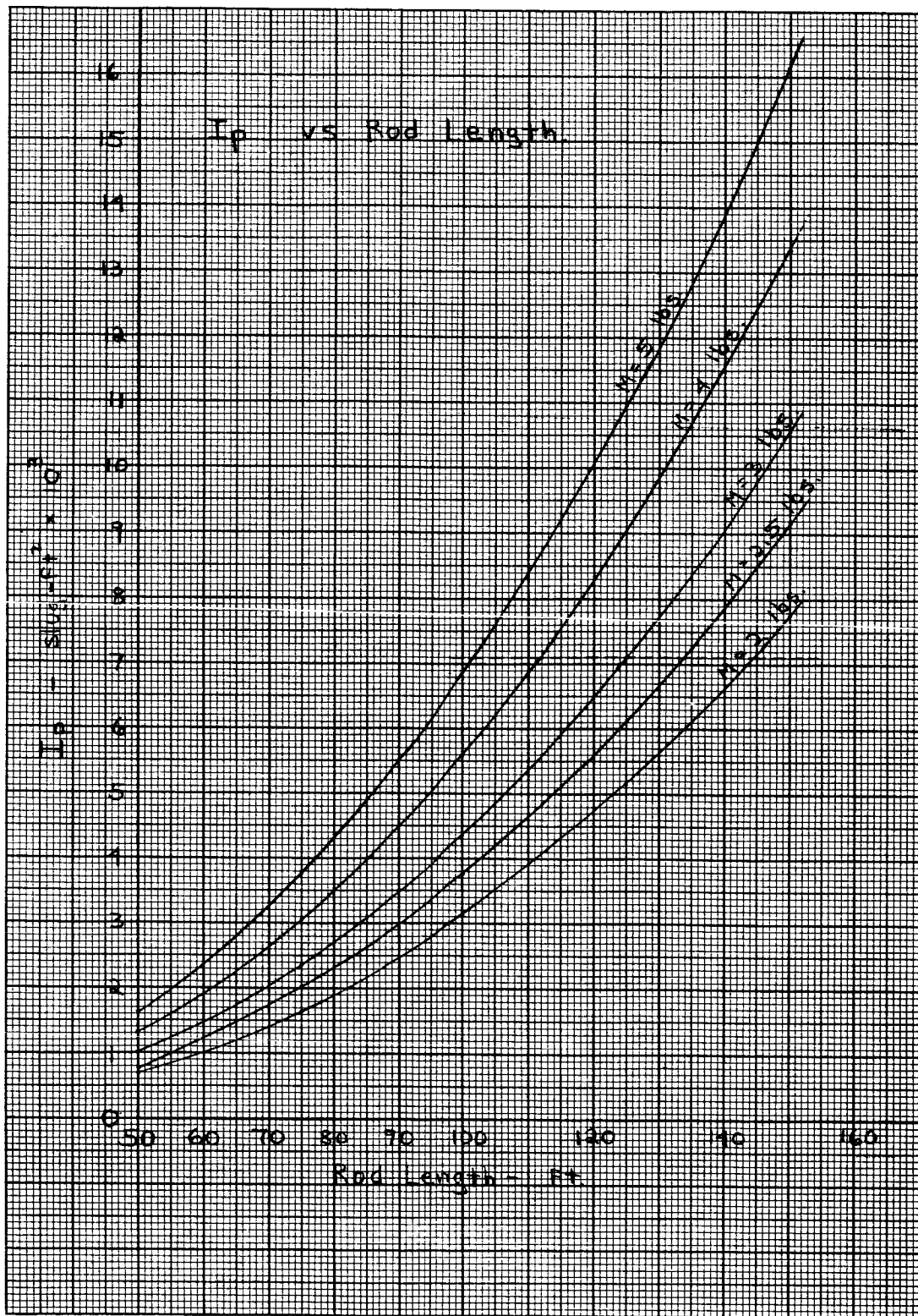


Figure 2.1-22.  $I_p$  vs Rod Length

Table 2.1-9. Performance Comparisons for ATS-A

	$\theta_P$ (deg)	$\theta_R$ (deg)	$\theta_Y$ (deg)
Previous TM-2 Configuration	1.9	.3	4.3
Recommended TM-2 System	1.8	.3	3.3
Increase in Accuracy	.1	-	1.0

Figures 2.1-23 and 2.1-24 are plots of the performance of the two systems for 150 hours in orbit.

#### 2.1.6.1.2 Optimization of ATS-D/E

##### 2.1.6.1.2.1 Conclusions

The system parameters recommended for the ATS-D/E gravity gradient control system are shown in Table 2.1-7 .

This system provides a weight saving of 14.19 pounds compared to the original GSFC design, and 6.18 pounds compared to a system based upon TM-2 parameters and employing 100-foot primary rods with 10-pound tip masses.

The recommended parameters are based primarily upon a tradeoff among three factors: pointing accuracy, weight and damper spring constant.

##### 2.1.6.1.2.2 Discussion

#### A. Solar Torque, Thermal Bending, and Magnetics

The optimization procedure for the ATS-D/E system is similar to that employed for the ATS-A system.

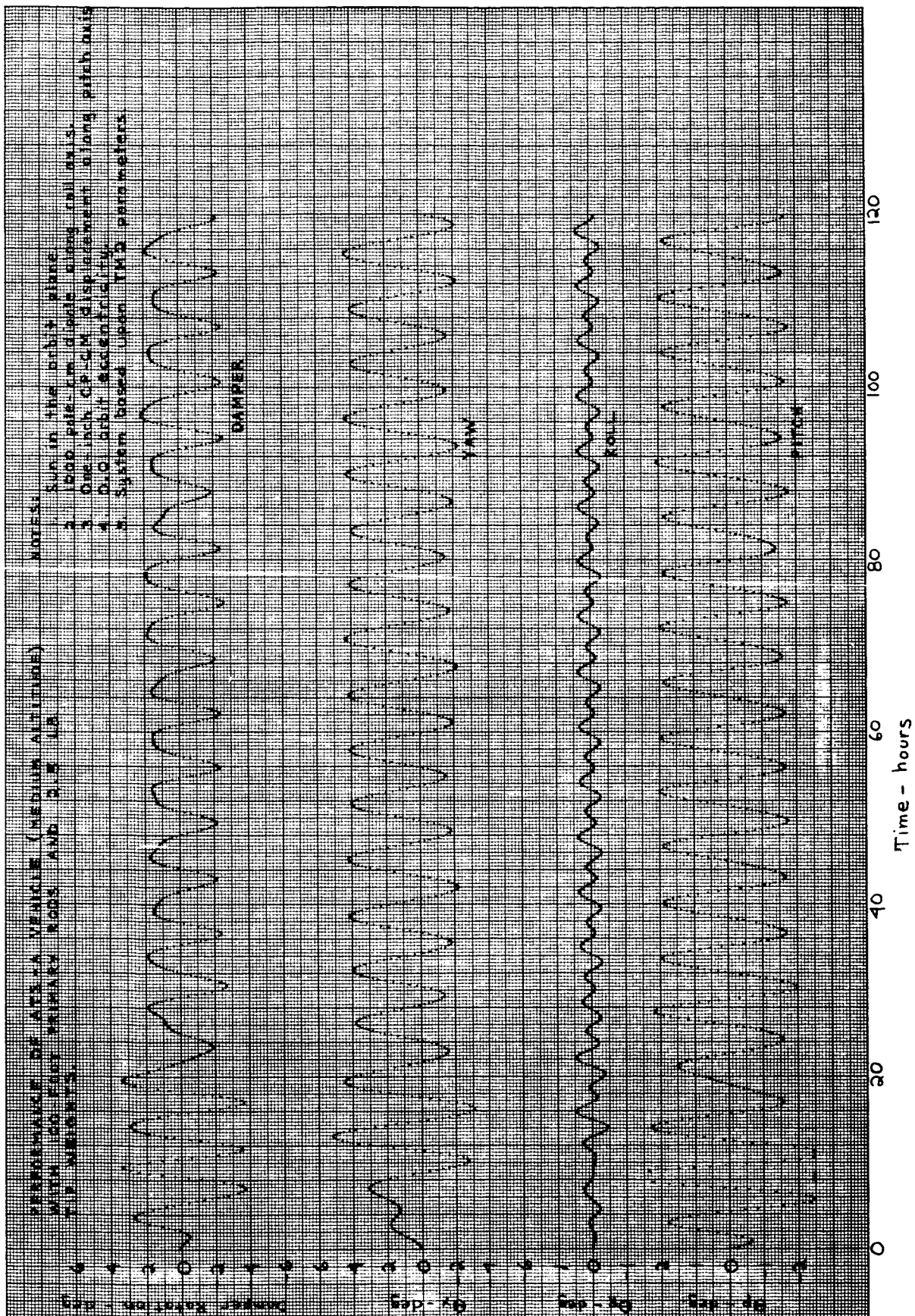


Figure 2.1-23. Performance of ATS-A Vehicle (Medium Altitude) With 100-Foot Primary Rods and 2.5 lb. Tip Weights



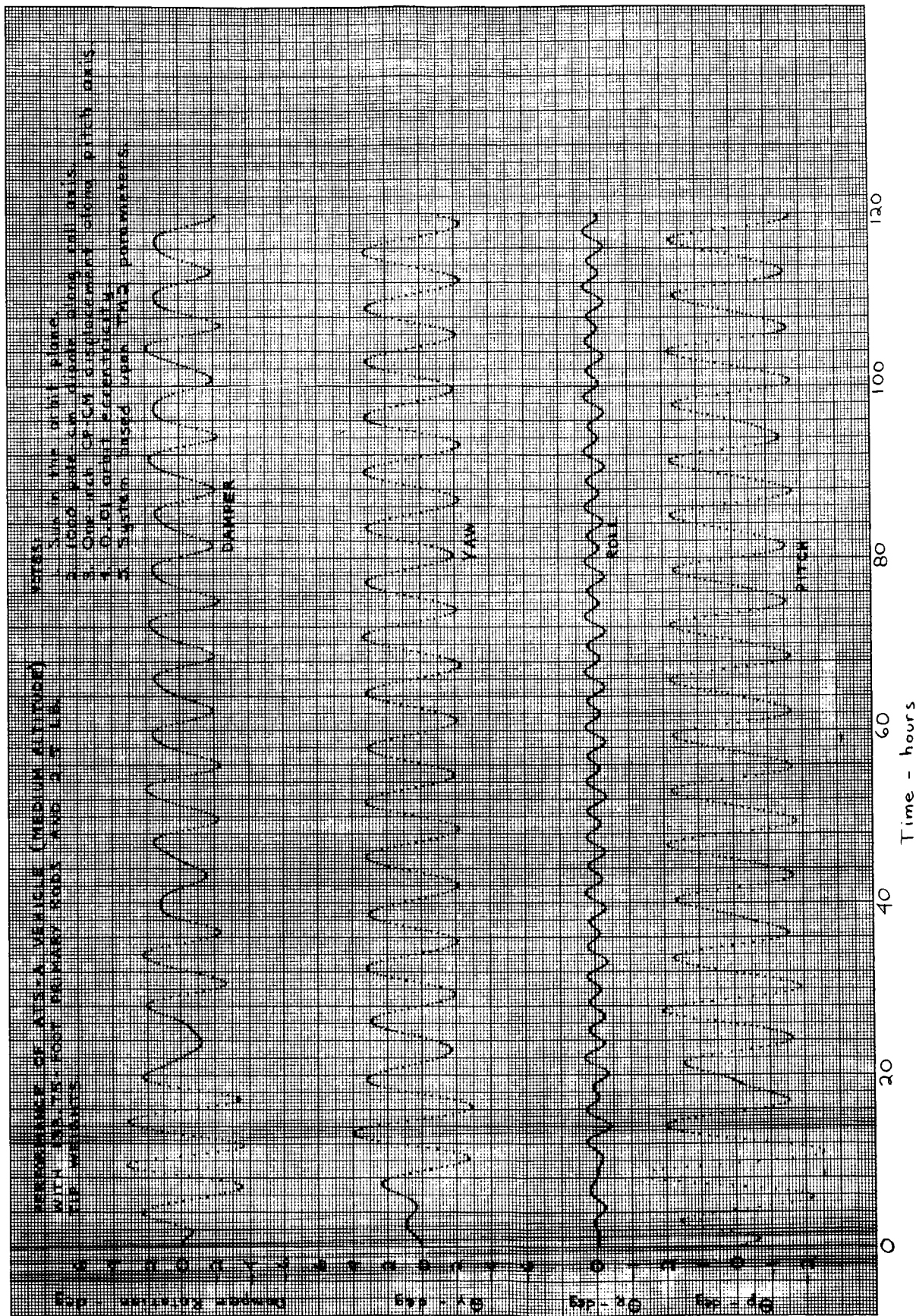


Figure 2.1-24. Performance of ATS-A Vehicle (Medium Altitude) With 133.75-Foot Primary Rods and 2.5 lb. Tip Weights

The primary sources of error for the ATS-D/E system are:

1. Vehicle magnetic dipole moment
2. Solar pressure torques caused by rod thermal bending and CP-CM displacement
3. Thruster torques.

The effects of the dipole moment and solar pressure torques were determined individually by GAPS III computer runs. Errors were obtained for a 100-foot primary rod with 10-pound tip masses. These are listed in Table 2.1-10.

Table 2.1-10. Error Sources for ATS-D/E

Error Source	Steady-state, zero-to-peak error		
	$\theta_P$	$\theta_R$	$\theta_Y$
1. 1000 pole-cm dipole along the roll axis	0	0	0.4
2. Thermal bending and solar pressure torques. Sun in the orbit plane.	1.1	1.1	4.0
3. Thermal bending and solar pressure torques. Sun inclined $23.45^\circ$ to the orbit plane.	1.0	1.0	1.9

These errors were scaled to provide plots of errors as a function of primary rod length and tip mass weight. Scaling equations were developed in the same manner as was done for the ATS-A system. These are given below.

1. Magnetics

$$\theta_{YAW} = \frac{1.175}{.000898M \ell^2 + .1452 \times 10^{-6} \ell^3}$$

$$\theta_{PITCH} = 0$$

## 2. Thermal Bending and Solar Pressure Torques - Sun in the Orbit Plane

$$\theta_{\text{YAW}} = \frac{11.75 \times 10^{-6} \ell^3}{.000898M \ell^2 + .1452 \times 10^{-6} \ell^3}$$

$$\theta_{\text{PITCH}} = \frac{33.94 \times 10^{-6} \ell^3}{.00944M \ell^2 + .1525 \times 10^{-5} \ell^3}$$

## 3. Thermal Bending and Solar Pressure Torques - Sun Inclined $23.45^\circ$ to the Orbit Plane.

$$\theta_{\text{YAW}} = \frac{5.58 \times 10^{-6} \ell^3}{.000898 M \ell^2 + .1452 \times 10^{-6} \ell^3}$$

$$\theta_{\text{PITCH}} = \frac{30.85 \times 10^{-6} \ell^3}{.00944 M \ell^2 + .1525 \times 10^{-5} \ell^3}$$

where  $\theta_{\text{PITCH}}$  and  $\theta_{\text{YAW}}$  are in degrees, M is in slugs, and  $\ell$  is in feet. Roll errors are ignored since they are comparable to the pitch errors and usually less.

Figures 2.1-25 through 2.1-29 are plots of pitch and roll errors as a function of primary rod length and tip mass weight. The shapes of these curves are similar to the corresponding curves for the ATS-A system.

Disturbance torques caused by the stationkeeping thruster are potentially the largest cause of yaw error.

### B. Thruster

This analysis covers the worst case for thruster induced torques about the yaw axis. By linearly summing the errors caused by rod mounting misalignments, rod lack of straightness,

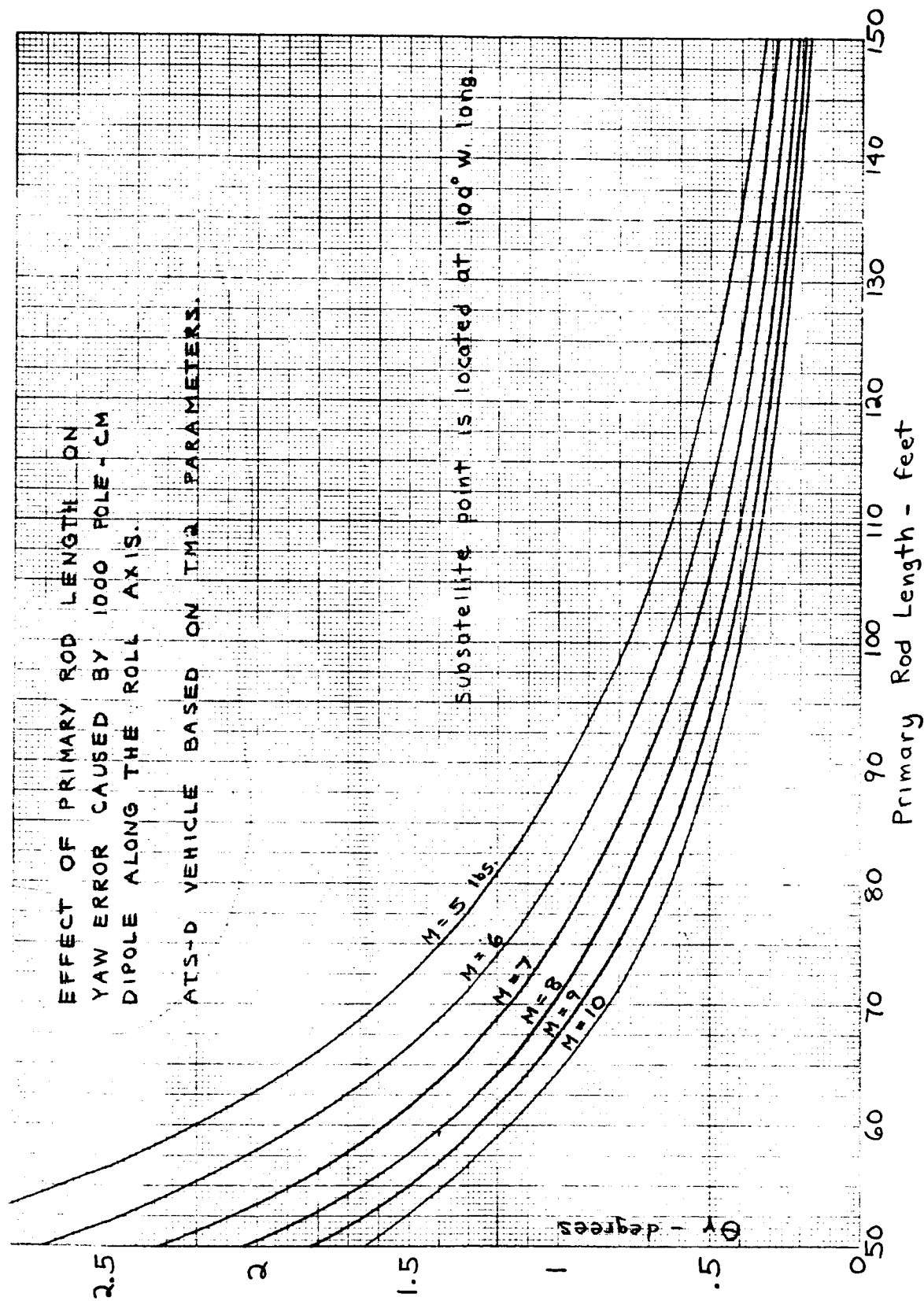


Figure 2.1-25. Effect of Primary Rod Length on Yaw Error Caused by 1000 Pole-CM Dipole Along the Roll Axis.  
ATS-D Vehicle Based on TM2 Parameters

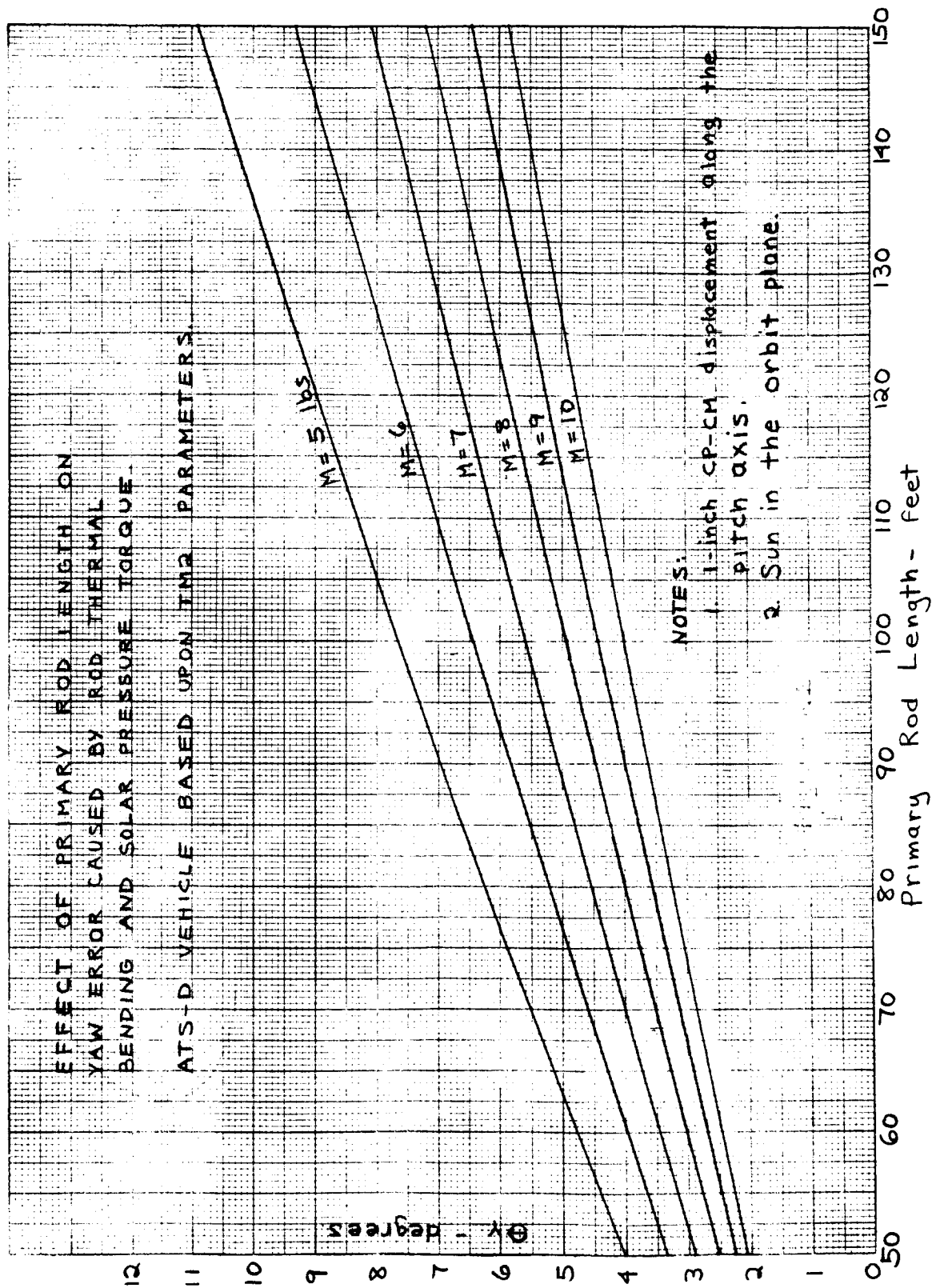


Figure 2.1-26. Effect of Primary Rod Length on Yaw Error Caused By Rod Thermal Bending and Solar Pressure Torque. ATS-D Vehicle Based Upon TM2 Parameters

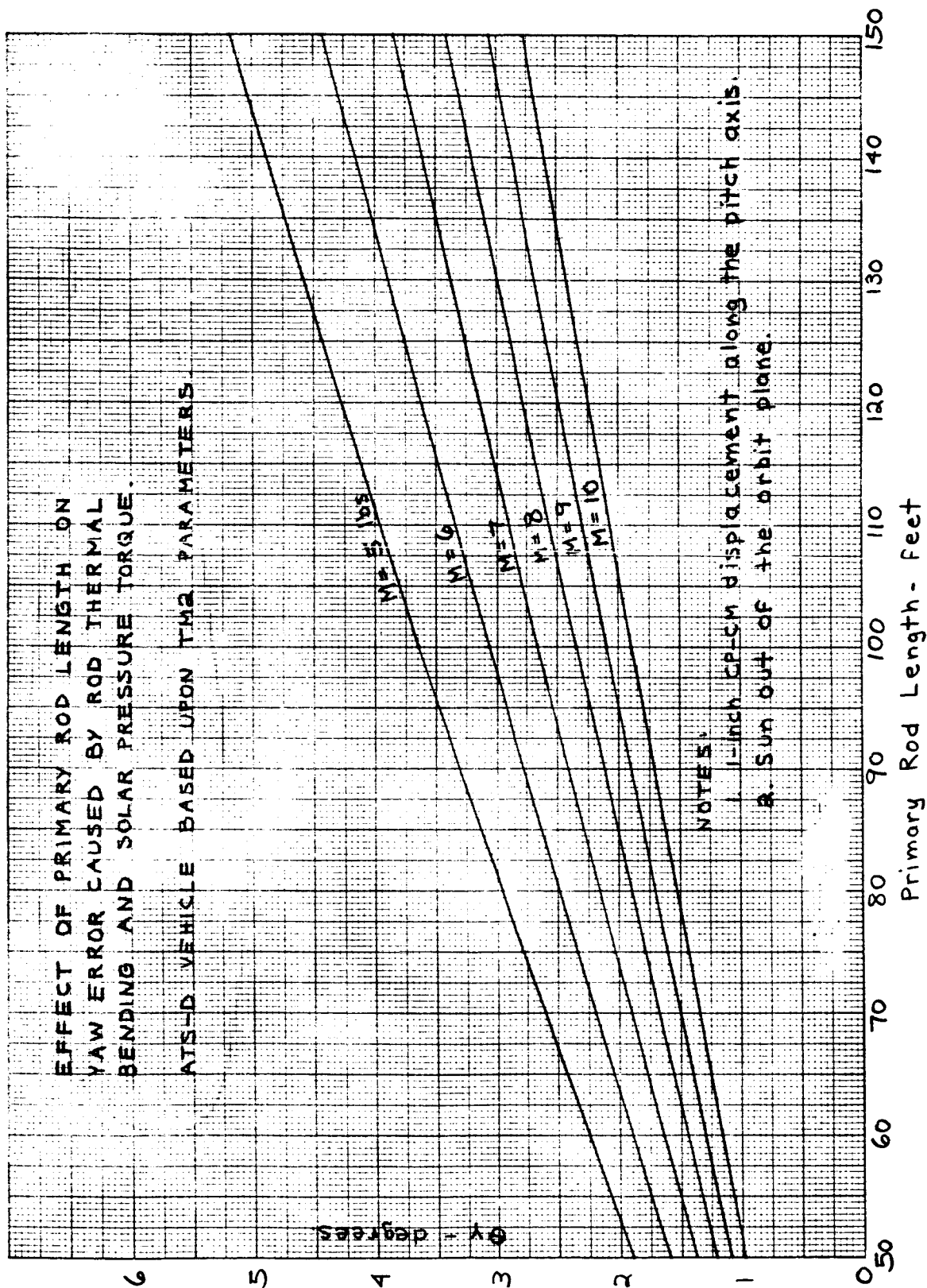


Figure 2.1-27. Effect of Primary Rod Length on Yaw Error Caused By Rod Thermal Bending and Solar Pressure Torque. ATSD Vehicle Based Upon TM2 Parameters

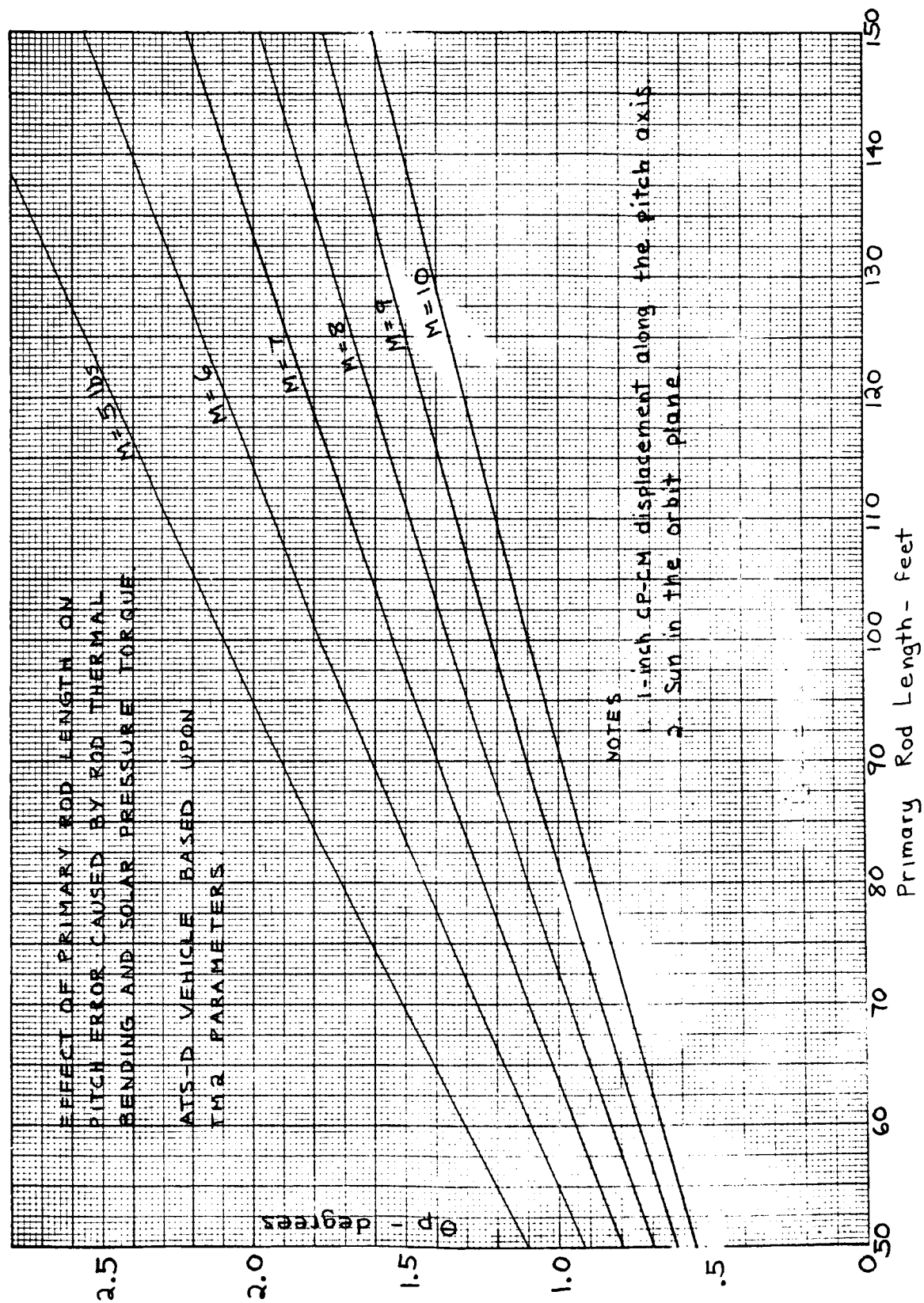


Figure 2.1-28. Effect of Primary Rod Length on Pitch Error Caused By Rod Thermal Bending and Solar Pressure Torque. ATS-D Vehicle Based Upon TM2 Parameters



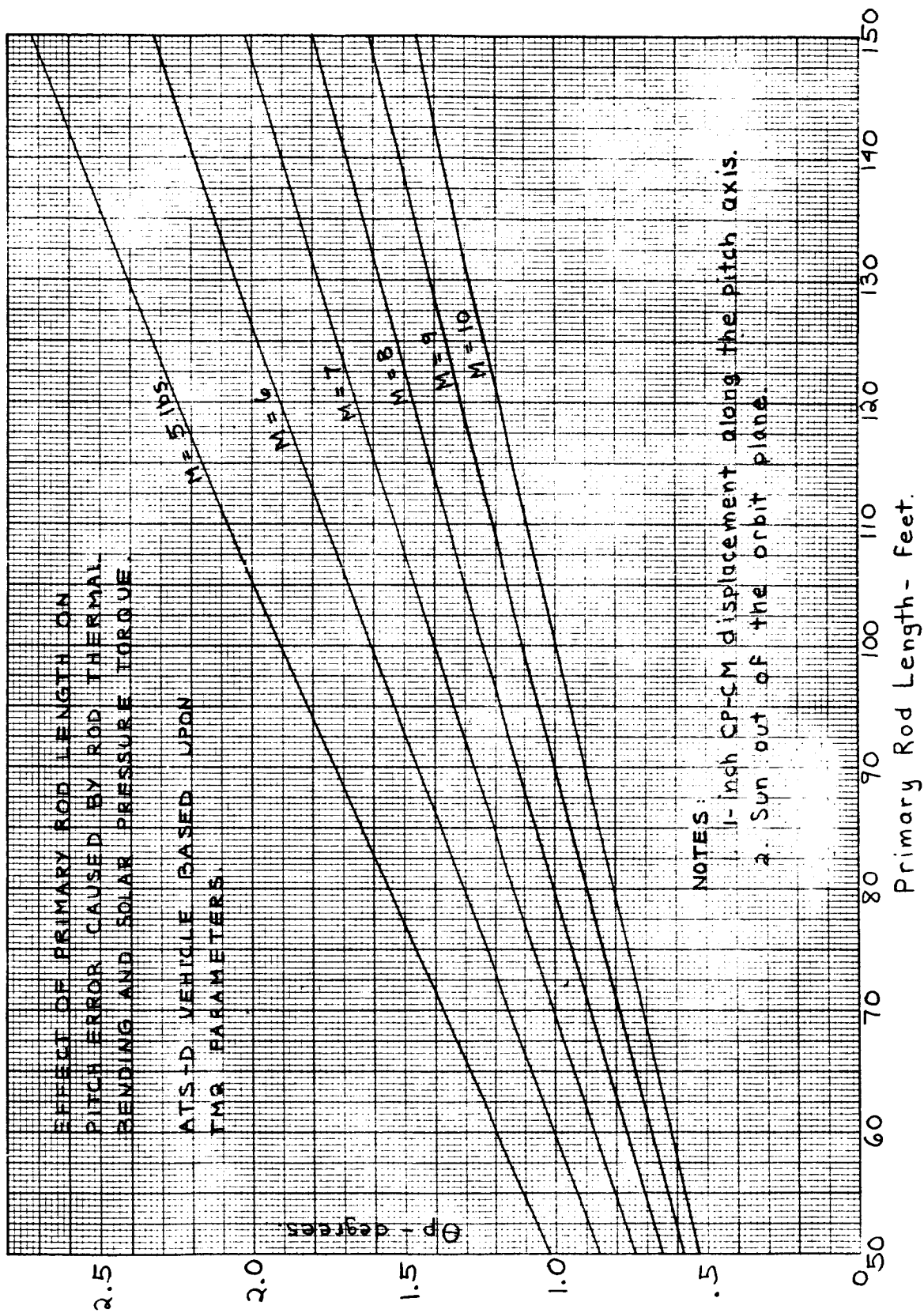


Figure 2.1-29. Effect of Primary Rod Length on Pitch Error Caused By Rod Thermal Bending and Solar Pressure Torque. ATS-D Vehicle Based Upon TM2 Parameters



thermal bending, initial manufacturing tolerances, and thrust vector offset a pessimistic "worst case" has been assumed.

These errors and their effects have been calculated and plotted for a variety of tip weights and rod lengths.

The assumptions for the analysis are:

1. Rod configuration is per Spec SVS-7316B
2. Silver-plated Copper-Beryllium Rods are used.
3.  $\Delta x$ ,  $\Delta z$ , Linear Mounting errors of Thruster, are Zero.  $\Delta y$ , equals 0.3 inches.
4. Body Moments of Inertia about Geometric Center are Zero.
5. Damper Moments of Inertia about Geometric Center (G.C) are negligible.
6. Linear addition of all shifts along the Z axis. This yields maximum yaw torque.
7. Rods bend circularly due to thermal considerations
8. Solar pressure is ignored
9. The System is linear, i.e., linear addition of errors is permissible.
10. Errors are assumed to be of extreme values.
11. C.M. - G.C. Misalignment = 0.3 inch = 0.025 minute of arc with rods stowed or with perfect extension.
12. Absorbtivity of rod  $\alpha = 0.15$

13. Maximum Thrust Vector Misalignment =  $1^{\circ}$
14. Sun Angle out of orbit plane =  $23.45^{\circ}$
15. Total System Weight = 585 pounds  
= 18.18 slugs
16. Thruster Force Level  $0.5 \times 10^{-5}$  lb Nominal
17. Inertia Rods half angle  $\zeta = 25.66^{\circ}$
18. Nominal G.C. to Thruster Force Center mounting distance = 2.333 feet
19. Rod Angular mounting error is  $0.5^{\circ} = \nu$

Definition of the symbols used in Figure 2.1-30 are:

$CM_I$	-	Initial Center of Mass of contracted rod configuration
$CM_R$	-	Center of Mass with rods extended and allowed to bend to extremes of tolerance envelope, and with maximum angular mounting error.
$CM_B$	-	Center of Mass with rods bent thermal gradients. Mounting and envelope errors are ignored.
$CM_T$	-	Center of Mass when $CM_I$ , $CM_R$ and $CM_B$ are summed.
$(X_1, Y_1, Z_1)$	-	Orthogonal reference axis set.
G.C.	-	Geometric Center of physical configuration with rods stowed or optimum extended.
$(\Delta x, \Delta y, \Delta z)_I$	-	Coordinates of $CM_I$ - G.C. offset due to Mfg. uncertainties.

$(\Delta x, \Delta y, \Delta z)_R$  - Coordinates of  $CM_R$  - G.C. offset due to angular offsets and non-straightness of rods.

$(\Delta x, \Delta y, \Delta z)_B$  - Coordinates of  $CM_B$  - G.C. offset due to thermal bending.

$\Delta x_T = \Delta x_I + \Delta x_R + \Delta x_B$   
 $\Delta y_T = \Delta y_I + \Delta y_R + \Delta y_B$   
 $\Delta z_T = \Delta z_I + \Delta z_R + \Delta z_B$

Coordinates of Final Center of Mass with respect to Geometric Center.

$\overline{TV}$  = Thrust Vector.

$F_x, F_y, F_z$  = Components of Thrust Vector

$e_x, e_y, e_z$  = Moment Arms of  $\overline{TV}$  about G.C.

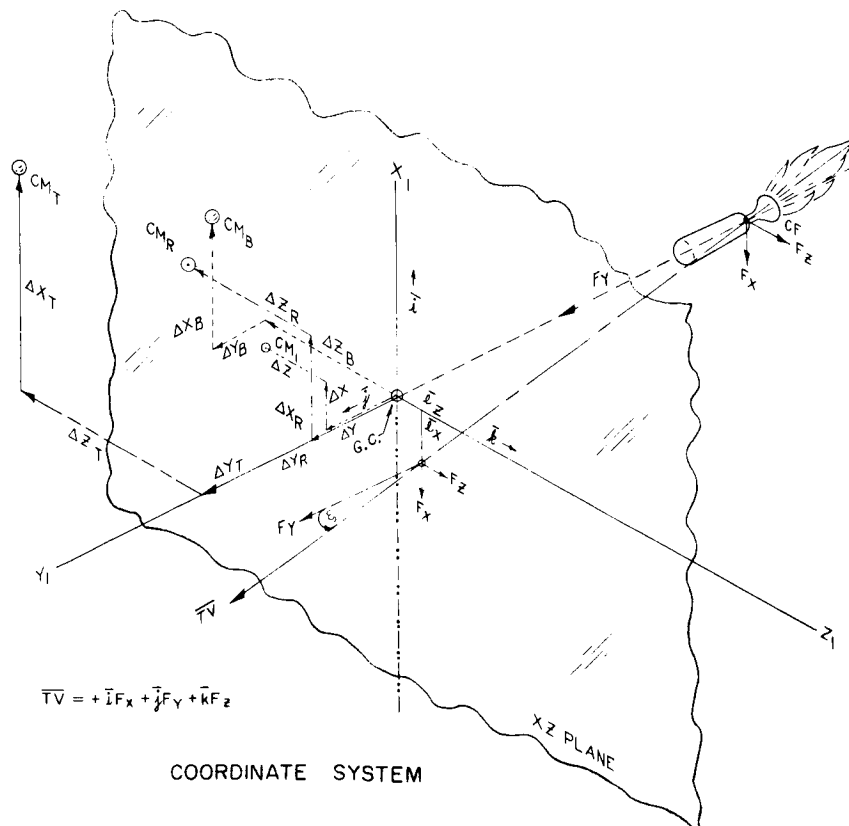


Figure 2.1-30. Coordinate System

### 1) Initial Mass Moment

The maximum radial offset of the Center of Mass of the stowed rod configuration from the Geometric Center, is defined as 0.3 in. (0.025 ft). If the rods are perfectly extended the same offset holds. The maximum error in yaw is obtained if this offset lies entirely along the  $Z_1$  axis.

$$\begin{aligned} \text{Then } Mm_I &= \text{Total Mass} \cdot \text{offset} \\ &= \frac{585 \text{ lb. sec}^2}{32.174 \text{ ft.}} \times 0.025 \text{ ft.} \\ Mm_I &= 0.45456 \text{ slug-ft.} \end{aligned}$$

### 2) Mass Moment - Rod Errors

The Mass Moment due to rod angular misalignments and permissible error envelope is:

$$\begin{aligned} Mm_R &= 4 \left\{ \frac{W_t}{g} \left( l \sin \nu + \frac{1}{2} \text{ ft.} + 0.005 \frac{\text{ft.}}{\text{ft.}} l' \right) \right. \\ &\quad \left. + \frac{\rho l}{g} \left( \frac{l \sin \nu}{2} + \frac{1}{2} \text{ ft.} \right) \right\} \end{aligned}$$

where

$$\begin{aligned} g &= \text{Gravitational Constant} = 32.174 \text{ ft/sec}^2 \\ l &= \text{Rod length (total) in feet} \\ l' &= \text{Rod length (in excess of 100 feet) in/feet} \\ W_t &= \text{Tip weight} \\ \rho &= \text{Rod weight/lineal foot} = 0.0156 \text{ Lb/ft} \\ \nu &= \text{Mounting angle error} = \frac{1}{2}^\circ \text{ max.} \end{aligned}$$

To simplify the equation the offsets of the rod below  $l = 25$  feet and for  $l = 100$  feet are assumed to cancel.

Thermal Bending Offsets. Definitions are:

$r$	=	Radius of rod = 0.25 inch = 0.02083 feet	$\frac{\text{Units}}{\text{feet}}$
$l$	=	Rod length	feet
$k$	=	Thermal Conductivity of rod material	$\frac{\text{Btu}}{\text{ft}^2 \cdot \text{hr}} \bigg/ \frac{^\circ\text{F}}{\text{ft}}$
$R$	=	Rod Radius of Curvature	ft
$\alpha$	=	Rod absorbitivity = 0.15	—
$\lambda$	=	Rod to solar flux angle of incidence	deg.
$\mu$	=	Coefficient of thermal expansion	$\text{ft/ft} \bigg/ ^\circ\text{F}$
$\rho$	=	Reflectivity = $(1 - \alpha) = 0.85$	—
$\tau$	=	Thickness of rod wall	ft
443	=	Solar flux	$\frac{\text{Btu}}{\text{hr} \cdot \text{ft}^2}$

The Radius of Curvature is defined as:

$$R = \frac{2 \tau k}{443 (\mu \alpha r)} \cdot \frac{1}{\sin \lambda}$$

for silver plated beryllium-copper rods

$$\mu = 9.9 \times 10^{-6} \frac{\text{ft/ft}}{^\circ\text{F}}$$

$$\alpha = 0.15$$

$$k = 75 \frac{\text{Btu/ft}^2 - \text{hr}}{\text{°F/ft}}$$

$$\tau = 1.66 \times 10^{-4} \text{ feet}$$

$$l = 50, 75, 100, 125 + 150 \text{ feet (for present purposes)}$$

Also from system geometry

$$\sin \lambda = \sin (\cos^{-1} (\cos \zeta \cos \lambda_o))$$

where

$$\begin{aligned} \zeta &= \text{half angle of rods - referred to } X_1 \text{ axis} \\ &= 25.66^\circ \end{aligned}$$

$$\begin{aligned} \lambda_o &= \text{angle between } x_1 \text{ axis and solar flux with Sun in } X_1, Z_1 \text{ plane} \\ &= 23.45^\circ \end{aligned}$$

For worst case

$$R = \frac{2 \tau k}{443 \mu \alpha r} \cdot \frac{1}{\sin (\cos^{-1} (\cos \zeta \cos \lambda_o))}$$

$$R = 3243.9 \text{ feet.}$$

Tip Deflection (for Circular Bending) is:

$$h = R \left( 1 - \cos \left[ \frac{180^\circ}{\pi R} \cdot l \right] \right)$$

The mass moments for the tip mass vs rod length field are:

$$M_{mB} = \frac{4 \rho l h}{3} + M_t \cdot h \text{ slug-ft.}$$

Since the total mass is to be held constant, any change in rod or tip masses must be reflected into the vehicle mass.

$$\begin{aligned} \text{Vehicle mass} &= \text{Total mass} - \text{tip mass} - \text{rod mass} \\ \text{Total mass} &= 18.18238 \text{ slugs (Refer: Hughes ATS Configuration Review Document)} \end{aligned}$$

The vehicle mass times 0.025 ft yields the vehicle moment.

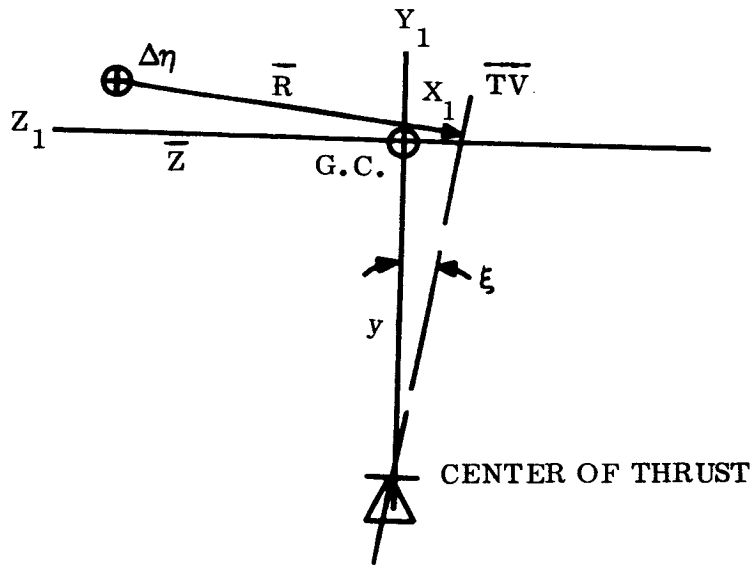
Summing the mass moments due to the Vehicle, Misalignment and error envelope, tip deflection and rod bending, and dividing the sum by the total mass yields the centroidal distance from the Geometric Center.

$$\bar{Z} = \frac{Mm_V + Mm_R + Mm_B}{M_T} \text{ feet}$$

The results of these calculations are:

	$\bar{Z}$ feet			
	Tip wts.			
Rod length (feet)	6	8	10	12
50	.082588	.100321	.118056	.135791
75	.116187	.143494	.170800	.198107
100	.158739	.198251	.237645	.277279
125	.217497	.273559	.329620	.385682
150	.287298	.362540	.437784	.513026

When all errors sum along  $Z_1$  the maximum error torque occurs.



Yawing moment is  $\overline{TV} \times \overline{R}$

$$\begin{aligned} \overline{TV} \times \overline{R} &= TV R \cos \xi \\ &= 0.5 \times 10^{-5} (Z + (y + \Delta y) \sin \xi) \quad 0.99996. \\ &= 0.49998 \times 10^{-5} (\overline{Z} + 0.020585) \end{aligned}$$

The yaw angle errors caused by the thruster disturbance torques are plotted in Figure 2.1-31 for 6-, 8-, and 10-pound tip weights. For these calculations, the error due to the thruster was assumed to be constant with no oscillation.

### C. Choice of System Parameters

Figure 2.1-32 shows the variation of pitch moment of inertia with rod length and tip weight. Figure 2.1-33 shows the variation of damper characteristics with pitch moment of inertia.

Figure 2.1-34 shows the total yaw error as a function of rod length and tip mass. Figures 2.1-32 and 2.1-33 were used to determine the lines of constant damper spring constant which appear on Figure 2.1-34. This plot illustrates some of the relationships that were considered in choosing system parameters. Error decreases as the primary rod tip mass weight is increased. However, this increases total system weight, not only in the primary rod



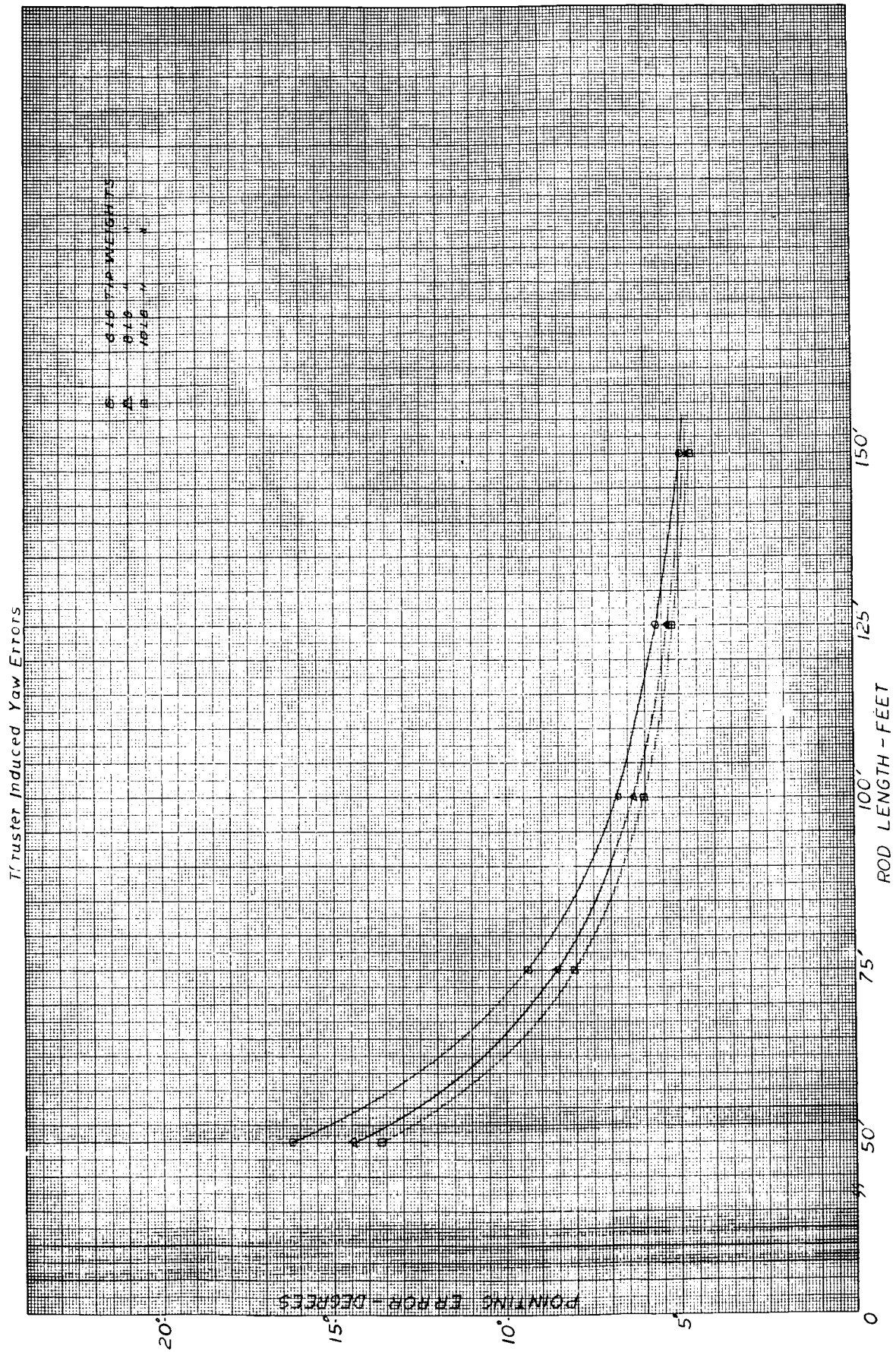


Figure 2.1-31. Thruster Induced Yaw Errors

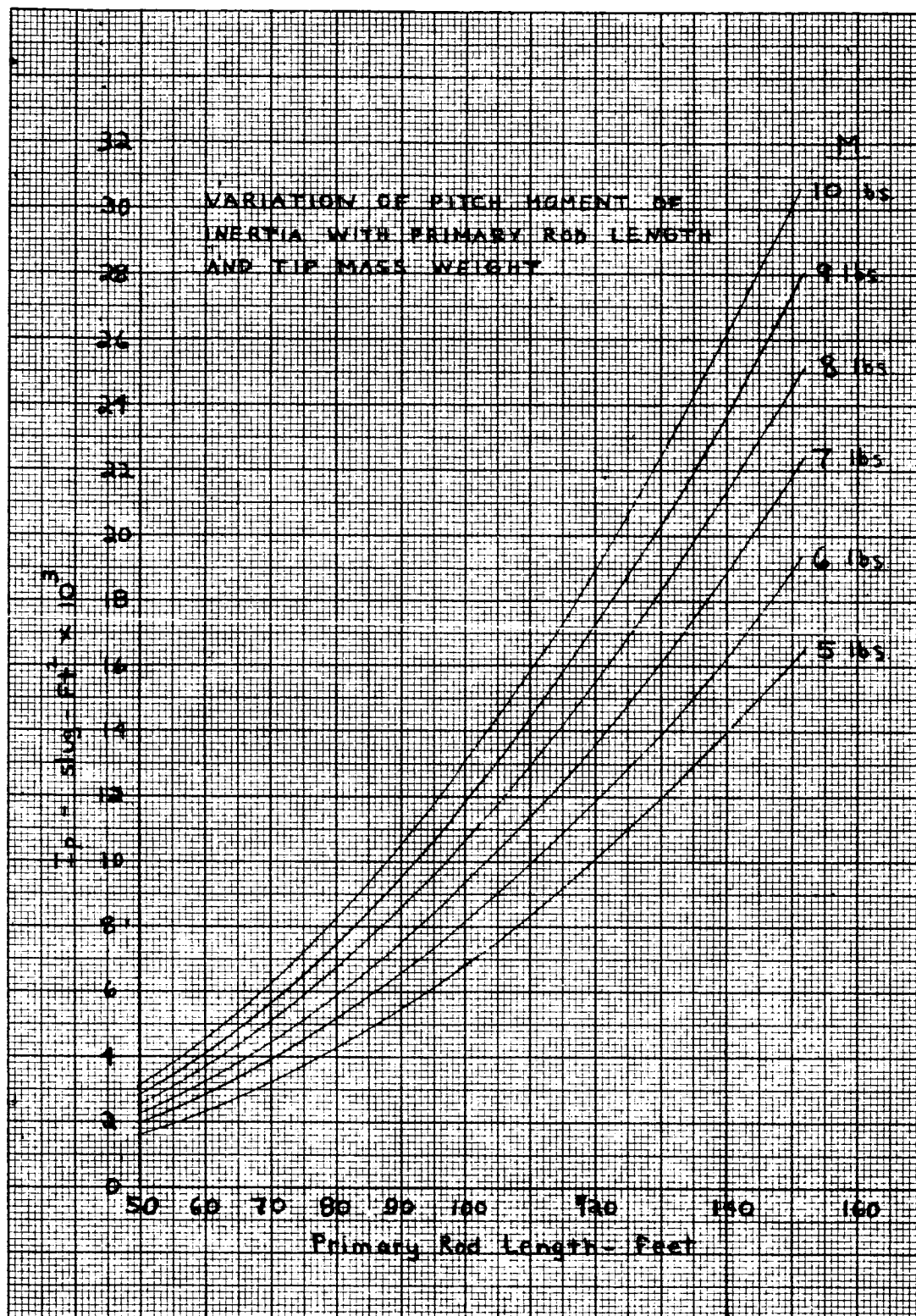


Figure 2.1-32. Variation of Pitch Moment of Inertia With Primary Rod Length And Tip Mass Weight

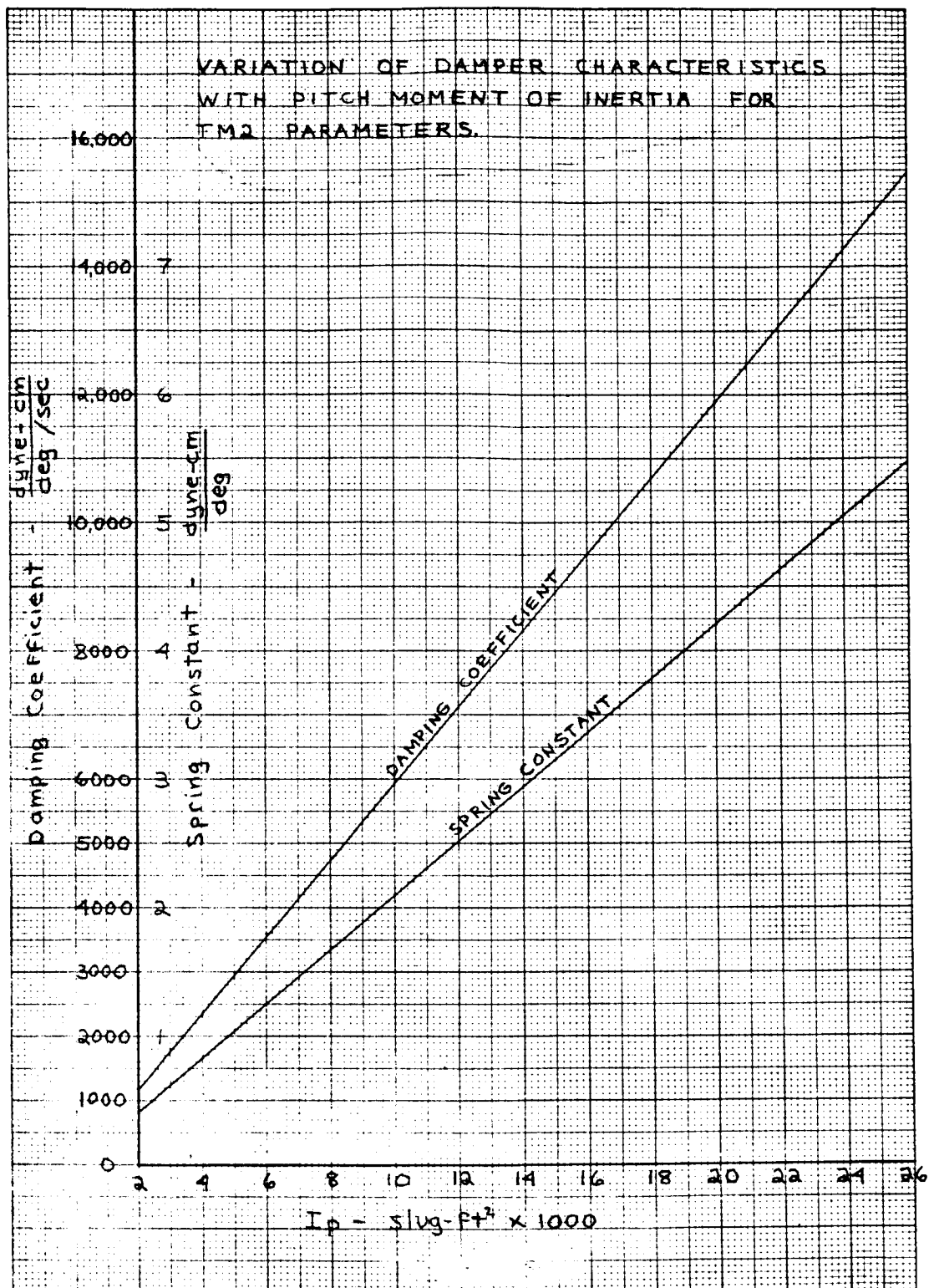


Figure 2.1-33. Variation of Damper Characteristics With Pitch Moment of Inertia For TM2 Parameters

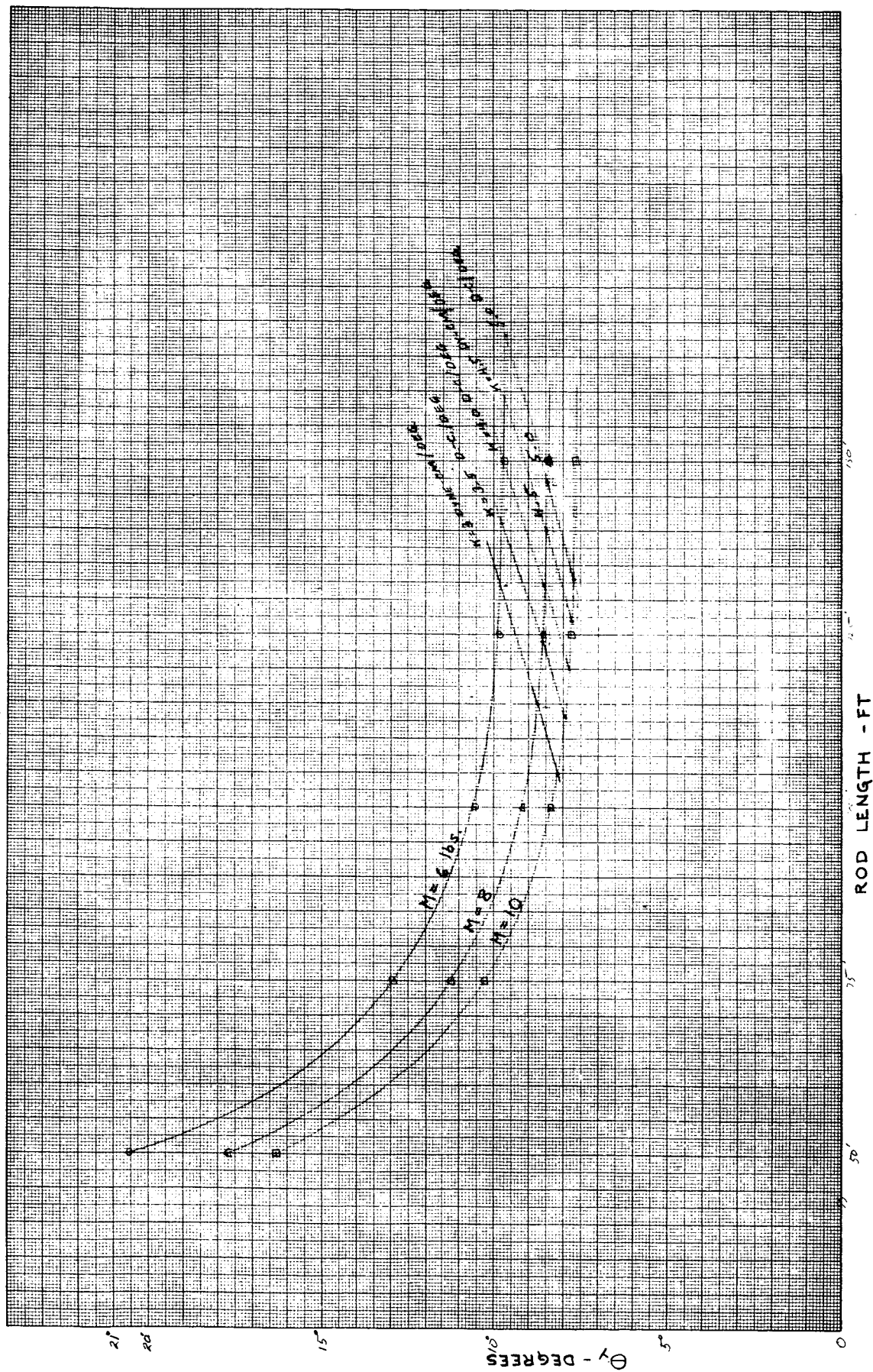


Figure 2.1-34. Total Pointing Error

tip weights, but also in the damper rod tip weights. For rod lengths below 150 feet, errors increase as the rod length is decreased. However, between 125 and 150 feet, accuracy improves only slightly with rod length. Increasing the rod length beyond 125 feet increases the pitch moment of inertia ( $I_P$ ), and the damper moment of inertia ( $.0325 I_P$ )

The damper moment of inertia must be increased by increasing the tip mass since the damper rod length is fixed. This would serve to increase the system weight which is undesirable.

Another important consideration is the design of the torsion wire suspension used in the hysteresis damper. The torsion wire must be small enough to provide the low levels of spring restoring torque required, and still be large enough to withstand the tension caused by damper cocking torques. For a given level of spring constant, increased accuracy requires larger tip masses, resulting in increased system weight.

Selection of the final system parameters was predicated on reducing the attitude control system weight. If the spring constant constructed for the original GSFC Configuration were employed, the new configuration would require a large moment of inertia. If this moment of inertia were achieved with the 10-pound tip weights originally planned, there would be little weight saving. To use 8-pound tip masses requires a rod length of 147 feet with a resulting pitch error of 1.94 degrees, which is higher than desired in view of the limited weight saving.

Consultations with STL have indicated that a low spring constant would be difficult to achieve, and a limit had to be placed on the spring constant. After discussions with STL on April 2nd, a limit of 3.5 dyne-cm/deg. was specified as a reasonable value.

After evaluating the performance associated with 8-pound and 10-pound tip weights, an 8-pound tip weight was selected. The anticipated performance associated with an 8-pound tip weight is given in Paragraph 2.1.6.1.2.2, and represents a good compromise among weight, performance, and engineering capability. The final configuration parameters are given in Table 2.1-7.

#### 2.1.6.1.2.3 Predicted Performance

Four computer runs were made using GAPS III. Two of these were for the standard comparison configurations with 100-foot rods and 10-pound tip weights, and two were for the new configuration. Cases with the sun in and out of the orbit plane were checked.

Figures 2.1-35 and 2.1-36 are the standard configuration and new configuration, respectively, with the sun out of the orbit plane. In this orbit, a large yaw bias error would be expected since the CM moves its greatest distance along the vehicle Z axis (pitch) due to thermal bending. (The oscillation due to thermal bending was not included in the optimization study.) The yaw bias is evident in both figures, but comparing yaw amplitudes, it is evident the new configuration has a considerably smaller oscillation amplitude than the old configuration. This reduced amplitude results in a significant yaw performance improvement for the new configuration.

Analysis of Figures 2.1-35 and 2.1-36 indicate that the performance improvement is more apparent than real. There is a distinct difference in the phasing and frequency of the oscillations of the two configurations. The old configuration (Figure 2.1-35) oscillates largely at orbital frequency, with a noticeable true orbital frequency component (due to thermal bending). These oscillations appear in both pitch and roll, and the pitch and roll oscillations are in phase. The new configuration has a very large second harmonic component in roll, and the pitch and roll oscillations are no longer in phase. (The largest of the peaks do not coincide.) It is felt that this phase shift is responsible for the improved yaw performance. Further studies are in process, but it appears that this phase relationship changes with time of year, and is a function of CM location as well. As a consequence, the actual yaw error may be higher than shown in this computer run. It is not expected, however, that the errors obtained from an inappropriate phasing will be worse than predicted by the optimization study. As a consequence the new configuration has been tentatively accepted as the nominal ATS-D/E Configuration.



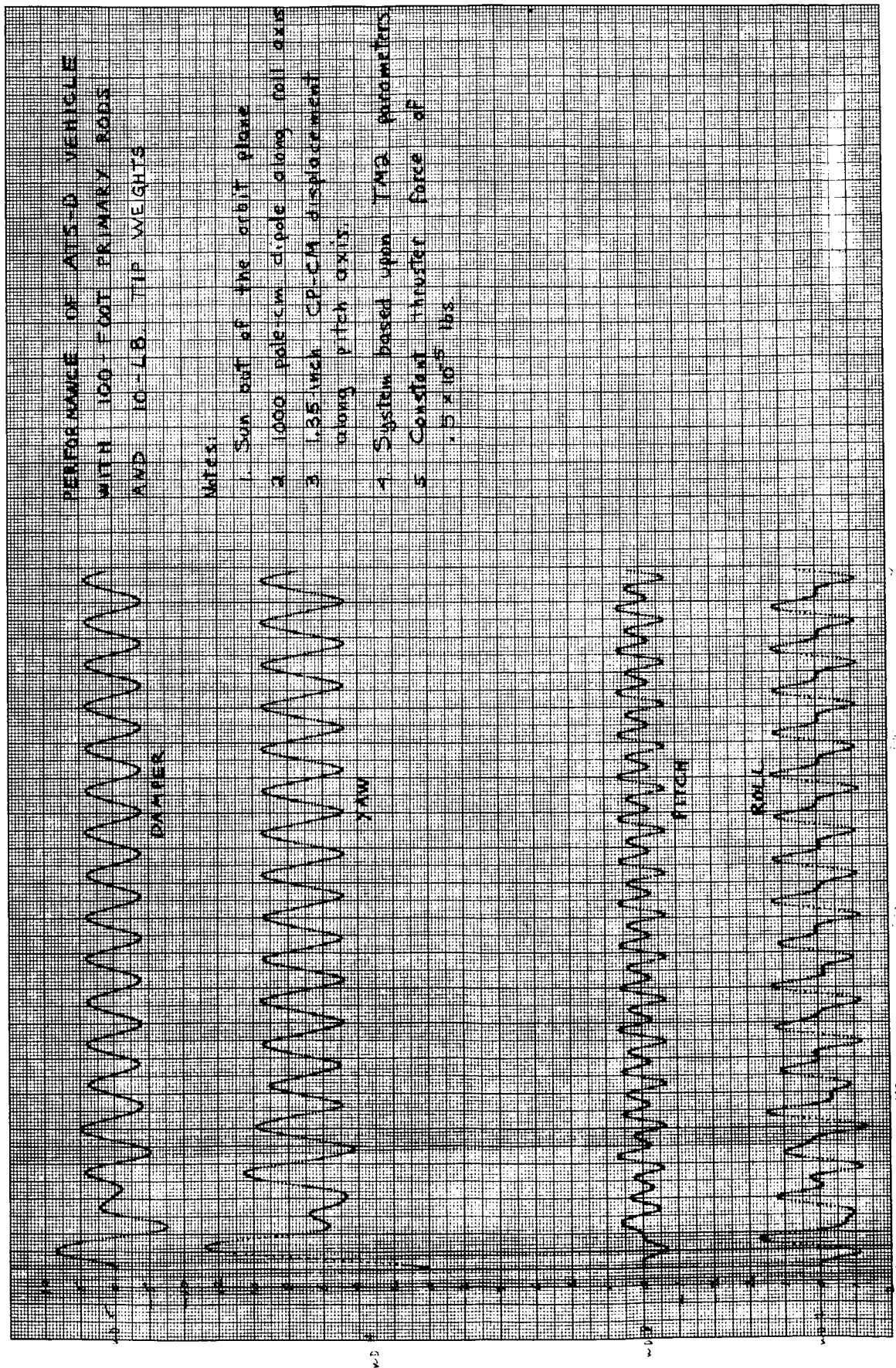


Figure 2.1-35. Performance of ATS-D Vehicle With 100-Foot Primary Rods And 10-lb. Tip Weights

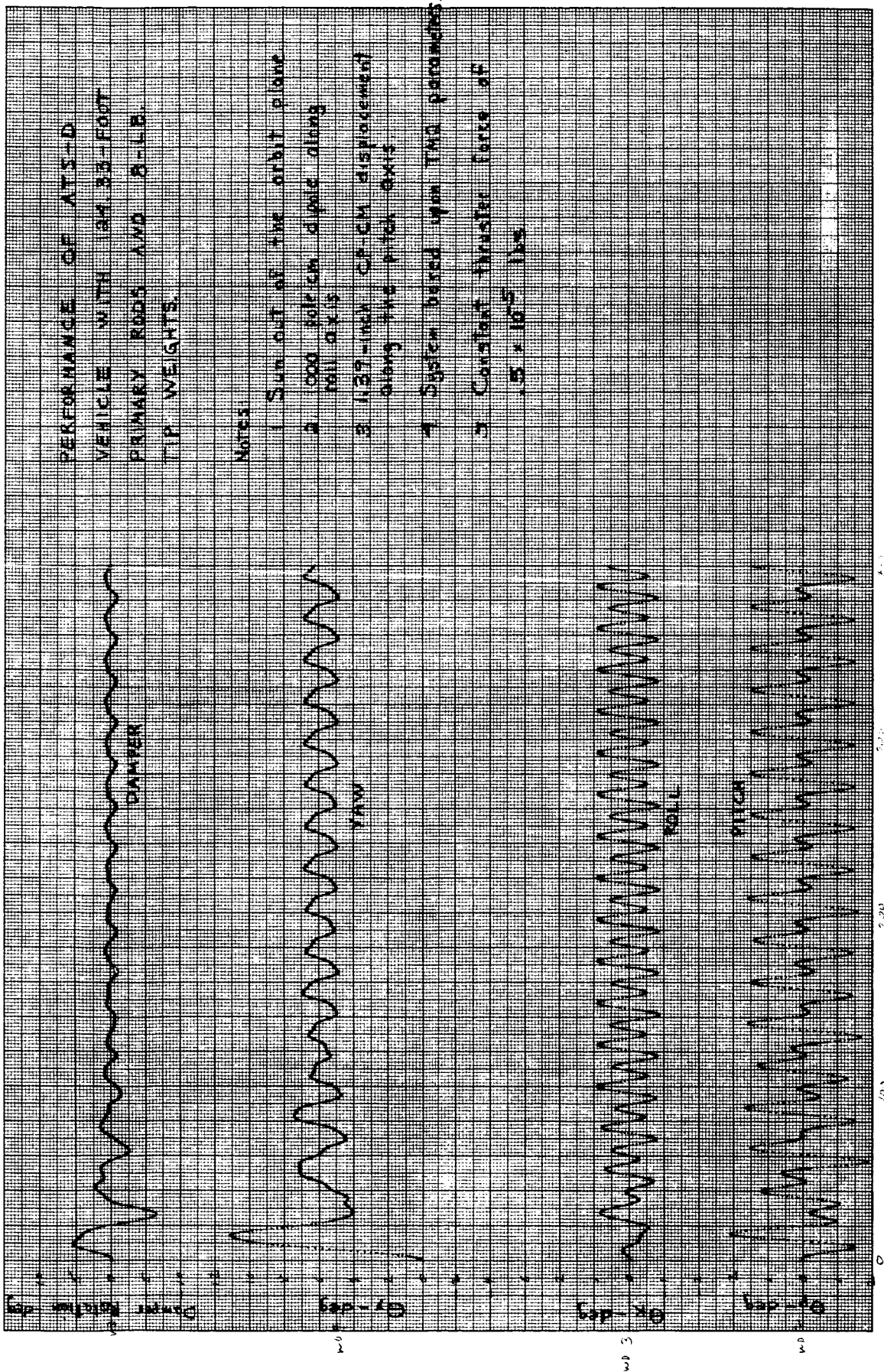


Figure 2.1-36. Performance of ATS-D Vehicle With 124.33-Foot Primary Rods And 8-lb. Tip Weights



On March 26, 1965, NASA/GSFC directed the use of a new set of non-dimensional ATS configuration parameters based on a series of optimization studies performed jointly by GE and NASA/Ames. Subsequent to that direction, GE established dimensional parameters for ATS - A, based on tradeoffs between performance and hardware implementation. (Paragraph 2.1.6.1, this report.) Thruster inversion studies were then re-initiated. Preliminary results of these studies are included in the following paragraphs.

#### 2.1.6.3.1 Summary and Conclusions

The nominal system for ATS-A has a moment of inertia of  $7107 \text{ slug-ft}^2$ . This is almost twice the moment of inertia of previous studies. As a consequence, the torque required to invert the satellite in 2.5 hours at full rod deployment is  $13 \times 10^{-4} \text{ lb-ft}$ . (For a 29-inch moment arm, this corresponds to a thrust level of about  $5.4 \times 10^{-4}$  pounds.) As per discussions with HAC on 16 March 1965, the current inversion thruster spec calls for a thrust level of  $2.9 \times 10^{-4}$  pounds ( $7 \times 10^{-4} \text{ lb-ft}$  torque for a 29-inch moment arm). If this torque level is employed, the time to invert is 3.8 hours. If the requirement for inversion in 2.5 hours is to be satisfied, the spacecraft inertia levels must be reduced by rod retraction prior to inversion. This approach was discussed with the GSFC gravity-gradient technical officer on 26 March 1965 and included in the current Orbit Test Plan, Paragraph 2.1.4.1 of this report. If the rods are retracted to 100 feet prior to inversion, a  $7 \times 10^{-4} \text{ lb-ft}$  torque level is acceptable for a 2.5-hour inversion time. On the other hand, if the 3.8-hour inversion time is acceptable, no rod retraction is required. However, the useful life of the inversion thrusters is time-limited by the amount of propellant carried. The longer inversion time would reduce the permissible number of the operations. About 1/2 hour is required to displace the satellite 30 degrees for transient evaluation of the gravity gradient dampers. (Refer Paragraph 2.1.4.1) The longer thrust times for inversion would place added operational constraints on the number of large angle displacements called for in the Orbit Test Plan.

Figures 2.1-37 and 2.1-38 show the response of the two systems with the sun in the orbit plane. The yaw bias has been reduced, but the amplitude of oscillation has increased. This is the result of the increase in sinusoidal disturbance torques acting on pitch and yaw with the sun in the orbit plane. The new configuration has superior yaw pointing accuracy in this orbit, but the pitch error is greater than the old configurations.

#### 2.1.6.2 Capture Studies

As mentioned in Paragraph 2.1.1, capture studies were suspended on 25 January 1965 to await final resolution of new configuration parameters. Status of efforts as of that date are included as Appendix C. Since publication of that report, the NASA requirement for a delay time between separation and initial boom deployment has been relaxed to 3.96 seconds. Capture studies, with the new parameters of Paragraph 2.1.6.1 will be resumed during the forthcoming quarter.

#### 2.1.6.3 ATS-A Inversion Maneuver

In September, 1964, the first results of GE inversion studies were presented at the ATS interface meeting, Hughes Aircraft Company. These studies were based on a thruster torque value of  $5 \times 10^{-4}$  lb-ft and indicated a total time for inversion of approximately 3.4 hours. An action item was placed on GE, at that same meeting, to re-evaluate the inversion requirements based on a maximum time for inversion of 2.5 hours. In addition, rise and decay time tolerances and thrust level tolerances were provided. At the November 1964 interface meeting, GE Spacecraft Department, results of this re-evaluation were presented. A torque level of  $8.7 \times 10^{-4}$  lb-ft with  $\pm 10\%$  tolerance was recommended for a 2.3-hour inversion maneuver. This study included considerations of thrust rise and decay transients, non-symmetrical torque profiles and a 30-degree maximum overshoot condition. For a 29-inch moment arm, the  $8.7 \times 10^{-4}$  lb-ft torque level corresponds to a thrust level of  $3.6 \times 10^{-4}$  pounds. A portion of this study was included in GE's Second Quarterly Report. Typographical errors resulted in a documented recommendation of a  $4.2 \times 10^{-4}$  pound thrust level but this was subsequently corrected to the  $3.6 \times 10^{-4}$  pound value.

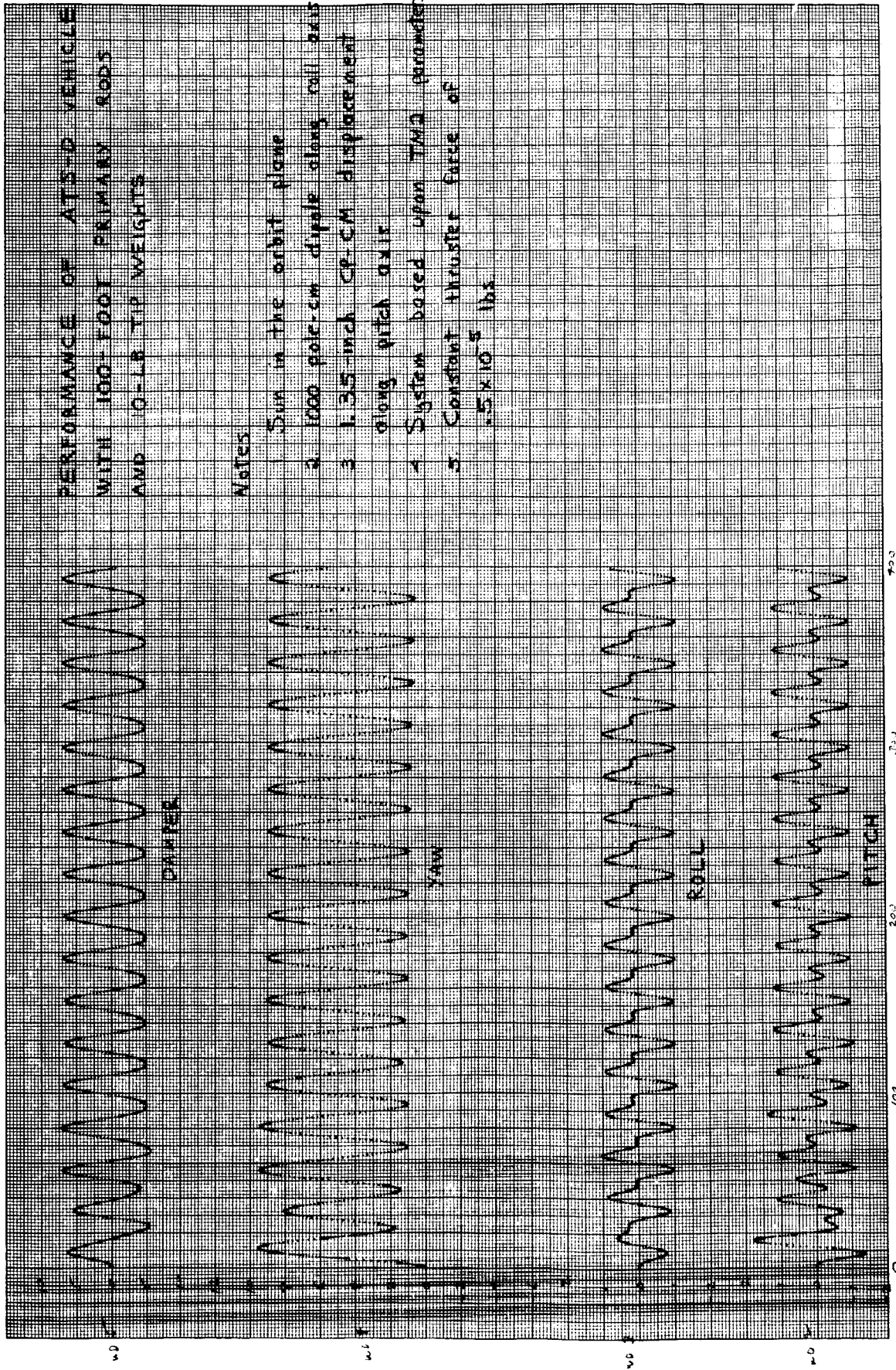


Figure 2.1-37. Performance of ATS-D Vehicle With 100-Foot Primary Rods And 10-lb. Tip Weights

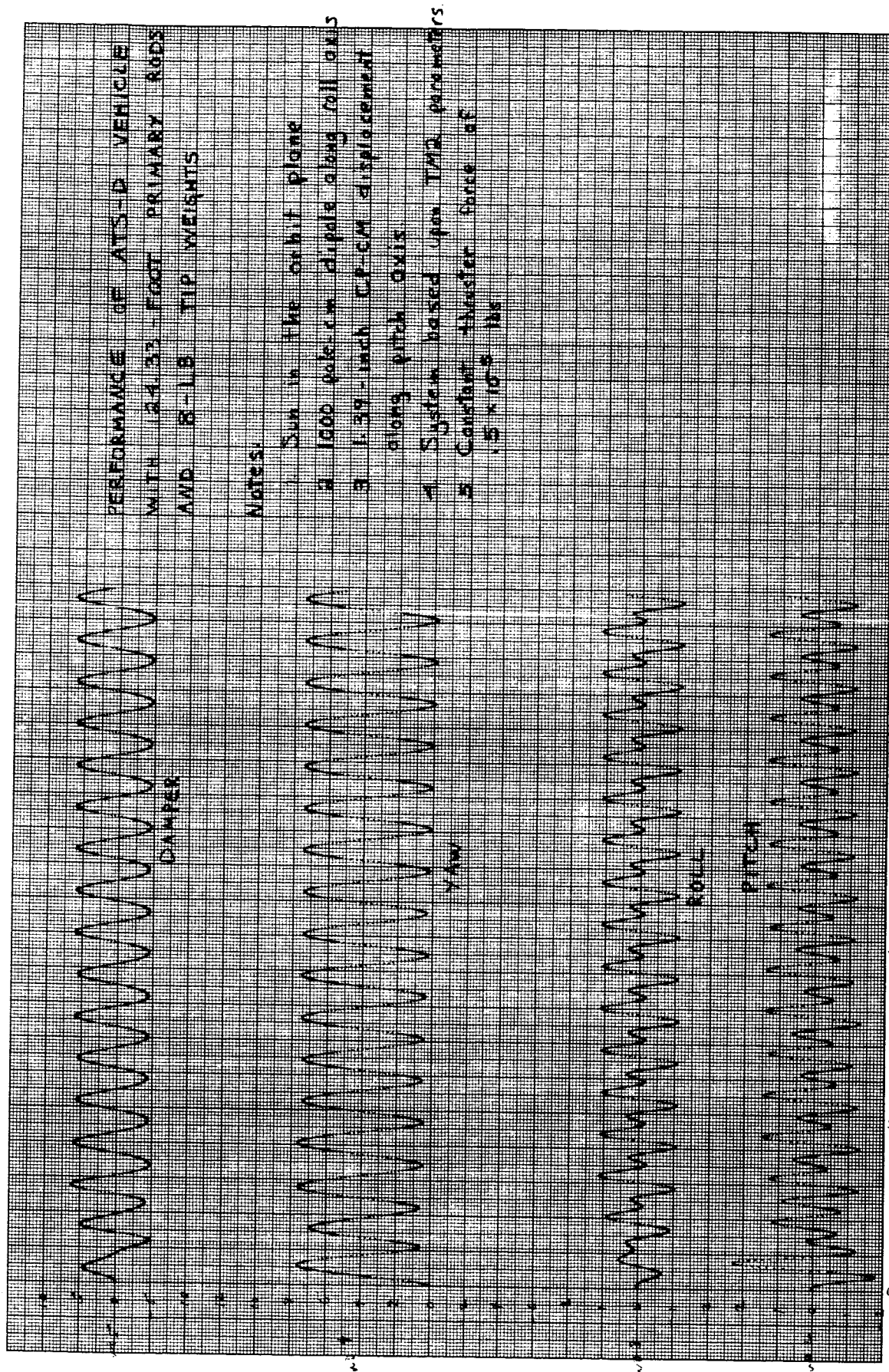


Figure 2.1-38. Performance of ATS-D Vehicle With 124.33-Foot Primary Rods And 8-lb. Tip Weights

#### 2.1.6.3.2 Discussion

For this preliminary study, the inversion maneuver was performed by applying square wave torques to the vehicle (one positive and one negative). These torques were turned on and off at appropriate intervals by means of a "preset timer". Inversion was "backward" (i.e., pitch up) for this study. It has been assumed that no attitude information is available to the ground station operator and that timing the thrusters is the only technique by which inversion can be achieved.

Figure 2.1-39 shows the results of a study with several values of thruster torques. From this figure, the nominal torque level is approximately  $13 \times 10^{-4}$  lb-ft. A limit on allowable vehicle overshoot due to thrust tolerances was placed at 30 degrees (Reference Second Quarterly Report). With this requirement, the torque range is  $11.5 \times 10^{-4}$  lb-ft to  $15.0 \times 10^{-4}$  lb-ft. The allowable torque tolerance about  $13 \times 10^{-4}$  is therefore -11.5% to +15.4% which is in agreement with the tolerance level specified in the Second Quarterly Report, assuming identical thrusters for forward and retro torques.

Since a torque level of  $7 \times 10^{-4}$  has already been selected, the timing sequence necessary to invert the fully deployed system was determined (Figure 2.1-40). The total time of the maneuver is 3.8 hours as shown. If the rods are retracted to 100 feet (reducing the moment of inertia to approximately one-half its current value), the inversion can be accomplished in 2.5 hours (Figure 2.1-41). To complete the inversion study, the case of non-identical thrusters, rise and decay time effects, etc., must be considered. The process must then be repeated for ATS-D/E. These studies are in progress.

#### 2.1.6.4 Response to Internal Disturbance Torques

Appendix D contains an analysis of system response to internally generated disturbance torques. This is now being programmed and will be used during the forthcoming quarter to evaluate known disturbances and specify tolerances on unknown disturbances.



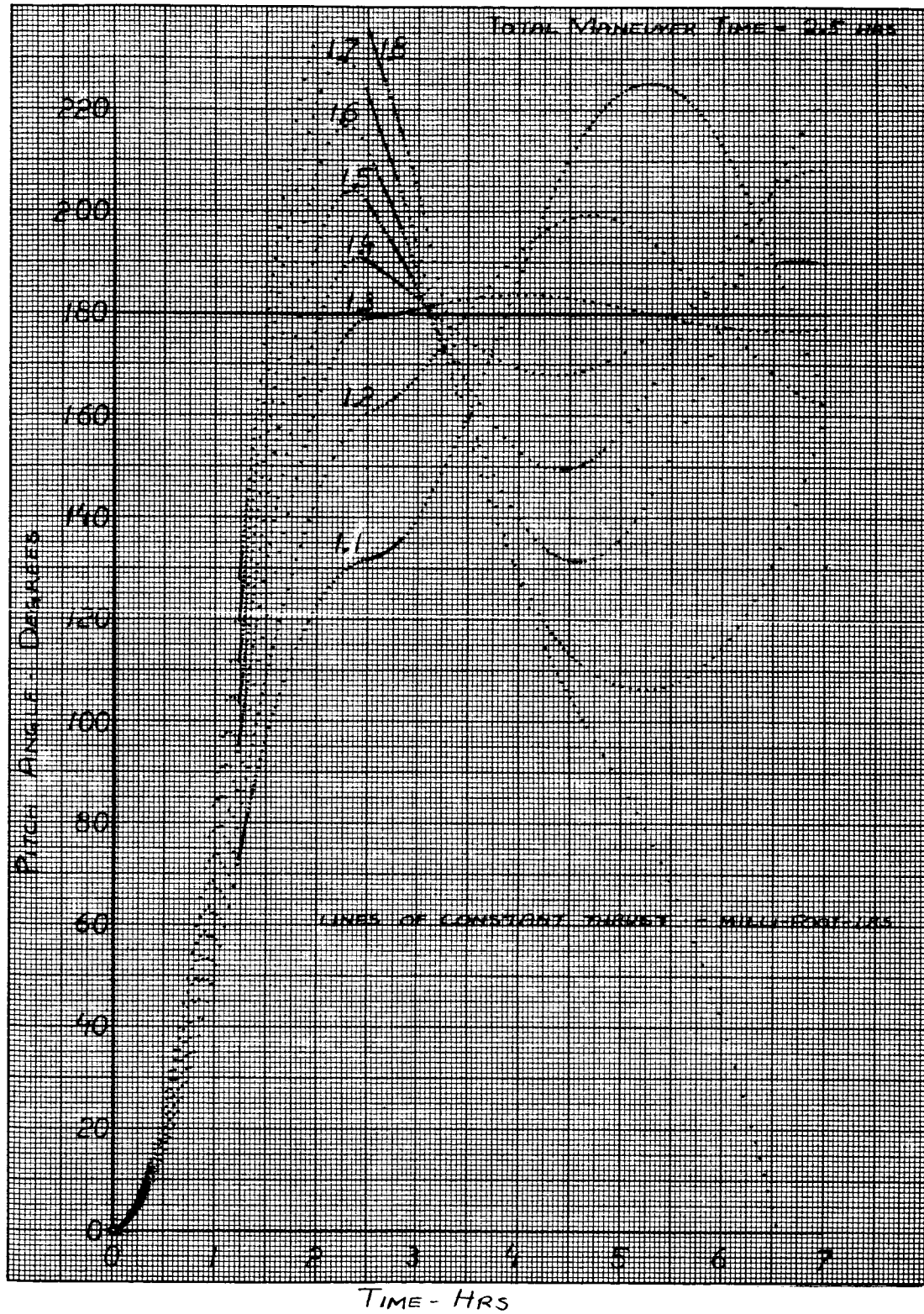


Figure 2.1-39. ATS-A Inversion With 133.75 Ft Rods

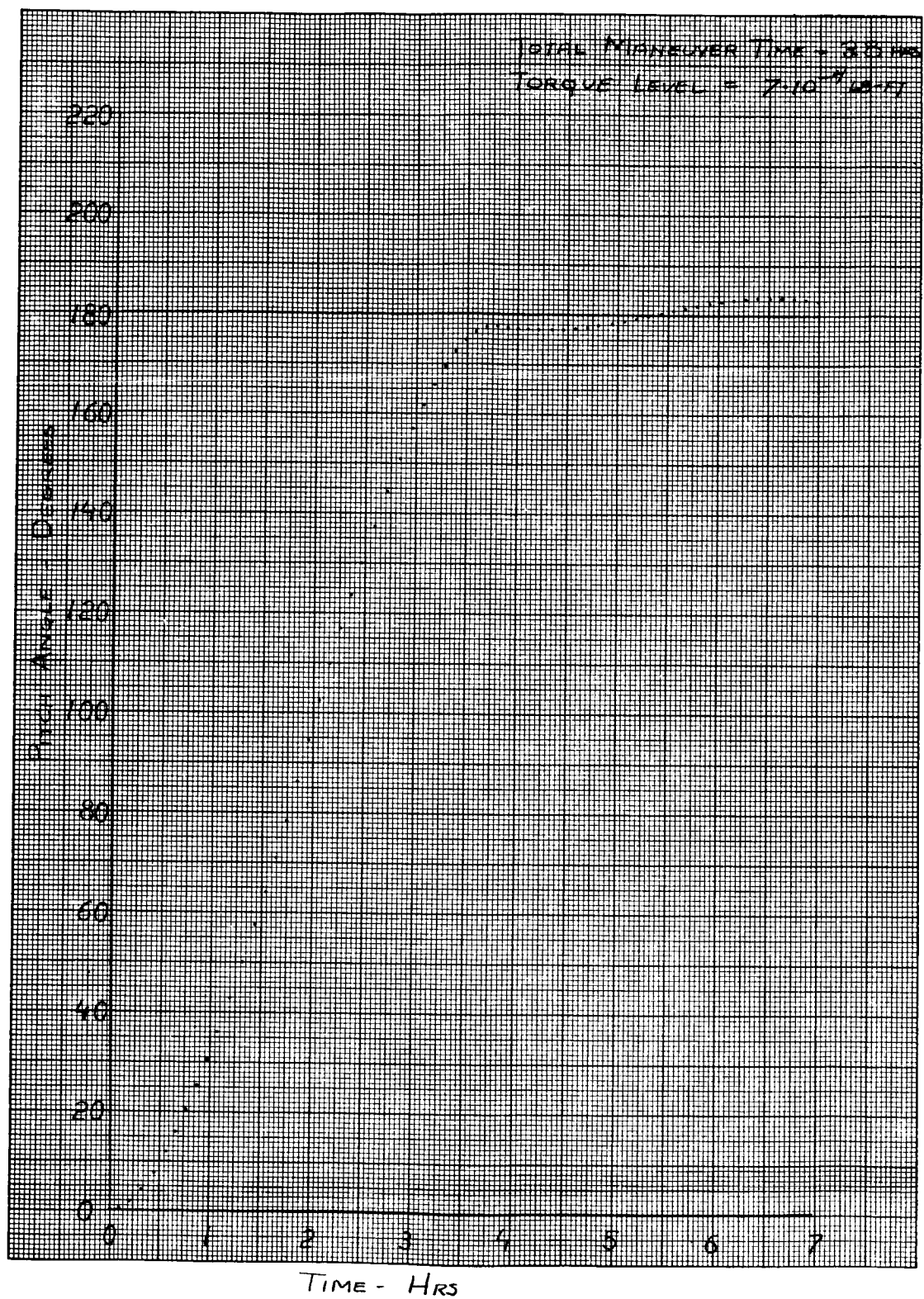


Figure 2.1-40. ATS-A Inversion With 133.75 Ft. Rods

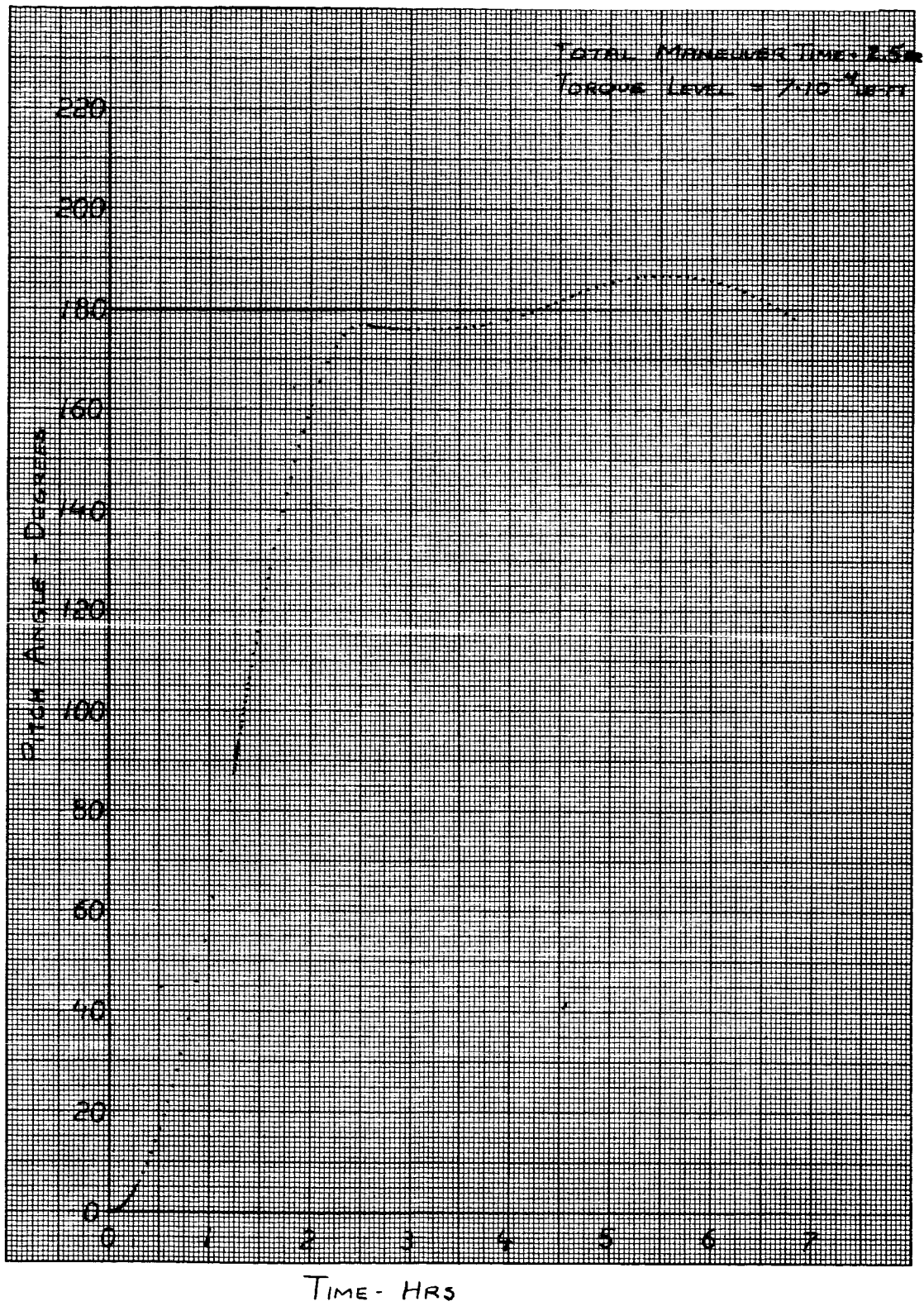


Figure 2.1-41. ATS-A Inversion With 100 Ft. Rods



## 2.1.7 REQUIREMENTS AND PERFORMANCE

### 2.1.7.1 Component Alignment Techniques

Emphasis was given to a definition of component alignment tolerances and measurement techniques. The recommended alignment procedure utilizes a collimated light source directed into a target mirror; the mirror is mounted on the component. It was planned to use epoxy to bond the mirror; however, difficulty was encountered in maintaining alignment during the curing time of the epoxy. The method was abandoned principally because the epoxy would neutralize the effectiveness of thermal coatings on some components and also because fixtures would be required to retain the target mirror even when epoxies were used with short curing time.

Studies indicate that a removable target fixture is the best solution to the alignment requirement.

### 2.1.7.2 Thermal-Vacuum Testing

In order to evaluate the performance of the Gravity Gradient Stabilization System components under realistic orbit thermal cycling, a solar vacuum test is proposed under the following conditions:

1. Use of a simulated sun
2. Cycling of the component under the extreme thermal conditions to be experienced by the ATS vehicles, and at the same cycling rate.
3. Housing the component in a thermally controlled environment representative of the Hughes structure

4. Installation of temperature sensors on the component and housing
5. Test chamber pressure established at  $10^{-5}$  Torr or lower.

The Solar Aspect Sensor, TV Camera, the Combination Passive Damper and Boom Subsystem are being considered for the solar-vacuum evaluation.

#### 2.1.7.3 Waivers to Thermal Test Requirements

NASA/GSFC approved a GE request to the thermal test requirements for component qualification as defined in NASA Specification S2-0102 with the following restrictions:

1. The thermal operating test may be deleted from the qualification program for only those components on which a performance test can be conducted during the thermal-vacuum test
2. The non-operating thermal storage test may be deleted from the qualification program of only those components whose storage test temperature is contained within the thermal vacuum test temperature range.

#### 2.1.7.4 Temperature Sensor Requirements

General Requirements for all ATS temperature sensors have been defined, including the expected temperature ranges, in the ATS System Memo No. 032. The memo was released on February 25th.

#### 2.1.7.5 Vibration Test Requirements

Structural/Dynamic test components for the Gravity Gradient Stabilization System will be delivered to the Hughes Aircraft Company for System Vibration Tests. The original vibration test requirements for these components was published in the Second Quarterly

Report (Para.2.1.10.2). These requirements were later amended by Revision V to the GE System Memo No. 018, dated February 23, 1965. These requirements supercede the former data.

The following requirements apply:

Each component will approximate the flight hardware in mass, c.g., dimensional envelope, and material. No functional tests are required for these components. HAC will be responsible for the installation, calibration, sensitivity checks, and recording instrumentation for all vibration monitors. A total of 6 accelerometers is required for instrumenting the gravity gradient components in the following locations:

Damper

2 Accelerometers

Channels 34 and 36\*

The exact location and sensitive direction of the accelerometers on the damper will be defined on a GE drawing after the GE damper/HAC structure final interface has been established. This drawing will accompany the GE damper to be used for the test.

Damper Boom

2 Accelerometers

Channels 8 and 14\*

The exact location and sensitive directions of the accelerometers will be defined on the damper boom drawing that will accompany the component.

Primary Boom Housing

1 Accelerometer

One of the Spare Channels

Location of accelerometer on the Primary Boom Housing will be defined on the component drawing.

TV Camera Housing

1 Accelerometer

One of the Spare Channels

---

\*As defined in Hughes Document - Reference No. 2222.3/100 ATS Vibration and Shock Qualification Test Plan.

Location of the accelerometer on the TV Camera housing will be defined on the component drawing.

#### TV Electronics

No Channel Request

The present HAC Channel 21\* will furnish useful data on the dynamic response of the TV electronics.

#### Power Control Unit

No Channel Request

The present HAC Channels 18, 19, and 20\* will furnish useful data on the dynamic response of the Power Control Unit.

#### Data Requirements

1. All data channels that pertain to GE components should be grouped so efficient data transmission can be made at the conclusion of the test.
2. The original tape or a copy is requested of all GE channel information including a record of the system input occurring at that time.
3. In order that analysis can be performed at GE the data should be on one-inch tape and be compatible with the GE tape system.

#### Personnel Requirements

It is requested that GE personnel witness the installation of all accelerometers associated with the Gravity Gradient Stabilization System.

It is requested that GE vibration specialists witness all testing associated with the Gravity Gradient Stabilization System.

---

\*As defined in Hughes Document - Reference No. 2222.3/100  
ATS Vibration & Shock Qualification Test Plan.

#### 2.1.7.6 Component Dipole Determination

All acceptance tests of prototype and flight components will include a magnetic dipole test. A maximum of 100 pole-cm magnetic dipole requirement has been placed on each ATS component. GE is planning to perform a gross dipole measurement on each GGSS component to a level of 100 pole-cm  $\pm$  100 pole-cm. Tests will be conducted at the GE facility using available test equipment. A set of Helmholtz coils will be used to establish a uniform magnetic field in the selected test area.

## 2.2 BOOM SUBSYSTEM

### 2.2.1 GENERAL

The Boom Subsystem of the ATS Spacecraft consists of four primary variable length booms which form an "X" configuration about the spacecraft, and two damper booms. The primary booms are motor driven, hence retractable, and incorporate a scissoring motor and associated mechanism which enable the boom apex angles to be varied. Since no requirement exists to vary the length of the damper boom, the self extending characteristic of the booms (the de Havilland Storeable Tubular Extendible Members) is utilized.

In accordance with the requirements for the subsystem, described in General Electric Specification SVS-7316B, the design incorporates the following:

#### 2.2.1.1 Primary Booms

The four primary booms are 150 feet long, 0.05 inches diameter of silver plated Berylco 25 (on the OD). The width of the stowed boom is 2.00 inches, hence the boom edge overlap is  $98^{\circ}$ . The silver plating is polished to afford an absorptance of approximately 0.10 to minimize thermal bending of the booms. In order to secure the proper moments of inertia, tip masses of 2.50 pounds are used for the ATS-A vehicle and tip masses of 10 pounds are used for the ATS-D/E.

#### 2.2.1.2 Damper Booms

The two damper booms are 45 feet long, 0.56 inches diameter, with a stowed width of 2.00 inches which results in an overlap of  $49.5^{\circ}$  for the boom. Like the primary booms, the material is Berylco 25, silver plated and polished on the OD for minimum solar absorptance and a consequent maximum straightness. Tip masses upon the damper booms are 1.90 pounds for the ATS-A and 7.14 pounds for the ATS-D/E vehicles.

#### 2.2.1.3 Erection Units

When stowed, the primary and damper booms are flattened to their two inch strip width, and wound up upon their respective spools. For deployment of the damper booms (since subsequent retraction is not required), their inherent erection capability is utilized. Thus, when stored, a cable fastened to each tip mass prevents their erection. Deployment is accomplished by severing the cable with an explosive bolt cutter.

Since the primary booms require their subsequent retraction and also a scissoring motion to change the apex angles of their "X" configuration, motors and gearing are used to provide this capability. Accordingly, each erection unit contains an erection motor and a scissoring motor.

Synchronization of the booms is required for both scissoring and deployment. Within each erection unit this is accomplished mechanically via gearing and a crank mechanism. Synchronization between erection units necessitates synchronization of the respective motors. Accordingly, shunt wound d-c motors are used for both scissoring and erection since they offer fine speed control, i.e., low speed variation with changes in torque load.

#### 2.2.1.4 Lubrication Techniques

Vacuum lubrication considerations and the recognized problems inherent with the operation of d-c motors in vacuum make hermetic operation desirable. To a considerable extent this is accomplished. All parts in the drive systems, except the slow speed elements, are hermetically sealed, and motion is transmitted across the hermetic boundary via a deformable bellows. This permits conventional lubricants to be used for the high speed drive elements, and an atmosphere in which the d-c motor can operate. Outside of the hermetic enclosure, lubrication is afforded by the judicious use of self-lubricating materials for bearings and gears, i.e., "Bartemp" bearings and  $M_oS_2$  impregnated polycarbonate gears.

#### 2.2.1.5 Reliability

Redundancy characterizes the design of the Boom Subsystem. A clutch mechanism is incorporated within the erection motor and the scissor motor to enable either motor to perform the two functions in the event of a failure. Despite the fact that the motors are mounted within a sealed enclosure, a low vapor pressure lubricant is intended. If the seal should fail, the low vapor pressure lubricant would continue to lubricate the d-c motor commutators.

#### 2.2.1.6 Instrumentation

To monitor performance, potentiometers will provide a measure of the deployed length of primary booms and the apex angle of the "X" configuration; the pressure within the hermetic enclosure will be monitored with a pressure transducer, and temperatures of the scissors motors and the vehicle structure adjacent to the erection units will be provided by thermistors. In addition, microswitches will enable the monitoring of the full extension of the boom and the emergency position of the clutch.

### 2.2.2 EXPLOSIVE CUTTERS

Reliability consideration for explosive devices, which include the prevention of inadvertant operation as well as the necessity for operation upon command, has resulted in the adoption of a dual squib system, each with a single bridgewire. Each bridgewire will be connected to a separate command channel with simultaneous energization for operation. Accordingly, Conax can now utilize Hercules CC No. 63 squibs (which were qualified for another program) for the cutter, thus eliminating the need for a new design and those additional reliability investigations which would have been necessary.

The ejectable connector has been modified by Conax, and is now made of plastic rather than aluminum. This improves ejection on firing and enables better shearing of the bridgewires which are routed through holes in the plastic with reduced chance of abrasion damage to their insulation during handling and vibration.



### 2.2.3 THERMAL MODEL

The requirements of the Thermal Model (T-2) of the Boom Subsystem have been established and transmitted to de Havilland. These requirements include the following design criteria:

#### 2.2.3.1 Boom Erection and Control Mechanism

1. The thermal model will consist of two end erection units and a center control box with each item capable of being separated from the remaining ones as is the case with the actual flight hardware.
2. Outline dimensions of the three units and construction of the external face plates shall be identical to flight hardware with regard to material, dimensions, assembly, and drawing details.
3. When assembled, the contact pressure and area between the center and end sections shall be the same as in the actual hardware. Simulation of the tie rod provision shall be made to hold the units together.
4. Internal equipments of the end sections and the center control box shall be simulated by a single thermal mass attached to the structure with a total thermal conductance equivalent to the actual hardware.
5. Location and protrusion of the squib and cable cutter shall be duplicated in size, shape, and mode of attachment to the structural plates. Thermal mass of the squib and cable cutter shall also be simulated.
6. Tip masses for the ATS-D/E configuration shall be removable. These weights should simulate the actual hardware in thermal mass and in mode of attachment to the erection packages.

7. Because of a recent change in vehicle design, detail specification of the surface finish for the erection mechanisms may be premature at this time. However, based on the original vehicle design, a polished aluminum surface with a total hemispherical emittance (  $\epsilon$  ) equal to 0.05 would be required.

#### 2.2.3.2 Primary Boom System

1. The thermal model will consist of two gear boxes and two primary boom system units.
2. Outline dimensions and construction of the external face plates for the gear box and the primary boom structure shall be identical to flight hardware with regard to material, dimensions, assembly, and drawing details. However, chem milling of the face plates is not required in the case of the primary boom structure. Instead, simulation should be made with flat plates of equivalent average thickness.
3. Mounting accommodations to the vehicle structure shall be identical to Hughes Aircraft requirements for primary boom flight hardware.
4. Mounting provisions for the gear box to the boom structure shall be identical to flight hardware.
5. Internal equipments of the gear box and primary boom structure shall be simulated by a single thermal mass attached to the structure with a total thermal conductance equivalent to the actual hardware.
6. The boom system shall be provided with removable tip masses having the same thermal mass and dimension as the actual hardware.
7. The gear box need not be hermetically sealed.

8. Two suitable heater units (simulating both drive motors) capable of variable heat dissipation up to 30 watts shall be provided in the gear box to simulate the scissoring and extension motors. The heaters shall be mounted in such fashion as to simulate the actual heat paths through the structure of the gear box. It is understood that the heat dissipation of the extension motor may peak at approximately 29 watts.
9. The outside surfaces of the gear box and primary boom structure shall be provided with a black anodize finish.

#### 2.2.4 DYNAMIC MODEL

The requirements of the Dynamic Model (T-3) of the Boom Subsystem have been established and transmitted to de Havilland. These requirements include the following design criteria:

1. The model shall simulate one complete spacecraft boom system.
2. The weight, center of gravity and moments of inertia of each of the three components (two primary boom assemblies and one damper boom assembly), shall be duplicated.
3. The basic structure of the primary boom system will be made from actual hardware.
4. A single mass having the center of gravity location, weight and attachments of the drive assembly will be substituted for the drive unit.
5. A single mass having the center of gravity, weight and attachment location of the primary boom extension mechanism will be substituted for each primary boom and will be attached rigidly to the basic structure (flex pivot need not be used).

6. The mass and center of gravity of the ATS-A tip weights will be duplicated. They are to be removable.
7. All attachment hardware shall be identical to that of flight models.
8. The weight, center of gravity location and inertias of the center and end sections of the damper boom system will be duplicated.
9. The contact geometry between the center and end sections will be as in the actual system.
10. The tie rod will be tensioned to the design tension load.
11. Detachable ATS-D/E weights will be provided for both primary and damper booms.
12. Surface finish is optional.

#### 2.2.5 PRESSURE TRANSDUCER

CIC's Model 6100 potentiometric pressure transducer has been selected. This unit affords redundant electrical contacts upon a film resistive element. Accordingly, the noise characteristic of wire wound pots is not affected, nor excessive sensitivity to wear out or corrosion under, say, dithering motion during vibration.

#### 2.2.6 D C Motors

Speed control of the shunt wound d-c motor is accomplished by modulating armature voltage. This necessitates a separate shunt winding for the brake each. Accordingly, to reduce brake power during motor operation, a new brake winding is being designed characterized by a greater number of turns of finer wire than Globe's normal design.

### 2.2.7 LUBRICATION

The G-300 silicone-bound grease contemplated for the sealed bearings and gears has caused concern, particularly for the high speed and highly loaded elements of the drive system, i.e., motor bearings and Spiroid gears. Accordingly, Shell's APL is being considered as an alternate.

Data exists which shows that the APL has a lower vapor pressure than the G-300. Because it is a petroleum base, it is anticipated that it can lubricate better than the G-300. However, it is not known if the APL is suitable for this application because of its low temperature characteristics. APL has been procured and will be tested upon Engineering hardware. If it is suitable for the application it will be used in lieu of G-300. If the APL is not suitable, MPB's Minipure, a Diester base grease, is intended with G-300 as the back-up.

### 2.2.8 THERMISTORS

Fenwal's GB32P82 thermistors have been chosen for monitoring the temperature of the scissors motors and the outside structural face of the erection units. These have been selected to function over the range  $-22^{\circ}\text{F}$  to  $250^{\circ}\text{F}$  with an accuracy of  $\pm 3.5\%$ .

### 2.2.9 PRIMARY ROD EXTENSION RATES

A discussion was presented in the Eighth Monthly Progress report of the primary rod extension and contraction rates on the structural integrity of the X-booms. The discussion was based on a dynamic analysis that was conducted during the reporting period. This analysis is included as Appendix E.

## 2.3 COMBINATION PASSIVE DAMPER

### 2.3.1 INTRODUCTION

Two dampers, one a hysteresis damper and the other an eddy-current damper, are combined with a clutching mechanism into a single package referred to as the Combination Passive Damper (CPD). These dampers (coupled to a damping boom) are alternately operated during the Applications Technology Satellite (ATS) mission to damp the vibrations of those vehicles that utilize gravity gradient stabilization techniques. In addition to providing damping torques, the CPD also must meet a requirement to restore the damper boom to a "null" position with respect to the satellite. This restoring torque is provided by a magnetic torsional restraint (abbreviated as T.R.) device incorporated in the eddy-current damper system, and by the torsion wire suspension (tendency to "untwist") in the hysteresis damper system.

#### 2.3.1.1 Basic CPD Functional Description

Basic functions currently incorporated in the CPD design and the associated hardware to perform these functions are listed below:

<u>Function</u>	<u>Associated Component(s)</u>
Damping	Hysteresis disc and magnets Eddy-Current (EC) Disc and Magnets
Torsional Restraint	Torsion Wire (Hysteresis Damper) Magnetic T.R. (EC Damper)
Suspension	Torsion Wire (Hysteresis Damper) Diamagnetic Cones and Magnets (EC Damper)
Clutching Mechanism	Solenoid actuator and Diaphragm Clutch
Boom Angle Indicator	Electro-Optical Device

Mode Indicator	Microswitches
Caging for Launch	Pyrotechnic Devices plus Mechanical Latches or Pins
Decaging Monitors	Microswitches
Temperature Sensing	Thermistors
Hard stops at $\pm 45^{\circ}$ rotation extremes	Mechanical stop
Soft stop between $40^{\circ}$ to $45^{\circ}$ at each extreme	Spring stop
Minimum Dipole	"Bucking" magnets properly oriented
Exclude Dust and Extraneous Light	Outer Cover

#### 2.3.1.2 Major Events During Reporting Period

- 4 Jan 1965      Received the proposal for the Hysteresis Damper from TRW/STL (Space Technology Laboratories).
- 20 Jan 1965      Meeting with STL at GE to discuss their proposal and costs for the Hysteresis Damper.
- 21 Jan 1965      Dynamics Research Corporation presented their proposal and cost for the Angle Detector. GE contracted with them for a 3 week study effort to definitize the problems.
- 2 Feb 1965      GE presented results of evaluation of STL proposal to NASA Goddard. An engineering evaluation model of the GE Hysteresis Damper was displayed and discussed at the meeting.
- 12 Feb 1965      A Design Review of the Combination Passive Damper was held at GE with GE personnel in attendance. Attendees included two consultants from GE Advanced Technology Labs, Schenectady, N.Y.
- 17 Feb 1965      Received NASA direction to "buy" the Hysteresis Damper. GE made preparations to obtain competitive bids.
- 25 Feb 1965      Dynamics Research Corporation presented to GE the results of their preliminary study for the Angle Detector and submitted a fixed price cost which was considerably higher than the previous CPFF cost.

- 5 March 1965      Hysteresis Damper Specification SVS 7331 signed off by NASA during a meeting at GE. At this same meeting, it was requested that GE redesign the boom caging mechanism for the CPD.
  
- 12 March 1965      RFQ for hysteresis damper sent to STL.
  
- 16 March 1965      Interface meeting at NASA Goddard. Hughes presented the new vehicle configuration which required various modifications to the CPD package to meet vehicle interface requirements. A major change was an extension of the damper boom shaft.
  
- 17-19 March 1965   Hughes personnel at GE to coordinate component locations and arrangements on the new vehicle structure. Systems optimization studies required study of several mounting positions. No final agreement reached.
  
- 19 March 1965      An in-house Angle Detector, utilizing a digital output, was conceived and costed at GE. A decision was made to use the GE angle detector in lieu of the proposed DRC design.
  
- 19-31 March 1965   Conceptual redesign effort on the CPD package to incorporate the GE angle detector, changes to accommodate the new HAC vehicle (including boom shaft extension), and a redesigned caging mechanism.

## 2.3.2 DESIGN EFFORT

### 2.3.2.1 Description of Configuration

#### 2.3.2.1.1 CPD Package Design (As of March 5th)

As noted in Paragraph 2.3.1.2, NASA indicated on March 5th that the caging concept which utilized straight pins was unacceptable. Because alternate schemes that might be employed (such as Marmon clamps, Vee blocks, etc.) would require a major redesign of the existing package, it was decided to discontinue detailed design effort until a decision was reached. About 25% of the design effort on the straight pin baseplate had been completed at the time work was stopped. In the interim, the design effort was concentrated on caging techniques. Therefore, this section describes the design status as of March 5th.

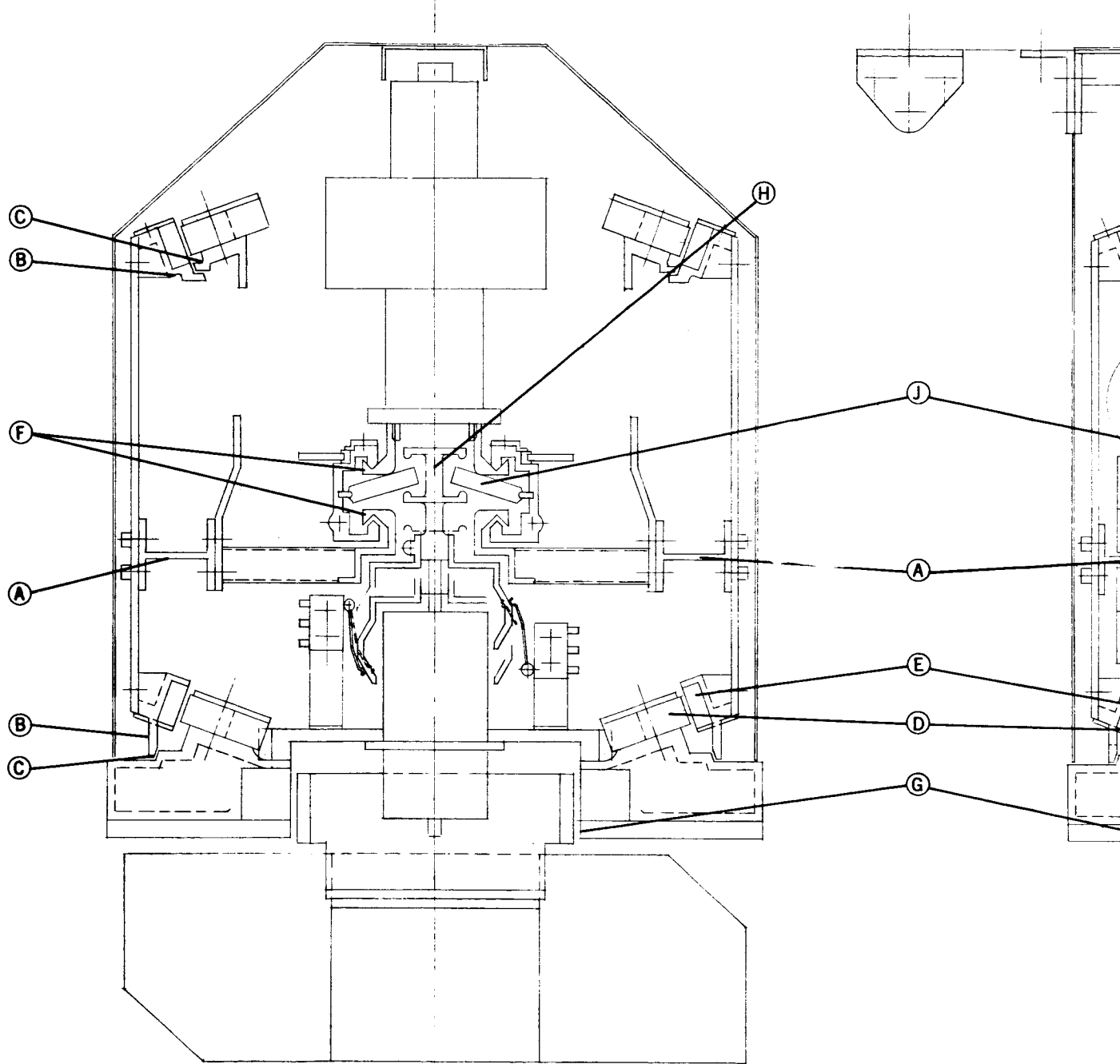


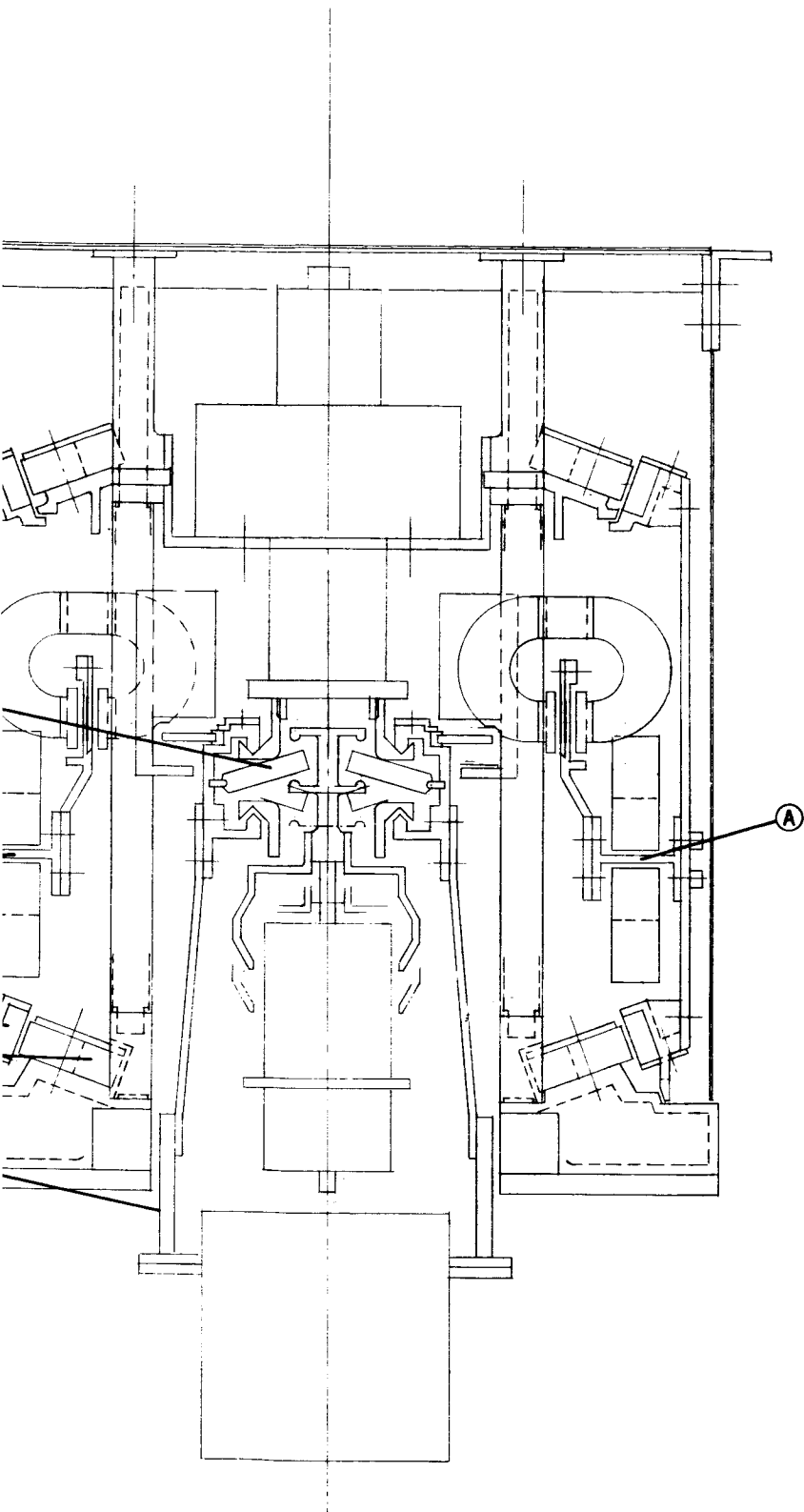
The layout drawing is shown in Figure 2.3-1 from which detailed manufacturing drawings of the damper were being prepared. This layout represents the refinements to the layout shown in Figure 2.3-2 of the Second Quarterly Report.

In addition to overall mechanical refinements necessary to provide manufactureable components, certain changes were made on functional components. The eddy current damping ring (A) of Figure 2.3-1 was changed from aluminum to copper. This change added weight but it was necessary to provide adequate damping as defined in systems studies. Axial stops (B) and tapered radial stops (C) were shown for the eddy current rotor. The nominal clearance between the suspension magnets (D) and the pyrolytic graphite (E) was set at .050 inch.

The stops, both axial and radial, were set at .040 inch nominal movement. Modifications were made to the details of the clutch design principally in the clearance between the clutch faces (F) which was increased from .1 inch to .14 inch. This increase will allow some clearance for operation in the failure mode which assumes that the damper not in use has become fixed in the most extreme axial position allowed by its stops. This change also increases the nominal axial movement of the damper boom shaft (G) from .1 inch to .14 inch when shifting from one damper to the other. The nominal clearance between the solenoid spool actuating surfaces (H) and the Belleville washer (J) was decreased from .1 inch to .07 inch.

The design of the base plate, which includes the provisions for the caging scheme as well as various other functions, was reduced from a concept to a detailed layout. Design of detailed parts from this layout was well underway when the work was held up to permit additional study of the caging mechanism. The originally proposed caging mechanism is shown in Figure 2.3-2. It consisted of four spring-loaded straight sided pins (1) which are restrained during launch by a cable (2). Built onto these four prime boom caging pins are appendages (3) containing smaller pins (4) which cage the eddy current damper. All pins fit into straight holes on the boom structure (5) and damper (6) respectively. Upon cable slacking (as the result of activation of pyrotechnic dimple motors) (7), the pins are



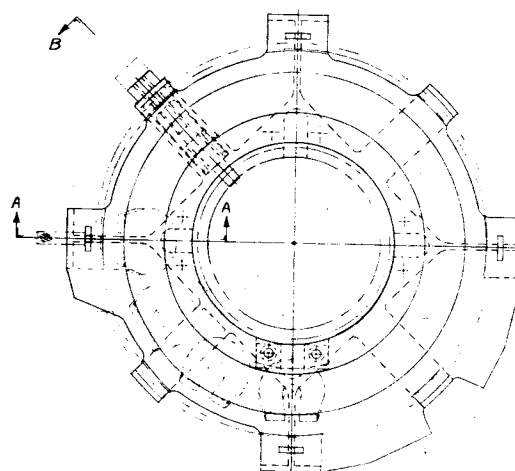
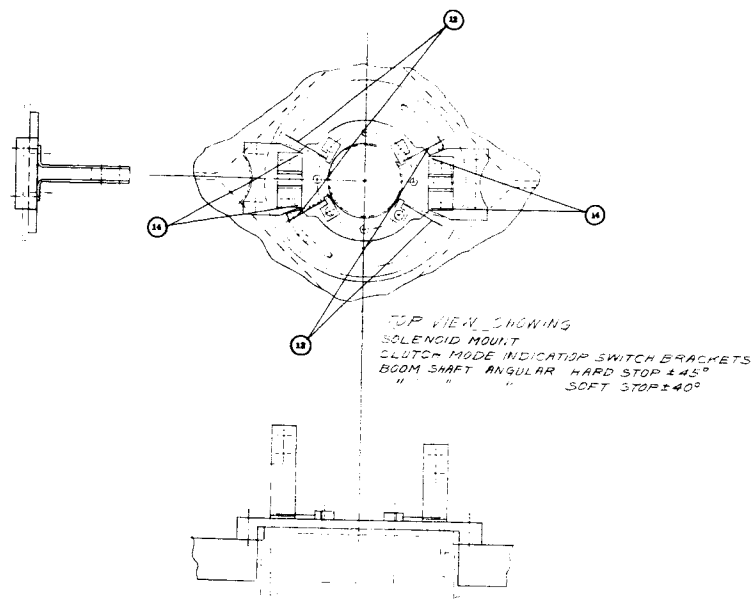


COMBINATION PASSIVE DAMPER  
FOR A.T.S.  
STAGE III ARRANGMENT  
FULL SCALE R. GREENE  
2/18/64

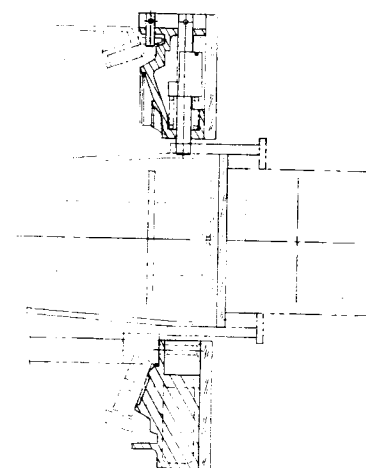
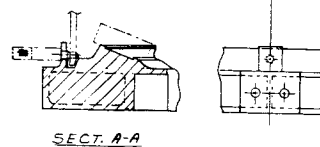
SK 56130 - 808 - 41

2

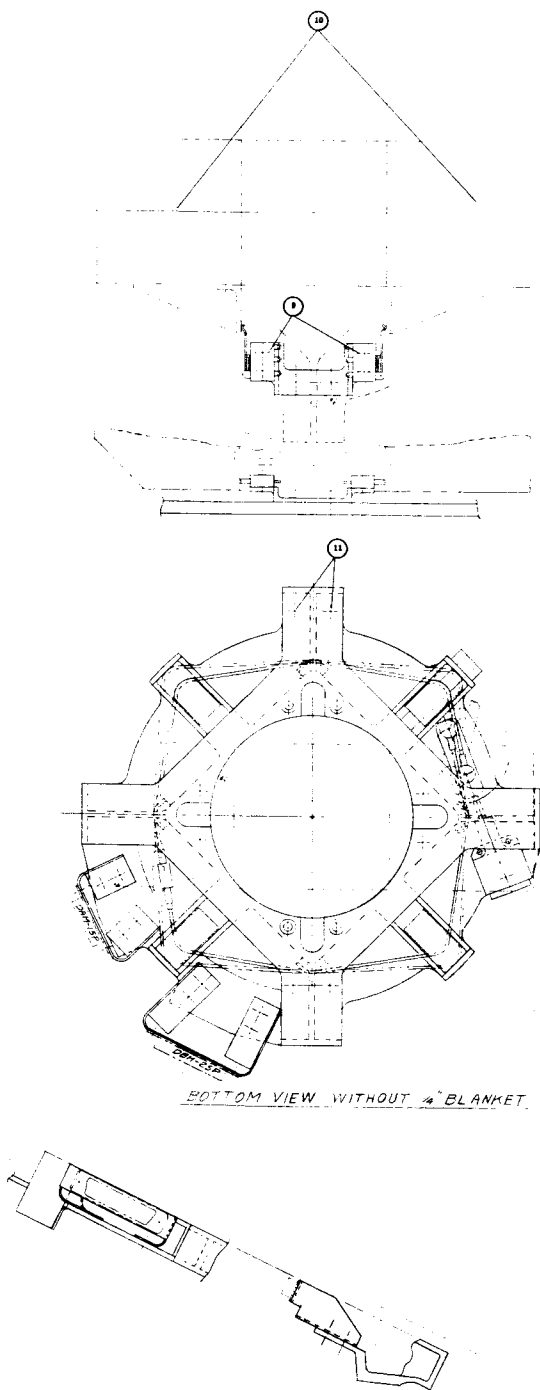
Figure 2.3-1. Combinative Passive Damper  
As of March 5, 1965 (GE Dwg. SK56130-808-41)



TOP VIEW



1



SK 56130-808-42

C.P.D. BASE PLATE

DRAWN BY: *A. S. S. S.*  
2/18/65

2

Figure 2.3-2. Straight Pin Caging Mechanism  
(GE Dwg. SK56130-808-42)

withdrawn from the holes by individual springs (8) of approximately 50-pound force. The normal withdrawal force is carefully controlled at assembly to be in the order of ounces. This system was selected over other methods because of its compactness, simplicity and similarity to release mechanisms used successfully on the Nimbus project. In addition to the caging elements provisions are made for mounting microswitches (9) which are positioned to indicate when the damper booms (10) initiate deployment. Mounting holes (11) are included on the baseplate to which can be mounted the "catches" for the electrical connector boom package. The connector is detached from the boom assembly by a pyrotechnic charge at boom deployment to allow free rotation of the damper boom during orbit. Mechanization for the hard and soft stops is also shown in Figure 2.3-2. The "soft" stops springs (12) are contacted by extensions (13) from the damper boom rotor at  $\pm 90^\circ$  rotation of the damper to provide a spring rate of 1000 dyne-cm/degree in the range of angular rotation of  $40^\circ$  to  $45^\circ$ . The "hard" stop limits (14) are contacted by the same extensions at the  $45^\circ$  rotations point to prevent rotation of the damper boom beyond this point.

#### 2.3.2.1.2 New Conceptual Layout

The changes in vehicle-damper package geometry has had a considerable effect upon the design of the CPD package. A conceptual layout of the damper elements is shown in Figure 2.3-3/4 including the baseplate. The modifications to the CPD necessitated by the changes in vehicle design will be discussed briefly, noting the essential differences from the design shown in Figure 2.3-1. In the CPD shown in Figure 2.3-3, the location of the damper boom (1) has been moved away from the baseplate, thus increasing the loads on the boom caging equipment at launch, and moments on the damper in operation. The inboard end of the damper package no longer must be configured to fit into a corner against a bulkhead. This allows the damper package to be "squared out" and the length between diamagnetic support rings (2) to be increased. This lengthening tends to counterbalance the increased boom moment for the eddy current damper. The increased eddy current rotor lengths will require a heavier structure to minimize deflection at launch. The increased distance from baseplate (3) to the boom (1) centerline allows the solenoid (4) to be longer and extend down into the boom shaft (5). The additional room may be

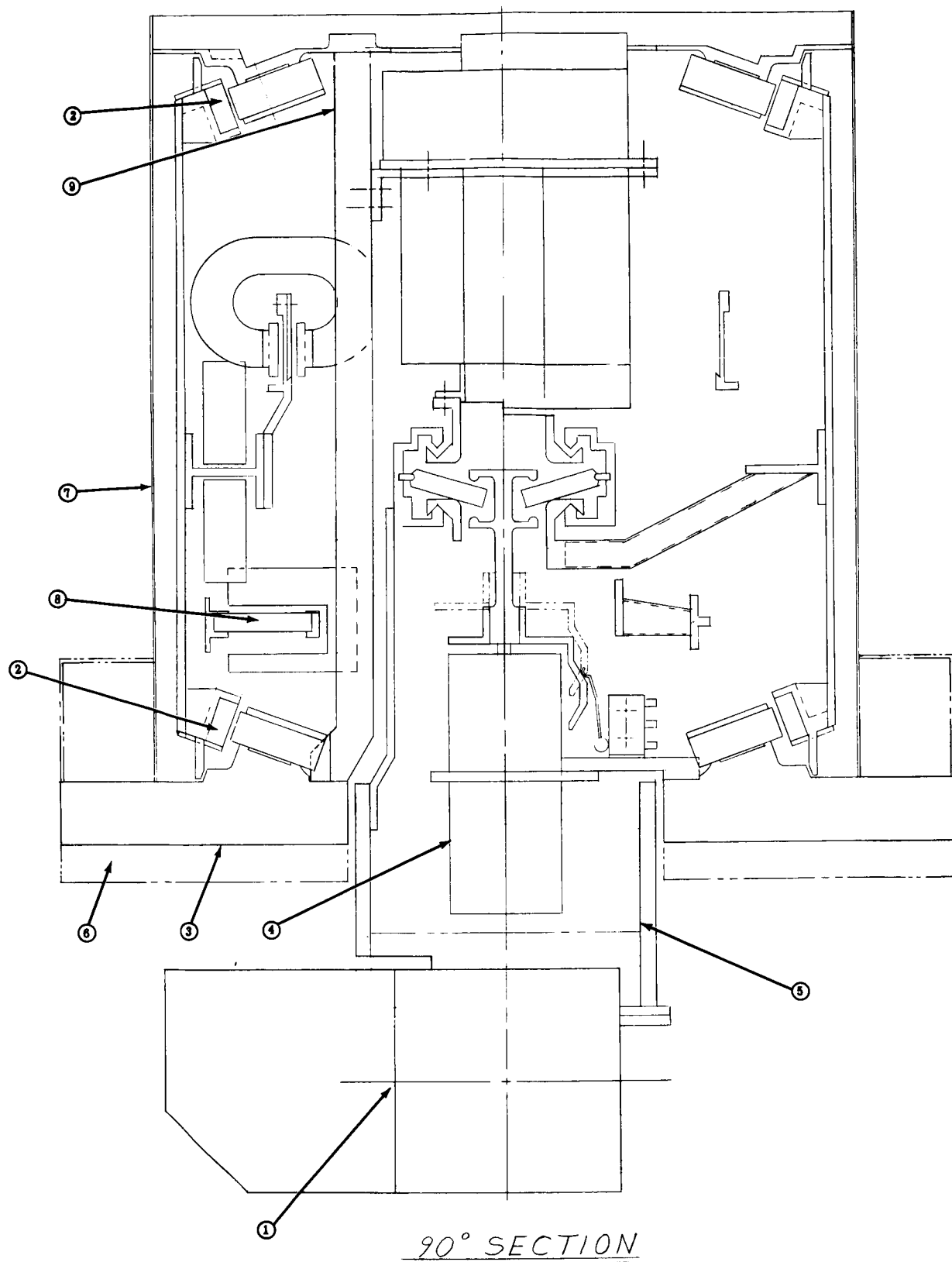


Figure 2.3-3/4 New CPD Concepts

important to permit a solenoid design which can meet force requirements. The change in vehicle-damper relationship changes the thermal conditions that require the use of thicker insulation (6), and that the case (7) of the damper package be of a relatively thick conductive metal.

An angle indicator (8), which has a digital readout, has been added to the design. The internal longitudinal rectangular structural tubes (9) have been offset to accommodate the angle indicator.

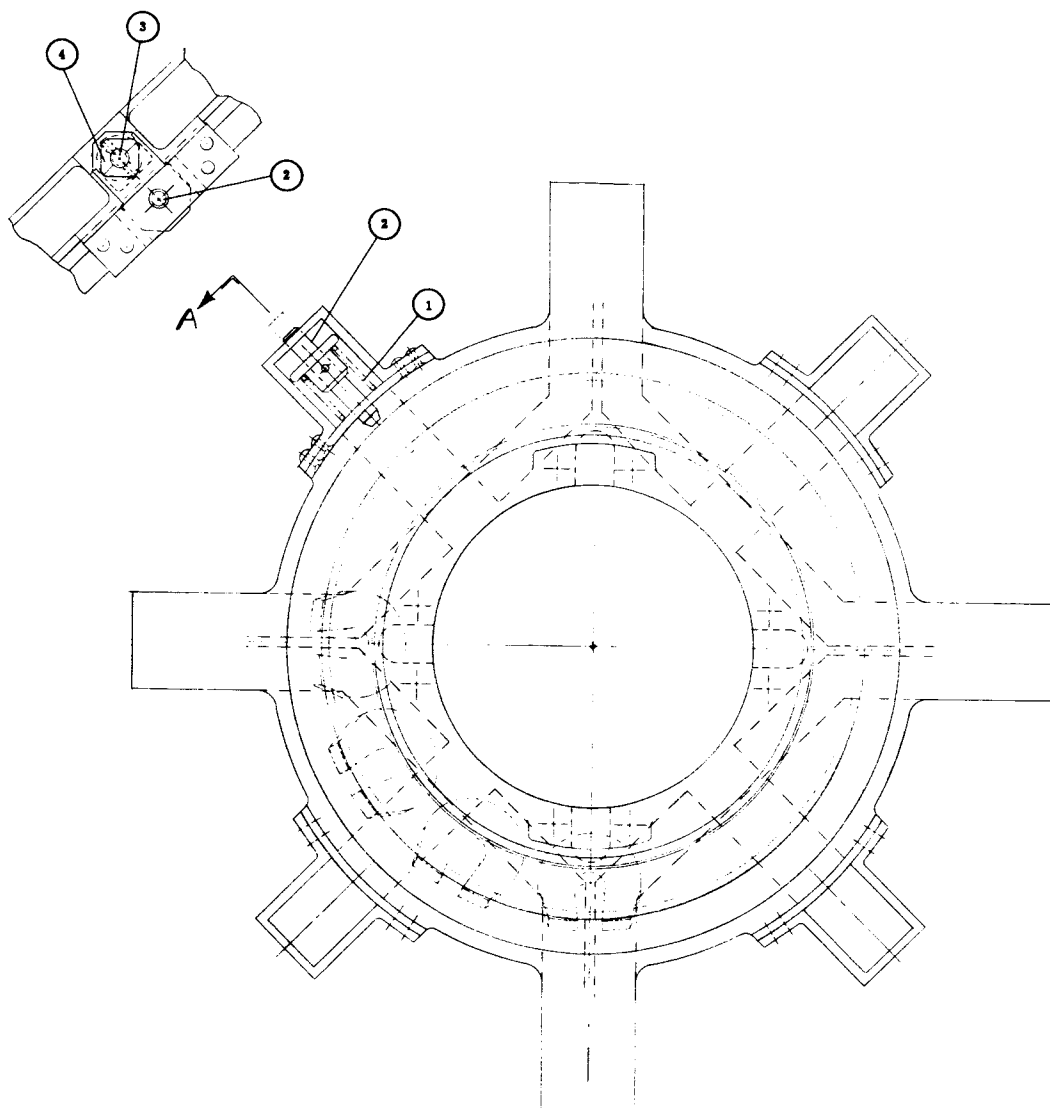
#### 2.3.2.1.3 Caging Damper Boom Support and Eddy Current Rotor

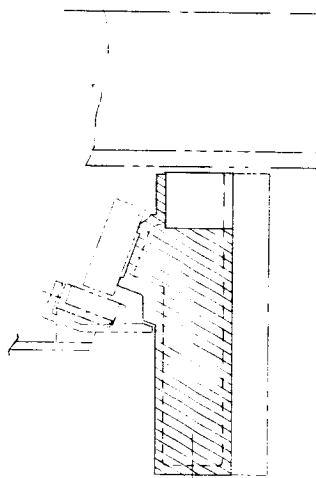
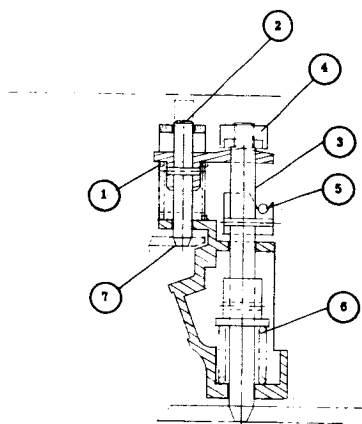
Objections have been raised to the straight-pin caging design shown in Figure 2.3-2. If by some remote possibility one of the eddy current rotor caging pins (4) of Figure 2.3-2 sticks, it would prevent the boom caging pin attached to it from withdrawing. A concept that eliminates this condition is shown in Figure 2.3-5. This design provides a separate spring (1) for the pin (2) caging the eddy current damper (7). The boom pin (3) has a threaded adjustment nut (4) which restrains the eddy current pin (2) in the caged mode while the boom pin is caged by the release cable (5). When the cable releases the boom pins, they can be withdrawn by the separate boom cage pin springs (6) even if the damper caging pins stick. This arrangement also reduces the tolerance of parallelism and location of the two pins (2) and (3) and their mating holes.

Other possible causes of malfunction include the effects of dirt, misalignment, cocking, brinelling, friction, and thermally induced binding. A number of caging concepts were investigated. Some of these are compared in Table 2.3-1. The columns titled Figure 2.3-2 and Figure 2.3-5 contain information regarding the straight pin and tapered pin designs. A brief functional description of each of the concepts in Table 2.3-1 is included below.

Concept No. 1 (C-1) embodies a clamp which is separated into two halves and pivoted about a bolt on the face of the baseplate. The bolt has a long clearance hole in the baseplate so the caging load is not carried through that path. The load is transferred from a vee ring on

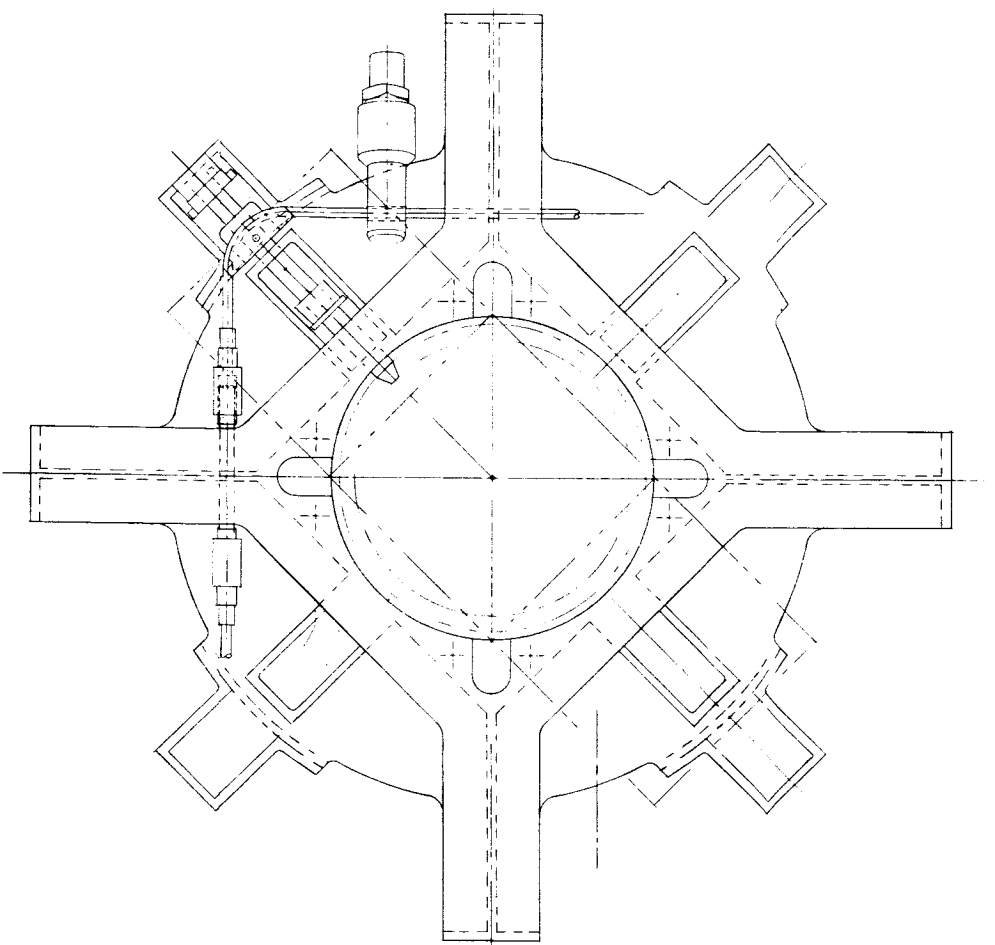






SECT. A-A

2



CPD BASE PLATE  
(TAPER PIN CAGING, BOOM SHAFT & EDDY CURRENT SHAFT)  
DRAWN BY: R. L. J.

Figure 2.3-5. CPD Baseplate Taper Pin Caging

3

TABLE 2.3-1. COMPARISON OF ATS-CPD CAGING CONCEPTS

DESIGNATION	FIG. 2.3-2		C-1	C-2	FIG. 2.3-5			C-4	C-5	C-7	C-8
GENERIC NAME	STRAIGHT PINS	DOUBLE VEE BLOCK CLAMP	PURE MARMAN CLAMP		TAPERED PINS	CAM PLATE	VEE BLOCK ON PIN	VEE BLOCK SCISSORS	SLIDING VEE BLOCK CLAMP		
1. Axial Load on Pins (20 lb boom @ 100g.)	Spring Only-50 lbs	2000 lbs each Block	N/A		23° Taper-712 lbs (no Fric.) 15° Taper-540 lbs (no Fric.) < 250 lb.-lb.	2000 lbs ea. Pad	2000 lbs. ea. Pin	N/A	2000 lbs each Block		
2. Bending Moment on Pins (Same Load)	~ 250 in.-lb.	~ 500 in.-lb.	N/A		23° -1000 lbs (Tension) 15° -700 lbs (Tension)	N/A	N/A	1000 lbs (Bending)	1500 in.-lb. on Block		
3. Band or Cable Load (Same Load)	75 lbs.	1000 lbs. (Bending)	1000 lbs (Tension)		Cable Cutter*	Bellows Motor Large Medium	Cable Cutter* Medium Small	Explosive Nut* Medium Boom Clamp- Medium EC-Large	1000 lbs Tension		
4. Pyrotechnic Device	Dimple Motor	Explosive Nut*	Cable Cutter*		Minimum Large						
5. Axial Space Req'd	Minimum	Large	Medium								
6. Radial Space Req'd	Large	Medium	Medium								
7. Some Operating Questions	1. Thermal Binding	1. Alignment	1. Release		1. Dirt Binding	1. Cam Plate Friction Loads	1. Cold Welding	1. Cold Welding	1. Sliding Block		
	2. Dirt Binding	2. Cold Welding	2. Rebound		2. Pin Cold Welding	2. Cold Welding		2. Reaction of Large Pyrotechnics	2. Complete Release		
	3. "Sequential" Operation	3. Reaction of Large Pyrotechnic	3. Cold Welding								
	4. Launch Damage	4. "Sequential" Operation	4. "Sequential" Operation								
8. Design Status	90% Complete	Concept Only	Concept Only		75% Complete	Rough Concept	Rough Concept	Conceptual Layout	Concept		
9. Design Questions	Mostly solved	1. Alignment	1. Release Device		1. Cable Release Device	1. Release Device	1. Release Device	1. Large Dia. EC Caging	1. EC Caging Success		
		2. Release Device	2. Jamming		2. Binding	2. Binding	2. EC Caging				
		3. EC Caging	3. Ring Catcher		3. EC Caging						
10. Relative Weight (Excluding EC Caging)	Light	Heavy	Medium		Light	Heavy	Medium	Heavy	Medium		
11. EC Damping	Integral	Separate	Separate		Integral	Separate	Separate	Separate (Heavy)	Integral		

\*Will Generate Exhaust Products

boom shaft to three vee blocks on the clamp and then through other vee surfaces on the clamp to matching lugs on the baseplate. Release is by a separation nut or a bolt cutter. Retraction of the two halves of the clamp is by two springs attached to the baseplate.

Concept C-2 is a conventional Marman configuration which clamps a tapered ring on the boom rotor to a matching ring on the face of the baseplate. A spacer between the two flanges is required to position the rotor properly. The spacer is pulled out by the clamp just after the clamp has released the rings. The clamp band is released by a bolt cutter. The band is retracted into stops by three or more springs attached to the baseplate.

The tapered pin design is shown in Figure 2.3-5. This is the preferred design. The mechanism is located in the baseplate except that the eddy-current caging pin and its separate spring, described earlier, project somewhat from the outside diameter of the plate. The pins will be held by a pretensioned cable in the caged position. The load in the cable is greater than for plain straight pins so that the release arrangement planned for the straight pin configuration will have to be altered. Preliminary design studies indicate that this design is the most reliable, satisfies the objections which have been raised as well, if not better than any of the other concepts considered. In addition, this concept involves the least alteration to work already completed and will be the lightest of the concepts considered.

Concept C-4 is a circular cam plate operating "dogs" with wedge-shaped points that engage a vee groove in the vee groove in the boom shaft. When the cam plate is rotated by pyrotechnic bellows motors, the follower surface of the dogs ride out on the cam slope and drop into grooves, releasing the boom. The dogs are retracted by springs. A shear pin holds the plate in the caged position until sheared by the action of the bellows motor.

Concept C-5 uses Marman clamp flanges the same as for C-2. The flanges are clamped by pins having heads of an inner cross section the same as a Marman clamp. The pins have a spacer like that described under C-2 to hold the boom shaft in its proper axial position. The pin guides have large clearance holes to allow the pins to align with the flanges. The pins are constrained (and released) by a cable similar to that for Figure 2.3-5. They are retracted by springs.

Concept C-7 provides vee block scissors for both the boom and eddy-current rotors. The scissors are like the clamp on C-1 and are mounted with clearance to the baseplate. The blocks have a cross-section like the Marman clamp, and the pin heads on C-5, and operate on Marman clamp type flanges. The scissors are released by an explosive nut or a bolt cutter and retracted by springs.

Concept C-8 uses a set of three vee grooved blocks that mate with a vee ring on the boom shaft, and three pins that mate with holes in the eddy-current rotor (similar to Figures 2.3-2 and 2.3-5). The blocks are mounted and guided on the face of the baseplate. They are held in the caged position by a slotted band. Pins threaded into the outside of the blocks form part of the guidance and hold the retracting springs. Nuts on these pins engage an arm on the eddy-current pins (again similar to Figures 2.3-2 and 2.3-5), and hold them in the caged position. When the band releases, both pins are retracted by their own springs. If the eddy current pin sticks, the boom pin (and block) can still retract as in Figure 2.3-5. Release is effected by redundant bolt cutters. Both the boom shaft and the eddy current rotor are released by the one actuation.

#### 2.3.2.1.4 Hysteresis Damper - GE Design

The detailed design drawings of the GE-designed Hysteresis Damper are approximately 75% complete for Stage III issue. All effort on this design has been discontinued at NASA's direction. The layout drawing (Figure 2.3-13) shows the general configuration of the GE Hysteresis Damper. The design of Stage III version of the damper is basically the same as that for the engineering model (Figure 2.3-6) which was built early in the reporting period. However, as indicated by the layout, a caging mechanism has been incorporated, along with various other minor changes, to improve the assembly, testing, and reliability of the damper.

Suspension and dipole characteristic tests on the engineering unit were performed and results are reported below in Paragraph 2.3.3.4, along with a detailed description of the Stage III design. No further tests were performed or planned because of NASA direction.

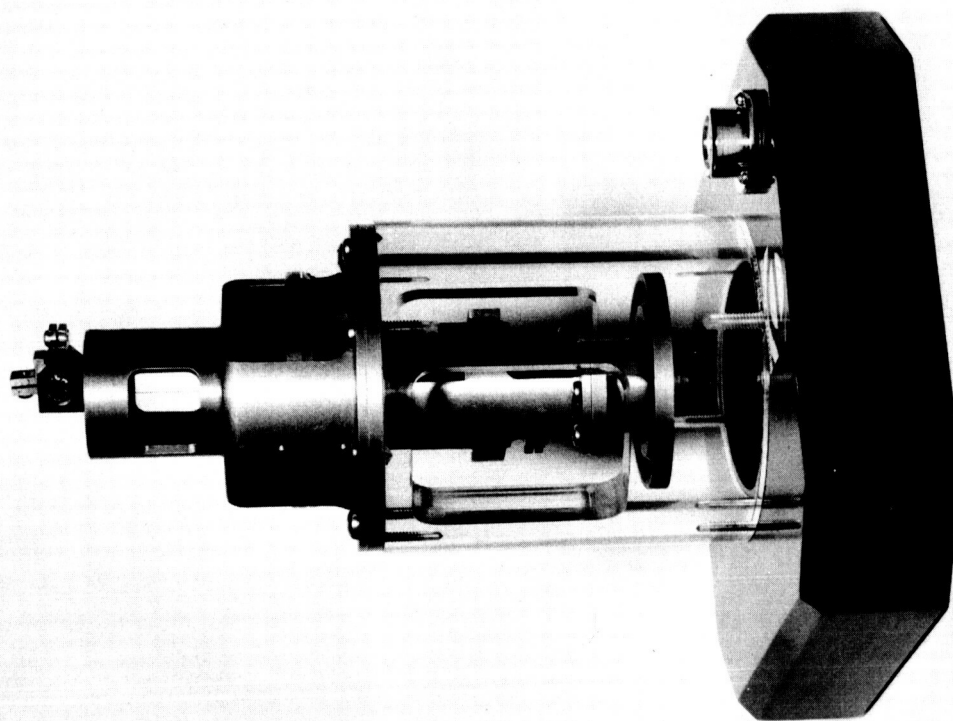


Figure 2.3-6. GE Hysteresis Damper Model

### 2.3.2.2 Interface Activities

#### 2.3.2.2.1 CPD to HAC Spacecraft Structure

As reported previously, a tentative agreement for mounting the CPD to the spacecraft by means of a truss arrangement was reached with Hughes Aircraft Company (HAC) on 17 November 1964. However, subsequent efforts to "freeze" this arrangement were unsuccessful since HAC was devoting their efforts to a redesigned vehicle and did not make layouts showing the "truss" mounting arrangement for GE concurrence. In this interim, GE continued the design effort on the CPD and provided mounting pads on the CPD baseplate such that fittings could be attached to accommodate almost any type of attaching structure which HAC might desire. At an interface meeting at NASA Goddard on 16 March 1965, HAC officially presented their redesigned vehicle structure. This new configuration provided more space for the CPD envelope, but also adversely affected the overall CPD design in several other respects as discussed below. From the NASA meeting, HAC personnel visited GE on 17-19 March to coordinate the gravity gradient experiment component locations and interfaces. During this joint effort, several constraints (such as vehicle dynamic balance, CPD thermal control, boom interference, structural attachment considerations, systems optimization studies, etc.) were considered. The general location of the CPD on the vehicle resulted in the following design changes to the CPD package:

1. To meet the thermal, dynamic balance, and boom interference considerations, the damper boom shaft was extended an additional 2 inches (approx.) away from the baseplate.
2. To meet systems requirements, the position of the CPD relative to the launch axis was adversely shifted, resulting in additional loads in the baseplate which, coupled with the additional moment arm of the extended boom shaft, requires complete redesign and analysis of the baseplate and caging mechanism.



3. The position of the CPD mounting pads were rotated  $45^{\circ}$  with respect to the vehicle (and the damper boom) which changes load paths through the baseplate. This shift may also adversely affect the mounting holes provided on the baseplate for switches and fittings which are provided for damper boom functions.
4. The exact method of mounting the CPD to the structure has not been determined and this, when established, may further alter the CPD concept.

GE is proceeding on a redesign effort on the overall CPD to accommodate the above design changes and other changes (Angle Detector) which are foreseeable as the result of recent perturbations.

#### 2.3.2.2.2 CPD to deHavilland Interface

The interface with the deHavilland Boom Package presently consists of three items:

1. Attachment of the Boom Package to the CPD Boom Shaft by means of simple flanges and four bolts.
2. Two limit switches mounted on the CPD which contact the end masses of the damper booms. These switches indicate boom extension.
3. The electrical connector on the damper boom package is explosively separated from the package at extension. A fitting to catch and absorb the energy of this connector is attached to the CPD baseplate by four bolts.

Item 1 has been resolved for some time; however, Items 2 and 3 are affected by the boom shaft extension of the CPD and the modifications necessary to the CPD baseplate to accommodate any new vehicle mounting requirements and/or a modified boom caging mechanism. Therefore, Items 1 and 2 are being considered in the redesign effort presently in progress on the overall CPD package.

#### 2.3.2.2.3 CPD to STL Hysteresis Damper Interface

During the reporting period considerable effort was expended to design the CPD such that the hysteresis damper as proposed in the initial STL proposal and the GE hysteresis damper packages would be interchangeable within the overall CPD package. This philosophy was necessary due to the uncertainty as to which hysteresis damper would be selected for the final configuration. The hysteresis damper envelope drawing was modified for the second RFQ to STL to provide this interchangeability. These modifications should not change the basic STL damper design since the new envelope was patterned to the STL drawing of the actual damper configuration which was well within the confines of the old envelope drawing.

#### 2.3.2.3 Specification Status

Table 2.3-2 lists the status of CPD specifications.

TABLE 2.3-2. CPD SPECIFICATION STATUS

<u>Specification Title</u>	<u>SVS No.</u>	<u>Status</u>
Combination Passive Damper	7314	Completely typed in preliminary form. Issuance being held pending resolution of damper requirements.
Passive Hysteresis Damper	7331	Issued on March 5, 1965.
Angle Detector	7315	Issued on Sept. 24, 1965 but must be revised to reflect the change to a digital device.
Solenoid	7333	Procurement changed from a specification controlled component to a piece-part procurement. Piece part drawing R-4606 has been prepared and awaiting final decision on parameters before issuance.

## 2.3.3 DEVELOPMENT ENGINEERING

### 2.3.3.1 CPD Design Review

The first Design Review for the CPD was held at GE on February 12, 1965. Two consulting engineers from the General Electric Advanced Technology Laboratories (L. G. Gitzendanner and B. D. Bedford) attended, together with several engineers from the Spacecraft Department whose assignments on the ATS Program assured critical comments of the CPD design. The morning session was devoted to a description of the components of the CPD and their function. Questions raised in this session were placed on the agenda for discussion during the afternoon.

The design Review confirmed the concept and design of the Combination Passive Damper. Several constructive comments made during the session will be incorporated in the fabrication and testing of the GE portion of the CPD.

### 2.3.3.2 Diaphragm Clutch Tests

The clutch diaphragm development entered an experimental phase in this quarter. Sample plain Belleville washers not designed for this specific application were tested. They did flip through, but there was less difference in flipping from one direction than from the other, than was indicated in the calculation. The washers tested did not have either the force or deflection required for the CPD clutch. Also it was found that the use of "fingers", needed to apply the load near the axis of the narrow washer, decreased the spring torque by one half or more. It was decided that it would be easier to develop a fluted diaphragm to the requirements of the CPD.

The corrugated Belleville washer shown in Figure 2.3-3 of the Second Quarterly Report was fabricated. It performed very poorly, by going only slightly past the mid point. Fabrication of this design was found to be much more difficult than the square fluted washer shown in Figure 2.3-7; therefore, this design has been given very low priority.

Shop drawings were made of the back-to-back fluted diaphragm shown in Figure 2.3-7 of the Second Quarterly Report. Tests already run on the square fluted design showed good promise of success, so no further work has been done on the back-to-back design. It was planned to use the square fluted diaphragm and tests were run to determine thinness and stress relieving techniques.

Figure 2.3-7 shows a square fluted washer, its pivot ring, and test housing. Figure 2.3-8 shows those parts assembled for testing. A number of tests have been run on washers of this general design. Figure 2.3-9 shows the results for one .014 inch thick washer. The decrease in load indicates yielding at the inner diameter. This had been indicated by the high stresses calculated during analysis. Visual inspection revealed no cracking or other failure. It should be noted that the washer will be flipped only about 60 times in actual service including ground testing.

Tests of a washer of the same design but .012 inch thick showed very little yielding and followed the curve obtained by analysis very closely. The loads, however, were lower than desired for the clutch. Figure 2.3-10 shows the results of tests on a diaphragm like that of test Figure 2.3-9 except a slot .1 inch deep (radially) and .12 inch wide was cut in the webs on the ID. The purpose was to relieve the high stresses at that point. This was accomplished because the yielding (change in load over a number of flips) was within experimental accuracy.

Due to changes in clutch geometry to improve failure mode operation it was desired to increase the stroke of the spring. This was done by using a smaller diameter pivot ring. The results on one spring is shown in Figure 2.3-11. The reason for the force increasing as a function of operating cycles has not been clearly established.

Another spring made to the same dimensions was tested and the results are shown in Figure 2.3-12. This washer showed much less increase in load with number of flips and also lower maximum load. More investigation is required.

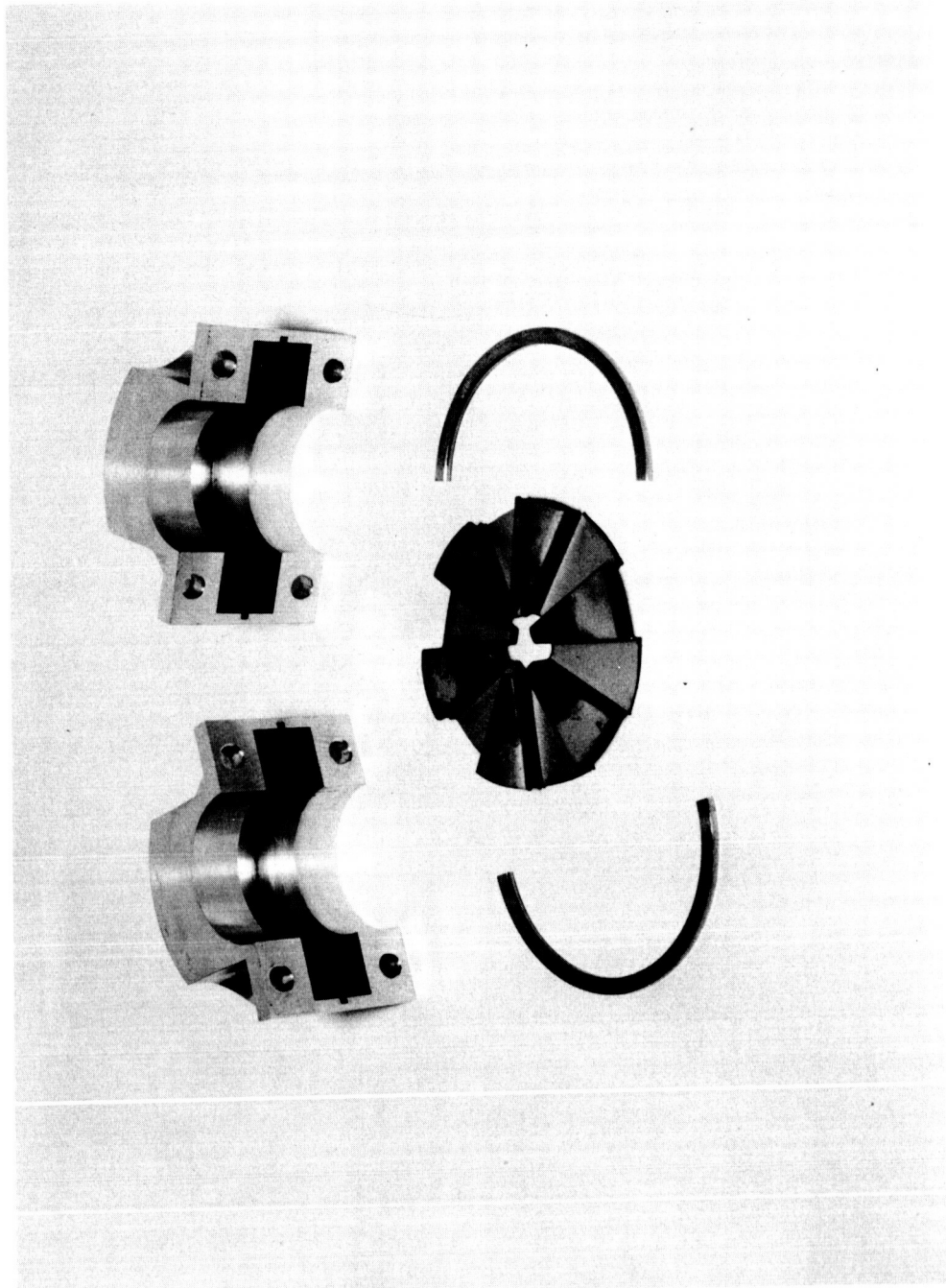


Figure 2. 3-7. Square Fluted Diaphragm

Shop drawings were made of the back-to-back fluted diaphragm shown in Figure 2.3-7 of the Second Quarterly Report. Tests already run on the square fluted design showed good promise of success, so no further work has been done on the back-to-back design. It was planned to use the square fluted diaphragm and tests were run to determine thinness and stress relieving techniques.

Figure 2.3-7 shows a square fluted washer, its pivot ring, and test housing. Figure 2.3-8 shows those parts assembled for testing. A number of tests have been run on washers of this general design. Figure 2.3-9 shows the results for one .014 inch thick washer. The decrease in load indicates yielding at the inner diameter. This had been indicated by the high stresses calculated during analysis. Visual inspection revealed no cracking or other failure. It should be noted that the washer will be flipped only about 60 times in actual service including ground testing.

Tests of a washer of the same design but .012 inch thick showed very little yielding and followed the curve obtained by analysis very closely. The loads, however, were lower than desired for the clutch. Figure 2.3-10 shows the results of tests on a diaphragm like that of test Figure 2.3-9 except a slot .1 inch deep (radially) and .12 inch wide was cut in the webs on the ID. The purpose was to relieve the high stresses at that point. This was accomplished because the yielding (change in load over a number of flips) was within experimental accuracy.

Due to changes in clutch geometry to improve failure mode operation it was desired to increase the stroke of the spring. This was done by using a smaller diameter pivot ring. The results on one spring is shown in Figure 2.3-11. The reason for the force increasing as a function of operating cycles has not been clearly established.

Another spring made to the same dimensions was tested and the results are shown in Figure 2.3-12. This washer showed much less increase in load with number of flips and also lower maximum load. More investigation is required.

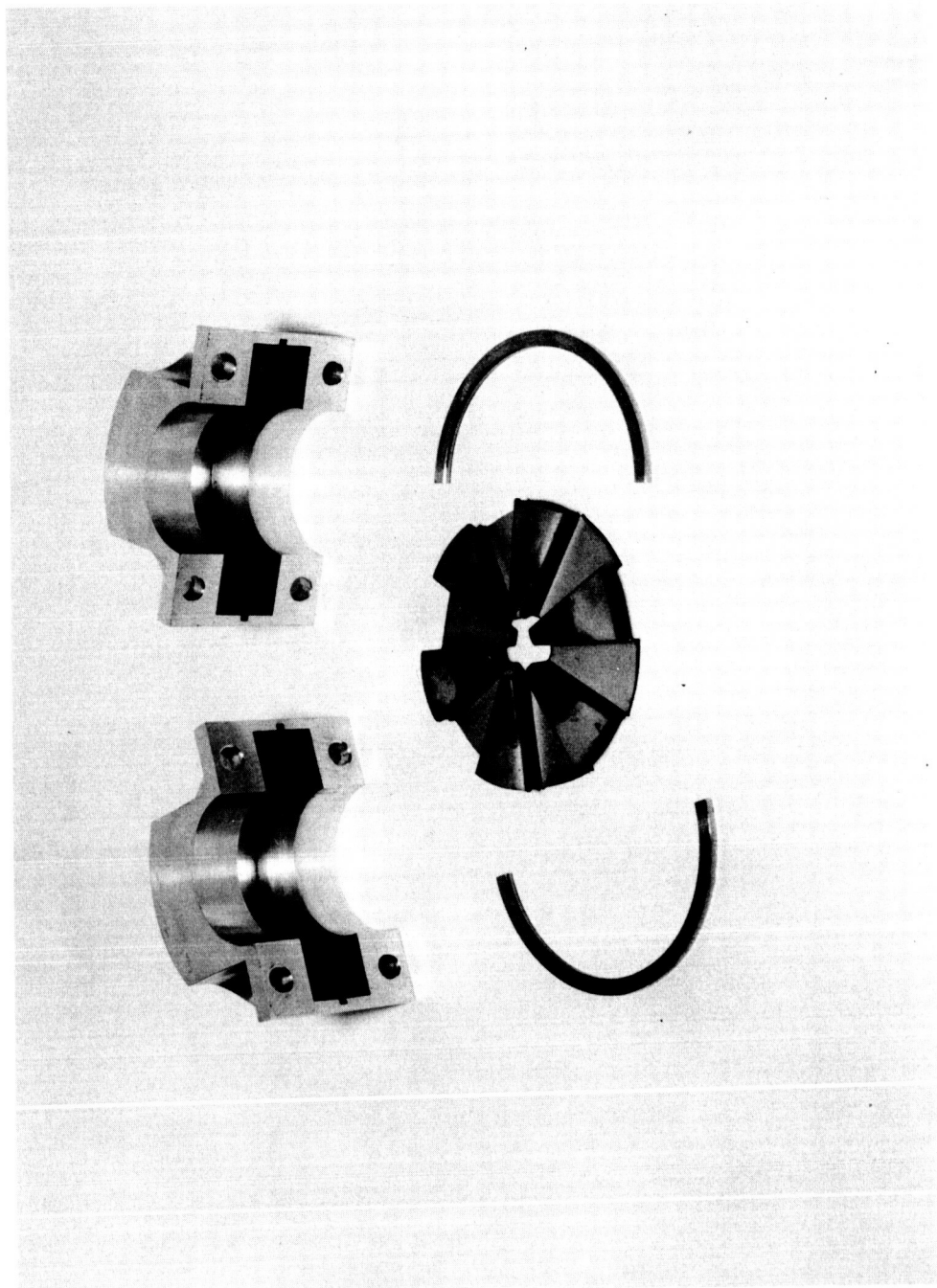


Figure 2. 3-7. Square Fluted Diaphragm

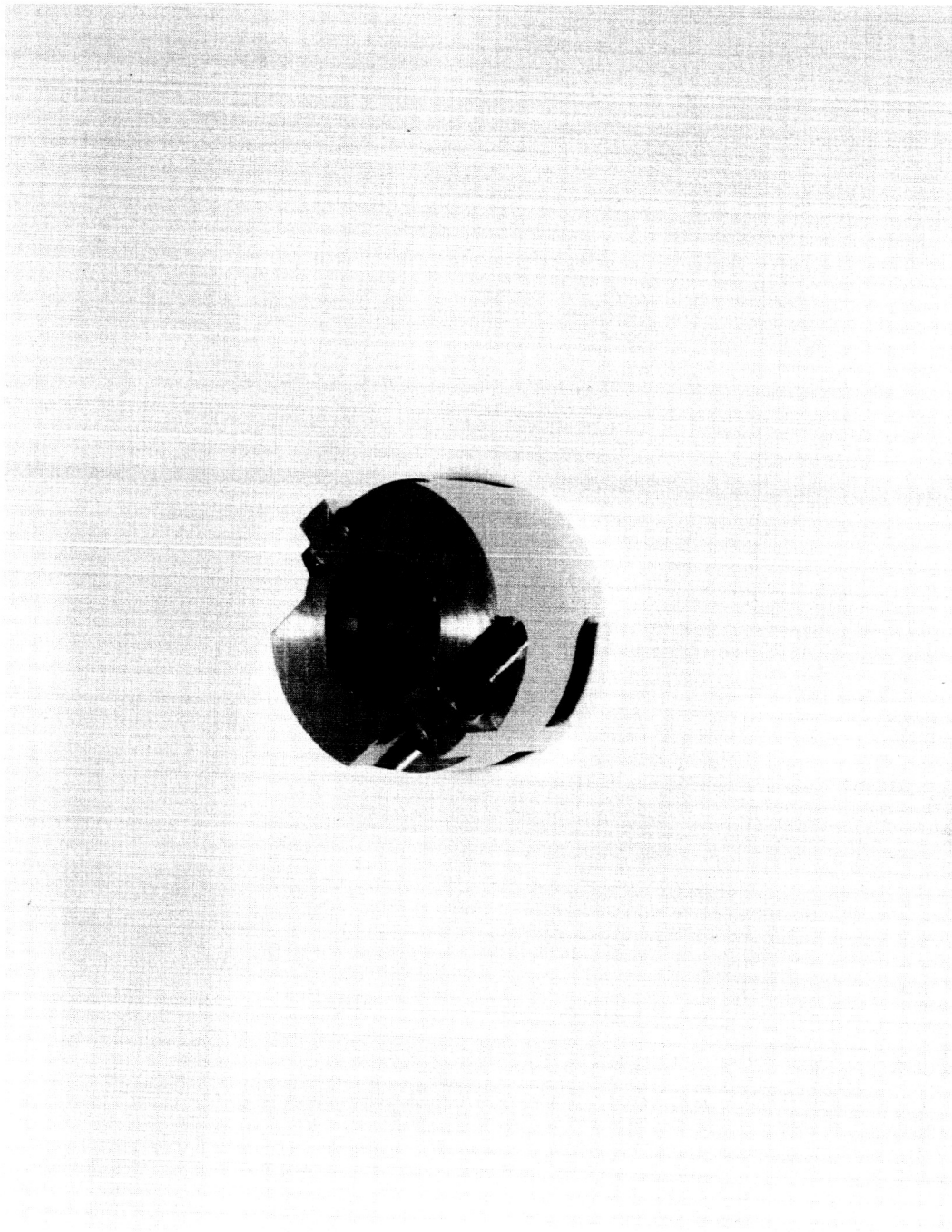


Figure 2.3-8. Fluted Diaphragm Assembled for Testing



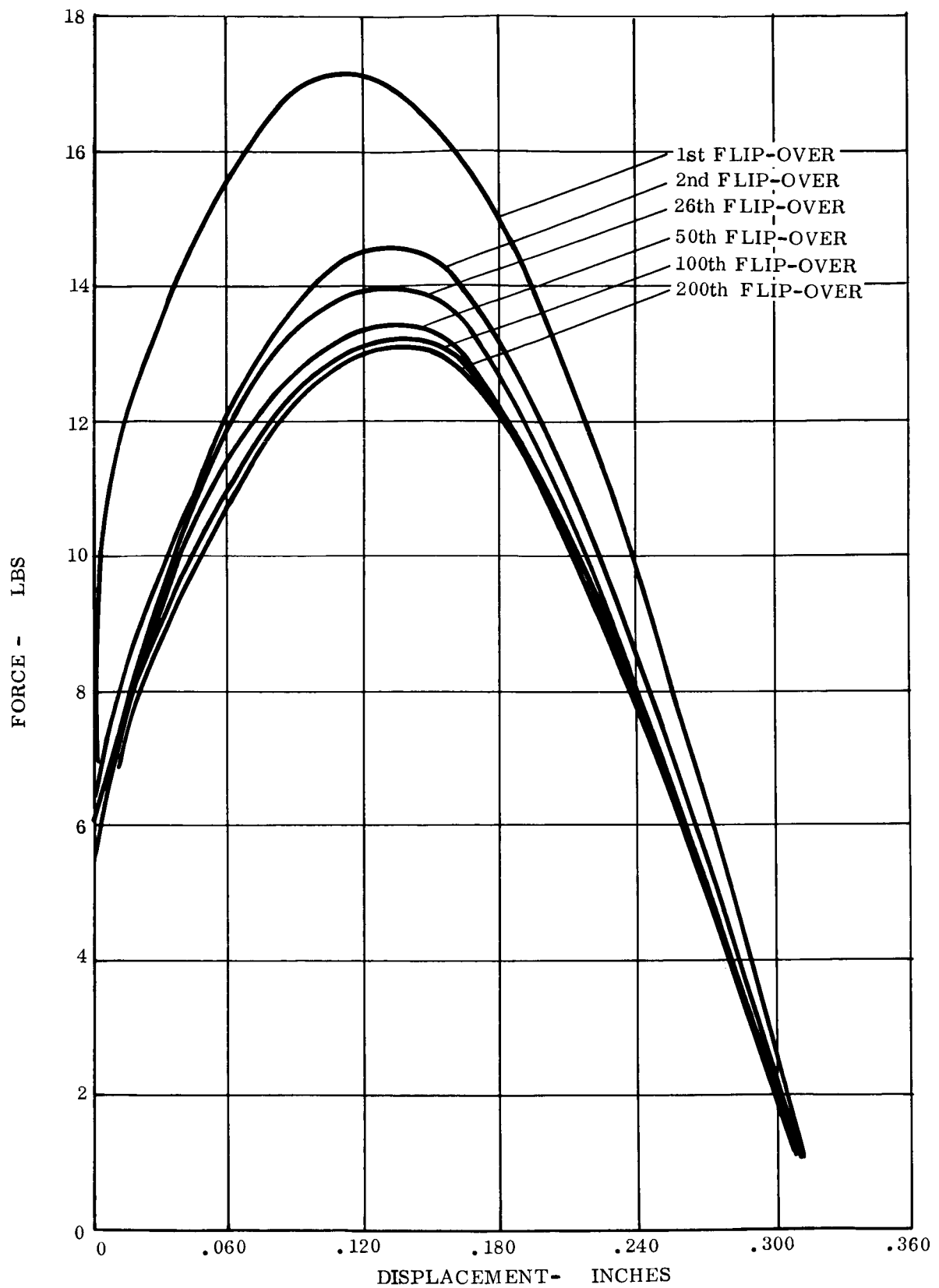


Figure 2.3-9. Force vs. Displacement for Square Fluted Diaphragm  
(.014 in. beryllium copper)

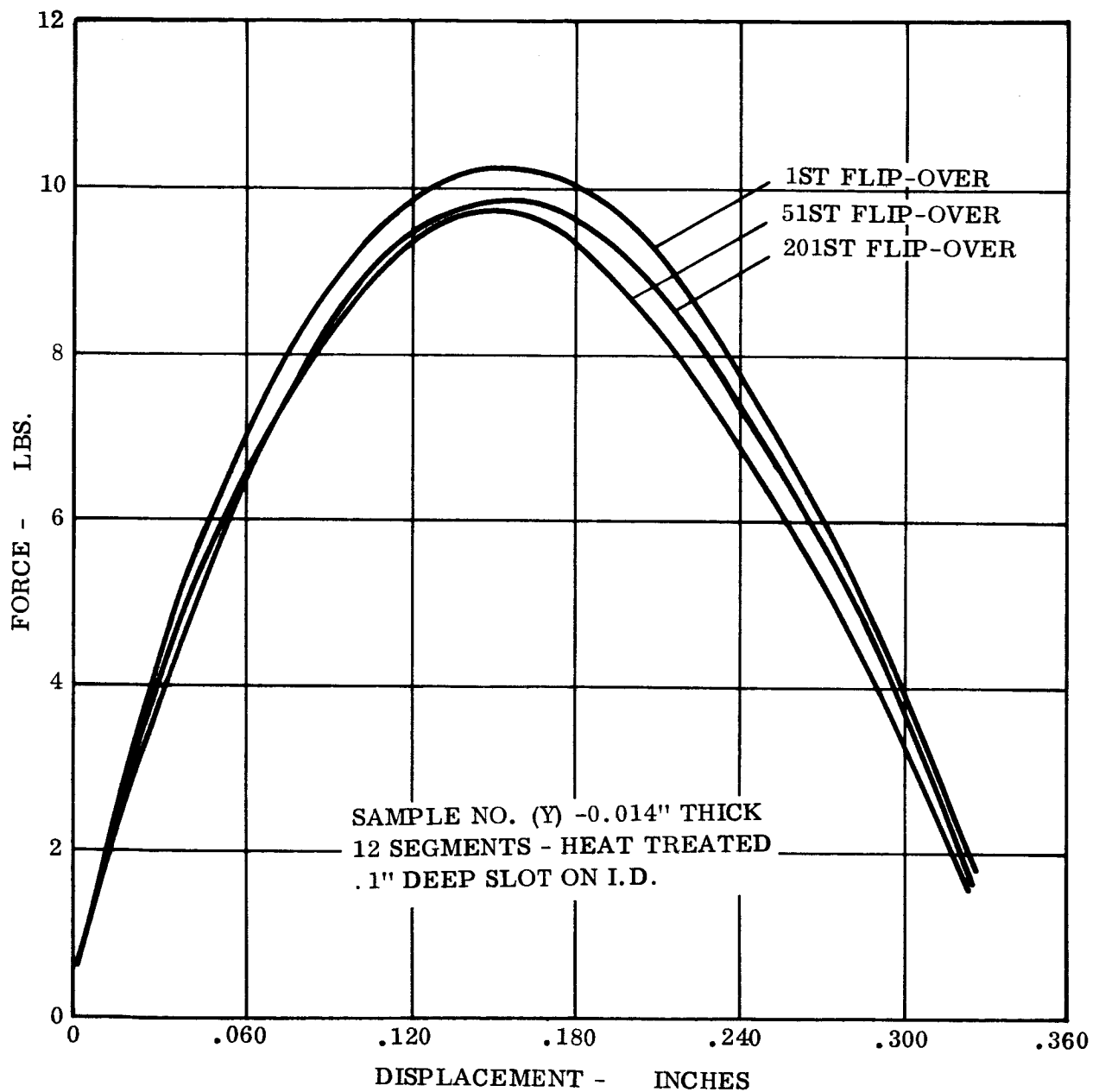


Figure 2.3-10. Force vs Displacement for Corrugated Belleville Spring (.012 in. Beryllium Copper)

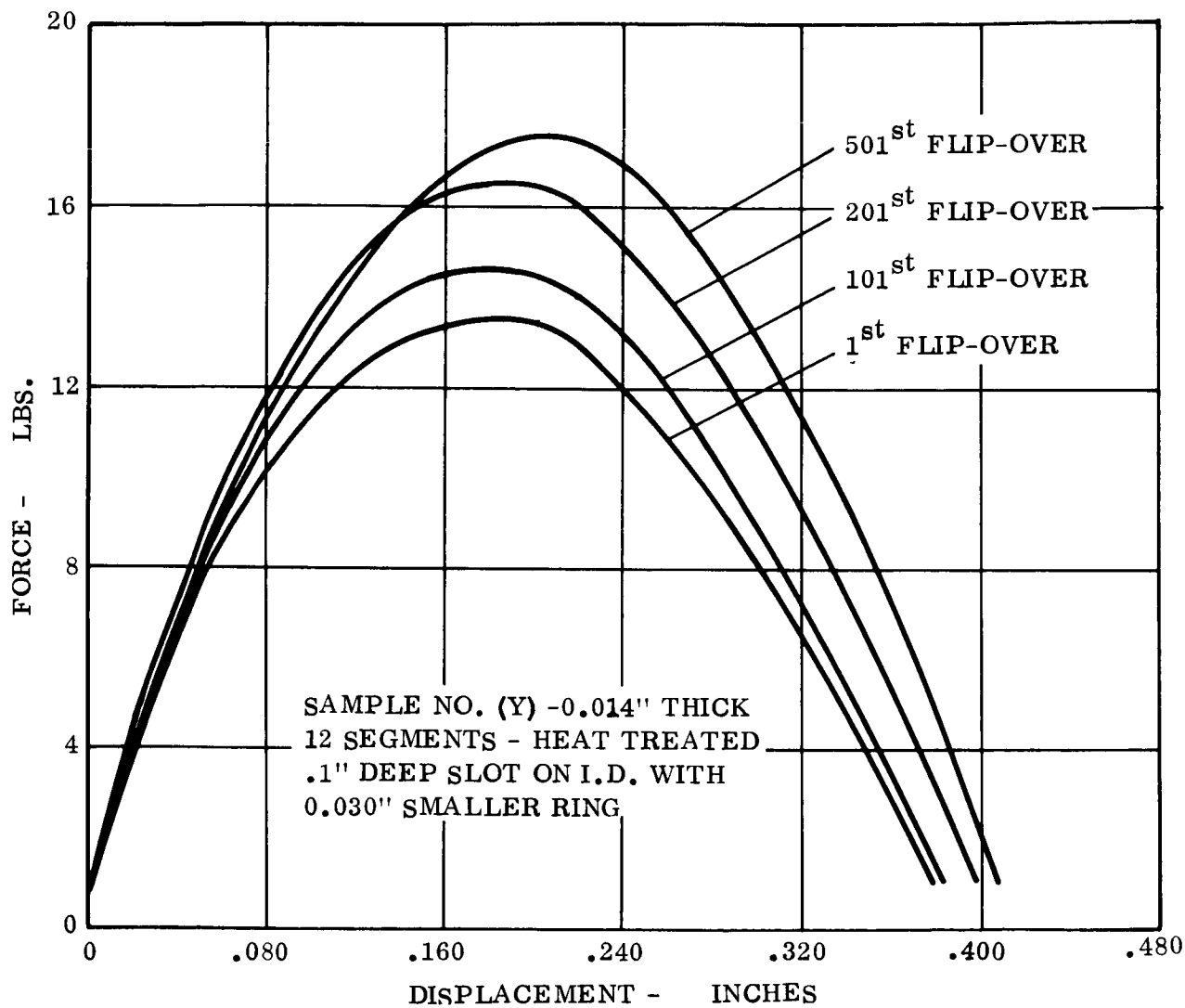


Figure 2.3-11. Force vs Displacement for Corrugated Belleville Spiral with Increased Stroke, First Sample

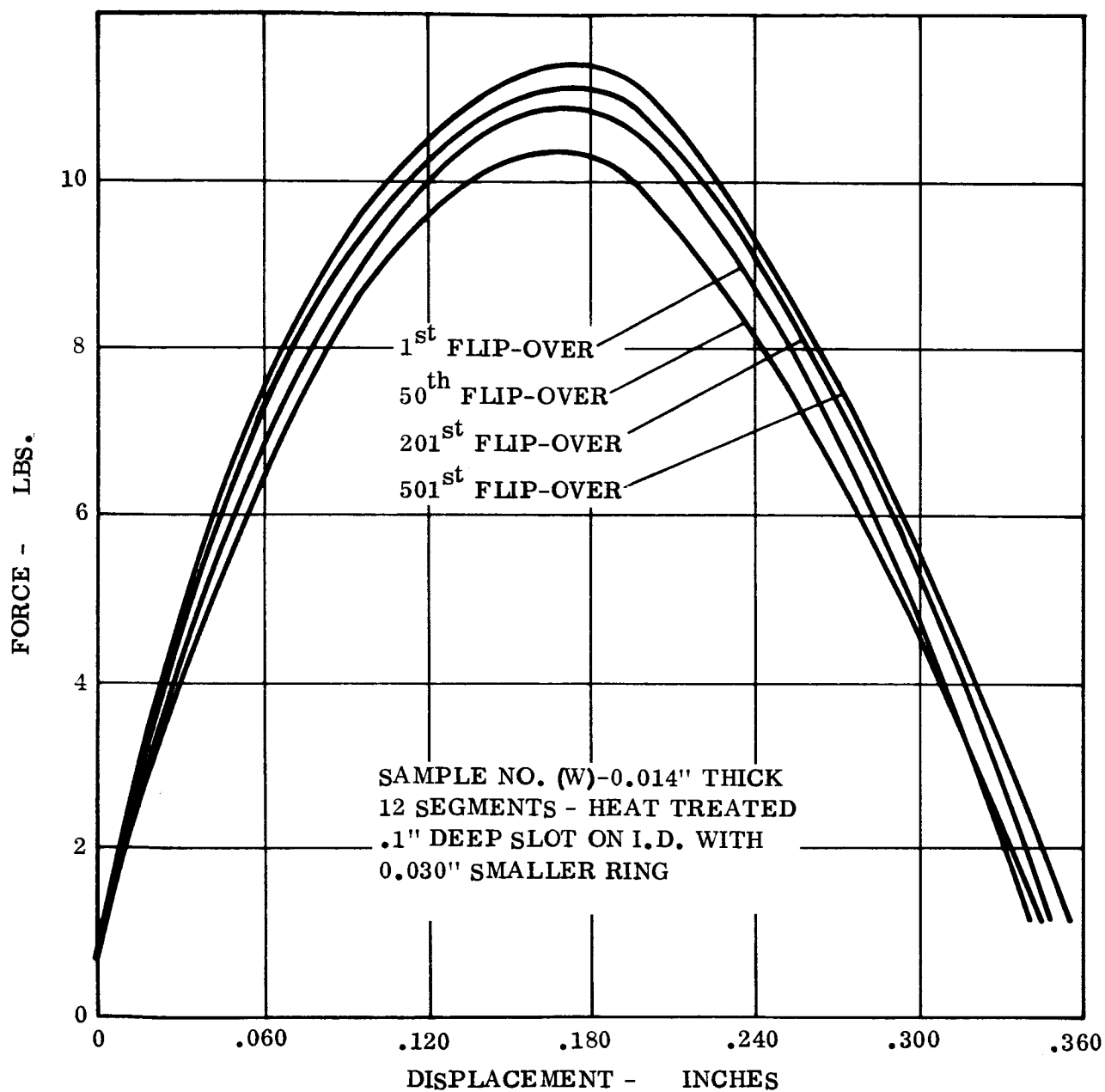


Figure 2.3-12. Force vs. Displacement for Corrugated Belleville Spring with Increased Stroke, Second Sample

All tests to date have shown the flipover points to be well within the .050 inch tolerance allowed in the clutch design.

The pivot rings used in the tests have been of Type 303 stainless steel. It has shown some grooving and copper wipe-off where the washer rubs. This type of stainless steel cannot be used in the damper because its magnetic permeability is relatively poor compared to the diamagnetic materials used in the damper. Molybdenum has been ordered for use in these rings. Its magnetic properties are satisfactory and it should provide a better bearing surface for the beryllium copper washer. It is planned to make simulated life tests of the washer-ring combination in a vacuum.

### 2.3.3.3 Eddy-Current Damper

#### 2.3.3.3.1 Damper Tests

Tests were conducted to measure the damping coefficient for the eddy-current damper disc, using copper, high purity aluminum, and raw stock aluminum. The damping coefficient of the copper disc surpassed the design goal of 1,500,000 dyne-cm-sec by 17%, but the aluminum disc fell short of the goal by 22% and 25%, respectively. The copper disc weighs about 1.0 pound, as compared to 0.3 pound, for aluminum. Two approaches were used to try to satisfy the design goal with aluminum discs. The first approach was to increase the magnet gap to permit the use of a thicker disc; the second approach was to increase the gap flux density by use of longer magnets. Both approaches proved inadequate, and use of the copper disc was specified.

#### 2.3.3.3.2 Location of Damping Magnets

Laboratory tests were conducted which showed that the functional characteristics of the magnetic torsional restraint element can be adversely affected by insufficient distance between the torsional restraint element and the eddy-current damping magnets. The locations of the damping magnets and the torsional restraint elements were rearranged on the

design layouts to improve the linearity and hysteresis characteristics of the torsional restraint. Subsequent tests confirmed that the revised arrangement reduced the adverse effects to about 10% of their original values.

#### 2.3.3.3.4 Diamagnetic Suspension

Diamagnetic repulsion force measurements were made to determine the effect of high temperature. A 13 percent loss in force was suffered when the pyrolytic graphite temperature was elevated to 200<sup>o</sup>F, as compared to the force previously determined for room temperature conditions. When the pyrolytic graphite was returned to room temperature, the full force was recovered, showing that the change was reversible. It should be noted that the suspension design of the current CPD is sufficiently conservative that no design changes will be required for the purpose of supporting the specified loads at the high temperatures.

Diamagnetic repulsion force measurements were made to determine the effect of pyrolytic graphite surface contaminants. The series of tests involved a pyrolytic graphite specimen subjected to various degrees of maltreatment, ranging from a perfectly clean specimen to a specimen with iron filings rubbed into the graphite surface. The general conclusion from these tests was that normal laboratory and assembly procedures would not contaminate the pyrolytic graphite severely enough to cause a reduction in suspension forces. No measurable force degradation was observed, for example, after a magnet was forcibly rubbed against the front surface of the graphite for 30 seconds or more. The same result was obtained after a piece of low carbon steel was forcibly rubbed against the graphite, scratching its surface and leaving graphite shavings on the surface. In the next test, the surface was covered with iron filings which were rubbed into the surface using a piece of low carbon steel. The excess filings were removed by tapping the specimen. Only a 33 percent reduction in force was suffered after this severe treatment. Only if a significant portion of the pyrolytic graphite should become so contaminated would the suspension be significantly degraded. The probability of this occurring is considered extremely small, under normal handling conditions.

A mathematical model was constructed to facilitate the optimization of the design for the diamagnetic suspension. A key feature of this model is the inclusion of the lateral attraction force of the magnetic torsional restraint. This lateral force acts as a load on the suspension, tending to move the rotor away from its null position, with a force whose magnitude is proportional to the rotor displacement off null. Its behavior is that of a negative spring force.

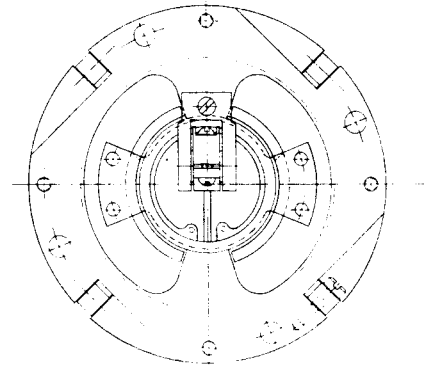
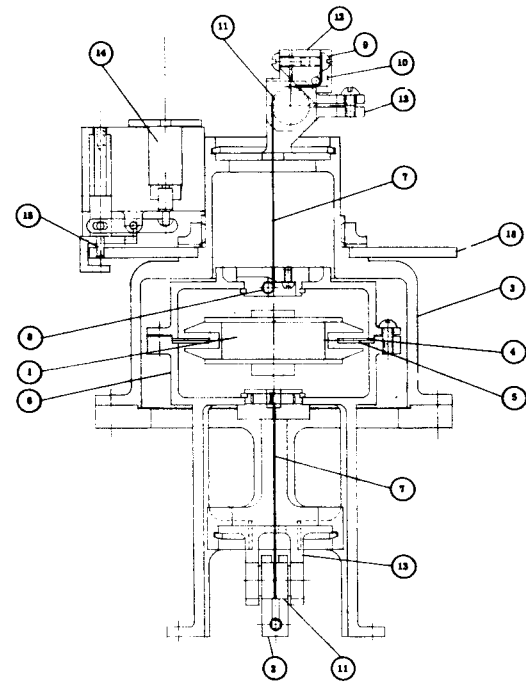
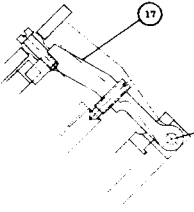
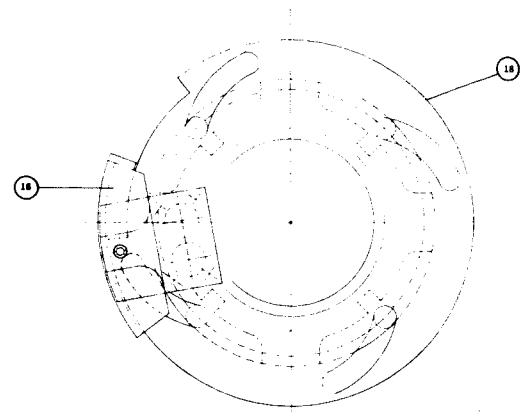
A digital computer program was written for a two-degree-of-freedom linear approximation of this mathematical model. This program has been used to aid in the selection of design parameters, and to evaluate the effect on the suspension of possible changes in the specified values for external cocking torque and radial force.

#### 2.3.3.4 Hysteresis Damper (GE Design)

##### 2.3.3.4.1 Mechanical Design

Figure 2.3-13 shows the Stage III layout of the hysteresis damper design. It consists of the following basic systems:

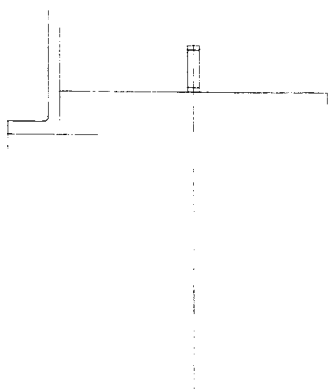
- |                |                       |
|----------------|-----------------------|
| (1) Damping    | (3) Caging            |
| (2) Suspension | (4) Support Structure |



1



18



*HYSTERESIS DAMPER*

*DRAWN BY: S. ANAGNOSTOPOULOS*

*DATE: 2-11-65*

SK 56130-808-43

2

Figure 2.3-13. Layout of the GE Hysteresis Damper Design

The damping system consists of a bar magnet (1) with pole pieces (2) supported on the component stator (3) and a thin ring of ferro-magnetic material (4) sandwiched between two thin aluminum rings (5) to support it in the component rotor (6). Discussions concerning the exact configuration and materials are contained in Paragraph 2.3.3.3.4 of this report.

The suspension system consists of two beryllium-copper wires (7) attached at one end to the rotor (6) and at the other end to the stator (3). The wires on the rotor end are wrapped around a pin (8) and anchored by placing the wire under a screw head (9) and then filling the wire hole and surrounding wire slots with SMRD-104 epoxy, a General Electric development. (10). The epoxy bonding will hold the wire in the event that the wire breaks near the anchoring screw. Since the reliability of the anchoring screw method is questionable, epoxy is necessary to provide additional assurance of a reliable attachment.

The wire on the stator end is wrapped  $90^{\circ}$  around a slotted flexure pivot (11) and then is bonded into a steel part (12) in a similar manner to the rotor end. The steel part is attached to the rotor of the flex pivot. Wire tension is controlled by twisting the flex pivot rotor, relative to the stator which is fixed to the damper stator, and locking it in place.

The stator ends of the suspension system (13) are constructed such that the rotor can be positioned in the radial and axial directions. The stator ends also allow for null adjustment of the torsional restraint system.

The flexure pivots have been selected to provide proper wire tension throughout the CPD temperature range and also to prevent the wires from breaking when the rotor "bottoms" on the stator stops during handling and testing.

The caging system consists of 2 dimple motors (14), a pin (15), a spring (16), four rotor holding arms (17), and disc (18) to change the position of the rotor holding arms. As shown in Figure 2.3-13, the four rotor holding arms are pivoted (19) on the damper mounting base and held in a "rotor locked" position by the slotted disc, so that they cage the damper rotor at its neutral position. The disc is held in a caged position by a pin (15). When it is desired

to uncage the damper, the dimple motor is detonated to cause the pin to release the disc from the damper stator. The disc position is then changed by approximately  $30^{\circ}$  ( rotates ccw as view from the top ). This rotation is produced by the spring located within the caging mechanism. Since the rotor holding arms are supported in slots in the disc, the arms are moved outward from the damper rotor causing the rotor to be released and become suspended on the wires alone. The spring tension acting between the disc and damper stator housing will maintain the damper in an uncaged mode.

The support structure is constructed basically of aluminum with 300 series stainless steel used for the flexure pivot holders. The caging device structure and disc are also aluminum. The pin and rotor support arms are 300 series stainless steel. All contacting surfaces are treated with Emralon 315 to eliminate any possibility of cold welding. Emralon 315 is a dispersion of TFE (teflon) in a special resin solution. This material provides a surface lubricant which is usable over a wide temperature range and is resistant to most chemicals. This material has been used and flown on the NRL eddy-current damper which was designed and built by GE.

#### 2.3.3.4.2 Results of Tests on GE Engineering Model

A series of tests were performed on the hysteresis damper engineering unit ( shown in Figure 2.3-6 ) to determine the dipole and suspension characteristics. The caged damper was suspended in a magnetic field, created by four-foot Helmholtz coils, with a wire having a torsional constant of 878.59 dync-cm/radian. The period of oscillation was measured with the magnet major axis perpendicular to the field and also parallel to the field. The measured dipole was essentially zero pole-centimeters with the magnet perpendicular to the field. The dipole was 506 pole centimeters when measured with the magnet parallel to the field. The test was performed in fields of 0.33 and 10.00 oersted. The dipole was then computed from the following formula:

$$K_m = \frac{K_w (P_2^2 - P_1^2)}{P_1^2 G_1 - P_2^2 G_2}$$

$K_m$	Magnet dipole in pole-centimeters
$K_w$	Wire Torsional Constant in dyne cm/radian
$P_1$	Period of oscillation, in seconds, in. 33 oersted field
$P_2$	Period of oscillation, in seconds, in. 10.0 oersted field
$G_1$	Field Strength in oersteds - 0.33
$G_2$	Field Strength in oersteds - 10.0

The suspension characteristics of the damper were checked on the LOFF. (See Figure 2.3-14.) Radial force and overturning torque tests were performed and axial force tests were omitted. The stiffeners in the axial direction far exceeds the minimum specified forces and, in fact, exceeds the normal capacity of the LOFF to measure this force level.

The radial force versus displacement tests indicated the characteristic curve was identical regardless of radial direction from which the force was applied, and it was also identical with the rotor rotated about  $40^\circ$  from the null position. The radial stiffness was found to be 244 dynes/0.001 inch displacement. ( This occurred with 0.428 pound wire tension. ) The radial force data agreed with calculated values.

The overturning torque restraint was determined to be 18,700 dyne-cm per degree. This data also agreed with the calculated value. It was previously reported that the data was approximately 5 percent from the calculated value. Since that time tests were performed on the flexure pivots and the data indicated the performance to be within 3 percent of the manufacturer's rating. On future units, all flexure pivots will be calibrated, and matched pairs will be used in each assembly to insure proper wire tension. The limitations of the fixtures used to assemble the engineering unit to properly tension the wire will also be overcome. It was originally thought that the wire tension was 0.45 pound. Later testing showed

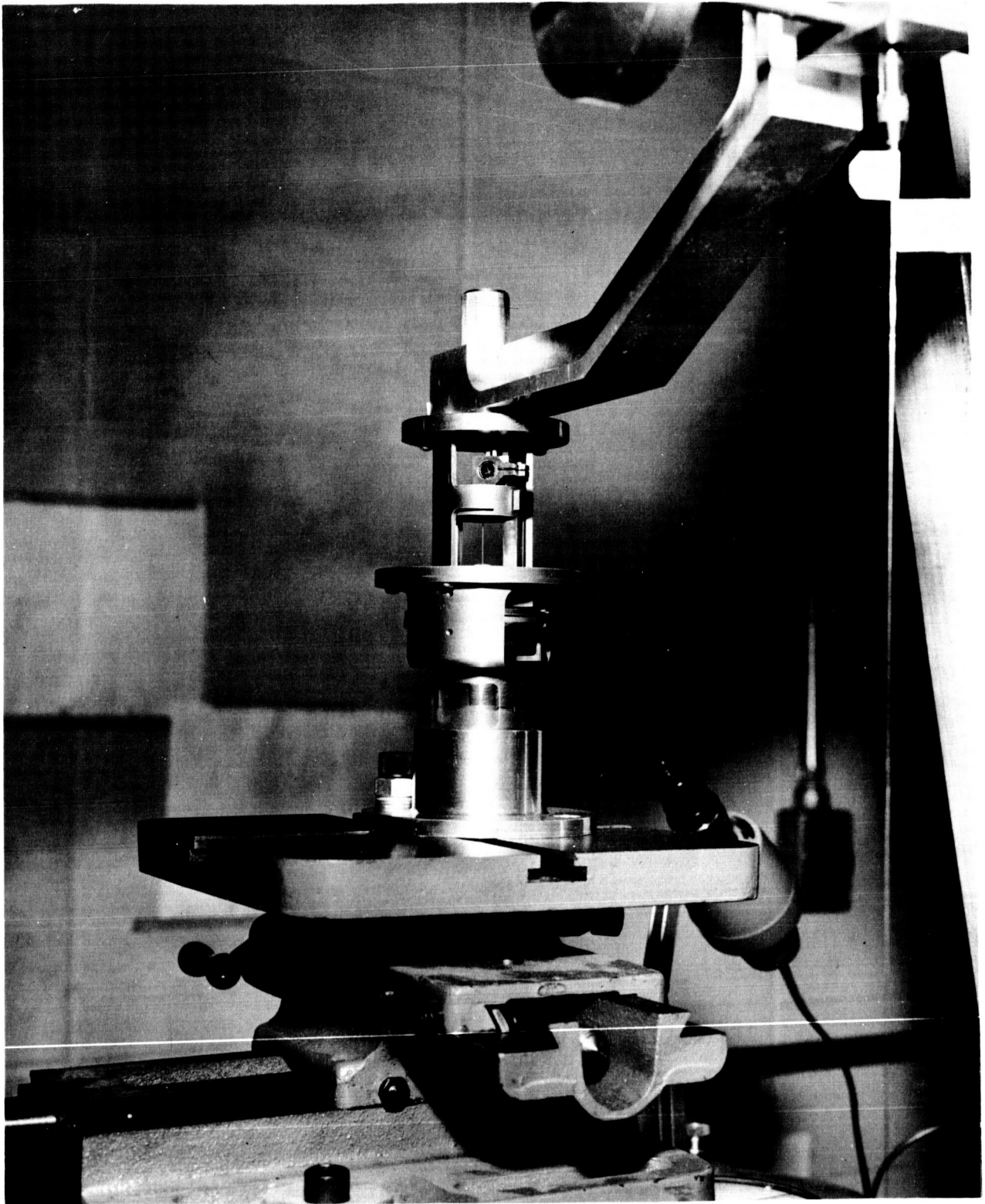


Figure 2.3-14. Load Carrying Capability Measurement Test Setup on the Low-Order Force Fixture

it to be 0.428 pound, or approximately 5 percent lower than that which the calculated values were obtained.

Tests were run on the epoxy bonding of the suspension system wires. In all tests run the wires broke prior to the epoxy bond. The epoxy used is SMRD-104. It is a flexible, sterilizable epoxy compound. Data is being accumulated on shear strength over varying temperature ranges and on long term creep.

These same tests gave data on the ultimate tensile stress of the wires for the ATS-A and ATS-D/E dampers. The data indicated the ultimate stress to be 139,000 psi. This was for beryllium-copper wire supplied with a rating of 110,000 to 135,000 psi. It is desired to use beryllium-copper wire with a rating of 190,000 to 225,000 psi ultimate tensile strength, therefore it will be heat treated to a hardness designation of "3/4 HT" to "HT."

#### 2.3.3.4.3 Tests on GE Hysteresis Damper Elements

In order to further verify the presence of ripple or variations in the level of hysteresis damping torque which was reported previously, the test setup was changed from the single to a double tension wire suspension. The double torsion wire suspension holds the damping disc from two tension wires, one from the above and one from below, and gives added stability to prevent lateral movement. It conforms closer to the Bell Telephone Laboratories test configuration. It has a disadvantage of allowing less than 360° rotation; the single tension wire permitted complete rotation. Appendix N contains the detailed results of the tests that were run. A summary of the information gained is included below.

The tests run on the double torsion wire showed no appreciable difference in damping level or magnitude of ripple from the results of the single torsion wire. Damping discs obtained from BTL were measured on both the single and double torsion wire suspension. These discs showed the same magnitude of damping and ripple as measured on discs that were fabricated by GE.

The test on the GE and BTL discs, with single and double torsion wire suspension, all indicate the presence of ripple. There seems to be very little doubt that ripple does exist in the discs as a result of theoretical analysis and test results.

#### 2.3.3.5 Angle Detector

##### 2.3.3.5.1 Design Status

GE has designed an angle detector meeting the requirements of Specification SVS-7315, to replace the one proposed by Dynamics Research Corporation (DRC). The decision to make the angle detector "in house" was made due to high costs, circuit complexity, and design problems associated with DRC's approach. The basic advantages of the GE design are: digital output, simple straight-forward circuits, redundant light source, temperature insensitive over the specified ranges, and lower cost.

##### 2.3.3.5.2 Description of GE Design

Angle detection is accomplished with the system shown in Figure 2.3-15 by using a coded disc (1) mounted to the damper boom shaft through which light is passed from one of two light sources (2) and (3) onto photo transistors (4). The disc code utilizes an expanded Gray code and by taking advantage of the increasing allowable error of angle detection going away from null, ( $\pm 1^\circ$  from  $+10^\circ$  to  $-10^\circ$  and  $\pm 10\%$  from  $+10^\circ$  to  $+45^\circ$  and  $-10^\circ$  to  $-45^\circ$ ), it is only necessary to use five bits. An additional five bits are used to compensate for radial and cocking motions of the damper boom shaft. Compensation is not required for axial motions. Typical outputs for any one shaft position would consist of three, ten-bit digital words, all of which are unique to that one position. The multiple words at each position are due to radial excursions of the damper boom shaft. The digital words will be catalogued and can be read directly or fed into a computer to give direct angular readout. The light supply consists of a fiber optic bundle (5), one end of which is divided into ten small bundles (6) each of which is aligned to a photo transistor (4). The other end is divided into two bundles (7) and (8) each of which is placed in the field of a collimated light beam coming from a tungsten filament lamp (9). The fiber optic bundle consists of approximately 5,000 individual fibers that are scrambled in such a manner that one-half of the

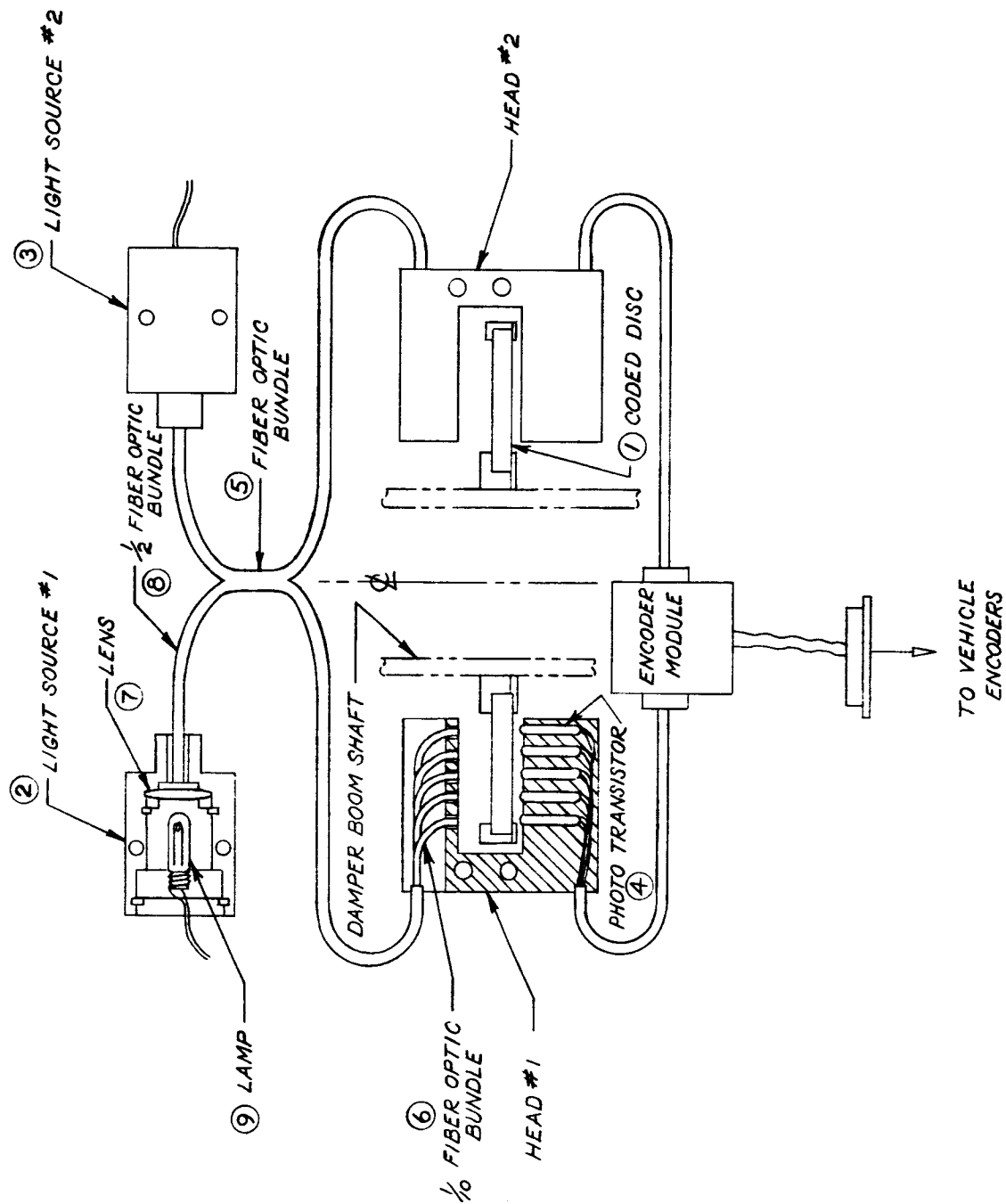


Figure 2.3-15. Boom Angle Detector



individual fibers opposite each photo transistor go to each light source, thereby producing a redundant light source because each lamp is capable of supplying the required light intensity for all ten photo diodes. Only one lamp will be used at one time; switching to the other lamp will be done by command. Depending on which lamp is selected, an average life of the lamps is from ten to fifty thousand hours. Lamp life is expressed as follows  $L \approx \frac{K}{V^{12}}$  where  $L$  = life in hours,  $V$  is the applied voltage and  $K$  is a constant. By derating the lamps 10 percent lamp life can be increased approximately three times. The photo transistors are used as a light activated amplifier. Signal processing is not required as the photo transistors are capable of handling the required voltages needed for telemetry. Figure 2.3-16 shows the electrical circuit of a typical "bit" circuit.

#### 2.3.3.6 Solenoid

The G. W. Lisk Company has been selected as the vendor for the solenoid. A solenoid was obtained from them, which has a winding closely resembling the anticipated electrical circuit of the final design. It is being used by the electronics group for circuit design evaluation. The voltage supplied to the solenoid will be regulated between 21.5 vdc and 26.5 vdc. This regulation helps in reducing the physical size of the solenoid. Previously the voltage supplied to the solenoid came from the unregulated bus. Two solenoids have been ordered per Dwg. No. R-4606 (This drawing has replaced the previously issued work statement, specification, and specification control drawing.) These solenoids will be build in accordance with the R-4606 drawing with the force requirement excepted. These units will provide information to engineering on the maximum force available in a package 3 inches long and 1.5 inches in diameter. The units will be tested with a diaphragm (clutch mechanism) assembly upon completion of the solenoid evaluation.

#### 2.3.3.7 Test Equipment

There has been no change in the status of first low order force fixture ( LOFF ), and it has been used daily for engineering development tests.

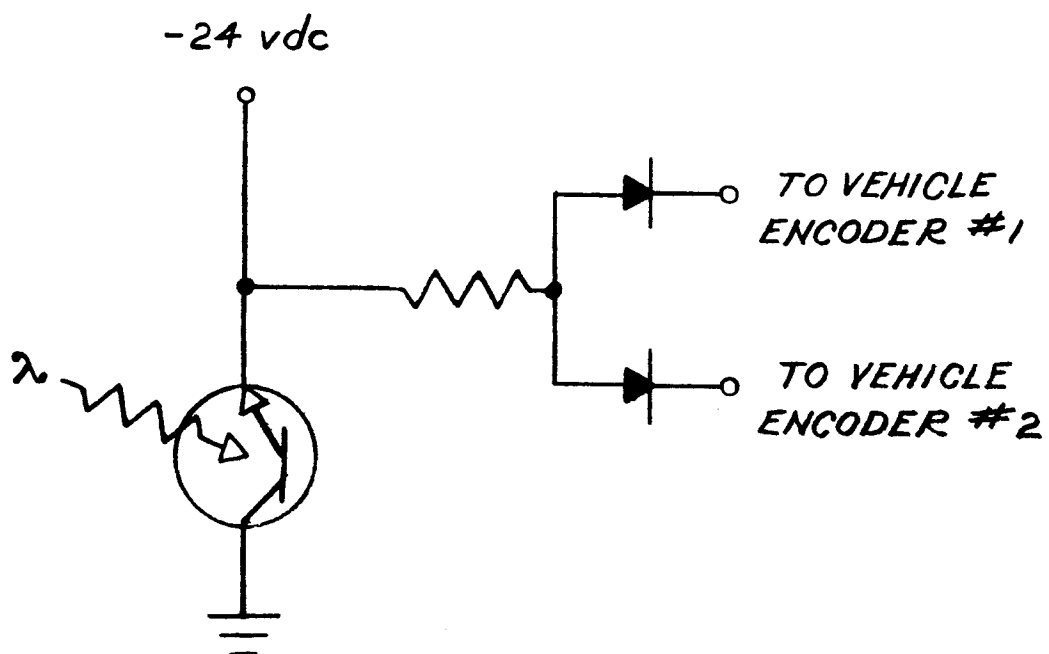


Figure 2.3-16. Typical Bit Circuit Boom Angle Detector

The LOFF No. 2 assembly is complete with the exception of the air bearing (anticipated arrival and installation is April 12th) and the CPD adapting fixtures . Design of fixtures will begin upon completion of CPD interface configuration.

The air bearing for the advanced damping test fixture (ADTF) was installed, with the torque/pickoff parts, and calibration of the system was started. Testing of the bearing indicated motoring torques and stiction torques to be less than 1.0 dyne-centimeter. Final system calibrations will be completed during the first week in April and damping tests will begin immediately. All fixtures have been completed with the exception of the CPD interface adaptors.

The four-foot Helmholtz coils used for dipole measurements have been in continuous use this quarter. CPD adapters have yet to be designed and built.

A magnetic test facility is presently being set up in a separate room at the Valley Force Space Technology Center. It will include a set of Helmholtz coils, 14 feet in diameter, a work stand and an adjustable height component/wire support. The room will be enclosed and relatively free from strong air currents. The smaller coils will also be placed in this room to provide a more versatile facility for dipole measurements.

## 2.4 ATTITUDE SENSOR SUBSYSTEM

### 2.4.1 SUBSYSTEM DESCRIPTION

The present electrical configuration of the Attitude Sensor Subsystem is shown in Figure 2.4-1. The principal component changes since the publication of the Second Quarterly Report are the deletion of the three-axis magnetic torquing coil and the definite incorporation of the two GFE infrared earth sensors on the medium altitude flight (ATS-A). As is the case with the TV camera subsystem, only one IR Earth Sensor will be flown on the two synchronous altitude flights, ATS-D and ATS-E.

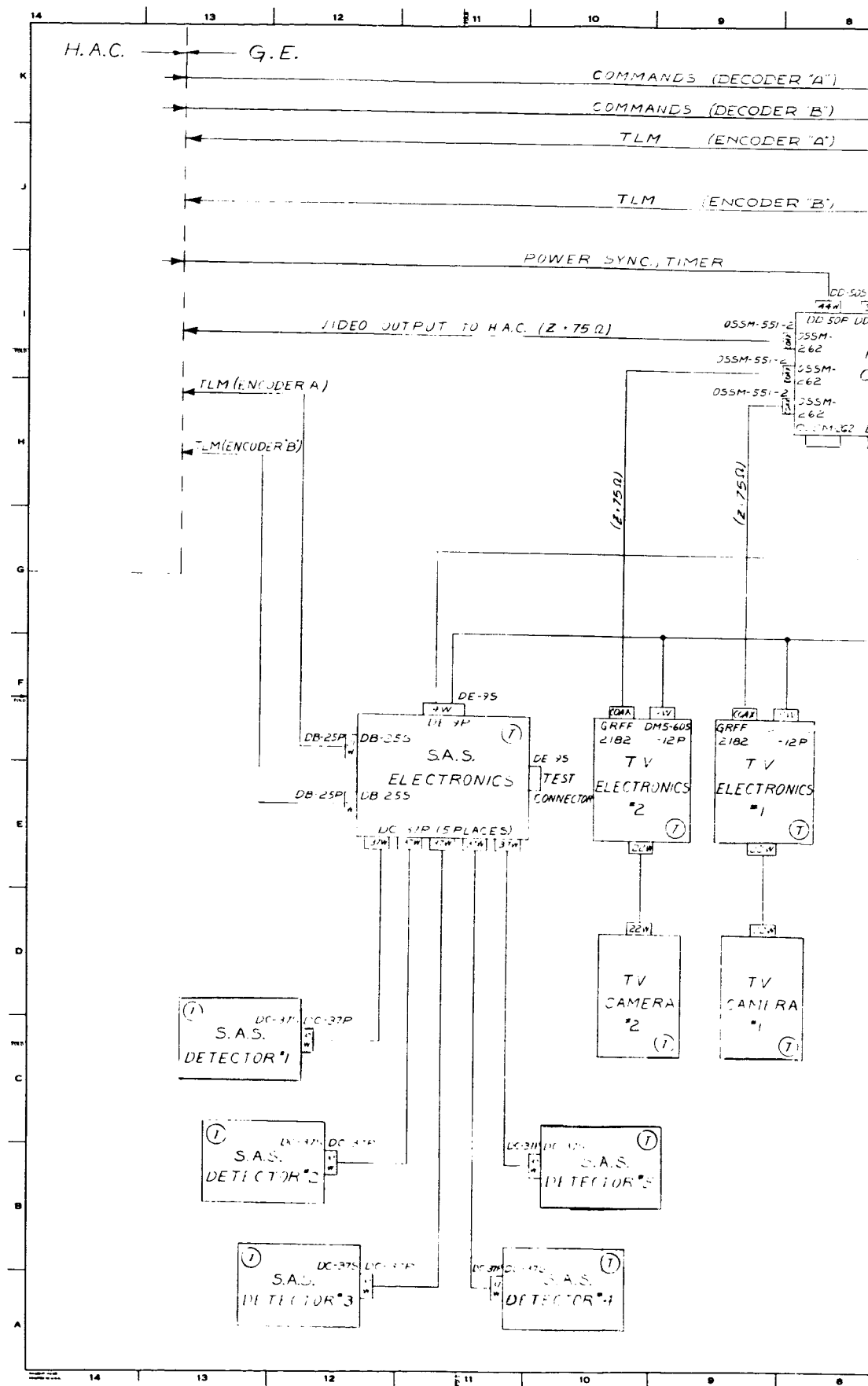
### 2.4.2 TV CAMERA SUBSYSTEM

#### 2.4.2.1 Design Activities

##### 2.4.2.1.1 Bandwidth Determination

An estimate of the overall bandwidth obtainable at the ground stations was made using assumed responses of the video amplifiers of the camera, of the down-link transmission and reception and of the ground recorder. In addition, a 10% worsening of reproduced data was assumed. Results indicated a final equivalent bandwidth between 2.25 and 3.46 mc/s based upon camera bandwidth extremes of 5.6 and 8.0 mc/s, down-link transmission and reception bandwidth extremes of 2.5 and 5.0 mc/s and ground recorder bandwidth extremes of 4.0 and 4.3 mc/s.

A Lear-Siegler TV camera Model 0431B was borrowed from the manufacturer for laboratory tests with scale model targets. With the model target having the best reflectance properties, an angular displacement of the target of 2.1 milliradians (0.12 degree) was observable using either the full camera bandwidth (5.5 mc/s) or a reduced bandwidth of 3.5 mc/s. Noise tests were also made using a random noise generator for inserting additional noise into the system. From these tests it was determined that a signal-to-noise





ratio of 20 db is the minimum usable. This signal to noise is based on peak-video signal to zero video signal level versus root mean square noise.

As a result of these tests and discussions with personnel from NASA/GSFC, the TV camera subsystem specification was revised to require a reduction in bandwidth from 8 mc/s to 3.5 mc/s by the insertion of a low-pass filter.

#### 2.4.2.1.2 Venting Investigation

The problem of venting the TVCS to ambient pressure at the time of launch was investigated. Without prior outgassing before launch, it was calculated that a vent hole of 1.5 inches would be required to obtain an internal pressure of  $10^{-5}$  mm Hg inside the electronics package. With complete prior outgassing, a vent hole of 0.25 inch is more than adequate to relieve internal pressure to a level less than  $10^{-5}$  mm Hg in the 100-minutes allowed before the camera is operated.

By reason of its smaller volume, the camera unit can theoretically be vented through a smaller size hole than the electronics unit, if its outgassing properties are comparable.

As a result of this investigation the TV Camera System specification was revised to require

- (1) That the minimum pressure at which corona can occur (if it can occur) be measured,
- (2) That the camera and electronics unit be outgassed in a high vacuum, and
- (3) That each camera and electronics unit be tested for any detectable signs of corona discharge.

### 2.4.2.2 Testing Activities

#### 2.4.2.2.1 Earth Simulation

It was decided that a simulation of the earth as seen by the TV camera would be needed for analysis of the accuracy of the attitude determination and to determine the repeatability of reading the target deflections. A three-foot plastic sphere was obtained and rendered opaque by lining it internally with white paper. The scaling factors were calculated using a  $1/2$  inch focal length lens on a vidicon camera. It is planned to simulate sunlight by means of a collimating mirror. An uncoated 60-inch parabolic reflector was obtained and arrangements have been made to have it aluminized. Preliminary tests have been made with an uncollimated light source and tests with sunlight are under consideration prior to the availability of the collimating mirror.

#### 2.4.2.3 TV Data Reduction

Distortions due to photographing a TV monitor may arise from at least two sources. Consider the geometry of a picture tube in Figure 2.4-2 with curved face and exaggerated face thickness.

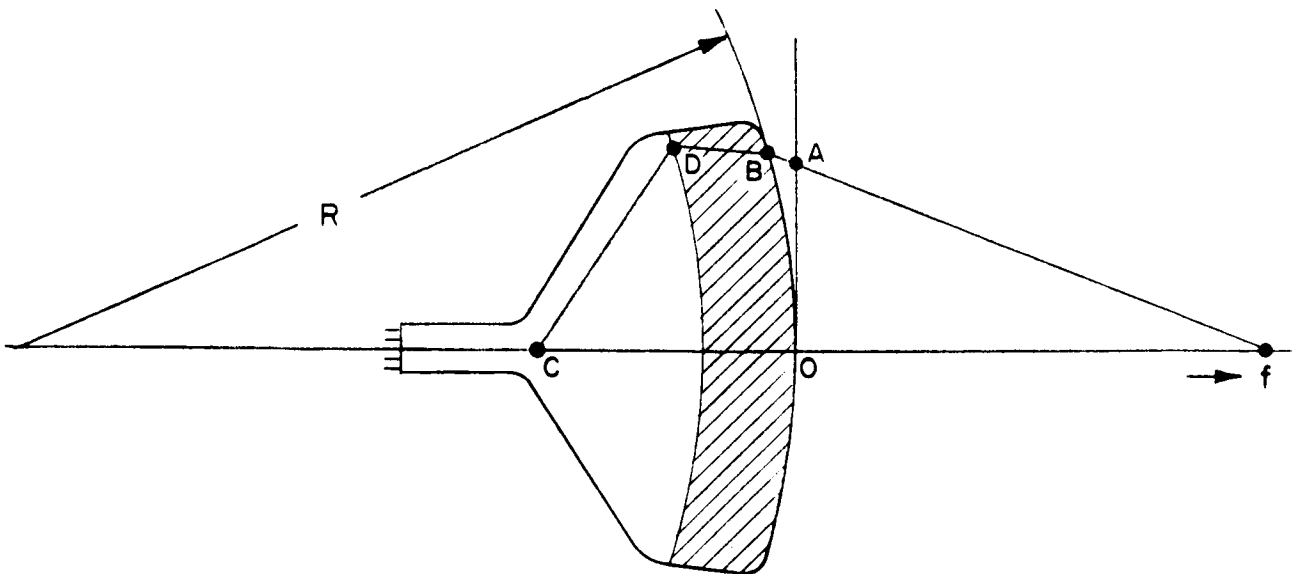


Figure 2.4-2. Geometry of a TV Picture Tube



A camera placed at f will focus properly on points in a vertical plane such as at A. A projection of the ray to B shows where the ray must emerge from the surface of the tube. If the index of refraction for the glass used is known, the point D at which the phosphor must be illuminated can be precisely located. From this drawing, three sources of error can be discerned:

1. The distance BA can be sufficient to result in defocusing if the camera is close
2. Ideally, the vertical distance at D and A should be equal but in fact differ due to BA
3. The vertical distances at D and A may also differ due to refraction within the glass.

For a 17-inch picture tube, the following values are typical:

R     $\approx$     25 inches,  
 BA    $\approx$     1 inch maximum,  
 Face thickness  $\approx$  1 centimeter,  
 Index of refraction  $\approx$  1.5 - 1.6.

Define the difference between vertical distances to D and A by an error E. It is this quantity E which we wish to minimize. An analytical solution to the problem is possible. However, by drawing the picture to scale, an assumption can be made which produces empirical results rather quickly. If this is done, it will be seen that, for camera distances of greater than about two feet, the effects of refraction are small compared to those due to face curvature and that in fact the rays all pass through the glass essentially parallel to the tube axis. With this assumption, if the vertical distance off axis is called y, a rather simple formula for the percentage error as a function of y can be obtained. This is,

$$\frac{E}{Y} = \frac{1}{R - \sqrt{R^2 - Y^2} + 1}$$

Setting  $\frac{E}{Y}$  at 1%, for example, it is found that with maximum deflection the camera distance  $f$  need be only about 7 feet. This suggests that while there are advantages to be had in a flat faced display tube, a less expensive solution might be to use camera distances of perhaps ten feet and a telescopic lens. If for some reason neither of these techniques proves desirable, then it is possible to remove barrel distortion by properly correcting the data once it is fed to a computer.

#### 2.4.3 POWER CONTROL UNIT (PCU)

The electrical design of the Power Control Unit continued during this quarter and was extended to include new requirements necessitated by changes in the Gravity Gradient Stabilization System. The packaging design also continued, although the effort was reduced somewhat pending definition of the new electrical requirements.

##### 2.4.3.1 Mechanical Design

A meeting with engineers from the Hughes Aircraft Company resulted in an agreement to change the outline dimensions of the PCU to permit a more suitable form factor for mounting in the satellite. The increased volume granted will provide the additional space required for the new functions and will allow a modest growth area.

A total of nine module drawings out of an anticipated fifteen different types have been released. Electronic parts have been ordered for the engineering units and assembly of the released modules is scheduled to begin the second week in April. No printed circuit board layouts have been released to date. Separate connectors to interface with each telemetry encoder and command decoder will be maintained in accordance with a request from the Hughes Aircraft Company. Regulated and unregulated power, synchronizing and timing signals will be combined into one connector as agreed with the HAC engineers.

##### 2.4.3.2 Electrical Design

The following paragraphs describe the electronic designs which were initiated or completed during this quarter. They are presented here in detail even though the results of recent

discussions with NASA/GSFC representatives have modified some of the design requirements since these circuits represent effort expended during this reporting period.

#### 2.4.3.2.1 Automatic Video Switch

The automatic video switch (Figure 2.4-3) alternates the signal going to the vehicle wide-band transmitter between the two Gravity Gradient TV Camera outputs whenever both systems are on at the same time. Transistor stages Q7 and Q8 act as an AND gate (negative logic) which in turn opens the AND gates consisting of Q2, CR4, and Q5, CR8 whenever both of its inputs are negative. These AND gates allow both phases of a square wave conditioned in Stages Q1 and Q4 to pass to the relay driver, Stages Q3 and Q6, which drive both the set and reset side of the Video Switch Relay. The rate of switching can be set by the timer frequency input selected from the vehicle clock.

Even though power is required for only 10 to 20 milliseconds in order to latch the Video Switch Relay in either position, it is applied to each relay coil (K1 and K2) on a 50% duty cycle basis during periods of operation. Operation in this mode keeps power dissipation within acceptable limits while reducing the number of circuits that would be required to derive the shorter pulse. This feature consumes approximately 0.5 watt during the time it is being used (i.e., when both TV systems are on); its standby power is about 40 milliwatts.

#### 2.4.3.2.2 Reference Power Supply (Figure 2.4-4)

In Figure 2.4.2-6 of the Second Quarterly Progress Report, reference power supply circuits were shown that made use of the -10 volt references coming from the HAC Telemetry Encoders. Because of the large tolerance on the output impedance of these reference voltages, they cannot be used without the insertion of buffer amplifiers, to get better than a  $\pm 0.5\%$  initial tolerance on the power supplies. It was determined that the reference power supply could be designed to use its own reference zener with fewer parts, less cost, and the same relative accuracy, while eliminating four HAC-GE interface wires.

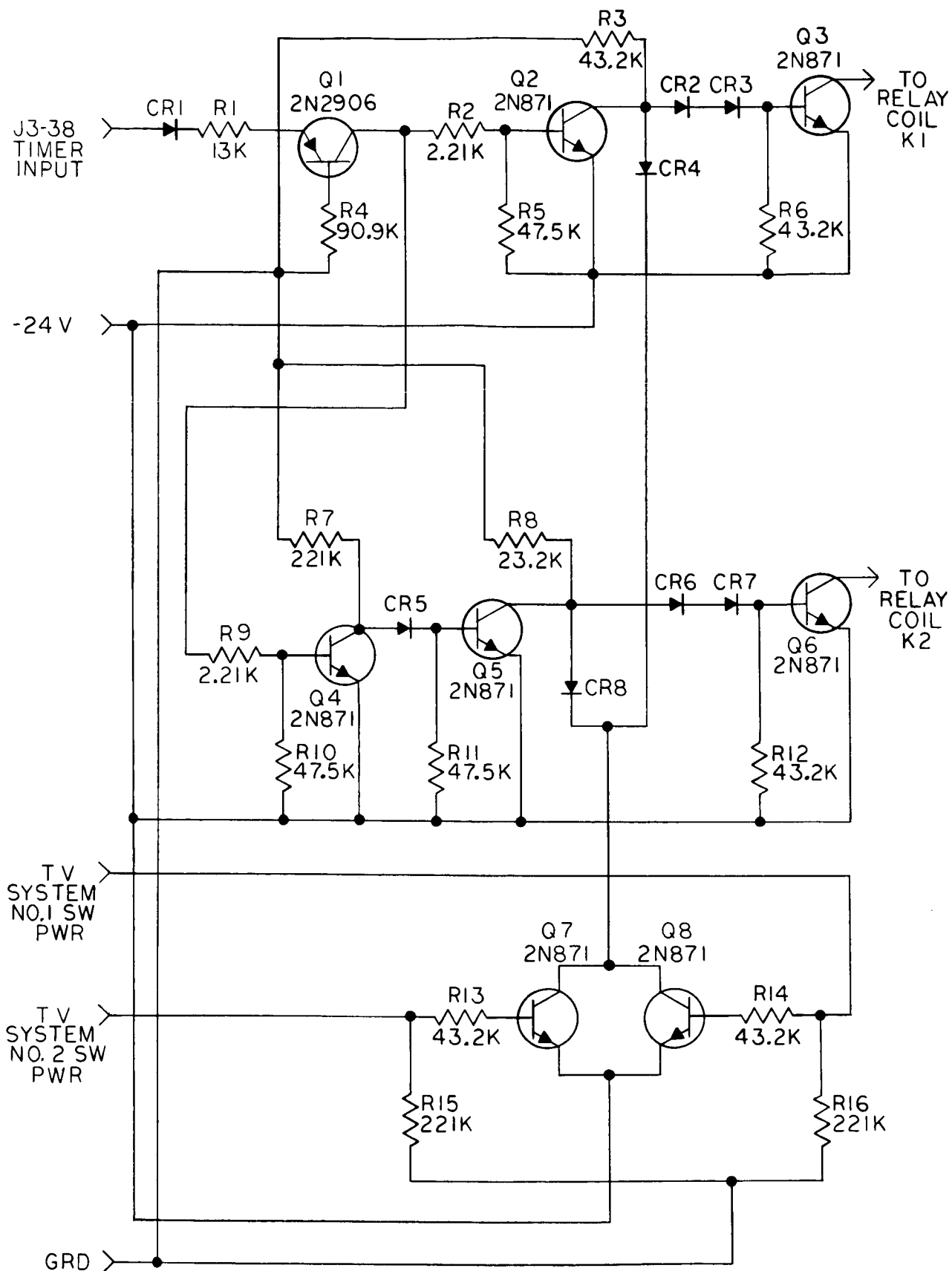


Figure 2.4-3. Automatic Video Switch

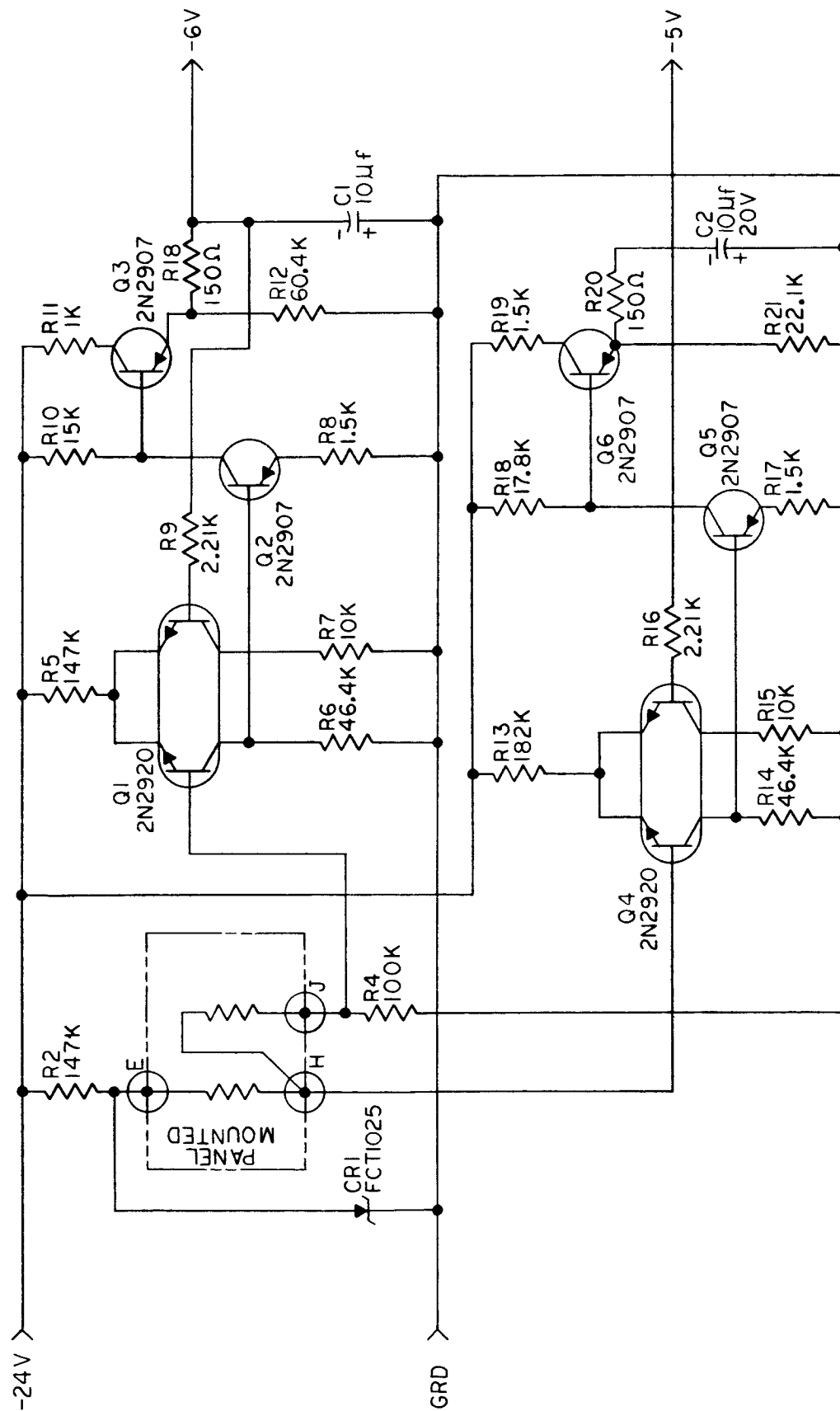


Figure 2.4-4. Telemetry Power Supply

The schematic shows two basic feedback type regulators which use the same reference element. The inaccuracies in the outputs arise from both the elements of the amplifiers as well as the stability of the reference element. The initial tolerance of the reference element is compensated by the resistor selection of the amplifier bias. The temperature drift is less than  $\pm 20$  millivolts. There could be  $\pm 5$  mv of drift in the reference due to variations in the current supplying the diode. Life test data from the diode manufacturer indicates good stability during 5000 hours of test at high stress conditions ( $\pm 3$  mv). This can be related to 3 years operation at our much lower stress level.

#### 2.4.3.2.3 Damper Clutch Solenoid Driver

In order to alleviate what was considered an unallowable weight penalty in the design of the damper clutch solenoid, it was agreed that some form of voltage regulation would be incorporated in the PCU to limit the voltage drive to both coils of this solenoid to -25 volts  $\pm 2.5$  volts instead of the -22.5 to -35 volt as would be experienced in the previous design by pulsing power to the device directly from the unregulated bus.

The schematic (Figure 2.4-5) shows the previously reported Solenoid Driver Circuit modified with a feedback network to clamp the negative excursions of output voltage two diode drops below the -24 volt bus (about 1.4 to 2 volts). As this voltage tends to go more negative than the reference, current will be drawn through the feedback transistor Q6 and rob available base drive current from the output Darlington, Q4 and Q5. Zener diode CR3 is used to establish the proper operating bias for Q6. R12 limits the available drive current to the output stage. CR5 prevents breakdown of the base-emitter junction of Q6 when the circuit is in standby. CR4 prevents leakage currents from triggering the circuit if the -30 volt bus is "ON" but the -24 volt bus is "OFF". C1 is used to roll off the amplifier to prevent unwanted oscillations.

#### 2.4.3.2.4 Separation Timer (Figure 2.4-5)

This circuit is used to control the start and stop of the initial boom deployment. Inputs from the Spacecraft Clock along with feedback position information from the rod position

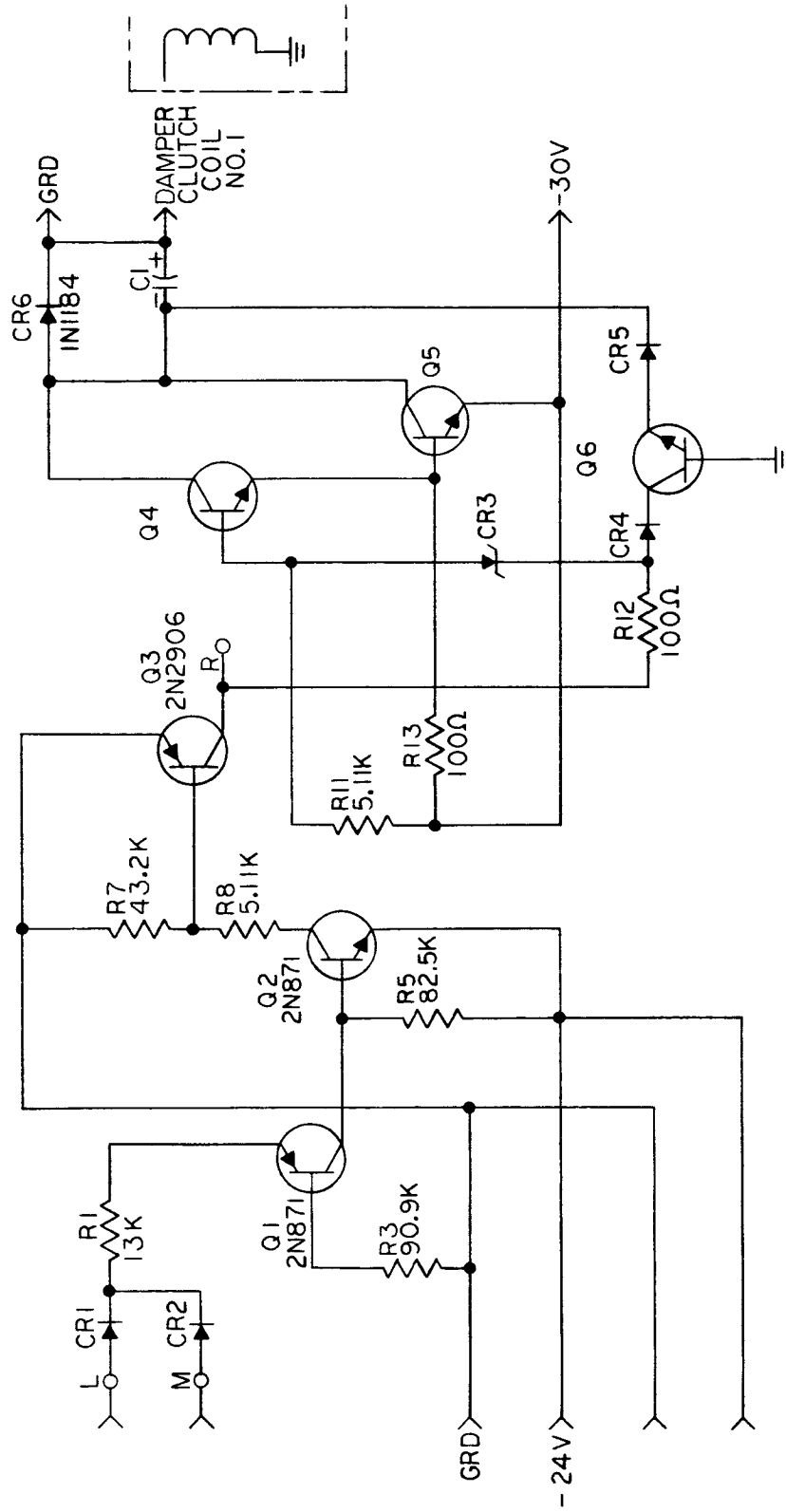


Figure 2.4-5. Damper Clutch Solenoid Driver

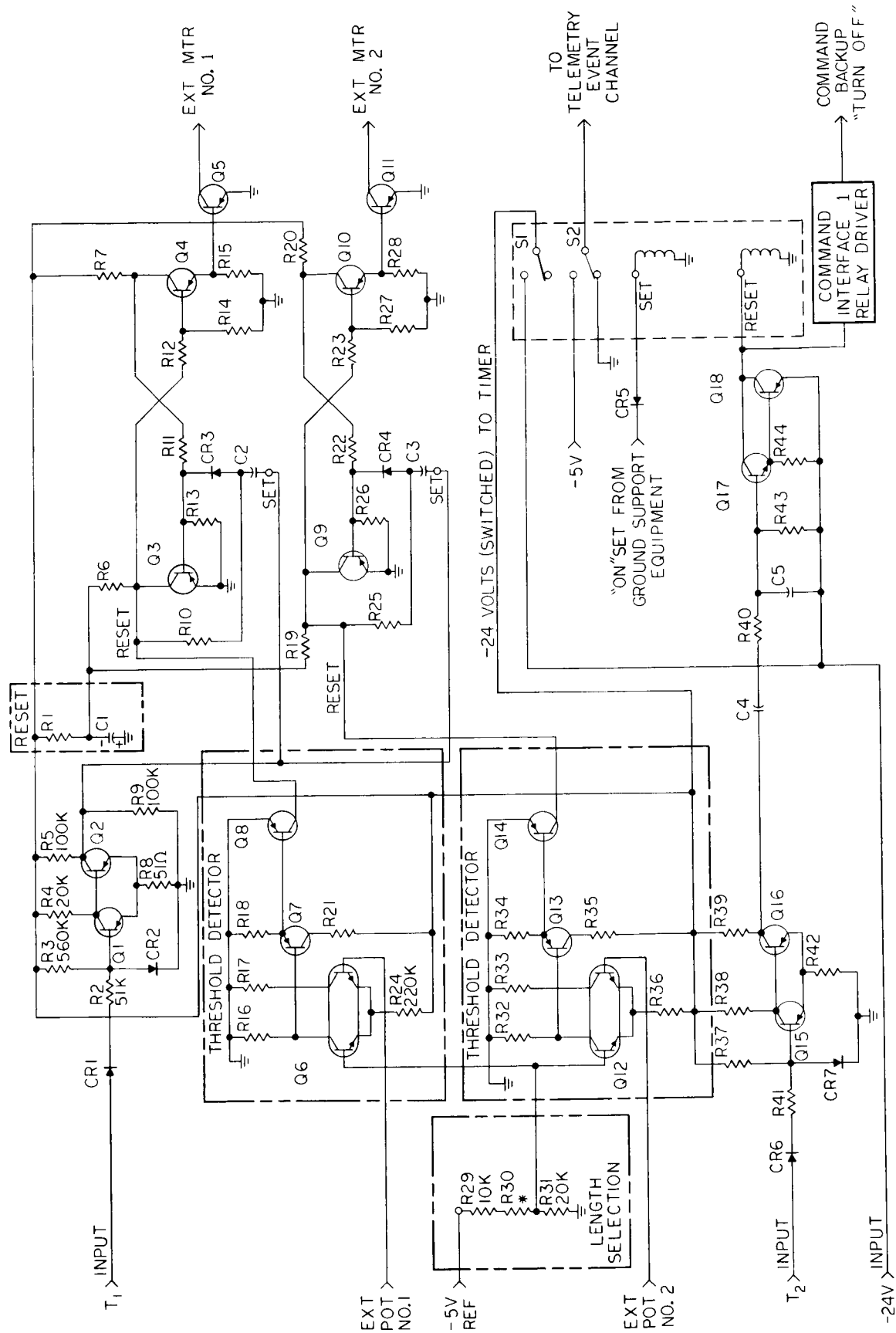


Figure 2.4-6. Separation Timer



potentiometers are used to accomplish the desired functions. The circuit requires an input separation signal, if the Spacecraft Clock inputs are not clamped in the RESET condition before separation, to inhibit premature extension of the gravity gradient booms.

Referring to the Figure 2.4-6, it can be seen that the motor driver outputs, (flip-flop stages Q3, 4, 5 and Q9, 10, 11) are reset on power turn-on by the delay action of R1, C1. The first rising edge of  $T_1$  will be conditioned in Schmitt Trigger Q1, 2 to SET both flip-flops which in turn is ORed with the extension motor command circuit to extend the motors. When the rods reach a predetermined length, the independent threshold detectors turn off their associated motor driver circuits. At the rising edge of the preprogrammed period,  $T_2$ , the Timer will be disabled by the RESET of relay K1, with a backup by ground command. The Separation Timer is thus restricted to be a "one shot" device and its RESET acts as a backup to shut off motor drive in the event of motor stalling or failure of the rod position indicator.

#### 2.4.3.2.5 Motor Driver Circuits (Figure 2.4-7)

In the second Quarterly Report, circuits were described that would perform the desired driving functions for the shunt wound motor. Stress analysis of the rods, however, has indicated that applying step acceleration/deceleration forces to the extension mechanism could cause failure of the rods. This problem can be eliminated by driving the armature of the extension/retraction shunt wound motor with a trapezoidal voltage function having rising and falling slopes of  $\pm 3$  volts/second (with a tolerance of  $\pm 1$  volt/sec) and the field winding (across which would also be a brake winding) with a step voltage waveform. The timing diagram (Figure 2.4-8) illustrates this sequence.

The logic diagram of Figure 2.4-7 shows how it is implemented. The slope generation is performed at a low power level and is gated into the selected power amplifier. The output of the gated slope generator is also detected whenever it is slightly above the standby voltage to control the setp function gating of the field power amplifier. The Separation Timer outputs are "ORed" into the extension drive command signal flow at appropriate points.

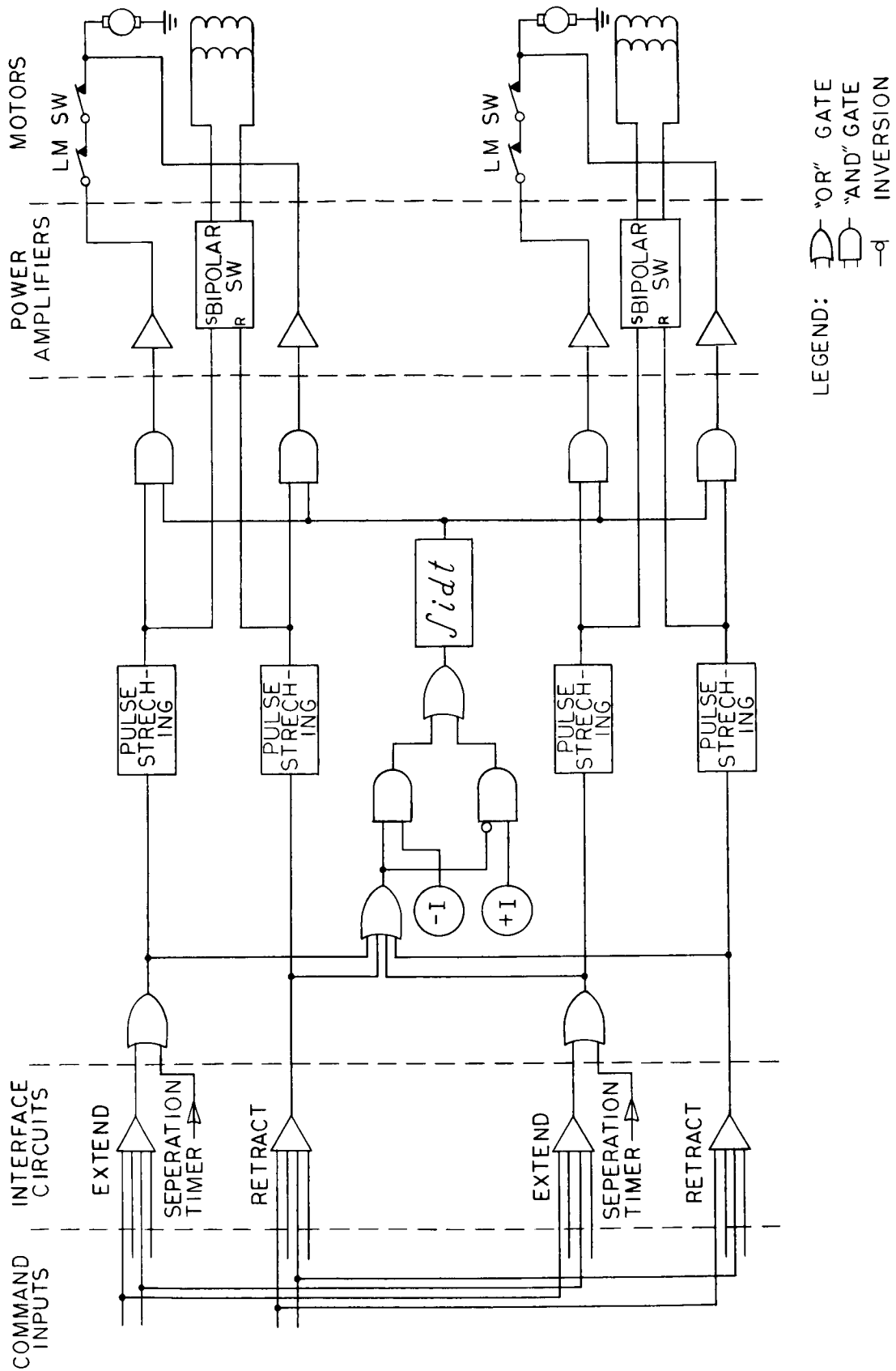


Figure 2.4-7. Rod Extension Motor Control Logic Diagram

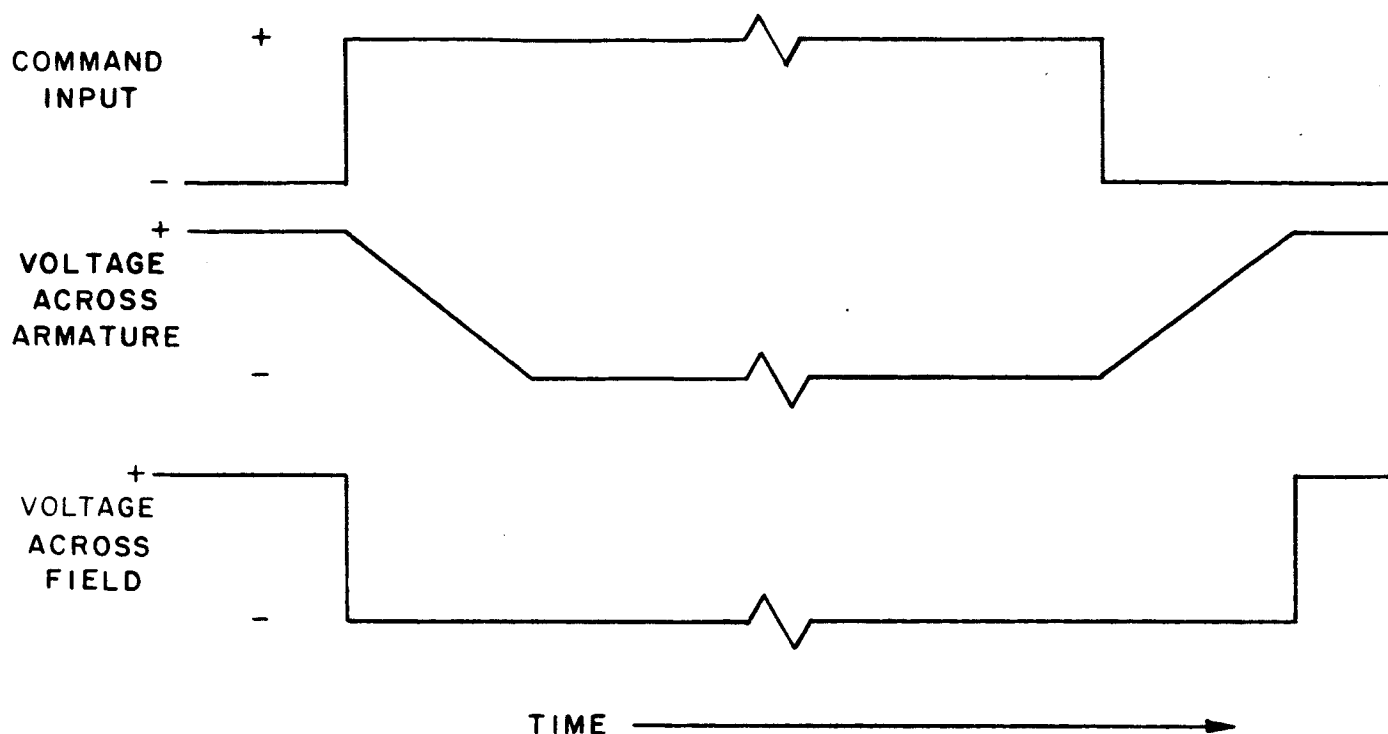


Figure 2.4-8. Rod Extension Motor Control Waveforms

#### 2.4.3.2.6 Digital-to-Analog Converter Networks

There has been some question as to the design justification behind the decision for compressing either four or five digital events on a single analog channel and still be assured of uniqueness of the telemetered signal received at the ground for any combination of event inputs. The following paragraphs detail the error analysis which justify the choice of either of the compression schemes.

The basis for the error analysis is, of course, the assumptions made for initial tolerances and drifts that will be experienced by individual parts. The initial tolerances are taken from the part specifications, and the drift tolerances are taken from long term test data. The "worst-case" errors expected at the output due to the various error sources are given in Table 2.4-1.

TABLE 2.4-1. RESULTS OF ERROR ANALYSIS FOR EXPECTED  
"WORST-CASE" ERRORS

Error Source		Output Error (Millivolts)
1.	Load current of Telemetry Encoder	-12.5 +2.5
2.	Telemetry Inaccuracy (including quantizing error)	<u>± 12.5</u>
3.	Switch offset (including IR drops of Ground Lead, etc.)	+0.0 -3.0
4.	Switch Dynamic Impedance	Negligible
5.	Initial Resistance Tolerance (using a R, 2R....2(n-1)R network and standard 1% resistance valves)	<u>± 35</u>
6.	Resistance Temperature Drift	<u>± 8</u>
7.	Long Term Resistance Drift	<u>± 15</u>
8.	Power Supply Initial Setup Tolerance	<u>± 5</u>
9.	Power Supply Drift with Load (Output Impedance)	<u>± 5</u>
10.	Power Supply Drift with Temperature (Zener & Amplifier d-c Drifts)	<u>± 10</u>
11.	Power Supply Drift with Life (Zener & Amplifier d-c Drifts)	<u>± 10</u>
12.	Power Supply Drift with Input Voltage	<u>± 10</u>
Total		-121
"Worst-Case"		+108

Examining the resistance ladder networks to determine the maximum allowable deviation of the output voltage from its nominal value, one finds that unique events in an  $R, 2R, \dots, 2^{(n-1)}R$  ladder must give voltage outputs with quantum spreads less than

$$\frac{5 \text{ volts}}{2^4 - 1} = 0.333 \text{ volts or } \pm 165 \text{ millivolts}$$

for a 4-Event Channel

and

$$\frac{5 \text{ volts}}{2^5 - 1} = 0.161 \text{ or } \pm 80 \text{ millivolts}$$

for a 5-Event Channel

It can be seen from the error analysis that the four-input ladder network always gives unique voltage levels readout at the ground stations for all combinations of input events.

It is also obvious that the 5-event combining network will not meet the unique readout voltage criterion in the "worst-case". If, however, one is willing to calibrate out the errors due to initial tolerance on resistors and the power supply initial set voltage, the uniqueness criterion can be met on the voltage variations of this calibrated output.

Additionally, if it is assumed that the errors contributed by different sources are statistically independent, and that "worst-case" limits are actually 3 sigma limits on parts, then it can be shown that the output error is within the 3 sigma distribution point of  $\pm 45$  millivolts in 99.73% of such networks constructed.

It is presently planned that four event ladder networks be used for this desired function in the PCU. However, it is believed that if a lack of telemetry channels becomes a problem in the system, the five event ladder network could be used with little design risk.

## 2.4.4 SOLAR ASPECT SENSOR

### 2.4.4.1 System Description

The solar aspect sensor to be used on gravity gradient oriented ATS flights A, D and E is a digital system composed of a single electronics unit and five solar detector assemblies. The Solar Aspect Sensor package is shown in Figure 2.4-9. Each of the solar detectors has a 128-degree by 128-degree rectangular field of view. When the sensors are placed on the spacecraft as shown in Figure 2.4-10, a full  $4\pi$  steradian coverage is obtained, with some small overlap areas.

#### 2.4.4.1.1 Detector

The detector is comprised of two Gray coded reticles, photocells, and the housing.

The Gray coded reticle is a small oblong block of fused quartz with a slit centered along the top surface, and a Gray coded pattern on the bottom surface. Sunlight enters the eye through the slit, casting a narrow band of illumination across the Gray coded pattern. The Gray coded reticle pattern provides for the generation of 8 bits of information. In any given bit, the band of sunlight either will or will not pass through the reticle pattern, depending on the angle of the reticle with respect to the sun.

Because the reticle has a Gray coded pattern, only one bit changes at a time. Were the opaque and clear areas on the reticle arranged in a conventional binary code, with simultaneous changes in more than one bit, there could be catastrophic errors in the determination of the angle, if the transitions were not perfectly synchronized.

It can be seen that in all 8 bits, no two of the transitions are in the same straight line. The width of the opaque or clear areas in the least significant bit is twice as wide as the resolution of the reticle. If the reticle pattern were in a conventional binary code, the width of the opaque or clear areas of the least significant bit would be equal to the resolution.

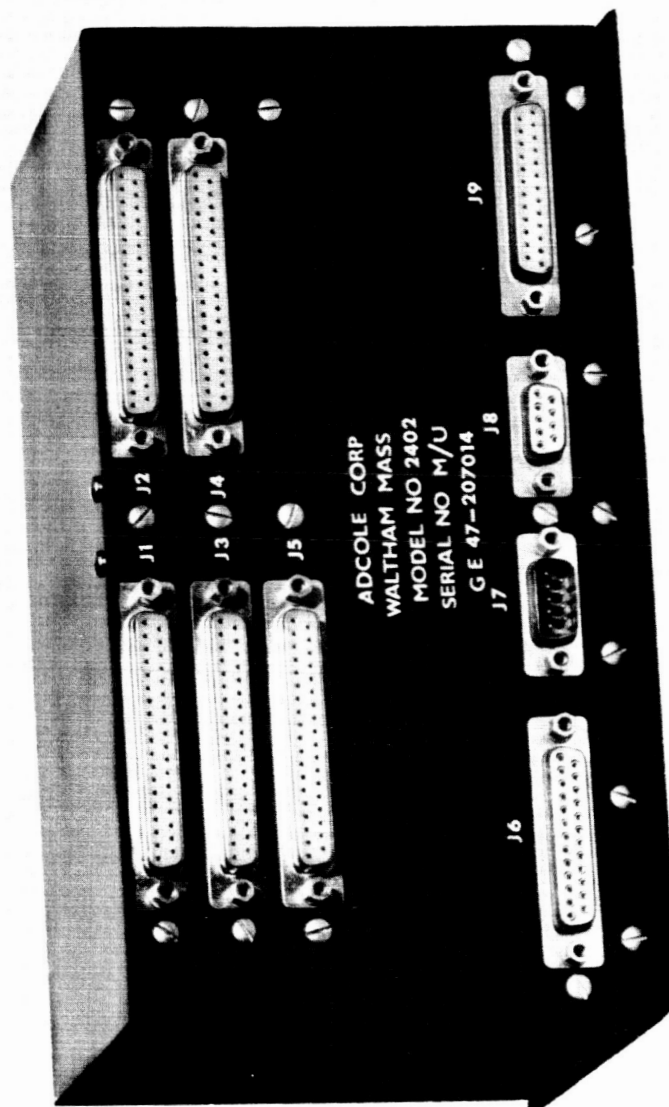
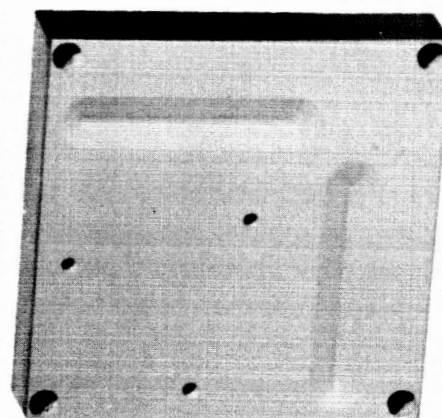


Figure 2.4-9. Solar Aspect Sensor Package



PHOTOGRAPH BY

HUTCHINS PHOTOGRAPHY, INC.  
BELMONT, MASS.

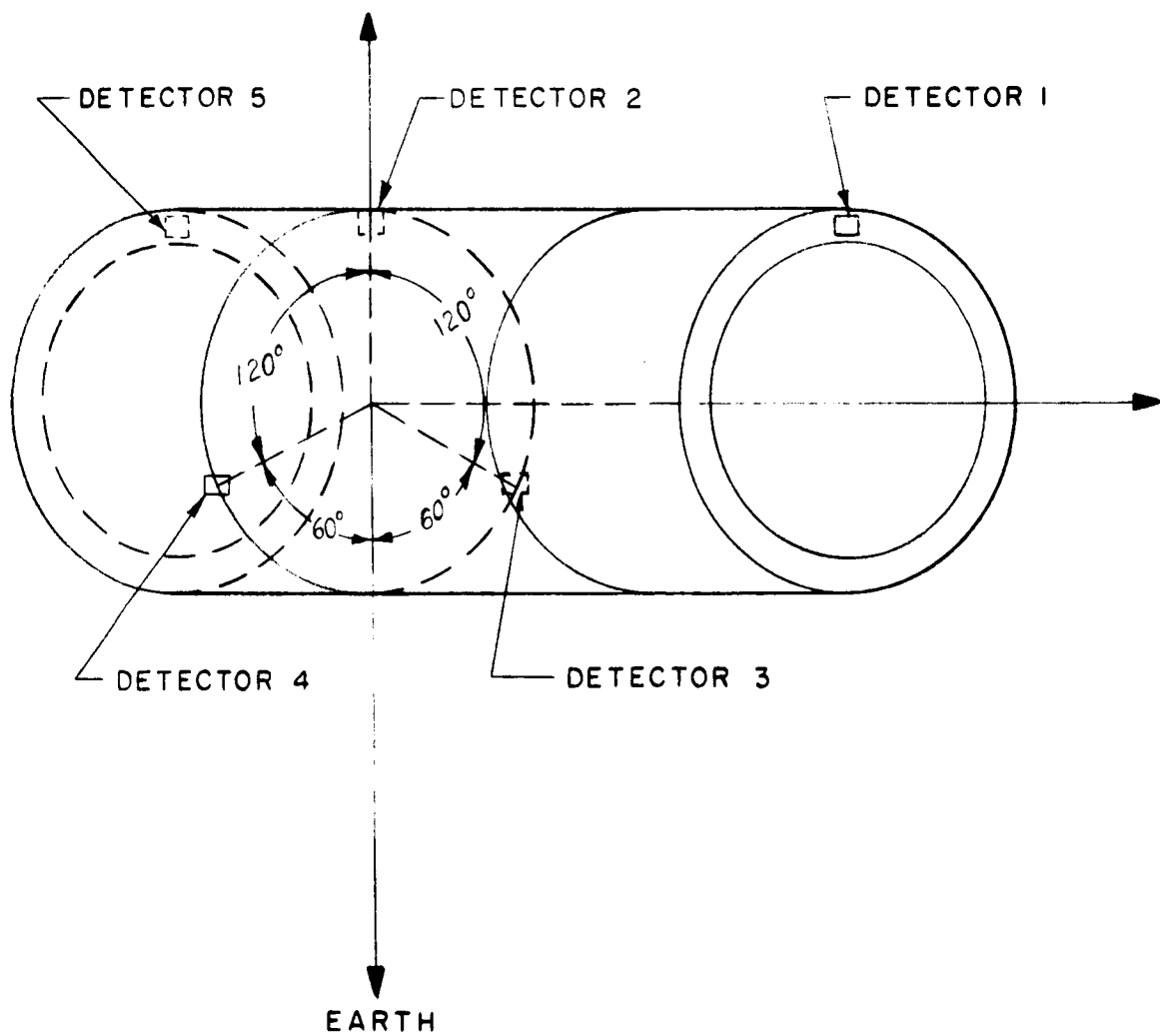


Figure 2.4-10 Solar Detector Locations on ATS Vehicle



However, the Gray coded reticle provides transitions in the more significant bits when the band of sunlight is halfway through an opaque area in the least significant bit.

Each of the 8 bits on the Gray coded reticle is superimposed on a photocell. The function of the cells is to detect the light (or note the absence of light) in the apertures at a given angle, and to produce measurable electrical signals correspondingly.

Silicon solar cells are used in the sensor. Their major limitation is the relatively small signal, on the order of 20 to 30 microamps, which requires amplification. However, their advantage over photoconductive materials is that they can readily withstand space environment, are very uniform, and have a linear relationship of incident light to output. The effects of ultraviolet and Van Allen belt radiation are minimized because the cells have the substantial shielding of the fused quartz block.

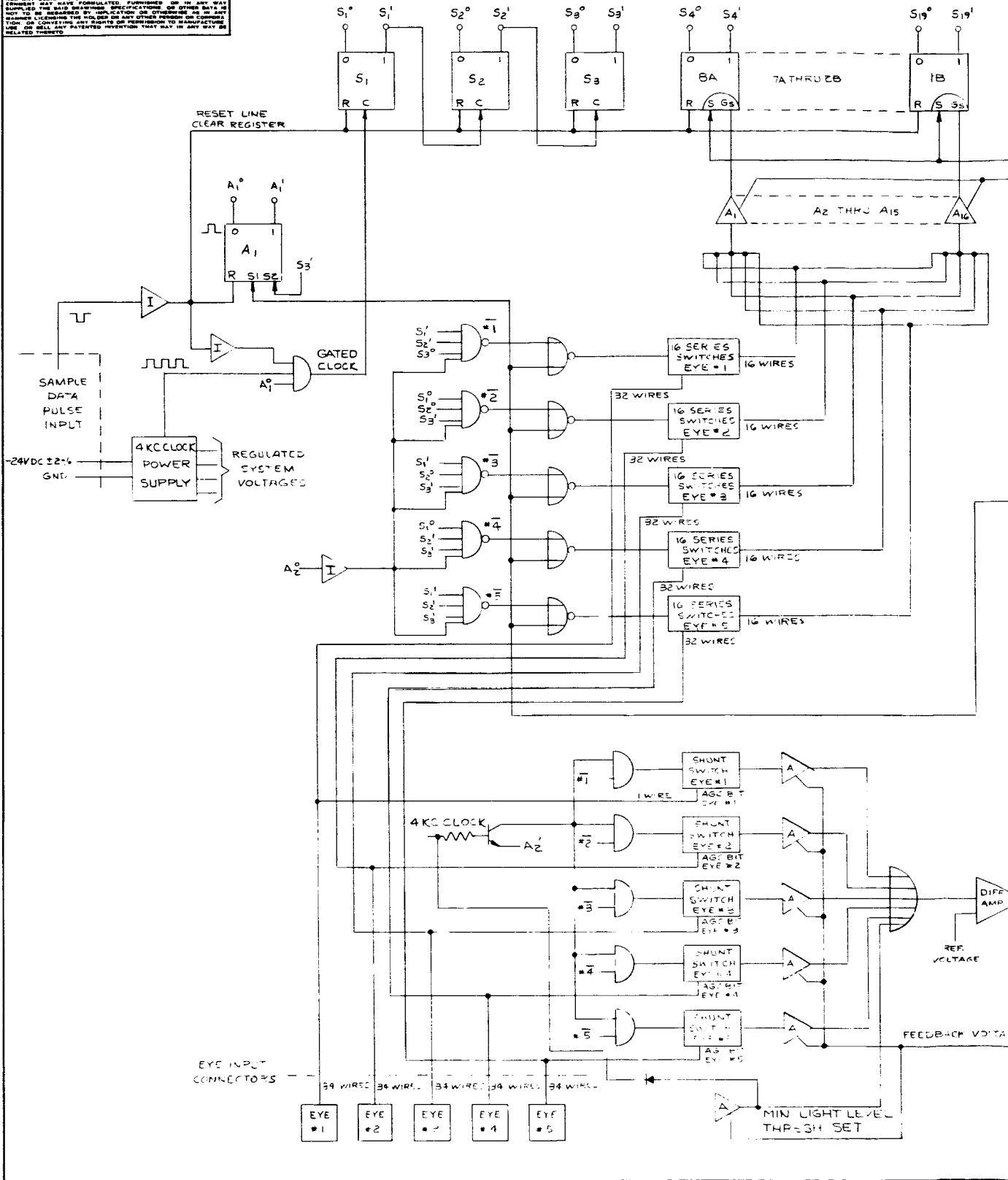
An additional wide open bit with a solar cell under it is included on sensors of this type. This is referred to as the AGC bit and is used to compensate for the variation in output of the solar cells under the Gray code bits which is a function of the angle of incidence.

#### 2.4.4.1.2 Electronics Unit

The block diagram of the electronics is shown in Figure 2.4-11 and described below.

The input sample data pulse causes the data register and identification to clear and sets the  $A_1$  flip flop to the "one" state. The  $A_1$  flip flop is used to control the 4 kc clock pulse generator and eye selection switches. With the  $A_1$  flip flop in the "one" state, clock pulses are generated and the eye selection circuit is activated. Clock pulses cause the identification binary counters  $S_1$  through  $S_3$  to count. The outputs of the binary counter  $S_1$  through  $S_3$  are decoded as shown and thus provide the scan system to select the eye that is most illuminated. When the counter reaches 010, it is decoded, inverted and used to open the shunt switch of eye number 1. If eye number 1 is the most illuminated eye, the current produced by the AGC bit would flow into the grounded base amplifier (this

NOTICE: WHEN GOVERNMENT DRAWINGS, SPECIFICATIONS OR OTHER DATA ARE USED FOR ANY PURPOSE OTHER THAN IN CONNECTION WITH A SPECIFICALLY RELATED GOVERNMENT PROCUREMENT OPERATION, THE UNITED STATES GOVERNMENT THEREBY INCUR NO LIABILITY, AND ANY OBLIGATION WHATSOEVER, AND THE FACT THAT THE GOVERNMENT MAY HAVE FORMULATED THEM, INCLUDING ANY AND ALL SUPPLIED THE SAID DRAWINGS, SPECIFICATIONS OR OTHER DATA IS NOT TO BE REGARDED AS AN IMPLICATION OR ENDORSEMENT, OR ANY OTHER LICENSE, TRADE OR OTHER RIGHTS OR PERMISSION TO MANUFACTURE, USE OR SELL ANY PATENTED INVENTION THAT MAY IN ANY WAY BE RELATED THEREBY.





current had previously been shunted by the closed switch) and cause a pulse to occur at the differential amplifier. If eye number 1 is not the most illuminated eye, no current or insufficient current would flow into the grounded base amplifier to cause a pulse to be produced at the differential amplifier. The binary counter will then continue to count and scan each eye until the most illuminated eye produces a pulse at the differential amplifier.

The  $A_2$  flip flop was set to the "one" state when  $S_1$  changed from a "one" to a "zero". In the "one" state the  $A_2$  flip flop enables the threshold switch.

The pulse produced by the differential amplifier when the proper eye is scanned causes the threshold detector switch to close. The negative going step voltage produced by the threshold switch causes the 500  $\mu$ s mono-stable multivibrator to be triggered.

The output of the one shot is inverted and used to drive the NOR gate inputs as shown. This ground level input together with the ground level input of the decoded identification will cause all series switches of the selected eye to close. Current from the illuminated solar cells of the selected eye will flow through the correct data register amplifier.

The output of the inverter connected to the one shot output is also connected to a pulse generator. This pulse generator will produce a set pulse that is coincident with the trailing edge of the 500  $\mu$ s pulse.

Flip flops  $S_4$  through  $S_{19}$  comprise the data register. These flip flops have an AC set (S) input and a gate set (G) input. The G input is a resistor that is used to bias a diode connected to the base of the "one" side transistor of the flip flop. The G inputs of all these flip flops are connected to the appropriate grounded base amplifier as shown. When current from the illuminated solar cells flows into these amplifiers, the output voltage increases. The set pulse is ended with the output of the amplifiers and the data flip flops will be set to a "one" or remain in a "zero" depending upon the amount of current flowing in each data bit amplifier from the data bit solar cells. The set pulse is also used to reset the  $A_1$  flip flop thus ending the sequence.

$S_1$ ,  $S_2$  and  $S_3$  now contain information to identify the selected eye and  $S_4$  through  $S_{19}$  contain the required sun angle information. The outputs of  $S_1$  through  $S_9$  is inverted and presented as a parallel output. The data at the output will remain until a new sample data pulse is received.

Total elapsed time in worst case from the end of the sample data pulse to new data at the output is 3.2 ms.

A detailed analysis of the electrical, mechanical, and optical errors is given in Appendix F.

#### 2.4.4.2 Subcontract Activities

A summary of the present status of the subcontract to the Adcole Corporation for the Solar Aspect System is given below.

All of Adcole's drawings are released. GE has approved the electrical, mechanical and optical design.

The wooden mockup is 95% complete.

The electronics test equipment is 80% complete.

The detector head test equipment is about 40% finished

General test plans for all units have been established.

90% of the parts have been ordered for the engineering unit.

The GE source control drawing for the temperature sensors to be incorporated into the detector head and electronics unit have been released.

## 2.5 QUALITY CONTROL

### 2.5.1 PROCEDURES

The requirements for subcontractor quality control are defined in NASA Spec. NPC-200-3, and GE Standing Instruction SI-217, 260. These specifications are included as part of negotiations with subcontractors who have been or will be engaged to supply components for the Gravity Gradient Stabilization System. When a contract is negotiated, GE furnishes the subcontractor with the applicable component specification and work statement (plus items referenced in these two documents) the approved parts list and the approved material and processes list. A cover letter informs the subcontractor of other related GE specifications which he may have on request.

### 2.5.2 THERMAL BENDING TESTS

A test is required to determine the thermal effect of rod bending to verify the results of the mathematical model. Preliminary plans were formulated which include test conditions and a schedule for performing such thermal testing.

The following Test Requirement documents were released:

TR No. 11008	Defines equipment requirements for damper testing
TR No. 11007	Defines equipment for Boom Subsystem Testing

### 2.5.3 SUBCONTRACT ACTIVITIES

Negotiations have been completed with deHavilland to supply components for the Boom Subsystem and with Adcole Corporation who will fabricate and test the Solar Aspect Sensor, including the sensor detectors. Additional negotiations were nearing completion at the close of the period with TRW/STL for the Passive Hysteresis Damper, and with Lear Siegler to furnish the TV cameras. Quality Control and Test Engineering has maintained liaison with

with the performing subcontractors, and participated in pre-negotiation activities with the others. Significant contacts with the subcontractors have included the following:

February 2, 1965	A meeting was held at deHavilland during which the total quality control requirements for the Boom Subsystem sub-contract were discussed. Action items that resulted from the meeting will require additions to the applicable work statement.
February 22, 1965	The Adcole Corporation was contacted to discuss their quality requirements with emphasis on the test plans and test equipment.
March 23, 1965	The requirements of NPC 200-3 and the GE quality control provisions were reviewed with Lear Siegler. Agreements were reached in these pre-negotiations discussions.
March 16-17, 1965	The detailed requirements for the wood mockup, thermal model and the dynamic model of the Solar Aspect Sensor were defined to Adcole as a result of rejection of the first wooden mockup received by GE.

#### 2.5.4 MATERIALS AND PROCESSES

A white thermal control coating is required for the Solar Aspect Sensor. Zinc Oxide white paint, Vitavar PV100, and Pyromark Standard White will be evaluated to determine their ability to meet the stability requirements of three years exposure to thermal radiation.

The Combination Passive Damper housing is constructed of welded, tubular 6061-T6 aluminum. Samples have been fabricated and will be evaluated for X-ray, weld penetration, hardness and tensile strength.

A review of the materials used in the bistable clutch solenoid uncovered problems in wear, friction and galling. Recommended materials changes have been made.



## 2.6 MANUFACTURING

During this reporting period, Manufacturing Engineering has maintained close liaison with Design Engineering in all design areas. This activity, in the early stages of the design effort - prior to drawing release - enables Manufacturing Engineering to identify the manufacturing methods required to produce the hardware and implement advanced plans for their availability by the time drawings are released to the shop. This activity also provides Manufacturing Engineering the opportunity to suggest features in the design, which will simplify the manufacturing operations while maintaining all functional requirements.

In addition to the above activity, Manufacturing Engineering has provided technical direction to the shop during the manufacture of Engineering test components. The following test components for the Combination Passive Damper were produced during this period:

One working model of the Hysteresis Damper

Three configurations of a modified Belleville type Spring with associated test fixtures for the Clutch Mechanism

One set of parts for the torsional restraint function of the Eddy Current Damper.

### 2.6.1 POWER CONTROL UNIT

The required tooling for potting electronic modules for the power control unit is complete. A total of seven module drawings have been released for fabrication.

## 2.6.2 MAKE OR BUY SCHEDULE

The following is the up-to-date make or buy plan on major end item components:

<u>ITEM</u>	<u>MAKE</u>	<u>BUY</u>
Hysteresis Damper		X
Combination Passive Damper (less Hysteresis Damper)	X	
TV Camera		X
Power Control Unit	X	
Sun Sensor		X
Angle Detector	X	
Damper Rod/Mechanism		X
Gravity Gradient Rods/Mechanism		X

The Make/Buy decision on these items represents a change from previously submitted plans.

On the Hysteresis Damper, the change was made in accordance with NASA request. The Angle Detector was changed based upon a less costly in-house design concept.

## 2.7 RELIABILITY AND PARTS & STANDARDS

### 2.7.1 INTRODUCTION

Emphasis during the quarter was directed toward an analysis of the Boom Subsystem since this design had been completed to the point of permitting reliability investigations. In addition, selected reliability studies were made when problem areas became apparent. Three test plans were evaluated for the primary boom sealed drive unit with the objective of selecting the plan which would provide the most information relative to the capability of the parts that comprise the unit.

Sampling rates of pyrotechnic devices were investigated based on historical data and the Spacecraft Department experience. This is discussed in the section on Technical Extracts.

The Parts Qualification Program recommended for ATS components is based on a trade-off of risk factor, "need" and cost. The parts selected to be qualified are presented together with the method used to select not only the component but also its qualification status.

### 2.7.2 BOOM SUBSYSTEMS EVALUATION

An initial reliability analysis of the Boom Subsystems has been prepared by the Reliability Engineering Operation.

The analysis is based on:

1. The operational sequence of events and duty cycles extracted from the latest "Orbit Test Plan" (OTP) issued by the ATS Systems Engineer for the System Design Review held on March 4, 1965, at VFSTC.

The OTP encompasses approximately any 196 days within a one year time period of the orbital mission. No attempt was made in this analysis to define any

operational cycles after this time period, and it assumed that the booms will remain in the last operational state occurring in the OTP.

2. Failure probabilities of the constituent part within each component based on operational use and standby periods occurring in the OTP.
3. Modifying failure rate factors resulting from the operational state of the part and the stress levels.

#### 2.7.2.1 Summary of Analytical Results

The estimated reliability for the Boom Subsystem for all operational modes is a composite of the Primary Boom and Damper Boom reliability, or

$$R_{(\text{Boom Subsystems})} = R_{(\text{Primary Booms})} \cdot R_{(\text{Damper Boom})} \quad (1)$$

The Primary Booms, in turn, are a composite of the estimated reliabilities of the normal and emergency modes of operation, wherein any one of two motors and associated gearing in each boom assembly is capable of performing both extension and scissoring of the booms, or

$$R_{(\text{Primary Booms})} = \left[ 1 - (1 - R_{\text{Normal}}) (1 - R_{\text{Emergency}}) \right] \quad (2)$$

Using estimated values shown in Paragraph 2.7.4.1, and demonstration values shown in Paragraph 2.7.4.2, the estimated reliability from Equation 1 above is:

$$\begin{aligned} R_{(\text{Boom Subsystem})} &= (.975) (.925) \\ &= (.902) \end{aligned} \quad (3)$$

It should be recognized that this estimated value is only for the Orbit Test Plan and is limited to the number of demonstration tests to be performed on the Damper Boom.

## **2.7.2.2 Functional Analysis General Information**

### **2.7.2.2.1 Duty Cycles**

The duty cycles for the Primary Boom System and the Combination Passive Damper (CPD) are shown in Tables 2.7-1 and 2.7-2. All three Boom duty cycles, normal mode and two emergency modes, show the extension, scissoring and "soak" periods which have been established for the ATS-A mission.

The CPD duty cycle has a direct relationship to the Primary Boom (X-Booms) duty cycle in that both dampers are exercised after each extension or scissoring action to determine the vehicle response to each dampers restraining torque.

### **2.7.2.2.2 Sequence of Events**

Tables 2.7-3 and 2.7-4 show the operational sequence of events which must occur to extend or scissor the X Booms in both the normal and emergency modes, as well as those required for the Eddy Current Damper and the Clutching Mechanism in the caging and uncaging modes.

### **2.7.2.2.3 Modifying Factors**

During the ATS mission, all equipments are either fully energized, cycled, or in the off state, according to the sequence in which their function is required. Thus, the parts, circuits, or components are subjected to various levels of stress relative to the operational state they are in.

Recognizing that the lifetime of a part is a function of the stress level and the interval of the applied stress, modifying factors are employed herein to account for the operational state of the parts, circuits, or components throughout the mission.

Table 2.7-1. System Duty Cycles Extracted from ATS-A Orbit Test Plan

Primary Boom System Event	Normal Mode Both Motors Operative			Emergency Mode Scissoring Motor Operative			Emergency Mode Extension Motor Operative		
	Ext.	Soak	Scissoring	Ext	Soak	Scissoring	Ext.	Soak	Scissoring
1. X-Booms deployed to 150' @ 2 ft/sec (nominal)	75 sec	5 days		33 hrs	5 days		75 sec	5 days	
2. Soak	25 sec	26 days		11 hrs	24 days		25 sec	26 days	
3. Retract X Booms to 100'									
4. Soak Time									
ECLIPSE PERIOD									
5. Scissor X Booms to 31° halfangle @ 1/8° per sec (nominal)			96 sec			96 sec			
6. Soak		10 days			10 days			10 days	
7. Scissor X Booms to 25°		10 days	48 sec		10 days	48 sec		10 days	
8. Soak		10 days			10 days			10 days	
9. Scissor X Booms to 15°		10 days	80 sec		10 days	80 sec		10 days	
10. Soak		10 days			10 days			10 days	
11. Scissor X Booms to 11°		10 days	32 sec		10 days	32 sec		10 days	
12. Soak		10 days			10 days			10 days	
13. Scissor X Booms to 19°		16 days	64 sec		16 days	64 sec		16 days	
14. Extend X Booms to 150'	25 sec	40 days		11 hrs	40 days		25 sec	40 days	
15. Soak		40 days	256 sec		40 days	256 sec		40 days	
16. Repeat scissor cycles @ 31°, 25°, 15°, 11°									
17. Scissor X Booms to 19°			64 sec			64 sec			
18. Retract X Booms to 50'	50 sec			22 hrs			50 sec		
19. Soak		16 days			16 days			16 days	
20. Repeat Scissor cycles @ 31°, 25°, 15°, 11°		40 days	256 sec		40 days	256 sec		40 days	
21. Scissor X Booms to 19°			64 sec			64 sec			
22. Extend X Booms to 100'	25 sec			11 hrs			25 sec		
23. Soak		7 days			7 days			7 days	
24. Retract X Booms to invert. Extend to stop. Retract to re-invert. Extend to stop.	20 sec	6 days		44 hrs	6 days		20 sec	6 days	
	220 sec	196 days	960 sec	132 hrs	194 days	960 sec	220 sec	196 days	Unknown

CURRENTLY UNDER INVESTIGATION

Table 2.7-2. System Duty Cycles Extracted from ATS-A Orbit Test Plan

PRIMARY BOOM SYSTEM				COMBINATION PASSIVE DAMPER		
Event	Ext.	Soak	Scissoring	Event	Sequence	Time (Days) Cumulative Total
1. X-Booms deployed to 150'	75 sec			CPD and Boom caged	4*	4
2. Soak		5 days				
3. Retract X-Booms to 100'	25 sec			Deploy Damper Boom, Uncage CPD	4	8
4. Soak		26 days		Check Performance of Damper #1	5	13
ECLIPSE PERIOD				Clutch to Damper #2	16	29
5. Scissor X-Booms to 31° halfangle @ 1/8° per sec (nominal)			96 sec	Clutch to Damper #1	7	36
6. Soak		10 days				
7. Scissor X-Booms to 25°			48 sec	Clutch to Damper #2	10	46
8. Soak		10 days				
9. Scissor X-Booms to 15°			80 sec	Clutch to Damper #1	10	56
10. Soak		10 days				
11. Scissor X-Booms to 11°			32 sec	Clutch to Damper #2	10	66
12. Soak		10 days				
13. Scissor X-Booms to 19°			64 sec	Clutch to Damper #1	16	82
14. Extend X-Booms to 150'	25 sec					
15. Soak		16 days		Clutch to Damper #2	10	92
16. Repeat Scissor cycles @ 31°, 25°, 15°, 11°		40 days		Clutch to Damper #1	10	102
17. Scissor X-Booms to 19°			256 sec	Clutch to Damper #2	10	112
18. Retract X-Booms to 50'	50 sec			Clutch to Damper #1	10	122
19. Soak		16 days		Clutch to Damper #2	16	138
20. Repeat scissor cycles @ 31°, 25°, 15°, 11°		40 days				
21. Scissor X-Booms to 19°			64 sec	Clutch to Damper #1	10	148
22. Extend X-Booms to 100'	25 sec			Clutch to Damper #2	10	158
23. Soak		7 days		Clutch to Damper #1	10	168
24. Retract X-Booms to invert. Extend to stop. Retract to re-invert. Extend to stop. (4 actuations)	20 sec	6 days		Clutch to Damper #2	10	178
				Clutch to Damper #1	18	196
TOTALS	220 sec	196 days	960 sec	(Damper #1 - Eddy Current) (Damper #2 - Hysteresis)	192 days	196 days

\*CPD caged

Table 2.7-3.

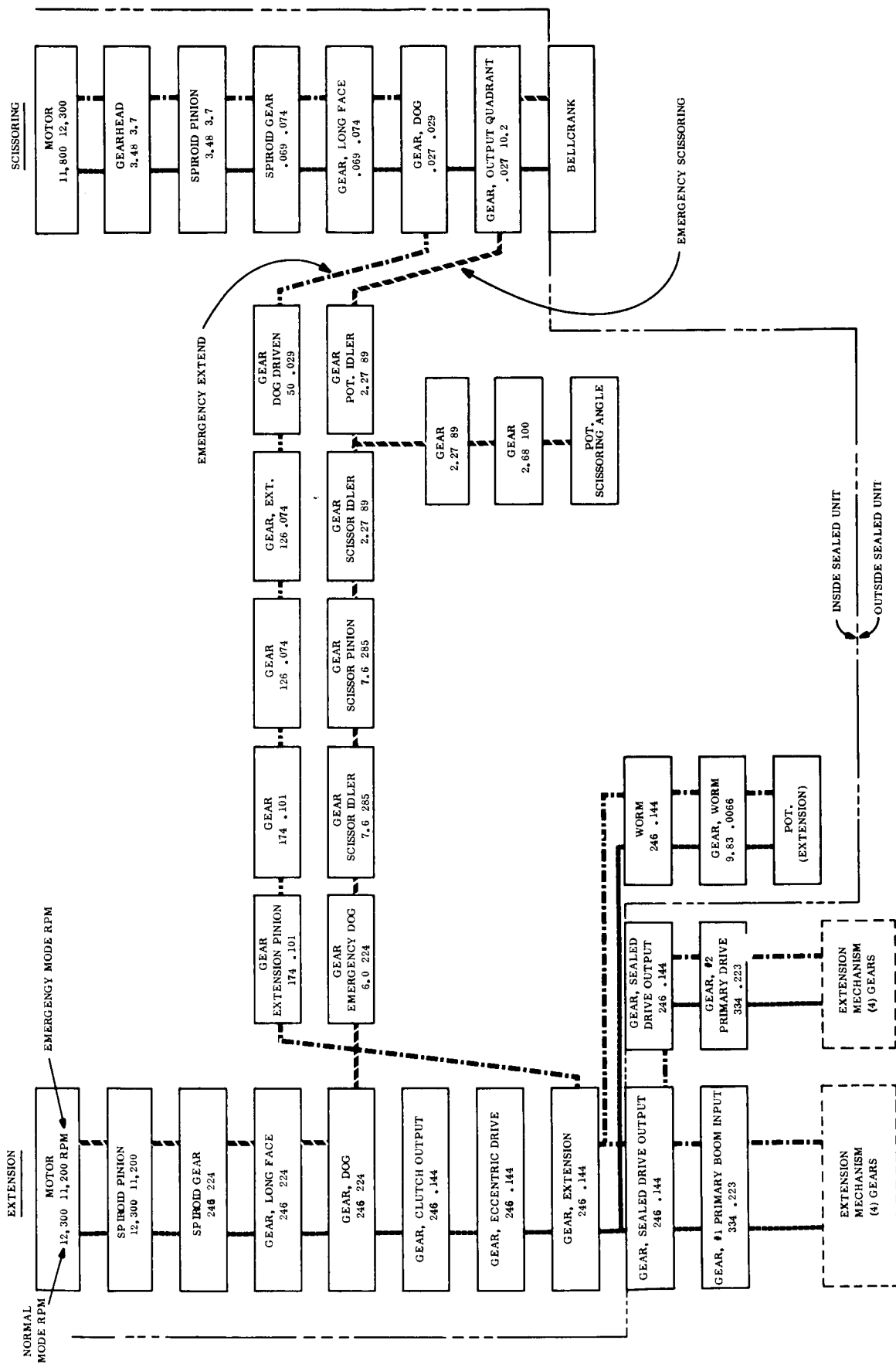
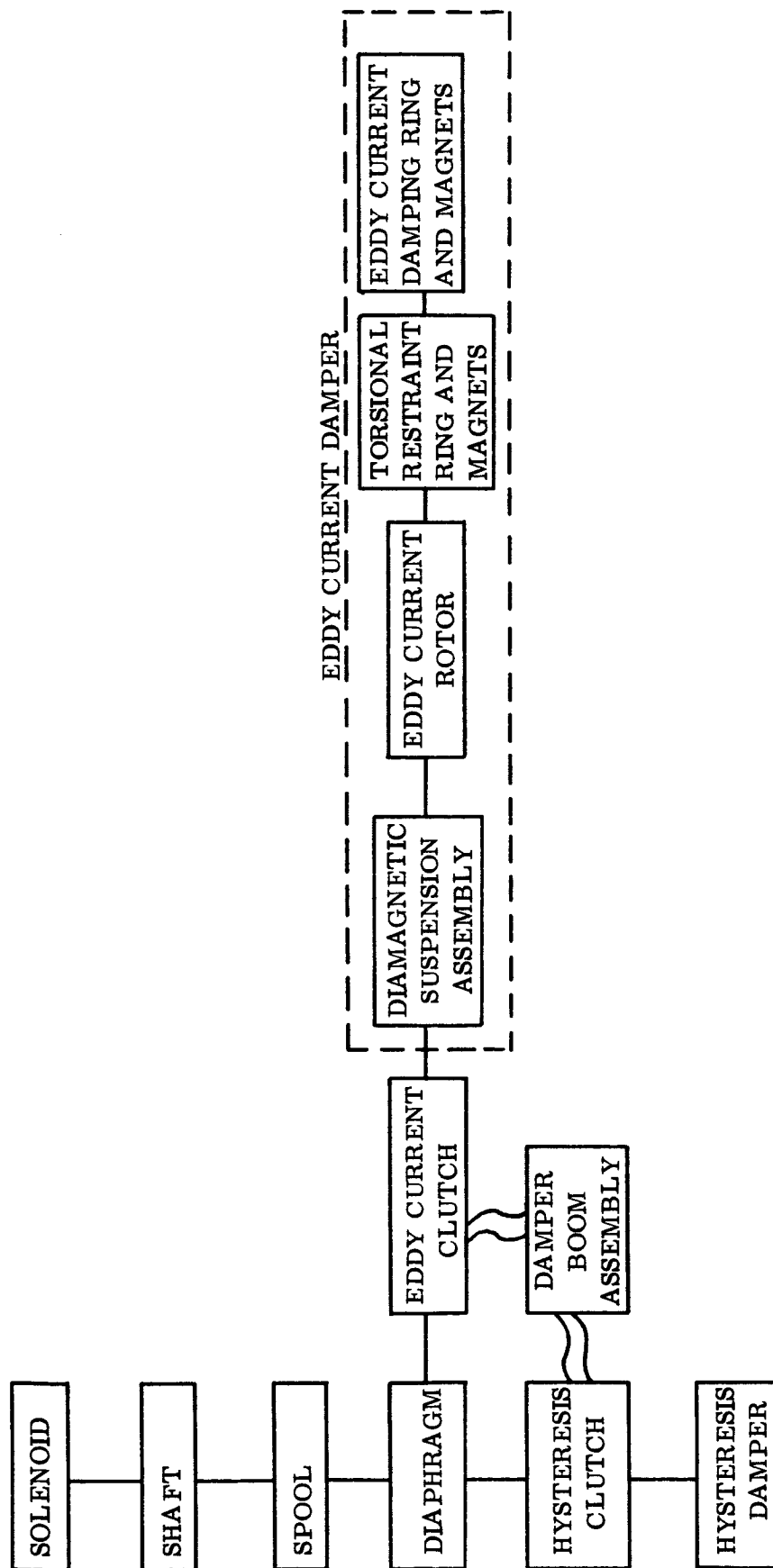




Table 2.7-4. Operational Sequence of Combination Passive Damper



As a reference point, one hour of continuous operation in the normal orbital space environment is used as a base and assigned a value of unity,  $K = 1$ . Other modifying factors used are:

Launch (non-operating)	$K = 100$
Launch (operating)	$K = 900$
All Equipment, Standby	$K = .015$
1st Hour of Cyclic State	$K = 4.0$

These factors are primarily used in the launch and orbital phases where periodic commands or diagnostic data transmission is required.

The effect of the modifying factors on the actual operating time of the components results in an "effective" operational time greater than, equal to, or less than the base value.

Table 2.7-5 shows the effect of the modifiers when applied to the Primary Booms.

#### 2.7.2.3 Primary Booms

The Primary Boom System has three functions in the ATS mission:

1. Extend and retract the X Booms to specified lengths of 50, 100, and 150 feet upon command.
2. Scissor the X booms, upon command, to half angles of  $19^{\circ}$ ,  $11^{\circ}$ ,  $15^{\circ}$ ,  $25^{\circ}$ , and  $31^{\circ}$ .
3. Retract the X Booms a specific length to cause vehicle inversion, then extend to capture.

To accomplish these functions, the controlling mechanisms of the four Booms are divided into two functional pairs. Each pair contains one motor and drive train for extension and one motor and associated mechanical linkage for scissoring. The motors, clutching mechanism, and part of the gear train and scissoring linkage are encased in a hermetically sealed

Table 2.7-5. Primary Boom Time-Stress Data for 196-Day Mission

Phase	Stress Factor K	Normal Mode						Emergency Mode Scissoring Motor Operative						Emergency Mode Extension Motor Operative					
		Time (t) (Hrs.)			Time-Stress (tk)			Time (t) (Hrs.)			Time-Stress (tk)			Time (t) (Hrs.)			Time-Stress (tk)		
		Deploy	Scissor	Common	Deploy	Scissor	Common	Deploy	Scissor	Common	Deploy	Scissor	Common	Deploy	Scissor	Common	Deploy	Scissor	Common
Launch	100	0.1	0.1	0.1	10	10	10	0.1	0.1	0.1	10	10	10						
Starts (1st Hr.)	4	9	15	24	36	60	96	15	24	36	36	60	96						
Operating	1	0.1	0.25	0.35	0.1	0.25	0.35	0.25	0.25	0.25	132	132	132						
Standby	0.015	4695	4689	4680	70.43	70.34	70.20	4689	4563	4548	68.45	70.34	68.22						
TOTAL		4704.2	4704.35	4704.45	116.53	140.59	176.55	4704.1	4704.35	4704.35	246.45	140.59	306.47						

NOTE 1 - This is based on the assumption that the extension motor will scissor the boom at the same rate as that of the scissoring motor. This assumption is necessary because the exact rate is unknown at the present time.

container. The D-C shunt motors are brush type motors which have a distinct speed control advantage with load variation over other motor types. Rotary solenoids are used to initiate clutching between the two motors upon ground command.

Table 2.7-6 shows the parts contained within the sealed drive assembly which will be operating or standing by in approximately a half atmosphere.

The seal of the container becomes the limiting item for this type of assembly, wherein total leakage of the contained gas may be catastrophic to the mission.

A pressure transducer is used as the sensory element to indicate possible leakage of this container, in order to provide ground command with a time period for an emergency course of action in case of total or partial leakage.

Temperature sensors are also provided to indicate internal temperature variations which may lead to degradation or catastrophic failure of parts within the sealed unit if the design parameters are exceeded.

Various microswitches and potentiometers are employed either to monitor and measure extension lengths and scissoring angles or to prevent damage to the drive units through over-extension or scissoring. Each pair of the Boom units has the capability for independent operation, although simultaneous motion between both units can be electrically controlled via the Power Control Unit.

Each pair of Boom drive units includes a rotary solenoid to provide emergency clutching between the extension and scissoring motors so that either motor is enabled to assume the function of the other, if any one motor fails. Table 2.7-3 shows the operational sequence of each motor and the associated linkage in the emergency modes. Although the scissoring and extension rates are dissimilar, each motor is essentially in standby redundancy to the other, so that total loss of the drive function cannot occur with a single motor failure.

Table 2.7-6. Primary Boom Subsystem Reliability Data

PARTS	TOTAL QUAN.	QUAN. (n)			FAIL. RATE $\lambda$ %/1000 HRS.	FAIL. RATE $\lambda$ %/10 <sup>4</sup> OPERATION	WORST CASE AVE. NO. OF CYCLES	QUAN. - FAIL. RATE-TIME-STRESS (n & tk)					
		DEPLOY	SCISSOR	COMMON				NORMAL MODE			EMERGENCY MODE		EMERGENCY MODE EXTENSION MOTOR OPERATIVE tk=116.5 tk=140.6 tk=176.6
								DEPLOY tk=116.5	SCISSOR tk=140.6	COMMON tk=176.6	DEPLOY tk=246.4	SCISSOR tk=140.6	
IN SEALED UNITS	GEARS	24	12	-	0.12			0.00017	0.00020	-	0.00031	-	SAME AS NORMAL MODE
	BEARINGS	28	10	8	0.50			0.00059	0.00071	0.00071	0.00123	0.000123	
	CONNECTORS	50P	-	50P	0.001			-	-	0.00009	-	0.00015	
	BELLOWS	3	1	2	0.60			0.00070	0.00169	-	0.00148	-	
	CAPACITORS	6	3	-	0.005			0.00002	0.00002	-	0.00004	-	
	POTS	2	1	1	0.168			0.00020	0.00024	-	0.00041	-	
	4 SWITCHES	4	-	4	-	0.11	24	-	-	0.00008	-	0.00013	
	MOTORS	2	1	1	-	3.0	15	0.00035	0.00042	-	0.00074	-	
	SOLENOID	1	-	1	-	3.5	1	-	-	0.00001*	-	0.00001*	
	**PRESS. XDUCER	1	-	1	3.500			-	-	0.00620	-	0.01073	
TOTAL							0.00203	0.00328	0.00709	0.00421	0.01230	0.01230	
REL.							0.9980	0.9967	0.9929	0.9958	0.9877	0.9877	
NOT IN SEALED UNIT	GEARS	12	-	-	0.012			0.00017	-	-	0.00035	-	SAME AS NORMAL MODE
	BEARINGS	64	-	-	0.50			0.00371	-	-	0.00788	-	
	CONNECTORS	37P	-	37P	0.001			-	-	0.00007	-	0.00011	
	4 SWITCHES	10	6	4	-	0.11	15	0.00008	0.00006	-	0.00016	-	
	FLEX. PIVOTS	6	-	-	-	0.022	15	-	0.00030	-	-	-	
	TOTAL							0.00396	0.00036	0.00007	0.00839	0.00011	
	REL.							0.9960	0.9996	0.9999	0.9916	0.9999	

\*TIME-STRESS FACTOR (tk) = 84.70 FOR ONE CYCLE OPERATION  
 \*\*THE ANALYSIS CONSIDERS THE PRESSURE TRANSDUCER AS AN INTEGRAL PART OF THE ASSEMBLY, AND THAT ITS FAILURE WOULD STOP ANY FURTHER OPERATION OF THE BOOMS. IT IS THE MAJOR FAILURE CONTRIBUTOR TO THE FAILURE EXPECTANCY OF THE PRIMARY BOOM SYSTEM, BUT IS CONSIDERED ESSENTIAL FOR PROOF OF ATMOSPHERIC INTEGRITY OF THE SEALED UNIT.

#### 2.7.2.3.1 Parts and Materials

All electronic parts have been selected from the Approved Parts List (ATS), 490L106, and all materials from the Approved Materials List (ATS), 490L107.

Each part selected for use in these components has been or will be qualified for the ATS mission requirements.

#### 2.7.2.3.2 Mathematical Model and Reliability Calculations

The mathematical model for the estimated reliability of the primary Booms for the 196-day mission is:

$$R_{(\text{Pri. Boom})} = \left[ \left( R_{\text{deploy}} \right) \left( R_{\text{scissor}} \right) \left( R_{\text{common}} \right) \right]^2$$

Expanding this basic model to include the redundancy achieved by the normal mode and the emergency modes of operation gives:

$$R_{(\text{Pri. Boom})} = \left[ \begin{array}{cc} 1 - 1 - R_{\text{normal deploy}} & 1 - R_{\text{emergency deploy}} \\ 1 - 1 - R_{\text{normal scissor}} & 1 - R_{\text{emergency scissor}} \\ R_{\text{emergency common}} \end{array} \right]^2$$

Inserting the reliability values from Table 2.7-4 in the mathematical model gives the reliability estimate for the Primary Boom of:

$$\begin{aligned} R_{(\text{Pri. Boom})} &= \left[ \begin{array}{cc} 1 - 1 - \{.9980\} \{.9960\} & 1 - \{.9958\} \{.9916\} \\ 1 - 1 - \{.9967\} \{.9996\} & 1 - \{.9967\} \{.9996\} \\ \{.9877\} \{.9999\} & 2 \end{array} \right] \\ &= \left[ .9999 \right] \left[ .9999 \right] \left[ .9876 \right]^2 \end{aligned}$$

$$=(.9874)^2$$

$$=.9750$$

#### 2.7.2.3.3 Explanation of Data Used in Reliability Calculations

The data used in Tables 2.7-5 and 2.7-6 have been revised to reflect the latest Primary Boom design and ATS system definition. The part quantities were obtained from the latest deHavilland Primary Boom design. The part failure rates utilized are the most factual obtainable for this application, whereby the basic MSD parts failure rates detailed in TRA-873-74 have been modified by applicable Interservice Data Exchange (IDEP) reports and industry program reports (Minuteman, Apollo, etc.). The operating and standby time periods were obtained from the system mission profiles delineated in Table 2.7-1.

#### 2.7.2.4 Damper Booms

The Damper Booms are two 45-foot, self erecting units which are mounted on the damper platform. When deployed, the damper booms act as a gravity anchor to the spacecraft.

Damper Boom release is the result of cutting a single retention tie bar of (.1875 inch aluminum) by means of a single pyrotechnic cable cutter, and using the stored energy in lift-off springs and the elastically wound tape to erect the booms. The same explosive action that initiates the cable cutter function also ejects a connector and wire pack which furnished the power for squib actuation.

At this time, 18 cable cutters are to be purchased to demonstrate firing and cutting capability in the Parts Qualification Program. Approximately 18 additional cable cutter assemblies will be functionally tested during engineering, acceptance and qualification tests of the entire Boom Subsystem.

The cumulative total of firings will, therefore, be approximately 36 for the cable cutter assembly and 18 for the complete Damper/Boom System.

Table 2.7-7 shows the demonstrated reliability resulting from the testing of 18 and 36 cable cutter assemblies or the complete Damper/Boom System where only one firing or deployment is required in the mission. The values shown are at three confidence levels for zero failures during testing.

A demonstrated reliability value of .925 at a 75% confidence level is used for the Damper Boom in the analysis shown in Paragraph 2.7.2.

### 2.7.3 COMBINATION PASSIVE DAMPER

The Combination Passive Damper (CPD) combines with the damper boom to damp the vibrations of gravity gradient stabilized vehicles. In addition to providing damping torques, the CPD also must meet the requirements for restoring the damper boom to a "null" position with respect to the satellite.

The CPD package consists of two dampers, one a passive hysteresis damper (PHD) and the other an eddy current damper (ECD), combined with a clutching mechanism that couples one or the other to the damper boom. The "null" position restoring torque is provided by a magnetic torsional restraint device in the eddy current damper, and by the torsion wire suspension in the hysteresis damper.

The hysteresis damper and the eddy current damper are mutually exclusive in operation but redundant in function. They use different methods of achieving the same end result, and in the present CPD design, are physically incapable of being operated simultaneously. A double acting solenoid actuator and diaphragm are the main elements of the clutching mechanism that is used to transfer from one damper to the other. This transfer must be accomplished at the "null" position or a position bias error will result. To be fully redundant in function, it has been assumed that a failure in the operating damper will not preclude an eventual transfer at the "null" position. Accomplishing this transfer may require one or more double clutching sequences, to enable the boom "null" and the damper "null" to come into opposition.



During operation of the dampers, the position of the damper boom is constantly monitored by the angle indicator. A portion of this indicator is attached to the damper boom structure and the remainder is attached to the static portion of the CPD, allowing the sensor to measure their relative positions. When it is desired to change from one damper to the other, the angle indicator output is monitored to determine when the damper boom will be in the "null" position. At that time, the solenoid is fired and the other damper is clutched. Since the torsional restraint kept this damper at "null" when it was not being used, both the damper and boom will be in the "null" position at the same time. Conversely, they will also deviate together and the damper torsional restraint will oppose their joint deviation and attempt to return both to the "null" position.

#### 2.7.3.1 Mathematical Model and Reliability Calculation

The mathematical model for the estimated reliability of the Combination Passive Damper for the 196-day mission is:

$$R_{CPD} = \frac{100 \left[ R_{ECD} + R_{clutch\ ass'y} \left( \frac{\lambda_{ECD}}{\lambda_{PHD} - \lambda_{ECD}} \right) (R_{ECD} - R_{PHD}) \right] + 92 \left[ R_{PHD} + R_{clutch\ ass'y} \left( \frac{\lambda_{PHD}}{\lambda_{ECD} - \lambda_{PHD}} \right) (R_{PHD} - R_{ECD}) \right]}{192}$$

where  $R_{CPD}$  is the reliability of the Combination Passive Damper,

$R_{ECD}$  is the reliability of the Eddy Current Damper,

$R_{PHD}$  is the reliability of the Passive Hysteresis Damper,

and the same subscripts apply to the failure rates.

This mathematical model is based on the fact that during the 196-day mission, detailed in Table 2.7-2, the eddy current damper will be clutched for a total of 100 days and the hysteresis damper will be clutched for a total of 92 days, after the CPD is uncaged.

No reliability calculation is presented in this report because of the lack of sufficient design or historical information. Design changes have prevented the development of the strength

and load factors which are necessary to prepare a computation of the individual reliability values. It is contemplated that these factors will be available in time to enable the inclusion of a CPD reliability calculation in the Fourth Quarterly Report.

#### 2.7.4 RELIABILITY FEATURES OF BOOM AND CPD

##### 2.7.4.1 Primary Booms

1. Both drive motors are in standby redundancy to each other
2. The sealed drive assembly is used to provide a normal (7 psia) atmosphere for vacuum sensitive parts
3. Pressure transducers provide timely indication of assembly seal failure
4. Lubricants within sealed drive assembly are being selected for stability in a long-term mission
5. Extension and scissoring limit switches prevent over travel of booms
6. Boom length or scissoring angle is measurable via potentiometers
7. Telemetry readout is provided to monitor all critical functions to prevent over-stressing of parts due to environmental extremes.

##### 2.7.4.2 Combination Passive Damper

1. Both dampers are in redundancy
2. All uncaging pyrotechnic devices are redundant and will be qualified in the parts qualification program

3. Design is simple, with moving parts kept to a minimum
4. Double acting solenoid and clutch will be exercised to demonstrate multi-mission operations during qualification tests
5. Temperature control will be provided to prevent low temperature extremes.

#### 2.7.5 RELIABILITY PROBLEM AREAS

During the course of the analysis, several problem areas became apparent which are in process of resolution, such as:

1. A single cable cutter (Conax) is used to initiate damper boom release. The cutter is used to sever a boom retention cable of .1875 inch aluminum.

This function is mandatory for damper boom release and subsequent 3-axis stabilization, and the failure of this device would be catastrophic to the mission.

Several alternate redundant designs have been investigated, but they have disadvantages which precluded their use.

This problem area has been discussed and evaluated in several design reviews, the decision was made to go with the present design.

2. The two squib firing circuits for squib actuation were series connected circuits wherein each circuit was signaled to fire by separate commands from the command decoders.

The latest configuration allows one command from either command decoder to fire both squibs simultaneously, which provides true redundancy for this function.

3. The mechanical complexity of the sealed drive assembly is a source of major concern from a reliability viewpoint. In any system containing many moving mechanical parts, the total weight of the unknown factors could approach or surpass the effect of the modifying factors that have been considered herein. The effect of these unknown factors (if any) can only be determined through results of engineering evaluation tests which verify the manufacturing process as well as the design.

#### 2.7.6 EVALUATION OF PRIMARY BOOM SEALED DRIVE UNIT TEST PLANS

The sealed drive unit, which is the most critical assembly within the Primary Boom System, is amenable to testing to qualify the assembly as well as the parts comprising the assembly in the scope of the Parts Qualification Program. Therefore, three test plans were evaluated by Reliability and Parts personnel to determine which plan would provide the most information about the capability of the parts and the assembly itself.

The test plans were based on the following alternatives:

1. Purchase and test 30 specimens of each part type
2. Purchase and test 20 specimens of each part type and one sealed drive unit. Also, use one of the engineering models for testing, resulting in a specimen size of 2 sealed drive units.

3. Purchase and test 5 specimens of each type and two sealed drive units. Also, use the engineering model for testing, resulting in a specimen size of three sealed drive units.

In all three test plans, five specimens of each part type are to be physically "torn down" and microscopically inspected by Materials and Processing after/during testing to verify processing integrity and/or failure criteria.

Five weighting factors were applied to each of the proposed tests as follows:

1. Percentage of the total population of parts represented by the number of parts to be tested.
2. Percentage of the failure probability represented by each part type in relation to the total sealed drive unit failure probability.
3. Probability of success represented by a test plan containing 100 dynamic mission equivalents.
4. Percentage of the application stress level at which mission profile tests can be conducted. (This percentage is raised to a power "K" to include the non-linear influence of stress level on failure rates.) The applied stress levels will vary from part to part dependent on construction, materials and environmental susceptibility. For example, a resistor can be stressed many times its use level in parts testing, whereas a motor cannot be stressed much above the manufacturer's rating without total destruction.
5. Percentage of failures attributed to parts and vendor supplied items uncovered by past programs.

Basic ground rules applied to all three test plans were:

1. 100 dynamic missions would be simulated in the parts qualification tests by repetitive stress cycles of those stresses applicable to each part type. Levels of stress would be one, two, etc. times those normally seen in the mission, extracted from component specification requirements.
2. Each sealed drive unit will be used to demonstrate 100 dynamic equivalent missions.
3. Parts used in the qualification tests will be equivalent to those purchased for the engineering model.
4. Two mechanical part types---gears and bearing---would not be tested in the parts qualification program.
5. Test Plan 2 would use one purchased sealed drive unit plus an engineering model for demonstration tests.
6. Test Plan 3 would use two purchased sealed drive units plus an engineering model for demonstration tests.

Table 2.7-8 shows the percentage of the population represented by a given specimen size at a given confidence level. This table is based on distribution-free statistics, where the required sample size is independent of the underlying distribution (Incomplete Beta Non-Parametric Tolerance Limits, Eisenhart, Hastay, Wallis; Techniques of Statistical Analysis, McGraw-Hill Book Company, Inc., New York, 1947, Chapter Two).

Table 2.7-9 shows the percentage of the failure probability of each part within the sealed assembly to the total failure probability of the sealed drive assembly, based upon average part failure rates, where:

Table 2.7-7. Cable Cutter Confidence Levels

Confidence Level	Demonstrated Reliability at 0 Failures	
	18 actuations	36 actuations
50	.962	.981
75	.925	.962
90	.879	.938

Table 2.7-8. Specimen Population

Sample Size	75% Confidence Level % of Population encompassed by the largest & smallest specimen of "n" specimens
2	8
3	18
4	35
5	65
10	75
15	83
20	87
30	92
40	94

Table 2.7-9. Percent Failure Probability

Item	No. Used In Sealed Drive Assembly	Average Failure Rate %/1000 Hrs	Fraction of Total Failure Rate
Gears	19	.012	.0015
Bearings	28	.05	.0065
Connectors	2	.001/PIN	.0033
Bellows	3	.60	.0777
Capacitors	11	.005	.0006
Pots	2	.30	.0389
$\mu$ Switches	4	.025	.0033
Motors	2	1.90	.2462
Solenoid	1	1.33	.1784
Press. Xducer	1	3.50	.4535

$$\lambda (\%) = \frac{\lambda_i}{\sum_{i=1}^n \lambda_i} \quad (4)$$

where  $\lambda_i$  = failure rate of  $i^{\text{th}}$  part  
 $i = 1, 2, \dots, n$

Table 2.7-10 shows the probability of success demonstrated by simulating 100 dynamic missions at various confidence levels ( $\chi^2$  distribution), where:

$$P \left\{ \lambda \leq \frac{\chi^2_{\alpha, 2(X+1)}}{2T} \right\} = C \quad (5)$$

which states, that if a component is tested which has an exponentially distributed lifetime for  $T$  actual test hours, and  $X$  failures are observed during this time, a confidence bound ( $C$ ) on the failure rate  $\lambda$  is given by Equation 5, where  $\chi^2$  is a  $\chi^2$  deviate with degrees of freedom,  $v = 2(X_1 + 1)$  and

$$C = \int_0^{\chi^2} f \left[ \chi^2 \mid 2(X_1 + 1) \right] d\chi^2 \quad (6)$$

It is assumed that the stress applied to the sealed drive unit in the contemplated dynamic mission tests will be the same as those in the mission. This is a simplifying assumption which can be modified or revised if a significant variability is indicated by system tests.

Table 2.7-10 shows the application of each weighting factor to all three test plans.

Table 2.7-11 classifies the failures revealed from component and systems tests on other programs, wherein the catastrophic failures were recorded and attributed to either

- (1) design procedures,
- (2) manufacturing processes,
- (3) parts,



Table 2.7-10. Demonstrated Success Probability

No. of Missions Demonstrated	Confidence Level (Percent)		
	75	90	95
20	0.933	0.891	0.861
40	0.966	0.944	0.928
60	0.977	0.962	0.951
80	0.982	0.972	0.963
100	0.987	0.977	0.970
150	0.991	0.985	0.980
200	0.994	0.989	0.985
250	0.996	0.991	0.988

Table 2.7-11. Classification of Failures, Other Programs

PROJECT	COMPONENT FAILURES						
	DESIGN	MFG.	MISC.	TEST	DFTG.	PART	VENDOR
OA O	33	51	6	4	1	14	65
NIMBUS	31	53	34	13	-	9	55
% of total DESIGN, MFG., PART & VENDOR FAILURES	20	33				8	38

- (4) test,
- (5) miscellaneous, or
- (6) vendor supplied items.

From this table, only items (1), (2), (3), and (6) were considered appropriate for use as weighting factors. For example, part failures showed up as only 8% of the total failures revealed, whereas vendor supplied components accounted for approximately 39% of all failures. Therefore, testing only 30 specimens of each part would not reveal the design and manufacturing failures which were found by tests of vendor supplied components.

#### 2.7.6.1 Conclusions

Test Plan II, Table 2.7-12 shows that a joint test of parts and assemblies would most thoroughly check out the design, manufacturing processes and all parts interaction as well as the parts themselves. The number of parts in Test Plan II provide a sufficient specimen size to be representative of the true population characteristics and the assemblies enough representation to uncover the inherent design and processing errors. The added knowledge of the joint method of testing was considered significant and Test Plan II was recommended as an adjunct to the Parts Qualification Program previously proposed to NASA.

### 2.7.7 TECHNICAL EXTRACTS

#### 2.7.7.1 Dimple Motors

Current thinking indicates that the dimple motors, similar or identical to the Hercules DM43B0, will be used to uncage (1) the Eddy Current Damper and the Damper Boom shaft, (2) the Hysteresis Damper, and (3) the Clutch Assembly. The DM43B0 dimple motor has a stated (on the Hercules data sheet) reliability of 99.9%. Presumably this is with 50% confidence and is based on their experience with both the S225D0 (Titan III Program) and the DM25J7 (various programs) rather than with the DM43B0 itself.



The reliability number of 99.9% appears to be derived from 600 ignition tests on the S225D0 which has an ignition setup configuration similar to the DM43B0. The case reliability has either been ignored or treated as unity due to the success achieved by the DM25J7 which has a case configuration closely approximating the DM43B0. A complete record of the S225D0 testing is on file in the Spacecraft Department.

This department has had the requirement that in the qualification of pyrotechnic assemblies, a minimum of 36 assemblies was required if the price per assembly was less than \$400 and a minimum of 18 if the price was \$400 or greater. The requirement for 36 is currently being studied and may be reduced to 24 assemblies. There is no historic documentation on the selection of these specific sample sizes, but the available information indicates that their ability to achieve a high degree of confidence is contingent on the pyrotechnic devices being applied redundantly.

Table 2.7-13 illustrates the reliability which could be demonstrated as a result of testing 18, 24, or 36 samples. These values are presented at three confidence levels for cases where either one or zero failures occur. Both the single and redundant application values are shown.

Table 2.7-13. Reliability Demonstrated for Pyrotechnic Sampling

Confidence Level	0 Failures		1 Failure	
	Single	Redundant	Single	Redundant
	18 samples		18 samples	
50%	.962	.998	.911	.992
90%	.879	.985	.805	.962
95%	.846	.976	.769	.946
	24 samples		24 samples	
50%	.972	.999	.932	.995
90%	.909	.992	.850	.978
95%	.883	.986	.821	.968

(Table continued on next page)

Table 2.7-13. Reliability Demonstrated for Pyrotechnic Sampling  
(Cont'd)

Confidence Level	0 Failures		1 Failure	
	Single	Redundant	Single	Redundant
	36 samples		36 samples	
50%	.981	.9996	.954	.998
90%	.938	.996	.898	.989
95%	.920	.993	.877	.984

During the testing of the Engineering Development, Prototype and Flight systems, as many as 108 devices may be functionally tested, approximately 36 at each stage. Assuming that 18 devices were qualification tested, the maximum demonstrated reliability would increase significantly after each subsequent stage. This fact is illustrated in Table 2.7-14 which shows the demonstrated reliability possible at the 95% confidence level if 36 units are tested at each hardware stage.

Table 2.7-14. Demonstrated Reliability at 95% Confidence Level

Hardware Phase	Maximum No. of Units	0 Failures		1 Failure	
		Single	Redundant	Single	Redundant
Qualification	18	.847	.976	.769	.947
Engineering Dev.	36	.946	.997	.917	.993
Prototype	36	.967	.9989	.949	.997
Flight	36	.976	.9994	.963	.9986

The figures in Table 2.7-14 provide sufficient evidence to justify the redundant use of duple motors, as currently planned in all three applications. This can be shown by the fact that over 5 units out of 100 may still fail after 54 have been tested with no failures. Since all three (Eddy Current, Hysteresis, Solenoid) units must fire to achieve complete success in this area, the combined chances of failure total 15 out of 100. Redundant usage would reduce this to less than 1 out of 100.

#### 2.7.7.2 Bridge Wires

Mechanical bridge wire failures have historically presented problems in the use of pyro-technic devices. Many of the structural defects have been overcome, however, in the method of bridge wire application that is used in the above dimple motors.

This fact, plus the intended redundant dimple motor usage, obviates the requirement for redundant bridge wires within the squibs.

#### 2.7.7.3 Driver Circuits

The present design provides the redundant dimple motors with redundant driver circuits. While decreasing the opportunity of failure due to open or low current circuits, it also increases the chance of premature firing of the squib due to a short circuit. A review of the circuit, however, reveals that the potential gain is far greater than the potential hazard from shorting which would result from the redundancy. The proposed circuit is composed primarily of seven transistors all of which are basically planar. Devices of this nature have an historical background which indicates that only 10% of their failures are due to short circuits, while 90% are due to either open circuits or out of specification values.

#### 2.7.7.4 Conclusions

The use of dimple motors to uncage the Combination Passive Damper elements is acceptable from a reliability standpoint if

1. The dimple motors are redundantly applied
2. Redundant driver circuits are used for the redundant motors.

If the above conditions are fulfilled and a mechanically strong bridgewire design is utilized, the use of one bridge wire per squib is also acceptable.

## 2.7.8 PARTS QUALIFICATION PROGRAM

Various parts proposed for use on the ATS equipment were not qualified to the practices described in the Hughes Aircraft Company Specifications. In order to define the type and specimen size of the parts which should be subjected to a qualification test cycle, a trade-off analysis approach was used. The tradeoff was based on three weighting factors; risk, need and cost.

The "risk" factor was based on:

1. Number of part type used in ATS
2. Effective operational time
3. Average failure rate of parts
4. Criticality of part in the equipment.

"Need" was based on:

1. Similarity of part type to other qualified parts
2. Available test or use data.

"Cost" was based on:

1. Cost of test specimens
2. Test Lab costs.

These three weighing factors were combined as  $\frac{\text{Risk} \times \text{Need}}{\text{Cost}} = \text{Merit.}$

Each part was then reviewed from the standpoint of ranking by merit value and the following selection approach was proposed.

1. Parts having "need" factors greater than 50 or parts having "risk" factors greater than 10, and parts having merit factors greater than 10 should receive parts "Qualification" tests, in addition to any testing requirements involved in the purchase of the parts normally provided by the vendor.
2. Those parts having a merit factor of from 1 to 10 by virtue of "risk or need" should receive a limited parts qualification; including dissection and examination of specimens in the GE-SD Materials and Processing Laboratory after testing.
3. Other parts having merit factors 1 to 10 shall receive no qualification testing at parts level other than that of dissection and examination.

Using the factors of risk "need" and cost, merit ratings were calculated for the parts or assemblies in the Gravity Gradient Stabilization Systems. This tradeoff analysis is summarized in Table 2.7-15. Following this analysis, the list of parts shown in Table 2.7-16 was prepared that specifies those parts or assemblies to be qualified and those that are not to be qualified.

The parts listed under Group A in Table 2.7-16 are those that require qualification testing. The purchase specifications were not available; however, a General Test Specification was written to permit estimation of the cost of the qualification tests. The plan was based on available Hughes' specifications, those written for other programs, and discussions with parts specialists. The plan consists of two parts:

1. A description of the tests to be made with reference to applicable MIL specifications (See Paragraph 2.7.8.2) and
2. Table 2.7.-17 which shows the paragraphs of 1. above which apply in each case, the tests to be made after each test condition, and the test conditions themselves.



Table 2.7-15. Relative Risk Analysis for ATS Parts Qualification Program

Description	Vendor Identification	n	t	c	$\lambda$	$\frac{c\lambda t}{1000}$	Need Factor	Weighted Cost	Merit	Comment	Significance
Connector	Amphenol	12	4000	1.0	0.001	16.0	10	2.8	57	MAC Tests	100 Spec x 350 Hrs.
Connector	DBM 255 NMC	2	4000	1.0	0.001	1.7	10	3.7	5	HAC NME Similar to NMC	
Connector	DCM 37P NMC	2	4000	1.0	0.001	2.7	10	3.3	8	HAC NME Similar to NMC	
Connector	DEH 25P-202	2	4000	1.0	0.001	1.7	100	3.4	50	No Data Available	
Transistor	Texas Instrument 2N2432	85	2000	1.0	0.045	76	0.1	2.2	3	GE R4343 Similar to R4048	
Transformer	Tresco	2	66	0.01	0.025	0.01	100	5.4	1	No Data Available	NASA Test in Process
Transformer	DC-AC (Special)	1	4000	0.1	0.025	0.1	100	12.9	1	No Data Available	
Transformer	UTC	1	4000	0.1	0.025	0.1	10	3.4	1	QPL-27 Mech Only	
Transformer	Raytheon	2	66	0.01	0.025	0.01	1	3.4	0	NASA MIL-T-39013	
Transformer	Edgetek	1	2050	1.0	0.025	0.5	100	3.8	13	No Data Available	
Solar Cell Assembly	Heliotek	5	2000	1.0	0.035	59	100	28.8	200	No Data Available	Also Investigate Clutch Adjustment Problem
Solar Cell Assembly	Hoffman	4	4000	0.1	0.035	0.6	10	1.9	30	GE Nimbus 55C Similar to 120C	
2-Way Clutch Solenoid		1	16 ~	1.0	1.33	0.5	100	31.9	2	No Data Available	
Rotary Solenoid	Ledex	2	17 ~	0.1	1.33	0.08	100	7.3	1	No Data Available	
Switch	Minn-Hon	8	1 ~	1.0	0.025	0.08	75	3.3	2	No Data Available	
Switch	6NN1-1	1	16 ~	0.01	0.025	0.01	75	2.1	1	No Data Available	Further Search of Data Sources should be made
Switch	Minn-Hon	8	1 ~	1.0	0.025	0.08	75	2.5	3	No Data Available	
Switch	2NM-1-3	8	1 ~	1.0	0.025	0.08	75	1.2	5	No Data Available	
Switch	12SM-4	8	11 ~	0.01	0.025	0.01	75	1.4	1	No Data Available	
Switch	Minn-Hon	2	400	0.1	0.10	0.4	100	0.7	30	No Data Available	
Lamp	Chicago Min. Lamp	2	400	0.1	0.10	0.4	100	0.7	30	No Data Available	Complete Data if CM 8 were used
Cable Cutter	Conax (Special)	2	17 ~	1.0	1.9	2.3	100	Special	200+	No Data Available	
Motor	Globe	114A143					75	16.4	11	No Data Available	
Motor	Globe	114A144					75	16.4	28	No Data Available	
Pressure Transducer	CIC	2	4000	0.05	3.5	14	100	14.7	190	No Data Available	
Thermistor	Fenwall	4	4000	0.05	0.06	0.5	25	4.8	6	Further search	Fenwall thermistor deleted 6 specimens tested Special squibs Data Available on Sprague 127P 500,000 revolutions tested at Bendix
Relay	GE	11	668	1.0	0.012	6.7	10	6.9	10		
Dimple Pyrotechnic Capacitor	(Special) Sprague	192P					100	Special	200+		
Potentiometer	Helipot	12	66	1.0	0.002	1.6	100	1.5	8		
Potentiometer	TSPR10K(2)L2	2	4000	0.01	1.4	1.1	100	3.6	0		
Potentiometer	Helipot	7223R10K(1)L2	2	4000	0.01	1.4	1.1	3.4	0		3 specimens - MIL environment 500,000 revolutions tested at Bendix 3 specimens - MIL environment
Bellows					0.6	728	100	9.0	300		

n = Number used per system  
 t = Effective Mission Risk Time based on Orbit Test Plan  
 c = Criticality per mission, e.g., Telemetry only = 0.01 Angle Detector = 0.10 In-Line Item = 1.00  
 $\lambda$  = Mission failure rate  
 Special = Pyrotechnic device to be qualified by GE

Table 2.7-16. ATS Parts Qualification Program

ITEM	DESCRIPTION	VENDOR/IDENT.	QTY	USE
GROUP A - PARTS REQUIRING QUALIFICATION*				
1	Connector	Amp - 47-205161	15	PCU CB to Chassis
2	Connector	Cannon - DBH 25P202	15	Boom Ass'y - Sealed Box
3	Transformer	Edgerton - TF5SXD922	15	SAS
4	Sensing Element Ass'y	Heliotek	15	SAS
5	Solar Cell	Hoffman - 55C	15	Angle Indicator
6	Lamp			
	Head Ass'y DRC	Chicago - Mini. Lamp		Angle Indicator
7	Cable Cutter	Conax	18	Damp. Boom
8	Pressure Transducer	--	15	Boom Ass'y - Sealed Box
9	Dimple Motors	--	18	Damper
10	Potentiometer (Scissors)	Helipot TSPR10K(2) L2	15	Boom Ass'y
11	Potentiometer (Ext.)	Helipot T223R10K(1) L2	15	Boom Ass'y
12	Transistor	--	15	Angle Indicator
13	Transformer	Spec D C - A C	15	Angle Indicator
14	Extension Limit Switch	Minn-Hon-2HM1-3	15	Boom Ass'y
15	Scissors Limit Switch	Minn-Hon-6HM1-1	15	Boom Ass'y
16	Motor - Boom Display	Globe	15	Boom Ass'y - Sealed Box
17	Motor - Scissors	Globe	15	Boom Ass'y - Sealed Box
18	Double Acting Solenoid	--	15	Damper
19	Sealed Drive Unit	deHavilland	2**	Boom Ass'y
GROUP B - NO QUALIFICATION REQUIRED*				
1	Connector	Cannon DBM 25SNMC-1-A106	5	Boom Ass'y
2	Connector	Cannon DCM 37PNMC-1-A106	5	Boom Ass'y
3	Transistor	TI 2N2432	5	SAS
4	Transformer	Tresco YS124	5	PCU
5	Transformer	UTC - DI - T36	5	Angle Indicator
6	Transformer	Raytheon R4077	-	PCU
7	Relay	R2314	5	PCU
8	Solenoid - Rotary	--	5	Boom Ass'y - Sealed Box
9	Switch	Min-Hon. 1HM-1	5	Solenoid/Clutch Position Switch Damper Boom Deployment
10	Switch	Minn-Hon. 12SM4T	5	Clutch Position - Boom
11	Bellows	--	5	Boom Ass'y - Sealed Box
12	Temp. Sensors	--	5 ea.	All
13	Thermistor	Fenwall 6B32P82C	5	Boom Ass'y - Sealed Box
14	Capacitor	Sprague 192P	5	Boom Ass'y - Arc Suppressor

\*Group A defines the parts which are to be subjected to a parts qualification program. The qualification program is to be basically the same as practiced by HAC on the ATS program and is described in the attached ATS General Test Specification.

\*\*Use sealed drive unit from Engineering Unit as one qualification unit.

Table 2.7-17. Group "A" Parts (Except 4, 5, 6, 7 and 9)

ITEM/TEST	1.2	1.3	1.4.1	1.4.2	1.5	1.6	1.7	1.8	1.9	1.10	1.11
1 and 2	1250 Vac	500 Vdc	-65C 1.3	1.3 1.2	-	202 1.2, 1.3	100G (10) 1.2	1.2 Monitored	1.2(150V) 1.3	-	120 Cycles Mating 1000 hrs - 300F 1.2, 1.3
1.10 Mating and demating force, contact voltage drop - 1.6, 1.9, 1.11											
3 and 13	100 Vac	100 Vdc	-65C 1.2, 1.3	1.2, 1.3	1.2, 1.3	202 105C	100G (10) 1.2, 1.3	1.2 Monitored	-	-	12 Wks - Cycles 1.2, 1.3
1.10 Performance checks using special circuit, temperature rise.											
18	-	100 Vdc	-65C 1.3	1.3	-	202 105C 1.3	100G (10) 1.3	1.3	-	-	1600 Operations 25C 1.3
14 and 15	-	100 Vdc	-65C 1.3	1.3	-	202 105C 1.3	100G (10) 1.3	1.3	-	-	1600 Operations 25C 1.3
16 and 17	100 Vac	100 Vdc	-65 Operation Torque 1.2, 1.3	Operation Torque 1.2, 1.3	1.2, 1.3	1.2, 1.3	100G (10) 1.2, 1.3	1.2, 1.3	-	-	1500 Hrs 50C 500 Cycles - 2
8	-	100 Vdc	-	-	-	-	50G (10) 1.2	Monitored 1.3	-	-	10,000 Cycles
1.10 Temperature cycling, MIL-202, method 102, cond. D, 100 cycles.											
10 and 11	750 Vac	500 Vdc	-65 1.3	1.2 1.3	1.3 Torque	105C 1.3 1.2	100G (10) Monitored 1.3 1.2	Monitored 1.3 1.2	-	-	20,000 cycles intermittent 65C Vac performance
1.10 Resistance temperature characteristic, electrical travel, resistance variation, torque - 1.4.1, 1.4.2											
12	-	-	-	-	-	202 105C	750	20G	-	-	1500 Hrs Operating
1.10 Helium leak, gross leak, temperature cycling, 20,000g acceleration.											

For example, all paragraphs of the test plan apply to Items 3 and 13. The withstanding voltage of Para. 1.2 is shown to be 100 vac. The insulation resistance is to be measured at 100 vdc. After both high and low temperature extremes, the tests of Para. 1.2 and 1.3 are to be repeated. Under thermal shock, Para. 1.6, the reference is to MIL-STD-202 and the high temperature is 105C. Under shock, Para. 1.7, the intensity is 100g and 10 repetitions, followed by the test of Para. 1.2 and 1.3. The vibration test, Para. 1.9, is required. Special tests are required, Para. 1.10, as specified in the part specification. The life test, Para. 1.11, is cyclic for 12 weeks, followed by the tests of Para. 1.2 and 1.3.

No details are given for Items 4, 5, 6, 7, and 9 because they will be tested by the respective vendor.

#### 2.7.8.1 ATS General Test Specification

##### 1. Methods of Examination and Test

1.1 Visual and Mechanical Inspection - The dimensions, marking, materials, finishes and surfaces shall be inspected.

1.2 Dielectric Withstanding Voltage - In accordance with Method 301 of MIL-STD-202. Test voltage and points of application specified in the individual part specification.

1.3 Insulation Resistance - In accordance with Method 302, Condition B of MIL-STD-202. Points of application specified in the individual part specification.

##### 1.4 Temperature Extremes -

1.4.1 Low Temperatures - The specimens shall be placed in a chamber and the temperature lowered to the temperature specified in the particular part specification and held at this temperature for 48 hours.

1.4.2 High Temperature - The specimens shall be placed in a chamber and the temperature raised to 100C and held at this temperature for 48 hours.

1.4.3 Functional Tests - The mode of operation and the tests to be performed are specified in the individual part specifications.

1.5 Thermal Vacuum -

1.5.1 High Temperature Vacuum - The specimens shall be placed in a vacuum chamber and the temperature raised to 65C. The pressure shall be reduced to  $10^{-6}$  Torr or lower. When stable conditions have been achieved, the specimens shall be operated and their temperature monitored for a period of 48 hours.

1.6 Thermal Shock - In accordance with Method 107, Condition C, of MIL-STD-202 or Method 503 of MIL-STD-810. The temperature extremes and the applicable method shall be as specified in the individual part specification.

1.7 Shock - In accordance with Method 202 of MIL-STD-202, Method 516-I of MIL-STD-810, or Method 2016, MIL-STD-750. Applicable method, number of shocks, magnitude and direction as specified in the individual part specification.

1.8 Vibration - In accordance with Table III and Table IV of SVS 7316A except that the levels shall be twice those listed.

1.9 Humidity - In accordance with Method 507 of MIL-STD-810. Conditions and cycles are given in the individual part specification.

1.10 Special Tests - As specified in the part specification.

1.11 Life - See the individual part specification.

### SECTION 3

#### NEW TECHNOLOGIES

In compliance with the provisions of the New Technologies clause in the applicable contract, GE has continued to maintain surveillance over the design and development of the Gravity Gradient Stabilization System for reportable items. One such new technology involves the economical use of a digital bit output from the proposed damper boom angle indicator.

Briefly, the damper boom angle indicator functions as follows: A coded disc is mounted to the damper boom shaft through which light is passed from one of two sources onto photo transistors. (Refer to Figure 2.3-15 for the plan of the angle detector.) The disc code utilizes an expanded Gray code. By taking advantage of the increasing allowable errors of angle detection away from null ( $+1^\circ$  from  $+10^\circ$  to  $-10^\circ$  and 10% from  $\pm 10^\circ$  to  $\pm 45^\circ$ ) it is only necessary to use five bits. (An additional five bits are used to compensate for radial and cocking motions of the damper boom shaft.) Typical outputs for any shaft position would consist of three, 10-bit digital words, all of which are unique to that one position.

The design of the angle detector is unique because it utilizes the reduced accuracy requirements from  $\pm 10^\circ$  to  $\pm 45^\circ$  to achieve maximum economy of digital bits. If a conventional Gray code (or a true binary code for that matter) were used to provide a digital readout for every degree from  $+45^\circ$  to  $-45^\circ$  (or 90 discrete bits of information), seven bits would be required for each of the two detector heads used in the system (i.e.,  $2^7 = 128$ , the next power of 2 above 90). In the proposed system, a change in the bits of word designation occur at the following angles (for both positive and negative values).

$\left. \begin{array}{c} 2 \\ 4 \\ 6 \\ 8 \\ 10 \end{array} \right\}$	$\left. \begin{array}{c} 1^\circ \\ \text{Accuracy} \end{array} \right\}$	12	$\left. \begin{array}{c} \\ \\ \\ \\ \\ \\ \\ \\ \\ \\ \end{array} \right\}$	$\left. \begin{array}{c} 10\% \text{ Accuracy} \end{array} \right\}$
		14		
		16		
		18		
		20		
		24		
		28		
		32		
		38		
		45		

Examination of the intervals indicates that any angle will be "read-out" to an accuracy of at least  $\pm 1^\circ$  or  $\pm 10\%$ , whichever is the greater. Because these limits represent the accuracy specified for the performance of the damper boom angle indicator, and only 15 bits of information are required to achieve this read-out (a total of 30 bits), the necessary intelligence can be achieved with 5 bits for each head.

## SECTION 4

### GLOSSARY

The following is a list of abbreviations and definitions for terms used throughout this report.

ADTF	Advanced Damping Test Fixture (used for CPD testing)
ATS-A	Medium Altitude Gravity Gradient Experiment (6000-nautical mile orbit flight)
ATS-D/E	Synchronous Altitude Gravity Gradient Experiment (24-hour orbit flight)
CPD	Combination Passive Damper
Crab Angle	Out-of-orbit angle flight caused by changes in X-rod angle
GE-MSD	General Electric Company Missile and Space Division
G <sup>2</sup> S/ATS	Gravity Gradient System/ATS
HAC	Hughes Aircraft Company
Local Vertical	Imaginary line extending from the satellite center of mass to the center of mass of the earth
LOFF	Low Order Force Fixture
MTBF	Mean Time Before Failure
MTTF	Mean Time to Failure
PCU	Power Control Unit
PIR	Program Information Request/Release, GE documentation
SAS	Solar Aspect Sensor
Scissoring	Changing the angle included between the primary booms in a manner that maintains a symmetrical configuration about the satellite yaw axis
STEM	Storable Tubular Extendable Member
Stiction Torque	That amount of initial torque required to overcome the initial effects of friction
SVA Fixture	Shock and Vibration Attachment Fixture
Thermal Twang	Sudden thermal bending which the booms will experience in passing from a region of total eclipse into a region of continuous sunlight or vice versa
TR	Torsional Restraint
TVCS	TV Camera Subsystem



## APPENDIX A. THE EFFECT OF ORBIT PARAMETER UNCERTAINTIES ON THE DETERMINATION OF SPACECRAFT ATTITUDE

### Introduction and Summary

The object of this study is to determine the influence of uncertainties in the satellite orbital elements on the determination of attitude, for the Applications Technology Satellite. Numerical results are based on a synchronous equatorial orbit, attitude data consisting of solar aspect information and the angle of polarization of received RF energy, and a ground station located at Mojave. However, all equations to be presented are given in appropriate generality.

Numerical results were obtained using the LGP-21 computer. The analysis of these results has led to the following conclusions: For the synchronous equatorial orbit, attitude determination is quite insensitive to errors in two of the orbital elements provided the orbit is of nominal eccentricity zero; namely,

$\Omega$  = the longitude of the ascending node,

$\omega$  = the longitude of perigee.

Attitude determination will be sensitive to errors in the remaining orbital elements.

$i_p'$  = the inclination of the orbit plane

$\epsilon_p$  = the mean satellite longitude

$e$  = the numerical eccentricity

$a$  = the semimajor axis

In order that errors in orbital elements should not result in errors of more than  $1^\circ$  in roll pitch, and yaw angles (using  $3\sigma$  confidence intervals) over a period of one week, it will suffice if the orbital elements can be estimated with the following accuracy:

$$\text{s.d. } (\Delta i_p') \leq 0.08^\circ$$

$$\text{s.d. } (\Delta \epsilon_p) \leq 0.04^\circ$$

$$\text{s.d. } (\Delta e) \leq 4 \times 10^{-4}$$

$$\text{s.d. } (\Delta a) \leq 0.5 \text{ km.}$$

The above results have been derived on the assumptions that:

1. The orbit is of nominal eccentricity zero, (i.e.,  $e$  is very close to 0)
2. The orbit is Keplerian.
3. Roll, pitch, and yaw angles are small.

# 1. Errors in Orbital Elements and Errors in Position

We consider a satellite in a geocentric orbit, of nominal eccentricity zero. The position of the satellite, in the geocentric equatorial coordinate system, will be specified by four quantities  $\Omega_p, i_p, u_p, r_p$ , defined as follows:

$\Omega_p$  = the longitude of the ascending node of the orbit,

$i_p$  = the inclination of the orbit,

$u_p$  = the argument of latitude of the satellite,

$r_p$  = the distance from the geocenter to the satellite.

The position of the satellite is computed from the elements of the satellite orbit. The elements are taken to be:

$\Omega'_p$  = the longitude of the ascending node,

$i'_p$  = the inclination of the orbit plane,

$\hat{\omega}_p$  = the longitude of perigee,

$e$  = the eccentricity,

$a$  = the semimajor axis,

$\epsilon_p$  = the mean longitude of the satellite, specified for a given time  $t_0$ , the epoch; we take  $t_0 = 0$ .

The position of the satellite, for a given time  $t$ , is computed by solving Kepler's equation

$$E - e \cdot \sin E = n \cdot t + \epsilon_p - \hat{\omega}_p$$

for the eccentric anomaly  $E$ , where  $n$  is the mean motion,

$$n = k_e \cdot a^{-3/2},$$

$k_e$  being the earth's gravitational constant.  $r_p$  is determined by

$$r_p = a (1 - e \cos E),$$

and  $u_p$  is determined from

$$\tan 1/2 E = \left\{ \frac{1-e}{1+e} \right\}^{1/2} \cdot \tan 1/2 (u_p - \hat{\omega}_p + \Omega'_p)$$

As was stated above, the orbit is assumed to be of nominal eccentricity zero.

Once the position of the satellite has been established, the following quantities are determined:

$(l'_1, m'_1, n'_1)$  = the direction cosines of the satellite-to-station line, in the local satellite orbit coordinate system.

$(l'_s, m'_s, n'_s)$  = the direction cosines of the sun line, in the local satellite orbit coordinate system.

This information, in conjunction with data from various sensors, is used to determine the attitude of the satellite. The attitude of the satellite is specified by angles  $\theta_B, \phi_B, \psi_B$ , the pitch, roll, and yaw angles.  $\theta_B, \phi_B, \psi_B$  are then functions of position (as well as sensor data) so that

$$\theta_B = \theta_B(\Omega_p, i_p, u_p, r_p),$$

$$\phi_B = \phi_B(\Omega_p, i_p, u_p, r_p),$$

$$\psi_B = \psi_B(\Omega_p, i_p, u_p, r_p).$$

Errors in position will result in errors in the determination of attitude. Differential errors  $d\Omega_p, di_p, du_p, dr_p$  will give rise to differential errors  $d\theta_B, d\phi_B, d\psi_B$ ; if it is assumed that the differential errors in sensor data are zero,

$$d\theta_B = \frac{\partial \theta_B}{\partial \Omega_p} \cdot d\Omega_p + \frac{\partial \theta_B}{\partial i_p} \cdot di_p + \frac{\partial \theta_B}{\partial u_p} \cdot du_p + \frac{\partial \theta_B}{\partial r_p} \cdot dr_p,$$

and similar equations hold for  $d\phi_B$  and  $d\psi_B$ .

Now compute  $du_p$  and  $dr_p$

as functions of the differentials of the orbital elements:

From the equation for  $\mathcal{N}_p$ ,

$$d\mathcal{N}_p = da \cdot (1 - e \cos E) + a \cdot (-de \cdot \cos E + e \sin E dE),$$

and taking  $e = 0$ ,

$$d\mathcal{N}_p = da - a \cos E de.$$

While from Kepler's equation,

$$dE - de \cdot \sin E - e \cos E dE = t \cdot dn + d\epsilon_p - d\bar{\omega}_p$$

taking  $e = 0$ , and solving for  $dE$ ,

$$dE = (\sin E) \cdot de + t \cdot dn + d\epsilon_p - d\bar{\omega}_p$$

From the definition of  $n$ ,

$$dn = k_e \cdot \left( -\frac{3}{2} a^{-\frac{5}{2}} \right) \cdot da = -\frac{3}{2} \cdot \frac{n}{a} \cdot da.$$

Differentiating the equation for  $\mathcal{U}_p$ , and setting  $e = 0$ ,

$$\begin{aligned} \left[ \sec^2 \frac{1}{2} E \right] \cdot dE &= \left[ -2 \tan \frac{1}{2} (u_p - \bar{\omega}_p + \Omega'_p) \right] \cdot de \\ &+ \left[ \sec^2 \frac{1}{2} (u_p - \bar{\omega}_p + \Omega'_p) \right] (du_p - d\bar{\omega}_p + d\Omega'_p) \end{aligned}$$

Now with  $e = 0$ ,  $E = u_p - \bar{\omega}_p + \Omega'_p$ , so that the above equation simplifies to

$$dE = \left[ -2 \sin \frac{1}{2} E \cos \frac{1}{2} E \right] \cdot de + (du_p - d\bar{\omega}_p + d\Omega'_p).$$

Solving for  $du_p$ ,

$$du_p = d\bar{\omega}_p - d\Omega'_p + dE + \sin E de$$

In this equation, substitute the expression for  $dE$ , giving

$$\begin{aligned} du_p &= d\bar{\omega}_p - d\Omega'_p + t \cdot dn + d\epsilon_p - d\bar{\omega}_p + 2 \sin E \cdot de \\ &= d\epsilon_p - d\Omega'_p - \left[ \frac{3}{2} \cdot \frac{n}{a} \cdot t \right] \cdot da + 2 \sin E \cdot de. \end{aligned}$$

Assuming that the partials

$$\frac{\partial \theta_B}{\partial \Omega_p}, \frac{\partial \theta_B}{\partial i_p}, \frac{\partial \theta_B}{\partial u_p}, \frac{\partial \theta_B}{\partial n_p}$$

have been computed (and the corresponding partials of  $\phi_B$  and  $\psi_B$ ), compute the corresponding partials with respect to the elements by:

$$\frac{\partial \theta_B}{\partial \Omega'_p} = \frac{\partial \theta_B}{\partial \Omega_p} - \frac{\partial \theta_B}{\partial u_p},$$

$$\frac{\partial \theta_B}{\partial i'_p} = \frac{\partial \theta_B}{\partial i_p}, \quad \frac{\partial \theta_B}{\partial \omega_p} = 0,$$

$$\frac{\partial \theta_B}{\partial a} = \frac{\partial \theta_B}{\partial n_p} - \frac{3}{2} \cdot \frac{n}{a} t \cdot \frac{\partial \theta_B}{\partial u_p},$$

$$\frac{\partial \theta_B}{\partial e} = 2 \sin E \cdot \frac{\partial \theta_B}{\partial u_p} - a \cos E \cdot \frac{\partial \theta_B}{\partial n_p},$$

$$\frac{\partial \theta_B}{\partial \epsilon_p} = \frac{\partial \theta_B}{\partial u_p}.$$

Let  $v_1, \dots, v_6$  denote the orbital elements, in the order in which they were introduced.

$$(\delta \theta_B)^2 = \sum_{i=1}^6 \sum_{j=1}^6 \frac{\partial \theta_B}{\partial v_i} \cdot \frac{\partial \theta_B}{\partial v_j} \cdot dv_i dv_j,$$

and approximately,

$$(\Delta \theta_B)^2 \doteq \sum_{i=1}^6 \sum_{j=1}^6 \frac{\partial \theta_B}{\partial v_i} \cdot \frac{\partial \theta_B}{\partial v_j} \cdot \Delta v_i \cdot \Delta v_j.$$

Now from the equation

$$\Delta \theta_B \doteq \sum_{i=1}^6 \frac{\partial \theta_B}{\partial v_i} \cdot \Delta v_i$$

it follows that

$$E(\Delta \theta_B) \doteq \sum_{i=1}^6 \frac{\partial \theta_B}{\partial v_i} \cdot E(\Delta v_i).$$

Assuming that the errors in estimating the  $\psi_i$  are not biased, i.e. that  $E(\Delta\psi_i) = 0$ , it follows that  $E(\Delta\theta_B) = 0$  and that

$$\text{Var}(\Delta\theta_B) = \sum_{i=1}^6 \sum_{j=1}^6 \frac{\partial \theta_B}{\partial \psi_i} \cdot \frac{\partial \theta_B}{\partial \psi_j} \cdot \text{Cov}(\Delta\psi_i, \Delta\psi_j).$$

Thus, given the variance - covariance matrix of the  $\psi_i$ 's, that is, given the values of the  $\text{Cov}(\Delta\psi_i, \Delta\psi_j)$ , we may compute  $\text{Var}(\Delta\theta_B)$ , approximately.

Furthermore, if the  $\Delta\psi_i$  are independent random variables, then

$$\text{Var}(\Delta\theta_B) = \sum_{i=1}^6 \left[ \frac{\partial \theta_B}{\partial \psi_i} \right]^2 \cdot \text{Var}(\Delta\psi_i).$$

Of course, it is hardly to be expected that the  $\Delta\psi_i$  should be independent, or even uncorrelated. Even so,  $\text{Var}(\quad)$  can be estimated in terms of the  $\text{Var}(\quad)$  as follows. Let

$$s(\Delta\theta_B; \Delta\psi_i) = \left| \frac{\partial \theta_B}{\partial \psi_i} \right| \cdot (\text{s.d.}(\Delta\psi_i))$$

and call  $s(\Delta\theta_B; \Delta\psi_i)$  the component of error in  $\theta_B$  due to error in  $\psi_i$ .

By Schwartz's inequality for a probability space,

$$\begin{aligned} |\text{Cov}(\Delta\psi_i, \Delta\psi_j)| &\leq \text{Var}(\Delta\psi_i)^{1/2} \cdot \text{Var}(\Delta\psi_j)^{1/2} \\ &= (\text{s.d.}(\Delta\psi_i)) \cdot (\text{s.d.}(\Delta\psi_j)). \end{aligned}$$

Hence it follows that

$$\begin{aligned} \text{Var}(\Delta\theta_B) &= \sum_{i=1}^6 \sum_{j=1}^6 \frac{\partial \theta_B}{\partial \psi_i} \frac{\partial \theta_B}{\partial \psi_j} \cdot \text{Cov}(\Delta\psi_i, \Delta\psi_j) \\ &\leq \sum_{i=1}^6 \sum_{j=1}^6 \left| \frac{\partial \theta_B}{\partial \psi_i} \right| \left| \frac{\partial \theta_B}{\partial \psi_j} \right| (\text{s.d.}(\Delta\psi_i)) (\text{s.d.}(\Delta\psi_j)) \\ &= \left[ \sum_{i=1}^6 \left| \frac{\partial \theta_B}{\partial \psi_i} \right| (\text{s.d.}(\Delta\psi_i)) \right]^2 = \left[ \sum_{i=1}^6 s(\Delta\theta_B; \Delta\psi_i) \right]^2 \end{aligned}$$

whence approximately,

$$\text{s.d.}(\Delta\theta_B) \leq \sum_{i=1}^6 s(\Delta\theta_B; \Delta\psi_i).$$

Thus to estimate s.d. ( $\Delta\theta_B$ ), it suffices to compute the  $|\frac{\partial\theta_B}{\partial v_i}|$  and to estimate the s.d. ( $\Delta v_i$ ). Of course, similar conclusions pertain to  $\phi_B$  and  $\psi_B$ .

Considering the partials  $\frac{\partial\theta_B}{\partial v_i}$ , it was seen that they are computable in terms of

$$\frac{\partial\theta_B}{\partial\Omega_p}, \quad \frac{\partial\theta_B}{\partial i_p}, \quad \frac{\partial\theta_B}{\partial u_p}, \quad \frac{\partial\theta_B}{\partial n_p}$$

i.e., in terms of the partials with respect to position, at least provided  $a$ ,  $E$ ,  $n$ , and  $t$  are specified. The quantities  $a$ , and  $n$  (which is computed from  $a$ ), are specified for the various orbits (medium and synchronous) being considered for the Application Technology Satellites.

As for  $t$ , it makes sense to consider the worst case. Thus, assuming orbital elements are supplied every week, the epoch  $t_0$  occurring at the beginning of the week, and predictions of position being made thereafter throughout the week on this basis,  $t$  would be at most equal to one week. If the basic unit of time is the minute, take

$$t = 1.008 \times 10^4 \text{ minutes.}$$

An estimate of  $|\frac{\partial\theta_B}{\partial a}|$ , valid throughout the week, is given by

$$|\frac{\partial\theta_B}{\partial a}| \leq |\frac{\partial\theta_B}{\partial n_p}| + \frac{3}{2} \cdot \frac{n}{a} \cdot (1.008 \times 10^4) \cdot |\frac{\partial\theta_B}{\partial u_p}|.$$

Specification of  $E$  affects only  $\frac{\partial\theta_B}{\partial e}$ . Again it is reasonable to consider the worst case. By Schwarz's inequality,

$$\begin{aligned} |\frac{\partial\theta_B}{\partial e}|^2 &= \left| \frac{\partial\theta_B}{\partial u_p} \cdot 2 \sin E - \frac{\partial\theta_B}{\partial n_p} \cdot a \cos E \right|^2 \\ &\leq \left[ \left( 2 \cdot \frac{\partial\theta_B}{\partial u_p} \right)^2 + \left( a \cdot \frac{\partial\theta_B}{\partial n_p} \right)^2 \right] \end{aligned}$$

and furthermore, there will be values of the eccentric anomaly  $E$  for which equality will hold above. Thus,

$$|\frac{\partial\theta_B}{\partial e}| \leq \left[ \left( 2 \cdot \frac{\partial\theta_B}{\partial u_p} \right)^2 + \left( a \cdot \frac{\partial\theta_B}{\partial n_p} \right)^2 \right]^{1/2}$$

will give a "perfect" estimate, for worst case analysis.



The above estimates will be used to compute bounds for  $\left| \frac{\partial \theta_B}{\partial a} \right|$ ,  $\left| \frac{\partial \theta_B}{\partial e} \right|$  and for the corresponding partials of  $\theta_B$ . The problem of estimating the  $\left| \frac{\partial \theta_B}{\partial v_c} \right|$  is thereby reduced to the problem of computing the partials of  $\theta_B$  with respect to position, which latter is a purely geometric problem, as will be shown; by this is meant that the partials of  $\theta_B$  with respect to position depend only on the relative positions of station, sun, and satellite, provided the local satellite orbit coordinate system is known. Knowledge of the local satellite orbit coordinate system requires knowledge of the velocity vector of the satellite, in addition to the satellite's position.

A word about units: The above formulas presuppose that angular quantities  $u_p$ ,  $du_p$ , etc., are measured in radians. The unit of time is the minute. the unit of distance is the mean equatorial radius, equal to

$$6378.145 \text{ km.},$$

( [3] , p. 92) , and

$$k_e = 0.07436574$$

( [3] . p. 92) .

Considering a synchronous equatorial orbit,

$$\dot{\iota}_p = 0^\circ \quad , \quad \Omega_p = 0^\circ$$

$$h_p = 22,766 \text{ n. miles}$$

( [1] , p. 9) .

---

\* See References at the end of this Appendix.

## 2. The Positions of Satellite, Station and Sun

We will assume that the sensor data to be used in determining the satellite attitude consists of:

- 1) The sun direction line from the satellite, supplied by the Solar Aspect Sensor;
- 2) The angle of polarization.

The relative positions of satellite, station, and sun are then relevant to this study.

Suppose the position of the satellite is given by definite values of  $\Omega_p$ ,  $i_p$ ,  $u_p$ , and  $r_p$ . Let

$\vec{r}_e$  = the vector from the geocenter to the satellite, in geocentric equatorial coordinates.

Letting  $\vec{i}_r$ ,  $\vec{j}_r$ ,  $\vec{k}_r$  be the unit vectors, originating at the geocenter, which define the local satellite orbit coordinate system, the following expressions for  $\vec{i}_r$ ,  $\vec{j}_r$ ,  $\vec{k}_r$  in the geocentric equatorial coordinate system may be written: ( (1), p. 6 )

$$\vec{i}_r = \begin{pmatrix} -\sin u_p \cdot \cos \Omega_p & -\sin u_p \cdot \sin \Omega_p \\ -\cos u_p \cdot \cos i_p \cdot \sin \Omega_p + \cos u_p \cos i_p \cos \Omega_p & \cos u_p \cdot \sin i_p \end{pmatrix}$$

$$\vec{j}_r = (-\sin i_p \cdot \sin \Omega_p, \sin i_p \cdot \cos \Omega_p, -\cos i_p)$$

$$\vec{k}_r = \begin{pmatrix} -\cos u_p \cdot \cos \Omega_p & -\cos u_p \cdot \sin \Omega_p \\ +\sin u_p \cdot \cos i_p \cdot \sin \Omega_p & -\sin u_p \cos i_p \cos \Omega_p, -\sin u_p \sin i_p \end{pmatrix}$$

Since  $\Omega_p$ ,  $i_p$ ,  $u_p$  are specified, these vectors can be computed. And since,

$$\vec{r}_e = -r_p \cdot \vec{k}_r$$

the vector  $\vec{r}_e$  may be computed.

The position of the station will be specified as follows. Let

$\lambda_1$  = right ascension of the station,

$\lambda_p$  = right ascension of the satellite,

$\delta_1$  = geocentric latitude of the station.

$\delta_1$  will be taken to be the latitude of Mojave,

$$\delta_1 = 35.33^\circ,$$

and the position of the station will be determined by specifying  $\lambda_1 - \lambda_p$ . Putting

$$\vec{E} = (E_I, E_J, E_K)$$

in geocentric equatorial coordinates,  $\cos \lambda_p$  and  $\sin \lambda_p$  are computed by putting

$$n = (E_I^2 + E_J^2)^{\frac{1}{2}}$$

and then setting

$$\cos \lambda_p = E_I/n, \quad \sin \lambda_p = E_J/n.$$

One then computes  $\cos \lambda_1$ ,  $\sin \lambda_1$  by

$$\begin{aligned} \cos \lambda_1 &= \cos \lambda_p \cdot \cos (\lambda_1 - \lambda_p) - \sin \lambda_p \cdot \sin (\lambda_1 - \lambda_p), \\ \sin \lambda_1 &= \sin \lambda_p \cdot \cos (\lambda_1 - \lambda_p) + \cos \lambda_p \cdot \sin (\lambda_1 - \lambda_p). \end{aligned}$$

Letting

$\vec{\eta}$  = the vector from the geocenter to the station, in geocentric equatorial coordinates,

compute  $\vec{\eta}$  by

$$\vec{\eta} = ( \rho \cos \delta_1 \cos \lambda_1, \rho \cos \delta_1 \sin \lambda_1, \rho \sin \delta_1 ),$$

where  $\rho$  is the radius of the earth at geocentric latitude  $\delta_1$ . The basic unit of length is the mean equatorial radius. For our purposes, it suffices to consider a spherical earth and to take  $\rho = 1$ .

Set

$\lambda_s$  = the right ascension of the sun,

$\vec{\omega}$  = vector of length 1 in the direction of the sun, in geocentric equatorial coordinates,

$\delta_s$  = the declination of the sun.

The sun direction  $\vec{\omega}$  is determined by specifying  $\lambda_s$ .

$\delta_s$  is then computed by

$$\tan \delta_s = \tan 23.45^\circ \cdot \sin \lambda_s ,$$

$23.45^\circ$  being the inclination of the ecliptic, and  $\vec{\omega}$  is computed by

$$\vec{\omega} = (\cos \delta_s \cos \lambda_s , \cos \delta_s \sin \lambda_s , \sin \delta_s )$$

Further, let  $\vec{e}$  be the vector of length 1 from the satellite to the station, in equatorial coordinates.

One has

$$\vec{e} = \frac{\vec{r} - \vec{E}}{|\vec{r} - \vec{E}|} .$$

The directions  $\vec{\omega}$  and  $\vec{e}$  are then written in the local satellite orbit coordinate system:

$$l'_1 = \vec{e} \cdot \vec{e}_v , \quad l'_s = \vec{\omega} \cdot \vec{e}_v ,$$

$$m'_1 = \vec{e} \cdot \vec{j}_v , \quad m'_s = \vec{\omega} \cdot \vec{j}_v ,$$

$$n'_1 = \vec{e} \cdot \vec{k}_v , \quad n'_s = \vec{\omega} \cdot \vec{k}_v .$$

Thus  $(l'_1, m'_1, n'_1)$  are the direction cosines of the station line, and  $(l'_s, m'_s, n'_s)$  those of the sun line, in the local satellite orbit coordinate system; and clearly these direction cosines are computable by the above formulas.

Thus, the directions of sun and station from the satellite, in the local satellite orbit coordinate system, are computable by the above formulas, once

$$\Omega_p, i_p, u_p, \pi_p, \lambda_1 - \lambda_p, \lambda_s$$

are specified.

Those configurations of sun, satellite and station where either,

1) the sun is not visible from satellite, or;

2) the satellite is below the station's horizon,

should not, of course, be considered. The satellite is below the station's horizon if and only if

$$(\vec{E} - \vec{r}) \cdot \vec{r} < 0.$$

It has been shown in [1], p. 14, that for an equatorial synchronous satellite orbit, and for a station at the latitude of Mojave, the satellite is visible from the station if and only if

$$-79.3^\circ \leq \lambda_1 - \lambda_p \leq +79.3^\circ$$

Accordingly, we shall only consider values of  $\lambda_1 - \lambda_p$  satisfying these inequalities.

If  $2\alpha$  is the angular diameter of the earth, as seen from the satellite, then one has

$$\cos \alpha = \frac{\sqrt{n_p^2 - 1}}{n_p};$$

while if  $\beta$  is the angle included between the sun line and the line from the satellite to the earth's center,

$$\cos \beta = \vec{\omega} \cdot \vec{k}_r = n'_s$$

If

$$n'_s < \cos \alpha$$

then  $\beta > \alpha$  and the sun is visible from the satellite. Accordingly, we restrict attention to those cases where the above inequality holds.

### 3. Errors in the Direction Cosines

The sensor data, in combination with the computed direction cosines

$$l'_1, m'_1, n'_1, l'_s, m'_s, n'_s$$

determine the satellite attitude. We must investigate errors in these direction cosines. Let there be given

$$d\Omega_p, d\dot{\iota}_p, du_p, dn_p,$$

differential errors in the quantities defining the satellites's position. Let

$$\vec{e}_I, \vec{j}_I, \vec{k}_I$$

be the unit vectors defining the equatorial coordinate system, as in [1] p. 6. We shall set

$$\vec{\omega}_\Omega = d\Omega_p \cdot \vec{k}_I$$

$$\vec{\omega}_{\dot{\iota}} = (d\dot{\iota}_p \cos \Omega_p) \vec{e}_I + (d\dot{\iota}_p \sin \Omega_p) \vec{j}_I,$$

$$\vec{\omega}_u = -(du_p) \cdot \vec{j}_I,$$

and

$$\vec{\omega} = \vec{\omega}_\Omega + \vec{\omega}_{\dot{\iota}} + \vec{\omega}_u.$$

Then from the equations defining  $\vec{e}_V, \vec{j}_V, \vec{k}_V$  in terms of  $\Omega_p, \dot{\iota}_p, u_p, n_p$ , one may verify that

$$d\vec{e}_V = \vec{\omega} \times \vec{e}_V,$$

$$d\vec{j}_V = \vec{\omega} \times \vec{j}_V,$$

$$d\vec{k}_V = \vec{\omega} \times \vec{k}_V.$$

Thus, the vectors  $d\vec{e}_V, d\vec{j}_V, d\vec{k}_V$  may be computed. From the fact that

$$l'_s = \vec{\omega} \cdot \vec{e}_V,$$

it follows that

$$dl'_s = \vec{\omega} \cdot d\vec{e}_V;$$

and similarly,

$$dm'_s = \vec{\omega} \cdot d\vec{j}_V,$$

$$dn'_s = \vec{\omega} \cdot d\vec{k}_V.$$

Thus, the differential errors in the direction cosines of the sun can be computed.

It should be noted that the derivation of the relation  $dl'_s = \vec{\omega} \cdot d\vec{r}_s$  presupposes that  $d\vec{\omega}$  is zero, or rather, negligible. One argues for this as follows: Any inaccuracy which one is likely to incur in predicting the satellite's position cannot make any appreciable difference in the satellite-sun direction cosines in an inertial coordinate system (and these direction cosines are the components of  $\vec{\omega}$ ). Indeed, if the inaccuracy were comparable to the diameter of the earth, an inaccuracy which is inconceivable in this context, this would give rise to an angular inaccuracy in the satellite-sun line of the order of the solar parallax, which is only  $8'' .80$ . Even this could be ignored quite safely in the present context.

Now let us consider errors in the satellite-station direction cosines. By the law of cosines,

$$|\vec{r} - \vec{E}|^2 = |\vec{r}|^2 + |\vec{E}|^2 - 2 \vec{r} \cdot \vec{E}$$

We will assume that the position of the station is known without error, so that  $d\vec{r} = 0$ . This implies that

$$\begin{aligned} |\vec{r} - \vec{E}| \cdot d|\vec{r} - \vec{E}| &= |\vec{E}| \cdot d|\vec{E}| - \vec{r} \cdot d\vec{E} \\ &= r_p \cdot dr_p - \vec{r} \cdot d\vec{E} \end{aligned}$$

so that  $d|\vec{r} - \vec{E}|$  may be computed if  $d\vec{E}$  is known. From

$$\vec{E} = -r_p \cdot \vec{k}_r$$

one sees that

$$d\vec{E} = -(dr_p) \vec{k}_r - (r_p) d\vec{k}_r$$

and since  $d\vec{k}_r$  is known,  $d\vec{E}$  is also, and so is  $d|\vec{r} - \vec{E}|$ . The definition of  $\vec{E}$  may be written

$$|\vec{r} - \vec{E}| \cdot \vec{E} = \vec{r} - \vec{E}$$

whence

$$(|\vec{r} - \vec{E}|) d\vec{E} = -(d|\vec{r} - \vec{E}|) \vec{E} - d\vec{E},$$

and thus we can compute  $d\vec{E}$ .

From

$$l_1' = \vec{e} \cdot \vec{r}$$

we see that

$$dl_1' = \vec{r} \cdot d\vec{e} + \vec{e} \cdot d\vec{r}$$

and similarly

$$dm_1' = \vec{j}_r \cdot d\vec{e} + \vec{e} \cdot d\vec{j}_r$$

$$dn_1' = \vec{k}_r \cdot d\vec{e} + \vec{e} \cdot d\vec{k}_r$$

NOTE: It is presupposed, in writing the formulas for  $\vec{\omega}$ ,  $d\vec{r}$ ,  $d\vec{j}_r$ ,  $d\vec{k}_r$ , that  $d\Omega_p$ ,  $di_p$ ,  $du_p$  are measured in radians.

#### 4. Errors in Altitude Determination

Assuming that the direction cosines  $l_1', m_1', n_1', l_s', m_s', n_s'$  have been computed for a given position of the satellite, the satellite attitude is computed using the following sensor data:

$(l_s, m_s, n_s)$  = the direction cosines of the sun from the satellite,  
in the satellite body coordinate system.

$\eta$  = the polarization angle.

The first step in computing the satellite attitude is to compute:

$(l_1, m_1, n_1)$  = the direction cosines of the station from the  
satellite, in the satellite body coordinate system.

If we define

$$\beta_1 = \cos^{-1} m_1$$

$$\psi_1 = \cos^{-1} n_1'$$



then for neutral attitude (no yaw, pitch, or roll) one has

$$\sin \beta_1 \cdot \sin \eta = \frac{l_1'}{\sin \psi_1},$$

$$\sin \beta_1 \cdot \cos \eta = -m_1' \cdot \tan \psi_1.$$

These formulas will be important for purposes of reduction.

One solves for  $l_1, m_1, n_1$  using the formulas:

$$\begin{aligned} \sin \psi_1 \cdot m_s = m_1 \cdot \sin \psi_1 \cdot \cos \nu - (m_1' l_s' - l_1' m_s') \sin \eta \cdot \sin \beta_1 \\ + (n_s' - n_1' \cos \nu) \cdot \cos \eta \cdot \sin \beta_1, \end{aligned}$$

$$l_1^2 + m_1^2 + n_1^2 = 1$$

$$\cos \nu = l_1 \cdot l_s + m_1 \cdot m_s + n_1 \cdot n_s$$

$$\cos \nu = l_1' \cdot l_s' + m_1' \cdot m_s' + n_1' \cdot n_s'$$

One computes  $\cos \nu$ , using the last equation, and  $\sin \psi_1$ , and then solves the first equation for  $m_1$ , keeping in mind that  $\beta_1$  is a function of  $m_1$ . Once  $m_1$  is known, the second and third equations can be solved for  $l_1$  and  $n_1$ . There is some ambiguity in this latter step; but this need not concern us in studying errors.

Differentiating the equation for  $m_1$ , and making use of the fact that

$$\begin{aligned} d(\sin \beta_1) &= \cos \beta_1 \cdot d\beta_1 = m_1 \cdot d\beta_1 \\ &= - \frac{m_1 \cdot dm_1}{\sin \beta_1}, \end{aligned}$$

we find that

$$\begin{aligned} &\left[ -\sin \psi_1 \cdot \cos \nu - (m_1' l_s' - l_1' m_s') \cdot m_1 \cdot \frac{\sin \eta}{\sin \beta_1} \right. \\ &\quad \left. + (n_s' - n_1' \cos \nu) \cdot m_1 \cdot \frac{\cos \eta}{\sin \beta_1} \right] \cdot dm_1 \\ &= -m_s \cdot d(\sin \psi_1) + m_1 \cos \nu d(\sin \psi_1) + m_1 \sin \psi_1 \cdot d(\cos \nu) \\ &\quad - \sin \eta \sin \beta_1 [d(m_1' l_s' - l_1' m_s')] + \cos \eta \sin \beta_1 [dn_s' - \cos \nu d n_1' - n_1' \cdot d(\cos \nu)] \end{aligned}$$

In deriving this we have ignored errors in the sensor data, i.e., we assume

$$dl_s = dm_s = dn_s = d\eta = 0.$$

Since the satellite is not expected to depart very far from neutral attitude, we are primarily interested in the case where attitude is neutral, i.e., pitch, roll, and yaw are zero. In this case,

$$\begin{aligned} l_1 &= l_1' , \quad m_1 = m_1' , \quad n_1 = n_1' ; \\ l_s &= l_s' , \quad m_s = m_s' , \quad n_s = n_s' ; \end{aligned}$$

further, we have available the formulas for  $\sin \beta_1 \cdot \sin \eta$  and  $\sin \beta_1 \cdot \cos \eta$  which were given above. Under these conditions, it has been shown (reference 2) that the coefficient of  $dm_1$  in the above equation may be written as

$$- \frac{1}{\sin^2 \beta_1} , \quad \frac{1}{\sin \psi_1} \cdot (\cos \gamma - m_1 m_s) (1 - n_1'^2)$$

Now from the relation  $l_1'^2 + m_1'^2 + n_1'^2 = 1$ , one sees that

$$l_1' \cdot dl_1' + m_1' \cdot dm_1' + n_1' \cdot dn_1' = 0.$$

Making use of this relation, one finds after some reduction that the right side of the equation for  $dm_1$  becomes

$$\frac{1}{\sin \psi_1} \cdot \left[ m_1' n_s' \cdot dn_1' + m_1' l_s' \cdot dl_1' - l_1' l_s' dm_1' + (1 - n_1'^2) dm_s' \right].$$

Thus, cancelling the factor  $\frac{1}{\sin \psi_1}$ , one finds that the equation for  $dm_1$  reduces to

$$\begin{aligned} &(\cos \gamma - m_1' m_s') (1 - n_1'^2) \cdot dm_1 \\ &= - \sin^2 \beta_1 \cdot \left[ m_1' n_s' dn_1' + m_1' l_s' \cdot dl_1' - l_1' l_s' dm_1' + (1 - n_1'^2) dm_s' \right]. \end{aligned}$$

Now we will find  $dl_1, dn_1$ . One has

$$d(\cos \nu) = l_1' \cdot dl_s' + m_1' \cdot dm_s' + n_1' \cdot dn_s' \\ + l_s' \cdot dl_1' + m_s' \cdot dm_1' + n_s' \cdot dn_1',$$

so that  $d(\cos \nu)$  is certainly computable. Further, from the equations in  $l_1, m_1, n_1$  one derives for neutral attitude:

$$l_1' dl_1 + m_1' dm_1 + n_1' dn_1 = 0.$$

$$l_s' dl_1 + m_s' dm_1 + n_s' dn_1 = d(\cos \nu)$$

Solving for  $dn_1$  and  $dl_1$ ,

$$(l_s' n_1' - n_s' l_1') \cdot dn_1 = -l_1' \cdot d(\cos \nu) - (l_s' m_1' - m_s' l_1') dm_1,$$

$$(n_s' l_1' - n_1' l_s') \cdot dl_1 = -n_1' \cdot d(\cos \nu) - (n_s' m_1' - n_1' m_s') dm_1,$$

These equations will define  $dn_1$  and  $dl_1$ , if

$$l_s' n_1' - n_s' l_1' \neq 0$$

and we will proceed in this section on the assumption that this is so. However, the case where this factor is zero is of interest to us, and we will have to reconsider this assumption in the next section.

Now we consider the errors in the attitude angles,  $\theta_B, \phi_B$ , and  $\psi_B$ , the pitch, roll, and yaw angles. We start with the equation

$$\sin \phi_B \cdot \cos \theta_B = m_1 n_1' + \sin \beta_1 \cdot \cos \eta \cdot \sin \psi_1$$

Differentiating, and setting  $\theta_B = \phi_B = \psi_B = 0$  (i.e., we consider neutral attitude), one obtains after some reduction

$$d\phi_B = \frac{m_1' dn_1'}{1 - n_1'^2} + \frac{n_1' dm_1}{1 - m_1'^2}.$$

Next one considers the equation

$$(l_1 \cdot n_s - l_s n_1) \cdot \sin \theta_B = (m_1 n_s - m_s n_1) \cdot [m_1 \cdot n_1' + \sin \beta_1 \cos \eta \sin \psi_1] \\ + (n_1 n_s' - n_s n_1').$$

Differentiating and setting  $\theta_B = \phi_B = \psi_B = 0$ , one obtains after a little reduction

$$(l_1' n_s' - l_s' n_1') \cdot d\theta_B = (m_1' n_s' - m_s' n_1') \cdot d\phi_B + (n_1' dn_s' + n_s' dn_1 - n_s' dn_1').$$

Starting now from the equation

$$(l_s n_1 - l_1 n_s) \cos \theta_B \sin \psi_B = (n_1 m'_s - n_s m'_1) \\ + (n_1 m_s - m_1 n_s) \cdot \left[ - m_1 m'_1 - \frac{l_1'}{\sin \psi_1} \cdot \sin \beta_1 \sin \eta \right. \\ \left. + m'_1 \sin \beta_1 \cos \eta \tan \psi_1 \right].$$

differentiating, setting  $\theta_B = \phi_B = \psi_B = 0$ , one obtains after considerable reduction

$$(l'_s n'_1 - l'_1 n'_s) \cdot d\psi_B = n'_1 \cdot dm'_s - n'_s \cdot dm'_1 + n'_s dm_1.$$

Of course, these formulas for  $d\theta_B$ ,  $d\phi_B$ ,  $d\psi_B$  will give the values of these quantities in radians.

One notes that the factor  $(l_s n_1 - l_1 n_s)$  occurs as the coefficient of  $d\theta_B$  and  $d\psi_B$  in the above formulas, and that if this factor is zero, those formulas are then indeterminate. We shall now consider what can be done about this.

## 5. Indeterminate Cases and Factors

In certain configurations, the sensor data and the computed direction cosines will not suffice to determine the attitude of the satellite. This happens when

$$\cos \nu - m'_1 m'_5 = 0$$

as is shown in reference [2]. Then we have a genuine indeterminate case. However, the equations which we have presented are indeterminate in other cases, notably when

$$l_s \eta_1 - l_1 n_s = 0$$

although this is not a case of genuine indeterminacy.

Before considering this in more detail, let us first consider the following two factors which will occur in the sequel as coefficients of quantities for which we are solving:

$$\eta'_1, (1 - \eta'^2_1)$$

We would have indeterminacy if either of these were zero. However, in the cases we are considering this does not happen.

Consider first  $\eta'_1$ . Since one has

$$\eta'_1 = \vec{e} \cdot \vec{k}_v;$$

$\eta'_1 = 0$  implies that  $\vec{e} \cdot \vec{k}_v = 0$ . Since  $\vec{e}$  is just a scalar multiple of  $\vec{\eta} - \vec{E}$ , one would have

$$(\vec{\eta} - \vec{E}) \cdot \vec{k}_v = 0.$$

By the law of cosines one then has

$$\begin{aligned} 1 &= |\vec{\eta}|^2 = |(\vec{\eta} - \vec{E}) + \vec{E}|^2 \\ &= |\vec{\eta} - \vec{E}|^2 + |\vec{E}|^2 + 2(\vec{\eta} - \vec{E}) \cdot \vec{E} \\ &= |\vec{\eta} - \vec{E}|^2 + |\vec{E}|^2 \end{aligned}$$

which is

$$|\vec{\eta} - \vec{E}|^2 = 1 - |\vec{E}|^2$$

since  $|\vec{E}| > 1$ , this is a contradiction. We conclude that  $\eta'_1 \neq 0$ .

Consider now the factor  $1 - n_1'^2$ . If

$$1 - n_1'^2 = 0$$

then since  $\vec{e} = (l_1', m_1', n_1')$  is a unit vector, one has

$$l_1' = m_1' = 0$$

and in particular

$$\vec{e} \cdot \vec{j}_v = m_1' = 0$$

Thus  $\vec{e}$  lies in the plane determined by  $\vec{r}_v$  and  $\vec{k}_v$  (in fact is collinear with  $\vec{k}_v$ ) and thus  $\vec{e}$  lies in the plane of the orbit. For the equatorial synchronous orbit, this implies

$$\delta_1 = 0^\circ$$

For the 6,000 n.mi.  $28^\circ$  inclined orbit, this would imply

$$|\delta_1| \leq 28^\circ$$

Since we are postulating a geocentric latitude  $\delta_1$  of  $35.33^\circ$ , it follows that with this value of  $\delta_1$ , we will have

$$1 - n_1'^2 \neq 0.$$

Typically, we deal with functions  $F$  of  $l_1', m_1', n_1', l_s', m_s', n_s'$  (as well as of sensor data):

$$F = F(l_1', m_1', n_1', l_s', m_s', n_s')$$

and we are interested in the differential  $dF$  of such a function, assuming there are no errors in the sensor data,

$$\begin{aligned} dF &= \frac{\partial F}{\partial l_1'} \cdot dl_1' + \frac{\partial F}{\partial m_1'} \cdot dm_1' + \frac{\partial F}{\partial n_1'} \cdot dn_1' \\ &+ \frac{\partial F}{\partial l_s'} \cdot dl_s' + \frac{\partial F}{\partial m_s'} \cdot dm_s' + \frac{\partial F}{\partial n_s'} \cdot dn_s'. \end{aligned}$$

Examples of such functions  $F$  are given by  $l_1, m_1, n_1, \theta_B, \phi_B, \psi_B$ .

From the relations

$$l_1'^2 + m_1'^2 + n_1'^2 = 1,$$

$$l_s'^2 + m_s'^2 + n_s'^2 = 1.$$

we see that

$$l_1' \cdot dl_1' + m_1' \cdot dm_1' + n_1' \cdot dn_1' = 0$$

$$l_s' \cdot dl_s' + m_s' \cdot dm_s' + n_s' \cdot dn_s' = 0$$

These relations can be used, for example, to eliminate  $dn_1'$  and  $dn_s'$  from the expression for  $dF$ .

In fact, if we define

$$D_{l_1'}(F) = \frac{\partial F}{\partial l_1'} - \frac{l_1'}{n_1'} \cdot \frac{\partial F}{\partial n_1'} \quad , \quad D_{m_1'}(F) = \frac{\partial F}{\partial m_1'} - \frac{m_1'}{n_1'} \cdot \frac{\partial F}{\partial n_1'} \quad ,$$

$$D_{l_s'}(F) = \frac{\partial F}{\partial l_s'} - \frac{l_s'}{n_s'} \cdot \frac{\partial F}{\partial n_s'} \quad , \quad D_{m_s'}(F) = \frac{\partial F}{\partial m_s'} - \frac{m_s'}{n_s'} \cdot \frac{\partial F}{\partial n_s'} \quad ,$$

then we have

$$dF = D_{l_1'}(F) \cdot dl_1' + D_{m_1'}(F) \cdot dm_1' \\ + D_{l_s'}(F) \cdot dl_s' + D_{m_s'}(F) \cdot dm_s' .$$

The reason for introducing the  $D_{l_1'}(F)$ , etc., is as follows: for the functions  $l_1, n_1, \theta_B, \phi_B$  it develops that the  $D_{l_1'}(F)$  etc., are divisible by the factor  $(l_s \cdot n_1 - l_1 \cdot n_s)$ , so that we can cancel it and thereby remove the spurious indeterminacy which was occasioned by this factor.

For some of these functions, the most important being  $\theta_B$ , the elimination of  $dn_s'$  is not possible when  $n_s' = 0$ . However, if  $n_s' = 0$ , then for an orbit of low or medium inclination one will have  $|l_s'| > 0$ ; in fact,  $l_s'$  will be reasonably close to -1 or +1. Thus if  $n_s' = 0$ , division by  $l_s'$  is possible and we can eliminate  $dl_s'$ . If we set

$$E_{m_s'}(F) = \frac{\partial F}{\partial m_s'} - \frac{m_s'}{l_s'} \cdot \frac{\partial F}{\partial l_s'} \quad ,$$

$$E_{n_s'}(F) = \frac{\partial F}{\partial n_s'} - \frac{n_s'}{l_s'} \cdot \frac{\partial F}{\partial l_s'} \quad ,$$

then we will have

$$dF = D_{l_1'}(F) \cdot dl_1' + D_{m_1'}(F) \cdot dm_1' \\ + E_{m_s'}(F) \cdot dm_s' + E_{n_s'}(F) \cdot dn_s' ,$$

The following formulas are very convenient in computing  $E_{m_s'}(F), E_{n_s'}(F)$ :

$$E_{m'_s}(F) = D_{m'_s}(F) - \frac{m'_s}{l'_s} \cdot D_{l'_s}(F), \quad E_{n'_s}(F) = -\frac{n'_s}{l'_s} \cdot D_{l'_s}(F).$$

From the formula given for  $dm_1$ , one sees that

$$\begin{aligned} n'_1 \cdot (\cos \nu - m'_1 m'_s) \cdot (1 - n_1'^2) \cdot D_{l'_1}(m_1) &= + m'_1 \cdot \sin^2 \beta_1 \cdot (n'_s l'_1 - n'_1 l'_s), \\ n'_1 \cdot (\cos \nu - m'_1 m'_s) \cdot (1 - n_1'^2) \cdot D_{m'_1}(m_1) &= + \sin^2 \beta_1 \cdot (m_1'^2 n'_s + l'_1 l'_s n'_1), \\ n'_1 \cdot (\cos \nu - m'_1 m'_s) \cdot (1 - n_1'^2) \cdot D_{l'_s}(m_1) &= 0, \\ n'_1 \cdot (\cos \nu - m'_1 m'_s) \cdot (1 - n_1'^2) \cdot D_{m'_s}(m_1) &= -n'_1 \cdot \sin^2 \beta_1 \cdot (1 - n_1'^2). \end{aligned}$$

Further, we have

$$\begin{aligned} n'_1 \cdot n'_s \cdot D_{l'_1}(\cos \nu) &= n'_s (n'_1 l'_s - n'_s l'_1), \\ n'_1 \cdot n'_s \cdot D_{m'_1}(\cos \nu) &= n'_s (n'_1 m'_s - n'_s m'_1), \\ n'_1 \cdot n'_s \cdot D_{l'_s}(\cos \nu) &= n'_1 (l'_1 n'_s - n'_1 l'_s), \\ n'_1 \cdot n'_s \cdot D_{m'_s}(\cos \nu) &= n'_1 (m'_1 n'_s - n'_1 m'_s). \end{aligned}$$

These formulas are used to derive the formulas given in the next section.

The choice as to whether one eliminates  $dn'_s$  or  $dl'_s$  may be determined by the relative magnitudes of  $l'_s$  and  $n'_s$ . If  $|n'_s| \geq |l'_s|$  then one may eliminate  $dn'_s$ , if  $|n'_s| < |l'_s|$  then eliminate  $dl'_s$ .



## 6. The Determinate Formulas

In this section we will present formulas for  $l_1, n_1, \phi_B, \theta_B, \psi_B$  in which the factor  $(l_s \cdot n_1 - l_1 n_s)$  does not appear. The formulas are developed by the method outlined in the previous section; we omit these derivations.

$$\begin{aligned}
 n_1' \cdot n_s' (\cos \nu - m_1' m_s') (1 - n_1'^2) D_{l_1'}(n_1) \\
 &= - l_1' n_s' (\cos \nu - m_1' m_s') (1 - n_1'^2) \\
 &\quad + m_1' n_s' (l_s' m_1' - m_s' l_1') \cdot \sin^2 \beta_1, \\
 n_1' \cdot n_s' \cdot (\cos \nu - m_1' m_s') (1 - n_1'^2) D_{m_1'}(n_1) \\
 &= - n_s' \cdot \{ l_1'^3 l_s' m_1' + l_1'^2 m_1' n_1' n_s' - l_1'^2 m_s' n_1'^2 \\
 &\quad + l_1'^2 m_1'^2 m_s' + l_1' l_s' m_1' n_1'^2 + m_1'^3 n_1' n_s' \}, \\
 n_1' \cdot n_s' (\cos \nu - m_1' m_s') (1 - n_1'^2) \cdot D_{l_s'}(n_1) \\
 &= + l_1'^2 n_1' (\cos \nu - m_1' m_s') \cdot (1 - n_1'^2), \\
 n_1' \cdot n_s' (\cos \nu - m_1' m_s') (1 - n_1'^2) D_{m_s'}(n_1) \\
 &= + n_1' \cdot (1 - n_1'^2) \cdot (l_1'^2 m_s' + m_1' n_1' n_s').
 \end{aligned}$$

We shall omit the formulas for  $E_{m_s'}(n_1)$  and  $E_{n_s'}(n_1)$ , and the corresponding formulas for  $l_1$  :

$$\begin{aligned}
 n_1' n_s' \cdot (\cos \nu - m_1' m_s') \cdot (1 - n_1'^2) \cdot D_{l_1'}(l_1) \\
 &= + n_1' n_s' \cdot (\cos \nu - m_1' m_s') (1 - n_1'^2) \\
 &\quad - m_1' n_s' \cdot (n_s' m_1' - n_1' m_s') \cdot \sin^2 \beta_1, \\
 n_1' n_s' \cdot (\cos \nu - m_1' m_s') (1 - n_1'^2) \cdot D_{m_1'}(l_1) \\
 &= + l_1' n_s' \cdot (n_s' m_1' - n_1' m_s') \cdot (n_1'^2 - m_1'^2), \\
 n_1' n_s' \cdot (\cos \nu - m_1' m_s') \cdot (1 - n_1'^2) \cdot D_{l_s'}(l_1) \\
 &= - n_1'^2 \cdot (\cos \nu - m_1' m_s') \cdot (1 - n_1'^2),
 \end{aligned}$$

$$\begin{aligned} n_1' n_s' \cdot (\cos \nu - m_1' m_s') (1 - n_1'^2) \cdot D_{m_s'}(\ell_1) \\ = + \ell_1' \cdot n_1' \cdot (n_s' m_1' - n_1' m_s') \cdot (1 - n_1'^2). \end{aligned}$$

The formulas for  $\phi_B$  are:

$$\begin{aligned} n_1' (\cos \nu - m_1' m_s') (1 - n_1'^2) \cdot D_{\ell_1'}(\phi_B) &= -\ell_s' \cdot m_1' \cdot (\ell_1'^2 + n_1'^2), \\ n_1' (\cos \nu - m_1' m_s') (1 - n_1'^2) \cdot D_{m_1'}(\phi_B) &= + \ell_1' \cdot \ell_s' (n_1'^2 - m_1'^2), \\ n_1' (\cos \nu - m_1' m_s') (1 - n_1'^2) \cdot D_{\ell_s'}(\phi_B) &= 0, \\ n_1' (\cos \nu - m_1' m_s') (1 - n_1'^2) \cdot D_{m_s'}(\phi_B) &= -n_1'^2 \cdot (1 - n_1'^2). \end{aligned}$$

It will be noted that  $n_s'$  does not appear as a coefficient in the formulas for the  $D(\phi_B)$ ; hence  $n_s' = 0$  is not a condition for indeterminacy in these formulas, and we do not need the  $E(\phi_B)$ . It is quite otherwise with  $\theta_B$ :

$$\begin{aligned} n_1' \cdot (\cos \nu - m_1' m_s') \cdot (1 - n_1'^2) \cdot D_{\ell_1'}(\theta_B) &= -m_1' \cdot m_s' \cdot (\ell_1'^2 + n_1'^2), \\ n_1' \cdot (\cos \nu - m_1' m_s') (1 - n_1'^2) \cdot D_{m_1'}(\theta_B) &= + \ell_1' m_s' \cdot (n_1'^2 - m_1'^2), \\ n_1' \cdot (\cos \nu - m_1' m_s') (1 - n_1'^2) \cdot D_{\ell_s'}(\theta_B) &= + \frac{n_1'}{n_s'} (\cos \nu - m_1' m_s') (1 - n_1'^2), \\ n_1' \cdot (\cos \nu - m_1' m_s') (1 - n_1'^2) \cdot D_{m_s'}(\theta_B) &= + \ell_1' m_s' \cdot \frac{n_1'}{n_s'} \cdot (1 - n_1'^2), \\ n_1' \cdot (\cos \nu - m_1' m_s') (1 - n_1'^2) \cdot E_{m_s'}(\theta_B) &= - \frac{m_s'}{\ell_s'} \cdot n_1'^2 \cdot (1 - n_1'^2), \\ n_1' \cdot (\cos \nu - m_1' m_s') (1 - n_1'^2) \cdot E_{n_s'}(\theta_B) &= - \frac{n_1'}{\ell_s'} \cdot (\cos \nu - m_1' m_s') (1 - n_1'^2). \end{aligned}$$

In the formulas for the  $D(\psi_B)$  it turns out that  $n'_S = 0$  is not critical, and hence we do not need to develop the  $E(\psi_B)$  :

$$\begin{aligned} n'_1 \cdot (\cos \gamma - m'_1 m'_S) (1 - n'^2_1) D_{l'_1}(\psi_B) &= -m'_1 \cdot n'_S \cdot (l'^2_1 + n'^2_1), \\ n'_1 \cdot (\cos \gamma - m'_1 m'_S) (1 - n'^2_1) D_{m'_1}(\psi_B) &= +l'_1 \cdot n'_S \cdot (n'^2_1 - m'^2_1), \\ n'_1 \cdot (\cos \gamma - m'_1 m'_S) (1 - n'^2_1) D_{l'_S}(\psi_B) &= 0, \\ n'_1 \cdot (\cos \gamma - m'_1 m'_S) (1 - n'^2_1) D_{m'_S}(\psi_B) &= +l'_1 \cdot n'_1 \cdot (1 - n'^2_1). \end{aligned}$$

Ordinarily, we would only be interested in computing  $d\theta_B, d\phi_B, d\psi_B$  (and not  $dl_1, dm_1, dn_1$ ). The above formulas permit us to compute these differentials directly, knowing only  $dl'_1, dm'_1, dl'_S, dm'_S$ , and, when  $n'_S = 0$ ,  $dn'_S$ . This is why we introduced the above formulas for the  $D(\phi_B)$ . The formula given in Section 4 above for  $d\phi_B$ , while not sensitive to the factor  $(l_S n_1 - l_1 n_S)$ , does require that one first compute  $dm_1$ , which we now can see is unnecessary. In fact, we have included expressions for the  $D(m_1), D(l_1), D(n_1)$  in this section and the previous section only because they are used to derive the corresponding expressions in  $\phi_B, \theta_B, \psi_B$ ; they are quite unnecessary in computing  $d\theta_B, d\phi_B, d\psi_B$ .

## 7. Numerical Results

The above equations were programmed for the LGP-21 computer. The configuration of sun, station, and satellite is specified in the program by the parameters

$$u_p, \lambda_1 - \lambda_p, \lambda_s$$

Various configurations were investigated, using combinations of the following parameter values:

$$\begin{aligned} u_p &= 0^\circ, 45^\circ, 90^\circ, 135^\circ, 180^\circ, 225^\circ, 270^\circ, 315^\circ; \\ \lambda_1 - \lambda_p &= 0^\circ, -70^\circ, +70^\circ; \\ \lambda_s &= 0^\circ, +90^\circ, -90^\circ. \end{aligned}$$

The program computes the partials of  $\theta_B, \phi_B, \psi_B$  with respect to  $\Omega_p, \dot{\Omega}_p, u_p$  and  $\lambda_p$ , and gives bounds for the partials of  $\theta_B, \phi_B, \psi_B$  with respect to  $e$  and  $a$ .

## 8. Analysis of the Results

For the synchronous equatorial orbit one has  $\dot{\Omega}_p = 0$ ; from the formula for  $\vec{j}_v$  one sees that this implies that  $\vec{j}_v = -\vec{k}_I$ ; from the formulas for  $\vec{\omega}_\Omega$  and  $\vec{\omega}_u$ ,

$$\vec{\omega}_u = + \frac{du_p}{d\Omega_p} \cdot \vec{\omega}_\Omega$$

One infers that

$$\begin{aligned} \frac{\partial \vec{c}_v}{\partial u_p} &= \frac{1}{du_p} \cdot (\vec{\omega}_u \times \vec{c}_v) = \frac{1}{du_p} \cdot \frac{du_p}{d\Omega_p} (\vec{\omega}_\Omega \times \vec{c}_v) \\ &= \frac{\partial \vec{c}_v}{\partial \Omega_p} \end{aligned}$$

similarly for  $\vec{j}_v$  and  $\vec{k}_v$ . One finds from this that

$$\frac{\partial \theta_B}{\partial u_p} = \frac{\partial \theta_B}{\partial \Omega_p}$$

similarly for  $\phi_B$  and  $\psi_B$ . Thus, it is unnecessary, for an equatorial orbit, to make a separate computation of the partials with respect to  $u_p$ . Further, since

$$\frac{\partial \theta_B}{\partial \Omega'_p} = \frac{\partial \theta_B}{\partial \Omega_p} - \frac{\partial \theta_B}{\partial u_p}$$

and similarly for  $\phi_B$  and  $\psi_B$ , we have

$$\frac{\partial \theta_B}{\partial \Omega'_p} = \frac{\partial \phi_B}{\partial \Omega'_p} = \frac{\partial \psi_B}{\partial \Omega'_p} = 0.$$

From the definition of the component of error, we see that

$$S(\Delta \theta_B; \Delta \Omega'_p) = 0,$$

similarly for  $\Delta \phi_B, \Delta \psi_B$ . We already have

$$S(\Delta \theta_B; \Delta \omega_p) = 0,$$

similarly for  $\Delta \phi_B, \Delta \psi_B$ .

We conclude that the attitude determination will be quite insensitive, for the geocentric equatorial orbit, to errors in  $\Omega'_p$  and  $\omega_p$ . This leaves only the four quantities

$$\dot{\Omega}'_p, e, a, \epsilon_p$$

as potential sources of sizable errors in attitude determination.

In considering the results obtained, one must take the following precaution: We have seen that in the case when  $(\cos \gamma - m'_1 m'_5) = 0$ , there is genuine indeterminacy, the sensor data and computed direction cosines do not suffice to determine the satellite attitude. Furthermore, as  $(\cos \gamma - m'_1 m'_5)$  approaches zero, we would expect the errors in attitude determination to increase without bound, if the determination is carried out using observed sun line and observed polarization angle. In consequence, if  $(\cos \gamma - m'_1 m'_5)$  were small, one would use another sensor combination to furnish data for attitude determination. Therefore, we have decided, rather arbitrarily, to ignore in our analysis all cases where

$$\cos \gamma - m'_1 m'_5 < 0.5,$$

on the grounds that in such cases the attitude of the satellite would be determined using a different sensor combination.

The remaining cases were examined for maximum values of the partials with respect to  $i'_p, e, a, \epsilon_p$ . It was found that

$$\left| \frac{\partial \theta_B}{\partial i'_p} \right|, \quad \left| \frac{\partial \phi_B}{\partial i'_p} \right|, \quad \left| \frac{\partial \psi_B}{\partial i'_p} \right| \leq 1.00^\circ,$$

$$\left| \frac{\partial \theta_B}{\partial \epsilon_p} \right|, \quad \left| \frac{\partial \phi_B}{\partial \epsilon_p} \right|, \quad \left| \frac{\partial \psi_B}{\partial \epsilon_p} \right| \leq 1.87^\circ,$$

$$\left| \frac{\partial \theta_B}{\partial e} \right|, \quad \left| \frac{\partial \phi_B}{\partial e} \right|, \quad \left| \frac{\partial \psi_B}{\partial e} \right| \leq 2.14 \times 10^2,$$

$$\left| \frac{\partial \theta_B}{\partial a} \right|, \quad \left| \frac{\partial \phi_B}{\partial a} \right|, \quad \left| \frac{\partial \psi_B}{\partial a} \right| \leq 1.07 \times 10^3.$$

These bounds are attained, by some one of the terms on the left of the various inequalities, for particular configurations of sun, station, and satellite. One concludes that

$$\begin{aligned} s(\Delta \theta_B; \Delta i'_p) &\leq s.d.(\Delta i'_p), \\ s(\Delta \theta_B; \Delta \epsilon_p) &\leq 1.87 \cdot s.d.(\Delta \epsilon_p), \\ s(\Delta \theta_B; \Delta e) &\leq 214 \cdot s.d.(\Delta e), \\ s(\Delta \theta_B; \Delta a) &\leq 1070 \cdot s.d.(\Delta a). \end{aligned}$$

We will investigate the accuracies required in the orbital elements if their contribution to errors in attitude determination are to amount to no more than  $1^\circ$ , using 3 $\sigma$  confidence limits. That is, we will require

$$3 \cdot s.d.(\Delta \theta_B) \leq 1,$$

similarly for  $\Delta \phi_B, \Delta \psi_B$ . Since

$$\begin{aligned} s.d.(\Delta \theta_B) &\leq s(\Delta \theta_B; \Delta i'_p) + s(\Delta \theta_B; \Delta \epsilon_p) \\ &\quad + s(\Delta \theta_B; \Delta e) + s(\Delta \theta_B; \Delta a), \end{aligned}$$

we will require that

$$\left. \begin{array}{l} S(\Delta\theta_B; \Delta i'_p), S(\Delta\theta_B; \Delta\epsilon_p), \\ S(\Delta\theta_B; \Delta e), S(\Delta\theta_B; \Delta a) \end{array} \right\} \leq \frac{1}{12} ;$$

we are thus apportioning errors equally to the four components. Similar requirements hold for the components of error in  $\phi_B$  and  $\psi_B$ .

In view of the results already obtained, the requirements are met if

$$s.d.(\Delta i'_p) \leq \frac{1}{12} = .083^\circ$$

$$s.d.(\Delta\epsilon_p) \leq \frac{1}{12} \cdot \frac{1}{1.87} = .045^\circ$$

$$s.d.(\Delta e) \leq \frac{1}{12} \cdot \frac{1}{214} = 3.89 \times 10^{-4}$$

$$\begin{aligned} s.d.(\Delta a) &\leq \frac{1}{12} \cdot \frac{1}{1070} = 7.78 \times 10^{-5} \text{ equatorial radii} \\ &= 4.96 \times 10^{-1} \text{ km.} \end{aligned}$$

## REFERENCES

- [1] Morris M. Levinson, Satellite Attitude Determination Via On-Board Earth Detector and Radio Sensor Information, Flight Dynamics Data Memorandum Number 4143-FD-007, Space Technology Center, General Electric Company, Valley Forge, Pennsylvania.
- [2] Morris M. Levinson, Satellite Attitude Determination Via On-Board Solar Aspect Sensor Measurements and Ground-based Polarization Angle Measurements, (to be published), Flight Dynamics Data Memorandum, Space Technology Center, General Electric Company, Valley Forge, Pennsylvania.
- [3] Robert Baker and Maud Makemson, An Introduction to Astrodynamics, Academic Press, New York, 1960.



## APPENDIX B

### TV ATTITUDE SENSORY ERROR ANALYSIS

#### INTRODUCTION

The purpose of this task, undertaken during February and March 1965, was to study the use of the TV sensor on the AFS satellite for attitude determination, and to indicate the magnitude of the estimation errors which result from such use.

#### RESULTS AND RECOMMENDATIONS

The major set of results from this task consists of numerical computations of the errors in locating the center of the image of the earth, using equispaced points along the illuminated perimeter. The full set of results are being delivered separately, but samples are included in this report. This type of processing is recommended for the long-term data reduction of TV imagery.

A source of error is the distortion introduced when the curved face of the television monitor is photographed. Analysis of this distortion indicates that significant reduction can be achieved by proper choice of the focal length of the camera lens. A very significant reduction will be possible if a long focal-length, telephoto lens is used, allowing the camera to be placed on the order of seven feet from the screen.

The sources of error throughout the system were categorized and recommendations for their minimization made. These categories are as follows:

- o Distortions which can be predetermined, such as optical (pincushion and barrel types), or electronic (non-linearities).
- o Distortions which vary slowly (not known in advance, but constant from frame to frame in operation)
- o Errors due to readout uncertainties, lack of resolution, and scan-to-scan quantization in raster presentation. Tend to be random and independent from one point on an image to another.

Treatment of these error types both in "quick-look" and "long-term" processing will of course vary. The accuracy demanded in "quick-look" processing is not as great as that in long-term processing; but for the latter, questions of volume of data must be considered. It is assumed that availability of a small digital computer can be justified for the long-term processing, in addition to some automatic readout equipment for converting image points to machine-readable form (x-y coordinate reader).

#### REMOVAL OF PREDETERMINED DISTORTIONS.

Every image photographed from, or presented on, the TV monitor, will have some distortions which may be pre-calibrated. Such calibration may take the form of empirical measurements (photographing round targets of equivalent earth size) through the identical camera-transmitter-received-monitor-camera chain. Deviations from circularity may be recorded in the form of a calibration table. Some distortions may be amenable to mathematical representation, such as that resulting from the transformation from a curved TV tube to a flat photographic film. The important factor about these distortions is that they may be calibrated out prior to operation, in both the quick-look and long-term mode of processing.

#### Quick-Look Removal of Predetermined Errors

It is recommended that quick-look attitude determination (for pitch and roll attitude angles) be accomplished through the use of specially prepared templates having a central hole and annular clear space whose radius is the same as the image of the earth's lighted portion on the display. These templates will be "eyeballed" to fit the portion of earth's perimeter which is visible. If altitude is approximately constant, the radius of the template's circular rim will be that of the apparent radius of the viewed earth (the horizon is viewed, which does not coincide with the great circle which would be viewed if the satellite were at infinite altitude.)

It may be possible to fabricate the templates through direct use of the camera chain to take account of distortions all at once. A circular target is photographed by the use of the TV camera, monitor, and 35mm camera chain. It will not be truly circular when the final image is developed, due to distortions. Its deviation from circularity will be the same as the deviation of the true earth when viewed from the satellite and transmitted through the identical chain. A set of templates made in this manner can thus be made up to be "pre-distorted templates" which should better fit the images actually received in operation, giving somewhat improved accuracy in the "quick-look" mode. It is recommended that a template be made for images of the earth in a number of different positions or quadrants of the field of view, since the distortions will not be the same over the entire monitor. In operation, the operator will select the proper "pre-distorted" template depending on the approximate location of the circular image. Fitting to the illuminated edge of the earth's image will be done through visual averaging, and should be sufficiently accurate for "quick-look" purposes.

#### Long-Term Removal of Predetermined Errors

If a computer is available for long-term image processing, the removal of predetermined errors will be accomplished in the same manner as the short-term errors to be described later. It is also possible to store in the computer tables of correction constants for mathematically-described predetermined errors, but this should not be necessary.

#### REMOVAL OF SHORT-TERM DISTORTIONS

Short-term distortions are principally electronic in nature, caused by failure of the camera to achieve true linearity, and other non-linearities all the way through the video chain. These cannot be calibrated in advance, since they are brought about by drifts in circuit parameters, component values, aging, etc. They may be constant from frame to frame, but

it is difficult to estimate how long an interval would elapse before they attain new values of errors.

#### Removal of Short Term Distortions in Quick-Look Processing

The only way to recognize short-term distortions is by the failure of the reference video marks transmitted with the image to occur at regular spacings. These video marks, originating at the vidicon target itself, are the only stable reference indications in the entire system. For quick look processing, the location of the center of the image through the use of templates will be made ~~with~~ reference to these markings, rather than to the edges of the film or TV monitor.

#### Removal of Short Term Distortions in Long-Term Processing

In order to use a computer for processing the received images, it will be necessary to read into the machine some reference indications which convert film coordinates to angular deviations. It is highly recommended that the coordinates of the reference video marks be fed into the computer each frame, or, if the indicated distortions seem to be constant from one frame to the next, at regular intervals of, say, ten frames. It should not be necessary to enter the coordinates of every reference mark; every ~~five~~ degrees should suffice. The result of entering the coordinates of the reference marks is that the computer can now construct its own conversion table from coordinates to angular deviations directly, thereby removing both predetermined (constant) and short-term (nonlinear) distortions. Distortions may make the earth's circular image badly contorted on the image, but if the reference video marks are entered, the computer can internally convert samples from the distorted circle to samples of a perfect circle. The processing of these input perimeter points is thereby greatly facilitated.

At a minimum, the corners (extreme reference video marks) should be entered every frame, to make unnecessary the precise mechanical alignment of each image.

## REMOVAL OF READOUT ERRORS

Errors which occur as a result of uncertainty in the locations of points on the image can be characterized as readout errors. These could occur due to the finite appearance of the earth's atmosphere, the quantization effect due to raster scanning, and the spreading of the light-dark boundary resulting from the forced reduction in video bandwidth. They can be removed only by smoothing over many samples of independent errors.

### Removal of Readout Errors in Quick Look Processing

The recommended method of reading out the images in the "quick look" mode, i.e. use of circular templates, allows for human smoothing over many samples of errors. The ability of the human to "eyeball" an annulus on a template to a "fuzzy" portion of a circle is quite remarkable. The eye actually performs a fairly sophisticated smoothing process, weighting good samples more than bad, fitting the curve with fairly good accuracy. This type of fitting is the only way to reduce readout errors in the quick-look mode.

### Removal of Readout Errors in Long-Term Processing

The more points are used in long-term processing of the circular image, the more accurate will be the estimation of the center of the circle. For example, if only two samples of earth's perimeter are entered into a computer, the computer can use these coordinates to estimate the center of a circle of given radius passing through the points directly. This circle will fit the noise as well as the "true" points. A more accurate estimate can be **obtained** through the use of three points on the circle rather than two, for with such a case an "average" circle can be computed which will "fit" the true circle and, in general not pass directly through the points themselves. Thus some error reduction

can be achieved. As the number of points increases, more samples of independent errors are obtained, with the result that the "smoothed" circle becomes closer and closer to the "true" circle we are trying to estimate. - The limit in number of points is reached when adjacent samples do not have independent errors.

A mathematical technique for performing this type of processing is described in the following section. The reference to "redundant samples" means that more than the bare minimum of two points is used as a basis for estimating the center of the circle. This process is fairly easily implemented on a small, fast digital computer, and the processing of the points should be accomplished in far less time than their entry into the machine. Computers in the CDC-914 class are admirably equipped for this task, as well as the removal of the other errors of the type we have indicated above.

Selection of the points to be used in a particular circular sample is not critical. In general, points should be equally spaced around the illuminated arc, to allow for the geometric averaging inherent in the maximum likelihood technique. This method weights those points entered whose geometric position is favorable to the accuracy of the computation, and gives less weight to those points whose locations are unfavorable to the accuracy of the estimate. Thus, a wide sample will allow for favorable points to be included. The number of points taken depends on the requirements for accuracy, and determination to extract as much as possible from the data without incurring exorbitant personnel costs.


## MAXIMUM LIKELIHOOD PROCESSING OF REDUNDANT CIRCULAR SAMPLES

The purpose of this memo is to describe the application of the technique of Maximum Likelihood Estimation to the problem of estimating the center of a circle of known radius, when presented with a set of measured points on its circumference. Two points on the circumference constitute the minimum information required for such an estimate, and yield a single point as the result. When more than two circumference points are measured, and it is assumed that each measurement contains errors, then a single point does not, in general, exist which will locate a circle passing through all the measurements. To properly process such a set of points, in which redundant information is present, a statistical estimation technique must be used which will result in a best estimate of the center of the circle: best in a statistical sense.

Such a technique is available with Maximum Likelihood Estimation. It yields an estimate for the location of a circle which, if considered the true circle, would have resulted in the set of measurements with maximum probability. That is, there is no other circle which will "better fit" the measurements. Implicit in the technique is the ability to take into account the statistical description of the way errors are introduced, and properly weight those samples which contribute least to estimation errors, while giving comparatively less weight to those samples whose average error performance, or geometric location, would introduce larger errors in the estimate.

This memo will derive the equations which must be solved to produce an estimate of the center of the circle, given a set of more than two samples on its perimeter. The errors in these samples are to be specified to the equations in terms of rms errors in horizontal and vertical coordinates at each point. If there is no reason to believe that points differ in their rms errors, then these may be considered constant for all measurements.

In addition to deriving the necessary equations for producing a maximum likelihood central estimate, this memo will also derive the equations which specify the expected error of the final estimate, in x and y coordinates, as a function of the number of measurement points, their locations, and their error statistics. Using these equations it will be possible to study the effects of measurement errors, number of points used, and geometric position of the sample segment on the final circular center estimate errors. Numerical values for center locational errors may then be calculated for a wide variety of these variables.

We begin by considering the geometry of Figure 1. The measurement points are indicated by the marks . Their coordinates in an arbitrary reference system are designated as  $X_1, Y_1$ , for the x and y positions of the 1<sup>th</sup> measured point. A total of N points are assumed. An estimate of the center of the circle, of known radius R, is shown as indicated by the coordinates  $\hat{X}$  and  $\hat{Y}$ . The circle of such radius, drawn using  $\hat{X}$  and  $\hat{Y}$  as its center, is as indicated in the figure.  $\hat{X}$  and  $\hat{Y}$  will be the maximum likelihood estimates of the true coordinates of the center of the circle, if the set of measured points "best fits" the circle as generated. To define how the points "fit" the circle generated by the estimate  $\hat{X}, \hat{Y}$ , we compute the probability of the indicated deviations between points  $x_1, y_1$  and the points on the solid circle at the same angular position in the x-y frame. These deviations are denoted by  $e_{x1}$  and  $e_{y1}$  for the x and y errors at the 1<sup>th</sup> point. In the absence of any measurement errors, of course, the Maximum Likelihood estimate of the center of the circle will be the true center, and all measured points will pass identically through the circle having  $\hat{X}$  and  $\hat{Y}$  as its center.

We begin by expressing the measured points in terms of the center of the assumed circle, the angular position of the measurement point on the circle, measured clockwise from the vertical, and the measurement errors in both directions at each point.



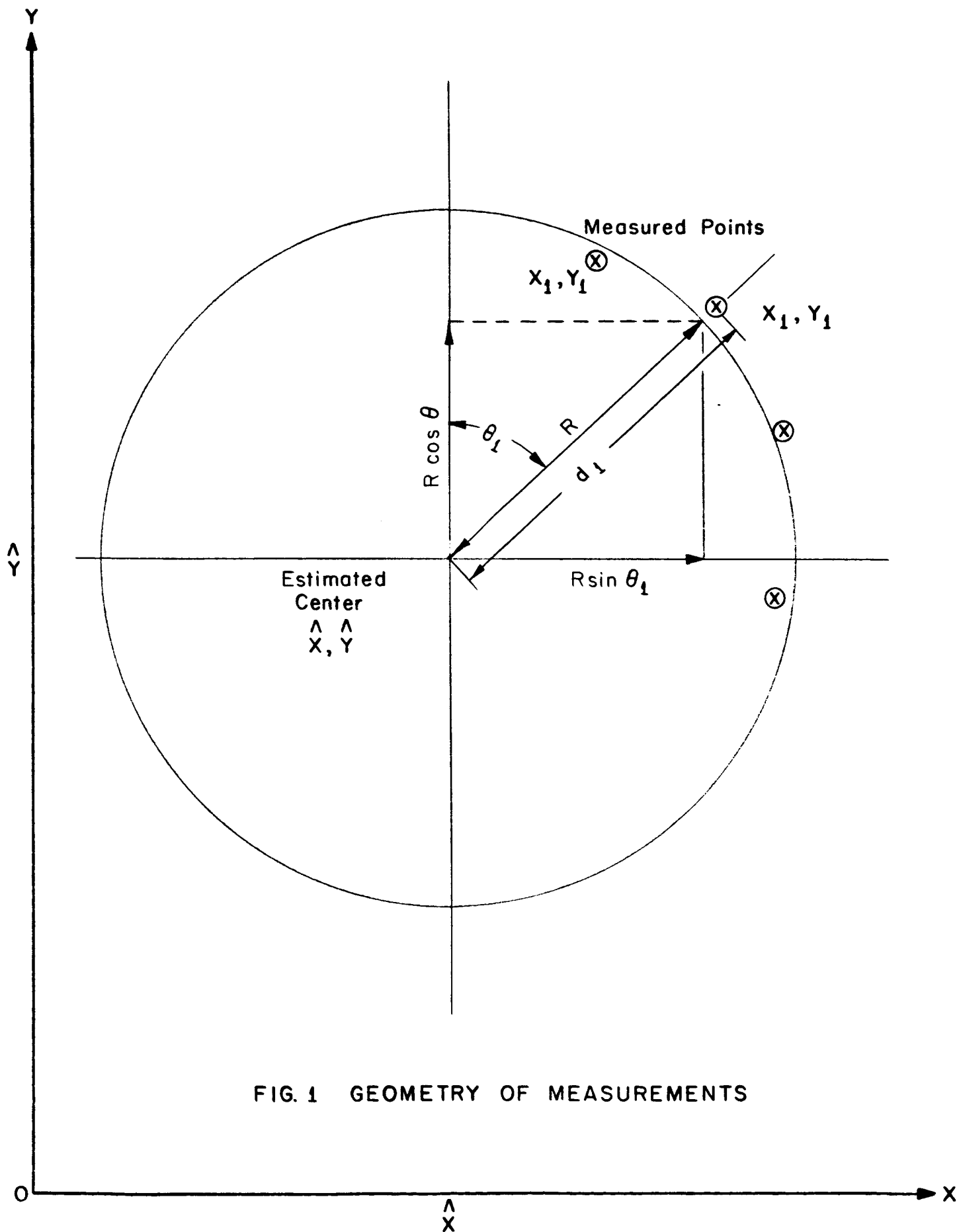


FIG. 1 GEOMETRY OF MEASUREMENTS

These points are:

$$x_1 = R \sin \theta_1 + \epsilon_{x1} + \hat{X} \quad (1)$$

$$y_1 = R \cos \theta_1 + \epsilon_{y1} + \hat{Y} \quad (2)$$

The total deviation of the measurement point is  $(\epsilon_{x1}^2 + \epsilon_{y1}^2)^{\frac{1}{2}}$ . When  $\hat{X}$  and  $\hat{Y}$  are chosen optimally, a function called the likelihood function is maximized. This function represents the probability of the indicated deviations from the circle. For this analysis,  $\epsilon_{x1}$  and  $\epsilon_{y1}$  will be considered to be independent errors, having Gaussian distributions of zero mean and standard deviations  $\sigma_{x1}$  and  $\sigma_{y1}$  respectively. The probability density function corresponding to an individual deviation  $\epsilon_{x1}$  and  $\epsilon_{y1}$  is thus given by the expression:

$$f(\epsilon_{x1}, \epsilon_{y1}) = \frac{1}{2\pi\sigma_{x1}\sigma_{y1}} \cdot e^{-\frac{1}{2} \left( \frac{\epsilon_{x1}^2}{\sigma_{x1}^2} + \frac{\epsilon_{y1}^2}{\sigma_{y1}^2} \right)} \quad (3)$$

The probability density function corresponding to the joint occurrence of the entire set of errors will be the product of all the individual density functions, if the errors are to be considered independent from sample to sample. The overall likelihood function is equal to this joint probability density function. Only the exponent is of interest. Since the individual density functions are of the form (3), the product of all the individual density functions is also of exponential form, with the exponent being the sum of the individual exponents.

The likelihood function is written:

$$L = K \cdot e^{-\frac{1}{2} \left[ \sum_{i=1}^N \frac{\epsilon_{xi}^2}{\sigma_{xi}^2} + \sum_{i=1}^N \frac{\epsilon_{yi}^2}{\sigma_{yi}^2} \right]} \quad (4)$$

where the constant K is immaterial, being the product of the individual constants. The likelihood function will be maximized by choosing  $\hat{X}$  and  $\hat{Y}$  to have values which will give deviations to minimize the summations in the exponent.

Minimization of the summations with respect to both  $\hat{X}$  and  $\hat{Y}$  is accomplished by setting the partial derivatives of the summation both to zero. In other words, the conditions of minimization of the exponential sums, or maximization of the likelihood functions, are as follows:

$$0 = \frac{\partial}{\partial \hat{X}} \left[ \sum_{i=1}^N \frac{\epsilon_{xi}^2}{\sigma_{xi}^2} + \sum_l \frac{\epsilon_{yl}^2}{\sigma_{yl}^2} \right] \quad (5)$$

$$0 = \frac{\partial}{\partial \hat{Y}} \left[ \sum_{i=1}^N \frac{\epsilon_{xi}^2}{\sigma_{xi}^2} + \sum_l \frac{\epsilon_{yl}^2}{\sigma_{yl}^2} \right] \quad (6)$$

These two equations will each contain terms in the set of measured coordinates, and in the unknowns  $\hat{X}$  and  $\hat{Y}$ . In principle these two equations in two unknowns can be solved to yield values for the unknowns. As we shall see, a closed form solution will not be possible, but a specific numerical computation may be made using a number of iteration techniques.

We start by performing the indicated partial differentiations:

$$0 = \sum_l \frac{\epsilon_{xl}}{\sigma_{xl}^2} \frac{\partial \epsilon_{xl}}{\partial \hat{X}} + \sum_l \frac{\epsilon_{yl}}{\sigma_{yl}^2} \frac{\partial \epsilon_{yl}}{\partial \hat{X}} \quad (7)$$

and

$$0 = \sum_l \frac{\epsilon_{xl}}{\sigma_{xl}^2} \frac{\partial \epsilon_{xl}}{\partial \hat{Y}} + \sum_l \frac{\epsilon_{yl}}{\sigma_{yl}^2} \frac{\partial \epsilon_{yl}}{\partial \hat{Y}} \quad (8)$$

The partial derivatives of the deviations  $\epsilon_{xl}$  and  $\epsilon_{yl}$  with respect to the estimate parameters  $\hat{X}$  and  $\hat{Y}$  are performed by differentiating a version of equations (1) and (2):

$$\epsilon_{xi} = x_i - \hat{X} - R \sin \theta_i \quad (9)$$

$$\epsilon_{yi} = y_i - \hat{Y} - R \cos \theta_i \quad (10)$$

When (9) and (10) are differentiated, we obtain the following results:

$$\frac{\partial \epsilon_{xi}}{\partial \hat{x}} = -1 - \frac{\partial}{\partial \hat{x}} (R \sin \theta_i) \quad (11)$$

$$\frac{\partial \epsilon_{xi}}{\partial \hat{y}} = -\frac{\partial}{\partial \hat{y}} (R \sin \theta_i) \quad (12)$$

$$\frac{\partial \epsilon_{yi}}{\partial \hat{x}} = -\frac{\partial}{\partial \hat{x}} (R \cos \theta_i) \quad (13)$$

$$\frac{\partial \epsilon_{yi}}{\partial \hat{y}} = -1 - \frac{\partial}{\partial \hat{y}} (R \cos \theta_i) \quad (14)$$

The partial derivatives of the trigonometric functions are found as

follows:  $\frac{\partial}{\partial \hat{x}} (R \sin \theta_i) = \frac{\partial}{\partial \hat{x}} \left[ \frac{R}{d_i} (x_i - \hat{x}) \right] = -\frac{R}{d_i} - \frac{(x_i - \hat{x})}{d_i^2} \frac{\partial d_i}{\partial \hat{x}}$

$$\frac{\partial}{\partial \hat{x}} (R \sin \theta_i) = -R \left[ \frac{1}{d_i} + \frac{(x_i - \hat{x})^2}{d_i^3} \right] \quad (15)$$

and from a similar computation,

$$\frac{\partial}{\partial \hat{y}} (R \sin \theta_i) = -\frac{R}{d_i^3} (x_i - \hat{x})(y_i - \hat{y}) \quad (16)$$

$$\frac{\partial}{\partial \hat{x}} (R \cos \theta_i) = -\frac{R}{d_i^3} (y_i - \hat{y})(x_i - \hat{x}) \quad (17)$$

$$\frac{\partial}{\partial \hat{y}} (R \cos \theta_i) = -R \left[ \frac{1}{d_i} + \frac{(y_i - \hat{y})^2}{d_i^3} \right] \quad (18)$$

Substituting (15 - 18) into (11)-(14), we obtain:

$$\frac{\partial \epsilon_{xi}}{\partial \hat{x}} = -1 + R \left[ \frac{1}{d_i} + \frac{(x_i - \hat{x})^2}{d_i^3} \right] \quad (19)$$

$$\frac{\partial \epsilon_{xi}}{\partial \hat{y}} = \frac{R}{d_i^3} (x_i - \hat{x})(y_i - \hat{y}) \quad (20)$$

$$\frac{\partial \epsilon_{yi}}{\partial \hat{x}} = \frac{R}{d_i^3} (x_i - \hat{x})(y_i - \hat{y}) \quad (21)$$

$$\frac{\partial \epsilon_{yi}}{\partial \hat{y}} = -1 + R \left[ \frac{1}{d_i} + \frac{(y_i - \hat{y})^2}{d_i^3} \right] \quad (22)$$

These expressions, together with the expressions in (9) and (10) with trigonometric functions replaced by ratios, may be substituted into the minimization form of equations (7) and (8), to yield the final forms:

$$0 = \sum_{i=1}^N \frac{(x_i - \hat{x}) \left(1 - \frac{R}{d_i}\right)}{\sigma_{xi}^2} \left[ -1 + R \left( \frac{1}{d_i} + \frac{(x_i - \hat{x})^2}{d_i^3} \right) \right] + \sum_{i=1}^N \frac{\left(1 - \frac{R}{d_i}\right) \left(\frac{R}{d_i^3}\right) (y_i - \hat{y})^2 (x_i - \hat{x})}{\sigma_{yi}^2} \quad (23)$$

$$0 = \sum_{i=1}^N \frac{\left(1 - \frac{R}{d_i}\right)}{\sigma_{xi}^2} \frac{R}{d_i^3} (x_i - \hat{x})^2 (y_i - \hat{y}) + \sum_{i=1}^N \frac{(y_i - \hat{y}) \left(1 - \frac{R}{d_i}\right)}{\sigma_{yi}^2} \left[ -1 + R \left( \frac{1}{d_i} + \frac{(y_i - \hat{y})^2}{d_i^3} \right) \right] \quad (24)$$

These equations can be somewhat simplified by combining some terms, but cannot be solved in closed form to give the value of  $\hat{x}$  and  $\hat{y}$  which will solve them.

The values  $d_i$  are found from  $d_i^2 = x_i^2 + y_i^2$ . The value  $R$  is constant.

A numerical solution for  $\hat{x}$  and  $\hat{y}$  is fairly easily obtained by a number of methods. It will be remembered that (23) and (24) are actually the derivatives of the exponent in the likelihood equation. When this exponent is minimized the derivatives will be zero. The exponent in question has the following form, as given in equation (4):

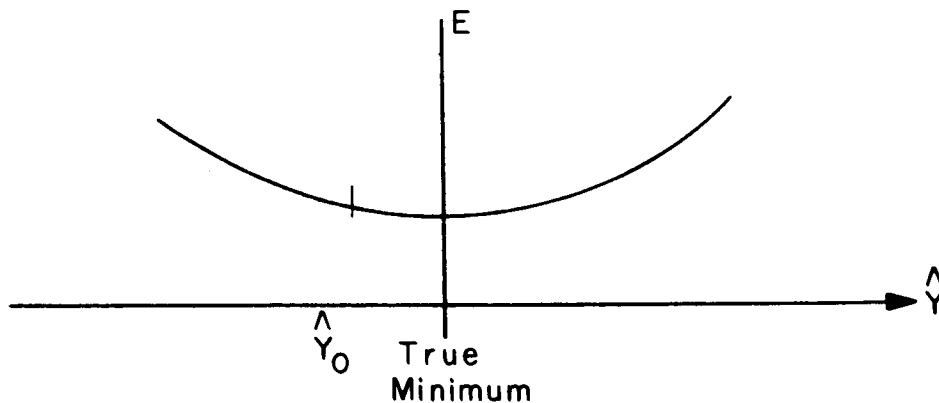
$$E = \sum_{i=1}^N \frac{\epsilon_{xi}^2}{\sigma_{xi}^2} + \frac{\epsilon_{yi}^2}{\sigma_{yi}^2} = \sum_{i=1}^N \left( \frac{x_i - \hat{x} - R \sin \theta_i}{\sigma_{xi}} \right)^2 + \left( \frac{y_i - \hat{y} - R \cos \theta_i}{\sigma_{yi}} \right)^2 \quad (25)$$

or removing the trigonometric functions,

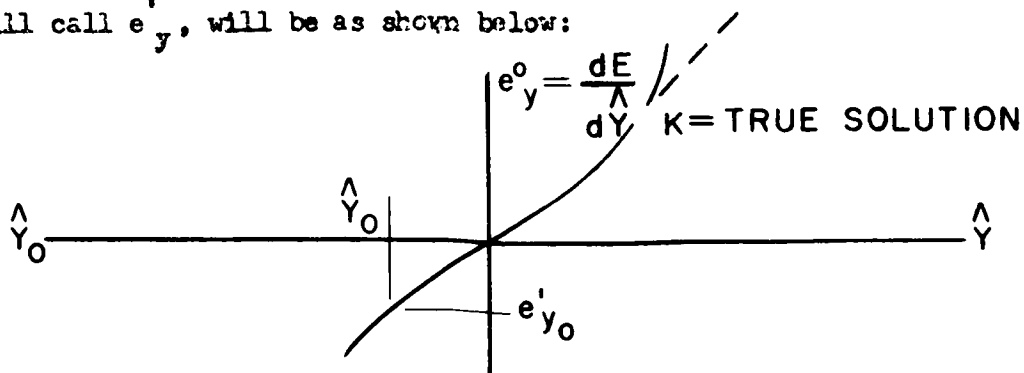
$$E = \sum_{i=1}^N \frac{(x_i - \hat{x})^2 (1 - R/d_i)^2}{\sigma_{xi}^2} + \sum_{i=1}^N \frac{(y_i - \hat{y})^2 (1 - R/d_i)^2}{\sigma_{yi}^2} \quad (26) \quad B-13$$

Note that if no errors are present, all the  $d_i$  are equal to  $R$  since all the points will be on the same circle. When this happens, of course equation (26) becomes equal to zero, and equations (23) and (24) are also satisfied, indicating that the maximum likelihood solution in the absence of errors is the true solution for the center of the circle.

To find a solution to (23) and (24) we may show the behavior of the exponent to be minimized, in the region near the true minimum. Let us assume that only one coordinate,  $\hat{X}$  or  $\hat{Y}$  needs adjustment to yield the true maximum likelihood solution. That is, we have somehow obtained the true solution for  $\hat{X}$  and have a trial value for  $\hat{Y}$  in the vicinity of the true value which will satisfy (23) and (24). Then  $E$  will have a value close to, but not precisely at its minimum, and an adjustment  $\Delta\hat{Y}$  is sought which will yield the final solution.



If the value of  $\hat{X}$  is the true minimizing value, then equation (23) will have right hand side equal to zero. Equation (24) will become zero on the right hand side when  $\hat{Y}$  is properly adjusted from the value  $\hat{Y}_0$  to the true solution. The relation between  $\hat{Y}$  and the right hand side of the equation (24), which we will call  $e'_y$ , will be as shown below:



The correction  $\Delta \hat{Y}$  to be added to  $\hat{Y}_0$  is approximately determined from the slope of the curve and the value of its trial value.

In the presence of slight errors in both  $\hat{X}$  and  $\hat{Y}$ , the more usual case, it is necessary to employ a technique based on the Taylor series expansion of the two derivative equations about the point  $\hat{X}, \hat{Y}$  which causes minimization. Call the values of  $\hat{X}$  and  $\hat{Y}$  which will satisfy (23) and (24)  $\hat{X}_m$  and  $\hat{Y}_m$  respectively. Call the right hand sides of these equations  $e'_x$  and  $e'_y$  respectively. Then

$$e'_x = e'_x \bigg|_{\substack{\hat{X}=\hat{X}_m \\ \hat{Y}=\hat{Y}_m}} + \frac{\partial e'_x}{\partial \hat{X}} \bigg|_{\substack{\hat{X}=\hat{X}_m \\ \hat{Y}=\hat{Y}_m}} \Delta \hat{X} + \frac{\partial e'_x}{\partial \hat{Y}} \bigg|_{\substack{\hat{X}=\hat{X}_m \\ \hat{Y}=\hat{Y}_m}} \Delta \hat{Y} \quad (27)$$

$$e'_y = e'_y \bigg|_{\substack{\hat{X}=\hat{X}_m \\ \hat{Y}=\hat{Y}_m}} + \frac{\partial e'_y}{\partial \hat{X}} \bigg|_{\substack{\hat{X}=\hat{X}_m \\ \hat{Y}=\hat{Y}_m}} \Delta \hat{X} + \frac{\partial e'_y}{\partial \hat{Y}} \bigg|_{\substack{\hat{X}=\hat{X}_m \\ \hat{Y}=\hat{Y}_m}} \Delta \hat{Y} \quad (28)$$

where  $\Delta \hat{X} = \hat{X} - \hat{X}_m$  and  $\Delta \hat{Y} = \hat{Y} - \hat{Y}_m$

The partial derivatives are found from (23) and (24), and are to be evaluated at  $\hat{X} = \hat{X}_m$  and  $\hat{Y} = \hat{Y}_m$ . Note  $e'_x$  and  $e'_y$  are both zero at the optimum point  $\hat{X}_m, \hat{Y}_m$ .

If at some trial point, we obtain values for  $e'_x$  and  $e'_y$  which are non-zero, the above two equations are solved simultaneously to find the values of  $\Delta \hat{X}$  and  $\Delta \hat{Y}$  which caused this value. The negatives of these increments are then the corrections to be applied to determine the true optimum.

# RESULTING ERROR OF ESTIMATE

In the absence of any measurement errors, the point  $\hat{X}$ ,  $\hat{Y}$  will be determined as the exact center of the circle. It is of interest to compute the average or expected deviation from this ideal point when the measurements are given errors. It is clear that the point  $\hat{X}$ ,  $\hat{Y}$  will differ from the ideal point by some value,  $\Delta\hat{X}$ ,  $\Delta\hat{Y}$ . The expected value of the quantity  $\overline{\Delta\hat{X}^2 + \Delta\hat{Y}^2}$  can be calculated for any specific measurement set, given the locations of the measured points (approximately), and the distributions of their errors. The method of calculation is as follows:

$$\Delta\hat{X} \cong \sum \frac{\partial \hat{X}}{\partial x_i} \epsilon_{x_i} + \sum \frac{\partial \hat{X}}{\partial y_i} \epsilon_{y_i}$$

$$\Delta\hat{Y} \cong \sum \frac{\partial \hat{Y}}{\partial x_i} \epsilon_{x_i} + \sum \frac{\partial \hat{Y}}{\partial y_i} \epsilon_{y_i}$$

where it is assumed that the  $\epsilon_{x_i}$  and  $\epsilon_{y_i}$  are small deviations from the measurement that would have been taken without errors. The partial derivatives are evaluated at the point  $\hat{X} = \hat{Y} = 0$ , since this is the value of the maximum likelihood estimate of the center of the circle in the absence of measurement errors, and we are considering only perturbations from this point, one at a time, caused by measurement errors.

We obtain the partial derivatives from differentiating (23) and (24) and retaining only those terms which do not vanish for  $\hat{X} = \hat{Y} = 0$  and thus  $d_1 = R$ . Differentiation is performed before setting these quantities to the values cited.

The partial derivatives needed are found from simultaneous solution of the results of differentiating these equations with respect to each  $X_i$  and  $Y_i$ .



If we differentiate equations (23) and (24) with respect to  $X_1$ , we obtain two equations in the two partials with respect to that variable, which may be solved simultaneously. If we differentiate (24) and (23) with respect to  $Y_1$  we obtain two equations which may be solved simultaneously to give the partials  $(\frac{\partial \hat{X}}{\partial Y_i})$  and  $(\frac{\partial \hat{Y}}{\partial Y_i})$ .

When differentiating (23) and (24), considerable simplification is possible if we anticipate that the derivatives will later be evaluated at  $\hat{X} = \hat{Y} = 0$ . This means that  $d_1 = R$ . Only one of the possible three terms in the derivatives of each summation will be retained. Each term under the summations must be differentiated with respect to  $X_1$  or  $Y_1$ ; we will refer to these terms with the subscript  $j$  to show the distinction.

Differentiating (23) with respect to  $X_1$ , we obtain:

$$\text{or } 0 = \sum_{j=1}^N \left[ \frac{X_j}{\sigma_{Xj}^2} \right] \left[ \frac{X_j^2}{R^2} \right] \frac{\partial}{\partial X_i} \left( \frac{-R}{d_j} \right) + \sum_{j=1}^N \left[ \frac{Y_j^2}{\sigma_{Yj}^2} \right] \left[ \frac{X_j}{R^2} \right] \frac{\partial}{\partial X_i} \left( \frac{-R}{d_j} \right) \quad (29)$$

$$0 = \sum_j \frac{X_j}{R} \left( \frac{X_j^2}{\sigma_{Xj}^2} + \frac{Y_j^2}{\sigma_{Yj}^2} \right) \frac{\partial}{\partial X_i} \left( \frac{-1}{d_j} \right) \quad (30)$$

The partial derivatives of  $d_j$  with respect to  $X_1$  is found from:

$$d_j^2 = (X_j - \hat{X})^2 + (Y_j - \hat{Y})^2 \quad (31)$$

from which is found the result:

$$\frac{\partial}{\partial X_i} \left( \frac{-1}{d_j} \right) = \frac{1}{d_j^2} \frac{\partial d_j}{\partial X_i} = \frac{1}{d_j^3} \frac{\partial}{\partial X_i} \left( (X_j - \hat{X})^2 + (Y_j - \hat{Y})^2 \right) \quad (32)$$

This is evaluated two ways depending upon whether  $i = j$  or  $i \neq j$ .

$$\left. \begin{aligned} \frac{\partial}{\partial X_i} \left( \frac{-1}{d_j} \right) &= \frac{1}{R^3} \left( -X_j \frac{\partial \hat{X}}{\partial X_i} - Y_j \frac{\partial \hat{Y}}{\partial X_i} \right) && \text{when } i \neq j \\ &= \frac{1}{R^3} \left( -X_j \frac{\partial \hat{X}}{\partial X_i} - Y_j \frac{\partial \hat{Y}}{\partial X_i} \right) + \frac{X_i}{R^3} && \text{when } i = j \end{aligned} \right\} \quad (33)$$

The difference between the two values is due to the fact that

$$\begin{aligned}\frac{\partial \hat{X}_i}{\partial X_i} &= 1 \text{ for } i = j \\ \frac{\partial \hat{X}_i}{\partial X_i} &= 0 \text{ for } i \neq j\end{aligned}$$

These values are substituted in (30) to yield:

$$0 = \sum_{j=1}^N \frac{X_j}{R^4} \left( \frac{X_j^2}{\sigma_{Xj}^2} + \frac{Y_j^2}{\sigma_{Yj}^2} \right) \left( -X_j \frac{\partial \hat{X}}{\partial X_i} - Y_j \frac{\partial \hat{Y}}{\partial Y_i} \right) + \frac{X_i^2}{R^4} \left( \frac{X_i^2}{\sigma_{Xi}^2} + \frac{Y_i^2}{\sigma_{Yi}^2} \right) \quad (34)$$

The  $R^4$  terms in the denominator may be cancelled to give the result in the form:

$$\sum_j K_j \left( X_j \frac{\partial \hat{X}}{\partial X_i} + Y_j \frac{\partial \hat{Y}}{\partial Y_i} \right) = X_i \quad (35)$$

$$\text{where } K_j = X_j \left( \frac{X_j^2}{\sigma_{Xj}^2} + \frac{Y_j^2}{\sigma_{Yj}^2} \right)$$

Expressed in terms of a linear equation in the unknowns,

$$\left[ \sum K_j X_j \right] \frac{\partial \hat{X}}{\partial X_i} + \left[ \sum K_j Y_j \right] \frac{\partial \hat{Y}}{\partial X_i} = K_i X_i \quad (36)$$

In a similar manner, we also differentiate (24) with respect to  $X_1$ , then

differentiate (23) and (24) with respect to  $Y_1$ . The results are:

$$\left[ \sum m_j X_j \right] \frac{\partial \hat{X}}{\partial X_i} + \left[ \sum m_j Y_j \right] \frac{\partial \hat{Y}}{\partial X_i} = m_i X_i \quad (37)$$

$$\left[ \sum K_j X_j \right] \frac{\partial \hat{X}}{\partial Y_i} + \left[ \sum K_j Y_j \right] \frac{\partial \hat{Y}}{\partial Y_i} = K_i Y_i \quad (38)$$

$$\left[ \sum m_j X_j \right] \frac{\partial \hat{X}}{\partial Y_i} + \left[ \sum m_j Y_j \right] \frac{\partial \hat{Y}}{\partial Y_i} = m_i Y_i \quad (39)$$

where  $K_j$  is as described above and

$$m_j = Y_j \left( \frac{X_j^2}{\sigma_{Xj}^2} + \frac{Y_j^2}{\sigma_{Yj}^2} \right)$$

Finally, we obtain the expressions for the partial derivatives from the simultaneous solution of equations (36) and (37) for  $\frac{\partial \hat{X}}{\partial x_i}$  and  $\frac{\partial \hat{Y}}{\partial x_i}$ ; and of equations (38) and (39) for  $\frac{\partial \hat{X}}{\partial y_i}$  and  $\frac{\partial \hat{Y}}{\partial y_i}$ . These are:

$$\frac{\partial \hat{X}}{\partial x_i} = \frac{C_1 m_i x_i - C_2 K_i x_i}{\Delta} \quad (40)$$

$$\frac{\partial \hat{Y}}{\partial x_i} = \frac{C_3 K_i x_i - C_4 m_i x_i}{\Delta} \quad (41)$$

$$\frac{\partial \hat{X}}{\partial y_i} = \frac{C_1 m_i y_i - C_2 K_i y_i}{\Delta} \quad (42)$$

$$\frac{\partial \hat{Y}}{\partial y_i} = \frac{C_3 K_i y_i - C_4 m_i y_i}{\Delta} \quad (43)$$

$$C_1 = \sum K_j Y_j \quad (44)$$

$$C_2 = \sum m_j Y_j \quad (45)$$

$$C_3 = \sum m_j X_j \quad (46)$$

$$C_4 = \sum K_j X_j \quad (47)$$

$$\Delta = C_3 C_1 - C_2 C_4 \quad (48)$$

Finally, from equations on page -10-, the means and variances of the final error of estimate may be calculated:

The means of  $\Delta \hat{X}$  and  $\Delta \hat{Y}$  are

$$\overline{\Delta \hat{X}} = \sum_i \frac{\partial \hat{X}}{\partial x_i} \overline{\epsilon_{xi}} + \sum_i \frac{\partial \hat{X}}{\partial y_i} \overline{\epsilon_{yi}} \quad (49)$$

$$\overline{\Delta \hat{Y}} = \sum_i \frac{\partial \hat{Y}}{\partial x_i} \overline{\epsilon_{xi}} + \sum_i \frac{\partial \hat{Y}}{\partial y_i} \overline{\epsilon_{yi}} \quad (50)$$

If we assume that the errors in individual points may be as likely positive as negative in both coordinates, then these means become zero. The estimating technique is therefore free of bias.

The variances in the errors will add, so that the variances in the resulting estimates will be the weighted sum of the variances of the measurements:

$$Var \Delta \hat{X} = \sum_i \left( \frac{\partial \hat{X}}{\partial x_i} \right)^2 \sigma_{xi}^2 + \sum_i \left( \frac{\partial \hat{X}}{\partial y_i} \right)^2 \sigma_{yi}^2 \quad (51)$$

$$Var \Delta \hat{Y} = \sum_i \left( \frac{\partial \hat{Y}}{\partial x_i} \right)^2 \sigma_{xi}^2 + \sum_i \left( \frac{\partial \hat{Y}}{\partial y_i} \right)^2 \sigma_{yi}^2 \quad (52)$$

Of course, the standard deviation of the estimate errors are found from the square root of the variances.

## COMPUTATION OF NUMERICAL VALUES FOR ESTIMATION ERRORS

To implement this process on a digital computer for the purpose of determining the center of the earth, the geometry of figure 2 is used. The angle  $\beta$  is defined by the illuminated crescent. The subtended arc is then divided into equal segments defined by  $N$  points  $x_1, y_1$ . Given the coordinate values of these points then and assuming values for  $\sigma_x$  and  $\sigma_y$ , numerical values are developed in the computer for use in equations 29 through 52. Angles  $\alpha$  and  $\beta$  are both used in the computer program to achieve the relationship between the position of the points  $x_1, y_1$  and the weighting of the values of  $\sigma_x$  and  $\sigma_y$ .

Two pages of sample results are included following Figure 2. Additional results will be furnished when runs are completed during the week ending 5 April, and the entire set compiled.

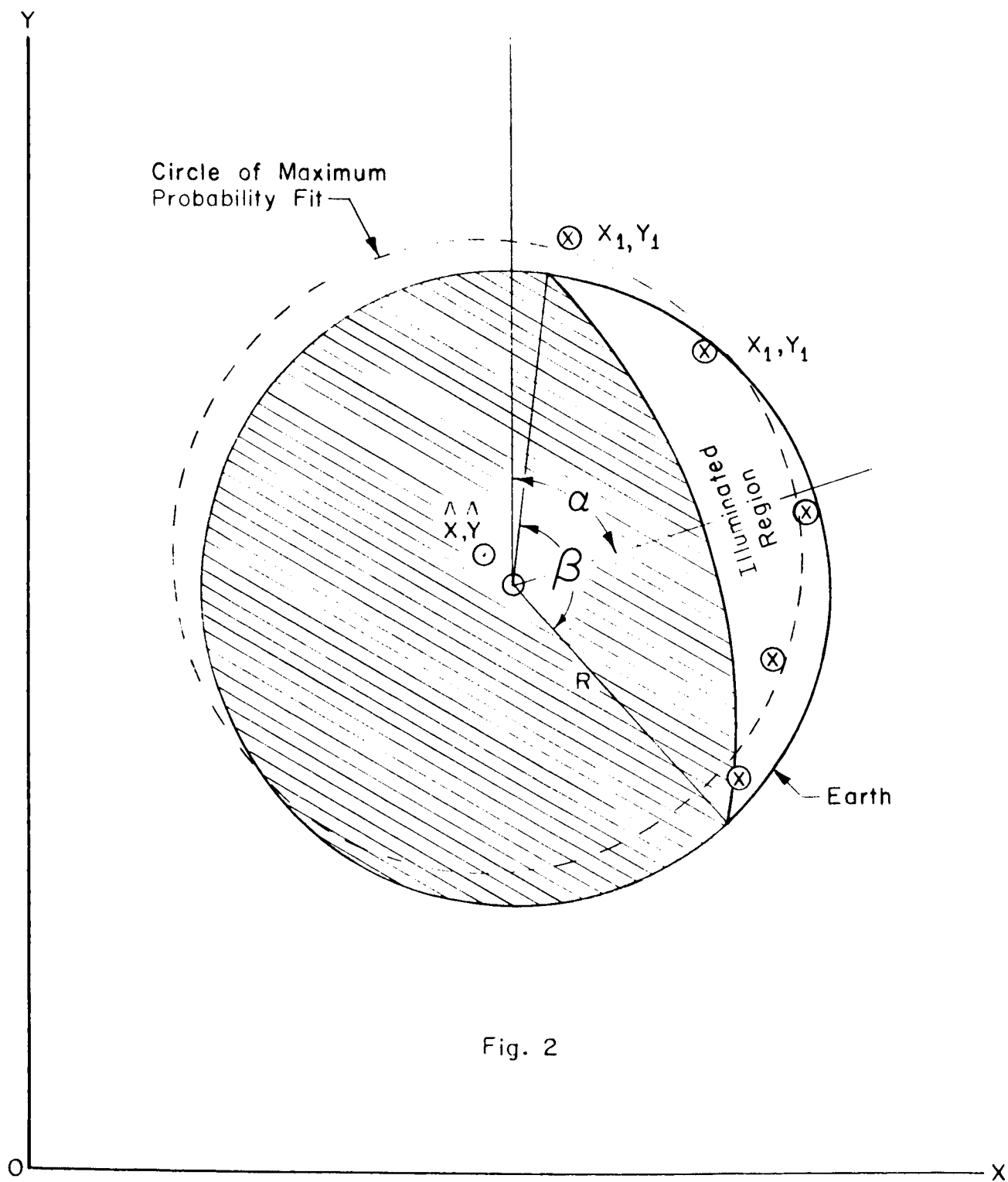


Fig. 2

Sigma x = .005'  
Sigma y = .005'

		$\sigma_x$ N=3	$\sigma_y$	$\sigma_x$ N=5	$\sigma_y$	$\sigma_x$ N=9	$\sigma_y$
ALPHA	BETA						
.'	15.'	.027087'	.002903'	.024217'	.002246'	.019767'	.001673'
.'	30.'	.013660'	.002953'	.012197'	.002275'	.009946'	.001691'
.'	45.'	.009239'	.003039'	.008231'	.002323'	.006701'	.001721'
.'	90.'	.005000'	.003536'	.004397'	.002597'	.003548'	.001888'
.'	135.'	.003827'	.004397'	.003280'	.003057'	.002604'	.002169'
.'	180.'	.003536'	.005000'	.002887'	.003536'	.002236'	.002500'
.'	270.'	.005000'	.003536'	.003039'	.003302'	.002183'	.002581'
30.'	15.'	.023503'	.013775'	.021002'	.012263'	.017139'	.009989'
30.'	30.'	.011922'	.007293'	.010624'	.006409'	.008655'	.005184'
30.'	45.'	.008144'	.005316'	.007222'	.004581'	.005867'	.003667'
30.'	90.'	.004677'	.003953'	.004023'	.003145'	.003214'	.002412'
30.'	135.'	.003977'	.004262'	.003225'	.003114'	.002502'	.002286'
30.'	180.'	.003953'	.004677'	.003062'	.003385'	.002305'	.002437'
30.'	270.'	.004677'	.003953'	.003107'	.003238'	.002289'	.002488'
60.'	15.'	.013775'	.023503'	.012263'	.021002'	.009989'	.017139'
60.'	30.'	.007293'	.011922'	.006409'	.010624'	.005184'	.008655'
60.'	45.'	.005316'	.008144'	.004581'	.007222'	.003667'	.005867'
60.'	90.'	.003953'	.004677'	.003145'	.004023'	.002412'	.003214'
60.'	135.'	.004262'	.003977'	.003114'	.003225'	.002286'	.002502'
60.'	180.'	.004677'	.003953'	.003385'	.003062'	.002437'	.002305'
60.'	270.'	.003953'	.004677'	.003238'	.003107'	.002488'	.002289'
90.'	15.'	.002903'	.027087'	.002246'	.024217'	.001673'	.019766'
90.'	30.'	.002953'	.013660'	.002275'	.012197'	.001691'	.009946'
90.'	45.'	.003039'	.009239'	.002323'	.008231'	.001721'	.006701'
90.'	90.'	.003536'	.005000'	.002597'	.004397'	.001888'	.003548'
90.'	135.'	.004397'	.003827'	.003057'	.003280'	.002169'	.002604'
90.'	180.'	.005000'	.003536'	.003536'	.002887'	.002500'	.002236'
90.'	270.'	.003536'	.005000'	.003302'	.003039'	.002581'	.002183'

Sigma x = .005'  
Sigma y = .010'

ALPHA	BETA	N=3		N=5		N=9	
.	15.'	.053826'	.005783'	.048172'	.004477'	.039348'	.003337'
.	30.'	.026625'	.005818'	.023881'	.004499'	.019531'	.003349'
.	45.'	.017433'	.005891'	.015698'	.004541'	.012867'	.003376'
.	90.'	.007906'	.006329'	.007217'	.004764'	.005982'	.003515'
.	135.'	.004591'	.007482'	.004252'	.005324'	.003574'	.003813'
.	180.'	.003536'	.010000'	.003286'	.006329'	.002646'	.004378'
.	270.'	.007906'	.006329'	.003986'	.005500'	.002692'	.004320'
30.'	15.'	.041959'	.025103'	.037565'	.022279'	.030689'	.018121'
30.'	30.'	.020654'	.013646'	.018538'	.011868'	.015174'	.009556'
30.'	45.'	.013388'	.010227'	.012061'	.008664'	.009907'	.006887'
30.'	90.'	.005857'	.007532'	.005373'	.005966'	.004458'	.004582'
30.'	135.'	.004844'	.007513'	.003949'	.005547'	.003071'	.004147'
30.'	180.'	.006060'	.008149'	.003890'	.005653'	.002895'	.004186'
30.'	270.'	.005857'	.007532'	.003619'	.005758'	.002759'	.004287'
60.'	15.'	.017752'	.031460'	.015896'	.028013'	.012988'	.022824'
60.'	30.'	.008779'	.016468'	.007870'	.014496'	.006435'	.011745'
60.'	45.'	.005916'	.011729'	.005264'	.010186'	.004287'	.008189'
60.'	90.'	.004579'	.007596'	.003500'	.006442'	.002652'	.005033'
60.'	135.'	.005853'	.006736'	.003824'	.005629'	.002751'	.004309'
60.'	180.'	.006555'	.006435'	.004332'	.005335'	.003062'	.004045'
60.'	270.'	.004579'	.007596'	.004117'	.005477'	.003101'	.004104'
90.'	15.'	.002952'	.027770'	.002274'	.024736'	.001690'	.020135'
90.'	30.'	.003135'	.014970'	.002381'	.013187'	.001757'	.010650'
90.'	45.'	.003407'	.011084'	.002540'	.009614'	.001858'	.007688'
90.'	90.'	.004326'	.007906'	.003150'	.006463'	.002256'	.005044'
90.'	135.'	.004819'	.007221'	.003795'	.005605'	.002686'	.004303'
90.'	180.'	.005000'	.007071'	.004326'	.005401'	.003099'	.004029'
90.'	270.'	.004326'	.007906'	.004199'	.005358'	.003421'	.003879'



Sigma x = u .005'

Sigma y = .020'

ALPHA	BETA	N=3		N=5		N=9	
.	15.'	.107478'	.011604'	.096370'	.008981'	.078742'	.006689'
.	30.'	.052897'	.011953'	.047960'	.009234'	.039315'	.006852'
.	45.'	.034325'	.012409'	.031487'	.009583'	.025943'	.007102'
.	90.'	.014577'	.013212'	.013565'	.009865'	.011387'	.007371'
.	135.'	.006842'	.013824'	.006570'	.010259'	.005840'	.007467'
.	180.'	.003536'	.020000'	.004143'	.013212'	.003614'	.008524'
.	270.'	.014577'	.013212'	.006342'	.010498'	.003906'	.008120'
30.'	15.'	.081694'	.049252'	.073173'	.043650'	.059768'	.035461'
30.'	30.'	.040773'	.028036'	.036492'	.024075'	.029821'	.019247'
30.'	45.'	.026969'	.022972'	.023909'	.018642'	.019599'	.014569'
30.'	90.'	.008364'	.015464'	.008078'	.012345'	.007104'	.009603'
30.'	135.'	.006327'	.014487'	.005553'	.010988'	.004252'	.008306'
30.'	180.'	.011004'	.015637'	.005822'	.010116'	.004311'	.007999'
30.'	270.'	.008364'	.015464'	.004680'	.011134'	.003913'	.008194'
60.'	15.'	.028451'	.052117'	.025608'	.046262'	.020992'	.037660'
60.'	30.'	.012877'	.027582'	.011827'	.024064'	.009805'	.019445'
60.'	45.'	.007481'	.019763'	.007065'	.016990'	.005933'	.013608'
60.'	90.'	.006430'	.013312'	.004478'	.011479'	.003278'	.008794'
60.'	135.'	.009950'	.013249'	.005552'	.011030'	.003936'	.008341'
60.'	180.'	.011285'	.012022'	.006554'	.010122'	.004482'	.007865'
60.'	270.'	.006430'	.013312'	.006395'	.010856'	.004500'	.008144'
90.'	15.'	.003137'	.030351'	.002383'	.026709'	.001758'	.021542'
90.'	30.'	.003700'	.019342'	.002758'	.016551'	.001997'	.013081'
90.'	45.'	.004549'	.016518'	.003241'	.012702'	.002313'	.010732'
90.'	90.'	.006020'	.014577'	.004546'	.011222'	.003226'	.008594'
90.'	135.'	.005090'	.014218'	.005528'	.010528'	.003905'	.007898'
90.'	180.'	.005000'	.014142'	.006020'	.012104'	.004507'	.008160'
90.'	270.'	.006020'	.014577'	.005934'	.010475'	.005309'	.007733'

Sigma x = .005'  
Sigma y = .040'

ALPHA	BETA	N=3		N=5		N=9	
.	15.'	.214870'	.024043'	.194914'	.018602'	.159604'	.013792'
.	30.'	.105617'	.025934'	.097932'	.020347'	.080841'	.015109'
.	45.'	.068376'	.026875'	.063948'	.021181'	.053057'	.015826'
.	90.'	.028504'	.027679'	.026729'	.020622'	.022540'	.015566'
.	135.'	.012238'	.027909'	.011907'	.020585'	.010876'	.015119'
.	180.'	.003536'	.040000'	.006424'	.027679'	.006046'	.017206'
.	270.'	.028504'	.027679'	.011684'	.021020'	.006820'	.016047'
30.'	15.'	.162932'	.098509'	.145919'	.087231'	.119124'	.070798'
30.'	30.'	.083911'	.059172'	.074402'	.049947'	.060508'	.039579'
30.'	45.'	.060282'	.055648'	.051048'	.042140'	.041234'	.032074'
30.'	90.'	.014515'	.032310'	.014360'	.026627'	.013327'	.021213'
30.'	135.'	.009981'	.028713'	.009455'	.022385'	.007125'	.017060'
30.'	180.'	.021415'	.030936'	.010316'	.019414'	.007653'	.015984'
30.'	270.'	.014515'	.032310'	.007436'	.022225'	.006738'	.016395'
60.'	15.'	.052760'	.098037'	.047597'	.086911'	.039075'	.070727'
60.'	30.'	.022750'	.052011'	.021191'	.045220'	.017707'	.036509'
60.'	45.'	.011693'	.037183'	.011680'	.031876'	.010054'	.025512'
60.'	90.'	.011068'	.025538'	.007113'	.022165'	.005003'	.016785'
60.'	135.'	.018944'	.027133'	.009707'	.022405'	.006828'	.016861'
60.'	180.'	.021560'	.023602'	.011740'	.020015'	.007855'	.015828'
60.'	270.'	.011068'	.025538'	.011682'	.022420'	.007851'	.016655'
90.'	15.'	.003789'	.039002'	.002776'	.033457'	.002008'	.026433'
90.'	30.'	.005618'	.031211'	.003920'	.025961'	.002756'	.020043'
90.'	45.'	.007544'	.029544'	.005164'	.024078'	.003593'	.018416'
90.'	90.'	.010157'	.028504'	.007929'	.021437'	.005598'	.016309'
90.'	135.'	.005671'	.028322'	.009673'	.020755'	.006823'	.015383'
90.'	180.'	.005000'	.028284'	.010157'	.026902'	.007878'	.016963'
90.'	270.'	.010157'	.028504'	.010064'	.021020'	.009615'	.015808'

Sigma x = .010'  
Sigma y = .005'

ALPHA	BETA	N=3	N=5	N=9			
.	15.	.027770'	.002952'	.024736'	.002274'	.020135'	.001690'
.	30.	.014970'	.003135'	.013187'	.002381'	.010650'	.001757'
.	45.	.011084'	.003407'	.009614'	.002540'	.007688'	.001858'
.	90.	.007906'	.004326'	.006463'	.003150'	.005044'	.002256'
.	135.	.007221'	.004819'	.005605'	.003795'	.004303'	.002686'
.	180.	.007071'	.005000'	.005401'	.004326'	.004029'	.003099'
.	270.	.007906'	.004326'	.005358'	.004199'	.003879'	.003421'
30.	15.	.031460'	.017752'	.028013'	.015896'	.022824'	.012988'
30.	30.	.016468'	.008779'	.014496'	.007870'	.011745'	.006435'
30.	45.	.011729'	.005916'	.010186'	.005264'	.008189'	.004287'
30.	90.	.007596'	.004579'	.006442'	.003500'	.005033'	.002652'
30.	135.	.006736'	.005853'	.005629'	.003824'	.004309'	.002751'
30.	180.	.006435'	.006555'	.005335'	.004332'	.004045'	.003062'
30.	270.	.007596'	.004579'	.005477'	.004117'	.004104'	.003101'
60.	15.	.025103'	.041959'	.022279'	.037565'	.018121'	.030689'
60.	30.	.013646'	.020654'	.011868'	.018538'	.009556'	.015174'
60.	45.	.010227'	.013388'	.008664'	.012061'	.006887'	.009907'
60.	90.	.007532'	.005857'	.005966'	.005373'	.004582'	.004458'
60.	135.	.007513'	.004844'	.005547'	.003949'	.004147'	.003071'
60.	180.	.008149'	.006060'	.005653'	.003890'	.004186'	.002895'
60.	270.	.007532'	.005857'	.005758'	.003619'	.004287'	.002759'
90.	15.	.005783'	.053826'	.004477'	.043172'	.003337'	.039348'
90.	30.	.005818'	.026625'	.004499'	.023881'	.003349'	.019531'
90.	45.	.005891'	.017433'	.004541'	.015698'	.003376'	.012867'
90.	90.	.006329'	.007906'	.004764'	.007217'	.003515'	.005982'
90.	135.	.007482'	.004591'	.005324'	.004252'	.003813'	.003574'
90.	180.	.010000'	.003536'	.006329'	.003286'	.004378'	.002646'
90.	270.	.006329'	.007906'	.005500'	.003986'	.004320'	.002692'

sigma x = .010'

Sigma y = .010'

ALPHA	BETA	N=3		N=5		N=9	
.1	15.1	.054174	.005806	.048434	.004492	.039534	.003346
.1	30.1	.027320	.005906	.024394	.004550	.019892	.003382
.1	45.1	.018478	.006078	.016462	.004646	.013402	.003442
.1	90.1	.010000	.007072	.008794	.005194	.007096	.003776
.1	135.1	.007654	.008794	.006560	.006114	.005208	.004338
.1	180.1	.007072	.010000	.005774	.007072	.004472	.005000
.1	270.1	.010000	.007072	.006078	.006604	.004366	.005162
30.1	15.1	.047006	.027550	.042004	.024526	.034278	.019978
30.1	30.1	.023844	.014586	.021248	.012818	.017310	.010368
30.1	45.1	.016288	.010632	.014444	.009162	.011734	.007334
30.1	90.1	.009354	.007906	.008046	.006290	.006428	.004824
30.1	135.1	.007954	.008524	.006450	.006228	.005004	.004572
30.1	180.1	.007906	.009354	.006124	.006770	.004610	.004874
30.1	270.1	.009354	.007906	.006214	.006476	.004578	.004976
60.1	15.1	.027550	.047006	.024526	.042004	.019978	.034278
60.1	30.1	.014586	.023844	.012818	.021248	.010368	.017310
60.1	45.1	.010632	.016288	.009162	.014444	.007334	.011734
60.1	90.1	.007906	.009354	.006290	.008046	.004824	.006428
60.1	135.1	.008524	.007954	.006228	.006450	.004572	.005004
60.1	180.1	.009354	.007906	.006770	.006124	.004874	.004610
60.1	270.1	.007906	.009354	.006476	.006214	.004976	.004578
90.1	15.1	.005806	.054174	.004492	.048434	.003346	.039532
90.1	30.1	.005906	.027320	.004550	.024394	.003382	.019892
90.1	45.1	.006078	.018478	.004646	.016462	.003442	.013402
90.1	90.1	.007072	.010000	.005194	.008794	.003776	.007096
90.1	135.1	.008794	.007654	.006114	.006560	.004338	.005208
90.1	180.1	.010000	.007072	.007072	.005774	.005000	.004472
90.1	270.1	.007072	.010000	.006604	.006078	.005162	.004366

Sigma x = .010'

Sigma y = .020'

ALPHA	BETA	N=3		N=5		N=9	
.	15.	.107652'	.011566'	.096344'	.008954'	.078696'	.006674'
.	30.	.053250'	.011636'	.047762'	.008998'	.039062'	.006698'
.	45.	.034866'	.011782'	.031396'	.009082'	.025734'	.006752'
.	90.	.015812'	.012658'	.014434'	.009528'	.011964'	.007030'
.	135.	.009182'	.014964'	.008504'	.010648'	.007148'	.007626'
.	180.	.007072'	.020000'	.006572'	.012658'	.005292'	.008756'
.	270.	.015812'	.012658'	.007972'	.011000'	.005384'	.008640'
30.	15.	.083918'	.050206'	.075130'	.044558'	.061378'	.036242'
30.	30.	.041308'	.027292'	.037076'	.023736'	.030348'	.019112'
30.	45.	.026776'	.020454'	.024122'	.017328'	.019814'	.013774'
30.	90.	.011714'	.015064'	.010746'	.011932'	.008916'	.009164'
30.	135.	.009688'	.015026'	.007898'	.011094'	.006142'	.008294'
30.	180.	.012120'	.016298'	.007780'	.011306'	.005790'	.008372'
30.	270.	.011714'	.015064'	.007238'	.011516'	.005518'	.008574'
60.	15.	.035504'	.062920'	.031792'	.056026'	.025976'	.045648'
60.	30.	.017558'	.032936'	.015740'	.028992'	.012870'	.023490'
60.	45.	.011832'	.023458'	.010528'	.020372'	.008574'	.016378'
60.	90.	.009158'	.015192'	.007000'	.012884'	.005304'	.010066'
60.	135.	.011706'	.013472'	.007648'	.011258'	.005502'	.008618'
60.	180.	.013110'	.012870'	.008664'	.010670'	.006124'	.008090'
60.	270.	.009158'	.015192'	.008234'	.010954'	.006202'	.008208'
90.	15.	.005904'	.055540'	.004548'	.049472'	.003380'	.040270'
90.	30.	.006270'	.029940'	.004762'	.026374'	.003514'	.021300'
90.	45.	.006014'	.022168'	.005080'	.019228'	.003716'	.015376'
90.	90.	.008652'	.015812'	.006300'	.012926'	.004512'	.010088'
90.	135.	.009638'	.014442'	.007590'	.011210'	.005372'	.008606'
90.	180.	.010000'	.014142'	.008652'	.010802'	.006198'	.008058'
90.	270.	.008652'	.015812'	.008398'	.010716'	.006842'	.007758'

Sigma x = .010'  
Sigma y = .040'

ALPHA	BETA	N=3		N=5		N=9	
.	15.'	.214956'	.023208'	.192740'	.017962'	.157484'	.013378'
.	30.'	.105794'	.023906'	.095920'	.018468'	.078630'	.013704'
.	45.'	.068650'	.024818'	.062974'	.019166'	.051886'	.014204'
.	90.'	.029154'	.026424'	.027130'	.019730'	.022774'	.014742'
.	135.'	.013684'	.027648'	.013140'	.020518'	.011680'	.014934'
.	180.'	.007072'	.040000'	.008286'	.026424'	.007228'	.017048'
.	270.'	.029154'	.026424'	.012684'	.020996'	.007812'	.016240'
30.'	15.'	.163388'	.098504'	.146346'	.087300'	.119536'	.070922'
30.'	30.'	.081546'	.056072'	.072984'	.048150'	.059642'	.038494'
30.'	45.'	.053938'	.045944'	.047818'	.037284'	.039198'	.029138'
30.'	90.'	.016728'	.030928'	.016156'	.024690'	.014208'	.019206'
30.'	135.'	.012654'	.028974'	.011106'	.021976'	.008504'	.016612'
30.'	180.'	.022008'	.031274'	.011644'	.020232'	.008622'	.015998'
30.'	270.'	.016728'	.030928'	.009360'	.022268'	.007826'	.016388'
60.'	15.'	.056902'	.104234'	.051216'	.092524'	.041984'	.075320'
60.'	30.'	.025754'	.055164'	.023654'	.048128'	.019610'	.038890'
60.'	45.'	.014962'	.039526'	.014130'	.033980'	.011866'	.027216'
60.'	90.'	.012860'	.026624'	.008956'	.022958'	.006556'	.017588'
60.'	135.'	.019900'	.026498'	.011104'	.022060'	.007872'	.016682'
60.'	180.'	.022570'	.024044'	.013108'	.020244'	.008964'	.015730'
60.'	270.'	.012860'	.026624'	.012790'	.021712'	.009000'	.016288'
90.'	15.'	.006274'	.060702'	.004766'	.053418'	.003516'	.043084'
90.'	30.'	.007532'	.038684'	.005516'	.033102'	.003994'	.026162'
90.'	45.'	.009098'	.033036'	.006482'	.027566'	.004626'	.021464'
90.'	90.'	.012040'	.029154'	.009092'	.022444'	.006452'	.017188'
90.'	135.'	.010180'	.028436'	.011056'	.021056'	.007810'	.015796'
90.'	180.'	.010000'	.028284'	.012040'	.024208'	.009014'	.016320'
90.'	270.'	.012040'	.029154'	.011868'	.020950'	.010618'	.015466'

Sigma x = .020'

Sigma y = .005'

ALPHA	BETA	N=3		N=5		N=9	
.	15.	.030351'	.003137'	.026709'	.002383'	.021542'	.001758'
.	30.	.019342'	.003766'	.016551'	.002758'	.013081'	.001997'
.	45.	.016518'	.004549'	.013783'	.003241'	.010732'	.002313'
.	90.	.014577'	.006020'	.011222'	.004546'	.008594'	.003226'
.	135.	.014218'	.005090'	.010528'	.005528'	.007898'	.003905'
.	180.	.014142'	.005000'	.012104'	.006020'	.008160'	.004507'
.	270.	.014577'	.006020'	.010475'	.005934'	.007733'	.005309'
30.	15.	.052117'	.028451'	.046262'	.025608'	.037660'	.020992'
30.	30.	.027582'	.012877'	.024064'	.011827'	.019445'	.009805'
30.	45.	.019763'	.007481'	.016990'	.007065'	.013608'	.005933'
30.	90.	.013312'	.006430'	.011479'	.004478'	.008794'	.003278'
30.	135.	.013249'	.009950'	.011030'	.005552'	.008341'	.003936'
30.	180.	.012022'	.011285'	.010122'	.006554'	.007865'	.004482'
30.	270.	.013312'	.006430'	.010856'	.006395'	.008144'	.004500'
60.	15.	.049252'	.081694'	.043650'	.073173'	.035461'	.059768'
60.	30.	.028036'	.040773'	.024075'	.036492'	.019247'	.029821'
60.	45.	.022972'	.026969'	.018642'	.023909'	.014569'	.019599'
60.	90.	.015464'	.008364'	.012345'	.008078'	.009603'	.007104'
60.	135.	.014487'	.006327'	.010988'	.005553'	.008306'	.004252'
60.	180.	.015637'	.011004'	.010116'	.005822'	.007999'	.004311'
60.	270.	.015464'	.008364'	.011134'	.004680'	.008194'	.003913'
90.	15.	.011604'	.107478'	.000501'	.006370'	.006689'	.078742'
90.	30.	.011953'	.052897'	.009234'	.047960'	.006852'	.039315'
90.	45.	.012409'	.034325'	.009583'	.031487'	.007102'	.025943'
90.	90.	.013212'	.014577'	.009865'	.013565'	.007371'	.011387'
90.	135.	.013824'	.006842'	.010259'	.006570'	.007467'	.005840'
90.	180.	.020000'	.003536'	.013212'	.004143'	.008524'	.003614'
90.	270.	.013212'	.014577'	.010498'	.006342'	.008120'	.003906'

Sigma x = .020'  
Sigma y = .010'

ALPHA	BETA	N=3		N=5		N=9	
.	15.	.055540'	.005904'	.049472'	.004548'	.040270'	.003380'
.	30.	.029940'	.006270'	.026374'	.004762'	.021300'	.003514'
.	45.	.022168'	.006814'	.019228'	.005080'	.015376'	.003716'
.	90.	.015812'	.008652'	.012926'	.006300'	.010088'	.004512'
.	135.	.014442'	.009638'	.011210'	.007590'	.008606'	.005372'
.	180.	.014142'	.010000'	.010802'	.008652'	.008058'	.006198'
.	270.	.015812'	.008652'	.010716'	.008398'	.007758'	.006842'
30.	15.	.062920'	.035504'	.056026'	.031792'	.045648'	.025976'
30.	30.	.032936'	.017558'	.028992'	.015740'	.023490'	.012870'
30.	45.	.023458'	.011832'	.020372'	.010528'	.016378'	.008574'
30.	90.	.015192'	.009158'	.012884'	.007000'	.010066'	.005304'
30.	135.	.013472'	.011706'	.011258'	.007648'	.008618'	.005502'
30.	180.	.012870'	.013110'	.010670'	.008664'	.008090'	.006124'
30.	270.	.015192'	.009158'	.010954'	.008234'	.008208'	.006202'
60.	15.	.050206'	.083918'	.044558'	.075130'	.036242'	.061378'
60.	30.	.027292'	.041308'	.023736'	.037076'	.019112'	.030348'
60.	45.	.020454'	.026776'	.017328'	.024122'	.013774'	.019814'
60.	90.	.015064'	.011714'	.011932'	.010746'	.009164'	.008916'
60.	135.	.015026'	.009688'	.011094'	.007898'	.008294'	.006142'
60.	180.	.016298'	.012120'	.011306'	.007780'	.008372'	.005790'
60.	270.	.015064'	.011714'	.011516'	.007238'	.008574'	.005518'
90.	15.	.011566'	.107652'	.008954'	.096344'	.006674'	.078696'
90.	30.	.011636'	.053250'	.008998'	.047762'	.006698'	.039062'
90.	45.	.011782'	.034866'	.009082'	.031396'	.006752'	.025734'
90.	90.	.012658'	.015812'	.009528'	.014434'	.007030'	.011964'
90.	135.	.014964'	.009182'	.010648'	.008504'	.007626'	.007148'
90.	180.	.020000'	.007072'	.012658'	.006572'	.008756'	.005292'
90.	270.	.012658'	.015812'	.011000'	.007972'	.008640'	.005384'



Sigma x = .020'

Sigma y = .020'

ALPHA	BETA	N=3		N=5		N=9	
.	15.'	.108348'	.011612'	.096868'	.008984'	.079068'	.006692'
.	30.'	.054640'	.011812'	.048788'	.009100'	.039784'	.006764'
.	45.'	.036956'	.012156'	.032924'	.009292'	.026804'	.006884'
.	90.'	.020000'	.014144'	.017588'	.010388'	.014192'	.007552'
.	135.'	.015308'	.017588'	.013120'	.012228'	.010416'	.008676'
.	180.'	.014144'	.020000'	.011548'	.014144'	.008944'	.010000'
.	270.'	.020000'	.014144'	.012156'	.013208'	.008732'	.010324'
30.'	15.'	.094012'	.055100'	.084008'	.049052'	.068556'	.039956'
30.'	30.'	.047688'	.029172'	.042496'	.025636'	.034620'	.020736'
30.'	45.'	.032576'	.021264'	.028888'	.018324'	.023468'	.014668'
30.'	90.'	.018708'	.015812'	.016092'	.012580'	.012856'	.009648'
30.'	135.'	.015908'	.017048'	.012900'	.012456'	.010008'	.009144'
30.'	180.'	.015812'	.018708'	.012248'	.013540'	.009220'	.009748'
30.'	270.'	.018708'	.015812'	.012428'	.012952'	.009156'	.009952'
60.'	15.'	.055100'	.094012'	.049052'	.084008'	.039956'	.068556'
60.'	30.'	.029172'	.047688'	.025636'	.042496'	.020736'	.034620'
60.'	45.'	.021264'	.032576'	.018324'	.028888'	.014668'	.023468'
60.'	90.'	.015812'	.018708'	.012580'	.016092'	.009648'	.012856'
60.'	135.'	.017048'	.015908'	.012456'	.012900'	.009144'	.010008'
60.'	180.'	.018708'	.015812'	.013540'	.012248'	.009748'	.009220'
60.'	270.'	.015812'	.018708'	.012952'	.012428'	.009952'	.009156'
90.'	15.'	.011612'	.108348'	.008984'	.096868'	.006692'	.079068'
90.'	30.'	.011812'	.054640'	.009100'	.048788'	.006764'	.039784'
90.'	45.'	.012156'	.036956'	.009292'	.032924'	.006884'	.026804'
90.'	90.'	.014144'	.020000'	.010388'	.017588'	.007552'	.014192'
90.'	135.'	.017588'	.015308'	.012228'	.013120'	.008676'	.010416'
90.'	180.'	.020000'	.014144'	.014144'	.011548'	.010000'	.008944'
90.'	270.'	.014144'	.020000'	.013208'	.012156'	.010324'	.008732'

Sigma x = .020'  
Sigma y = .040'

ALPHA	BETA	N=3	z	N=5		N=9	
.	15.'	.215304'	.023132'	.192688'	.017908'	.157392'	.013348'
.	30.'	.106500'	.023272'	.095524'	.017996'	.078124'	.013396'
.	45.'	.069732'	.023564'	.062792'	.018164'	.051468'	.013504'
.	90.'	.031624'	.025316'	.028868'	.019056'	.023928'	.014068'
.	135.'	.018364'	.029928'	.017008'	.021296'	.014296'	.015252'
.	180.'	.014144'	.040000'	.013144'	.025316'	.010584'	.017512'
.	270.'	.031624'	.025316'	.015944'	.022000'	.010768'	.017200'
30.'	15.'	.167836'	.100412'	.150260'	.089116'	.122756'	.072484'
30.'	30.'	.082616'	.054584'	.074152'	.047472'	.060696'	.038224'
30.'	45.'	.053552'	.040908'	.048244'	.034656'	.039628'	.027548'
30.'	90.'	.023428'	.030128'	.021492'	.023864'	.017832'	.018328'
30.'	135.'	.019376'	.030052'	.015796'	.022188'	.012284'	.016588'
30.'	180.'	.024240'	.032596'	.015560'	.022612'	.011580'	.016744'
30.'	270.'	.023428'	.030128'	.014476'	.023032'	.011036'	.017148'
60.'	15.'	.071008'	.125840'	.063584'	.112052'	.051952'	.091296'
60.'	30.'	.035116'	.065872'	.031480'	.057984'	.025740'	.046980'
60.'	45.'	.023664'	.046916'	.021056'	.040744'	.017148'	.032756'
60.'	90.'	.018316'	.030384'	.014000'	.025768'	.010608'	.020132'
60.'	135.'	.023412'	.026944'	.015296'	.022516'	.011004'	.017236'
60.'	180.'	.026220'	.025740'	.017328'	.021340'	.012248'	.016180'
60.'	270.'	.018316'	.030384'	.016468'	.021908'	.012404'	.016416'
90.'	15.'	.011808'	.111080'	.009096'	.098944'	.006760'	.080540'
90.'	30.'	.012540'	.059880'	.009524'	.052748'	.007028'	.042600'
90.'	45.'	.013628'	.044336'	.010160'	.038456'	.007432'	.030752'
90.'	90.'	.017304'	.031624'	.012600'	.025852'	.009024'	.020176'
90.'	135.'	.019276'	.028884'	.015180'	.022420'	.010744'	.017212'
90.'	180.'	.020000'	.028284'	.017304'	.021604'	.012396'	.016116'
90.'	270.'	.017304'	.031624'	.016796'	.021432'	.013684'	.015516'

Sigma x = .040'

Sigma y = .005'

ALPHA	BETA	N=3		N=5		N=9	
.	15.	.039002'	.003789'	.033457'	.002776'	.026433'	.002008'
.	30.	.031211'	.005618'	.025961'	.003920'	.020043'	.002756'
.	45.	.029544'	.007544'	.024078'	.005164'	.018416'	.003593'
.	90.	.028504'	.010157'	.021437'	.007929'	.016309'	.005590'
.	135.	.028322'	.005671'	.020755'	.009673'	.015383'	.006823'
.	180.	.028284'	.005000'	.026902'	.010157'	.016963'	.007678'
.	270.	.028504'	.010157'	.021020'	.010064'	.015808'	.009615'
30.	15.	.098037'	.052760'	.086911'	.047597'	.070727'	.039075'
30.	30.	.052011'	.022750'	.045220'	.021191'	.036509'	.017707'
30.	45.	.037183'	.011693'	.031876'	.011680'	.025512'	.010054'
30.	90.	.025538'	.011068'	.022165'	.007113'	.016785'	.005003'
30.	135.	.027133'	.018944'	.022405'	.009707'	.016861'	.006828'
30.	180.	.023602'	.021560'	.020015'	.011740'	.015828'	.007855'
30.	270.	.025538'	.011068'	.022420'	.011682'	.016655'	.007851'
60.	15.	.098509'	.162932'	.087231'	.145919'	.070798'	.119124'
60.	30.	.059172'	.083911'	.049947'	.074402'	.039579'	.060508'
60.	45.	.055648'	.060282'	.042140'	.051048'	.032074'	.041234'
60.	90.	.032310'	.014515'	.026627'	.014360'	.021213'	.013327'
60.	135.	.028713'	.009981'	.022385'	.009455'	.017060'	.007125'
60.	180.	.030936'	.021415'	.019414'	.010316'	.015984'	.007653'
60.	270.	.032310'	.014515'	.022225'	.007436'	.016395'	.006738'
90.	15.	.024043'	.214870'	.018602'	.194914'	.013792'	.159604'
90.	30.	.025934'	.105617'	.020347'	.097932'	.015109'	.080841'
90.	45.	.026875'	.068376'	.021181'	.063949'	.015826'	.053057'
90.	90.	.027679'	.028504'	.020622'	.026729'	.015566'	.022540'
90.	135.	.027909'	.012238'	.020585'	.011907'	.015119'	.010876'
90.	180.	.040000'	.003536'	.027679'	.006424'	.017206'	.006046'
90.	270.	.027679'	.028504'	.021020'	.011684'	.016047'	.006820'

Sigma x = .040'  
Sigma y = .010'

ALPHA	BETA	N=3		N=5		N=9	
.	15.	.060702'	.006274'	.053418'	.004766'	.043084'	.003526'
.	30.	.038684'	.007532'	.033102'	.005516'	.026162'	.003526'
.	45.	.033036'	.009098'	.027566'	.006482'	.021464'	.004326'
.	90.	.029154'	.012040'	.022444'	.009092'	.017188'	.006452'
.	135.	.028436'	.010180'	.021056'	.011056'	.015796'	.007810'
.	180.	.028284'	.010000'	.024208'	.012040'	.016320'	.009014'
.	270.	.029154'	.012040'	.020950'	.011868'	.015466'	.010618'
30.	15.	.104234'	.056902'	.092524'	.051216'	.075320'	.041984'
30.	30.	.055164'	.025754'	.048128'	.023654'	.038890'	.019610'
30.	45.	.039526'	.014962'	.033980'	.014130'	.027216'	.011866'
30.	90.	.026624'	.012860'	.022958'	.008956'	.017588'	.006556'
30.	135.	.026498'	.019900'	.022060'	.011104'	.016682'	.007872'
30.	180.	.024044'	.022570'	.020244'	.013108'	.015730'	.008964'
30.	270.	.026624'	.012860'	.021712'	.012790'	.016288'	.009000'
60.	15.	.098504'	.163388'	.087300'	.146346'	.070922'	.119536'
60.	30.	.056072'	.081546'	.048150'	.072984'	.038494'	.059642'
60.	45.	.045944'	.053938'	.037284'	.047818'	.029138'	.039198'
60.	90.	.030928'	.016728'	.024690'	.016156'	.019206'	.014208'
60.	135.	.028974'	.012654'	.021976'	.011106'	.016612'	.008504'
60.	180.	.031274'	.022008'	.020232'	.011644'	.015998'	.008622'
60.	270.	.030928'	.016728'	.022268'	.009360'	.016388'	.007826'
90.	15.	.023208'	.214956'	.017962'	.192740'	.013378'	.157484'
90.	30.	.023906'	.105794'	.018468'	.095920'	.013704'	.078630'
90.	45.	.024818'	.068650'	.019166'	.062974'	.014204'	.051886'
90.	90.	.026424'	.029154'	.019730'	.027130'	.014742'	.022774'
90.	135.	.027648'	.013684'	.020518'	.013140'	.014934'	.011680'
90.	180.	.040000'	.007072'	.026424'	.008286'	.017048'	.007228'
90.	270.	.026424'	.029154'	.020996'	.012684'	.016240'	.007812'

ph

Sigma x = .040'  
Sigma y = .020'

ALPHA	BETA	N=3		N=5		N=9	
.	15.	.111080'	.011808'	.098944'	.009096'	.080540'	.006760'
.	30.	.059880'	.012540'	.052748'	.009524'	.042600'	.007020'
.	45.	.044336'	.013628'	.038456'	.010160'	.030752'	.007480'
.	90.	.031624'	.017304'	.025852'	.012600'	.020176'	.009080'
.	135.	.028884'	.019276'	.022420'	.015180'	.017212'	.010740'
.	180.	.028284'	.020000'	.021604'	.017304'	.016116'	.012396'
.	270.	.031624'	.017304'	.021432'	.016796'	.015516'	.013684'
30.	15.	.125840'	.071008'	.112052'	.063584'	.091296'	.051952'
30.	30.	.065872'	.035116'	.057984'	.031480'	.046980'	.025740'
30.	45.	.046916'	.023664'	.040744'	.021056'	.032756'	.017148'
30.	90.	.030384'	.018316'	.025768'	.014000'	.020132'	.010608'
30.	135.	.026944'	.023412'	.022516'	.015296'	.017236'	.011004'
30.	180.	.025740'	.026220'	.021340'	.017328'	.016180'	.012248'
30.	270.	.030384'	.018316'	.021908'	.016468'	.016416'	.012404'
60.	15.	.100412'	.167836'	.089116'	.150260'	.072484'	.122756'
60.	30.	.054584'	.082616'	.047472'	.074152'	.038224'	.060696'
60.	45.	.040908'	.053552'	.034656'	.048244'	.027548'	.039628'
60.	90.	.030128'	.023428'	.023864'	.021492'	.018328'	.017832'
60.	135.	.030052'	.019376'	.022188'	.015796'	.016588'	.012284'
60.	180.	.032596'	.024240'	.022612'	.015560'	.016744'	.011580'
60.	270.	.030128'	.023428'	.023032'	.014476'	.017148'	.011036'
90.	15.	.023132'	.215304'	.017908'	.192688'	.013348'	.157392'
90.	30.	.023272'	.106500'	.017996'	.095524'	.013396'	.078124'
90.	45.	.023564'	.069732'	.018164'	.062792'	.013504'	.051468'
90.	90.	.025316'	.031624'	.019056'	.028868'	.014060'	.023928'
90.	135.	.029928'	.018364'	.021296'	.017008'	.015252'	.014296'
90.	180.	.040000'	.014144'	.025316'	.013144'	.017512'	.010584'
90.	270.	.025316'	.031624'	.022000'	.015944'	.017280'	.010768'

sigma x = .040'  
Sigma y = .040'

ALPHA	BETA	N=3		N=5		N=9	
.	15.'	.216696'	.023224'	.193736'	.017968'	.158136'	.013384'
.	30.'	.109280'	.023624'	.097576'	.018200'	.079568'	.013528'
.	45.'	.073912'	.024312'	.065848'	.018584'	.053608'	.013768'
.	90.'	.040000'	.028288'	.035176'	.020776'	.028384'	.015104'
.	135.'	.030616'	.035176'	.026240'	.024456'	.020832'	.017352'
.	180.'	.028288'	.040000'	.023096'	.028288'	.017888'	.020000'
.	270.'	.040000'	.028288'	.024312'	.026416'	.017464'	.020648'
30.'	15.'	.188024'	.110200'	.168016'	.098104'	.137112'	.079912'
30.'	30.'	.095376'	.058344'	.084992'	.051272'	.069240'	.041472'
30.'	45.'	.065152'	.042528'	.057776'	.036648'	.046936'	.029336'
30.'	90.'	.037416'	.031624'	.032184'	.025160'	.025712'	.019296'
30.'	135.'	.031816'	.034096'	.025800'	.024912'	.020016'	.018288'
30.'	180.'	.031624'	.037416'	.024496'	.027080'	.018440'	.019496'
30.'	270.'	.037416'	.031624'	.024856'	.025904'	.018312'	.019904'
60.'	15.'	.110200'	.188024'	.098104'	.168016'	.079912'	.137112'
60.'	30.'	.058344'	.095376'	.051272'	.084992'	.041472'	.069240'
60.'	45.'	.042528'	.065152'	.036648'	.057776'	.029336'	.046936'
60.'	90.'	.031624'	.037416'	.025160'	.032184'	.019296'	.025712'
60.'	135.'	.034096'	.031816'	.024912'	.025800'	.018288'	.020016'
60.'	180.'	.037416'	.031624'	.027080'	.024496'	.019496'	.018440'
60.'	270.'	.031624'	.037416'	.025904'	.024856'	.019904'	.018312'
90.'	15.'	.023224'	.216696'	.017968'	.193736'	.013384'	.158128'
90.'	30.'	.023624'	.109280'	.018200'	.097576'	.013528'	.079568'
90.'	45.'	.024312'	.073912'	.018584'	.065848'	.013768'	.053608'
90.'	90.'	.028288'	.040000'	.020776'	.035176'	.015104'	.028384'
90.'	135.'	.035176'	.030616'	.024456'	.026240'	.017352'	.020832'
90.'	180.'	.040000'	.028288'	.028288'	.023096'	.020000'	.017888'
90.'	270.'	.028288'	.040000'	.026416'	.024312'	.020648'	.017464'

hs

## APPENDIX C

### ATS-A CAPTURE STUDIES

#### DISCUSSION

The capture of ATS-A has been discussed both in the first and second quarterly progress reports. Since the issuance of these documents, the moments of inertia of the satellite body (with undeployed rods) have been revised upwards. The latest available numbers (reference - R. Wirth) are  $73.4 \text{ slug ft}^2$  along the x and y axis, and 74.1 along the z axis (the axis of symmetry of the cylindrical spacecraft body). The moment of inertia of the deployed configuration about the roll axis is approximately  $3600 \text{ slug ft}^2$  resulting in a moment of inertia growth ratio of 49:1. Since the spacecraft is yawed ninety degrees with respect to the orbital reference frame when positioned on the booster, the pitch bias rate is about the spacecraft roll axis, and the bias rate must be  $(49) (.0158) \cong .8 \text{ deg/sec}$ . From a preliminary computer run, which includes gravity gradient torques, the initial spacecraft bias (prior to rod deployment) necessary to place the vehicle at the zero attitude error position at the completion of rod deployment is  $-7.4$  degrees.

It has been stated that a time delay between separation from the booster and deployment of the rods is desirable. With the existing tolerances ( $\pm 1 \text{ deg/sec}$  pitch and yaw;  $\pm 1/4 \text{ deg/sec}$  roll - booster referenced coordinates) on spacecraft separation rates, the originally requested 20 second delay requirement cannot be met (reference - GE's Second Quarterly Report). Preliminary work on a 12 second delay indicated that a delay time of this magnitude was feasible and subsequent studies were concentrated on that condition. To be compatible with the electronic package, the actual time of deployment is 11.36 seconds for the secondary boom, and 11.88 seconds for the primary booms. The secondary boom is self-erecting, but the power required to "trigger" is available only before or after the deployment of the main booms. Deploying first was felt to improve the capture capability slightly.

Figure 1 indicates the performance during capture with the nominal bias rate, bias position, rod extension rate, and a "12 second delay" with a +1 deg/sec pitch down rate (uncertainty). Since the 12 second (11.88) delay was programmed in, the booster was biased an additional  $(-11.88 \text{ sec}) (.8 \text{ deg/sec}) = -9.6$  degrees resulting in a final bias angle of  $(-9.6 - 7.4) = -17$  degrees. At 2 ft/sec, the rod deployment phase (for 100-foot rods) is completed in 50 seconds. This is short compared to the printout interval of the computer program, and the vehicle appears to "jump" at the initiation of the run. All runs were extended to 48 hours.

Figure 1 shows large amplitude oscillations approaching to within 16 degrees of the 90-degree position. This marginal capture capability poses serious difficulties, particularly with regard to acceptable tolerances on such things as booster rates, rod extension rates, etc.

Figure 2 shows the system performance with a rate uncertainty of -1 deg/sec. The performance is comparable to that of Figure 1, but of slightly less amplitude. This is due to the reduced absolute inertial rate of the satellite following rod deployment.

To determine variations about the nominal, several additional runs were made. Figure 3 is the nominal rod extension rate and a pitch rate of uncertainty of +1 deg/sec. However, the bias rate imparted by the booster was assumed to be .6 deg/sec rather than the prescribed .8 deg/sec. This run captured easily. If the rate uncertainty had been negative, however, the vehicle would have tumbled (Figure 4). While this vehicle righted itself again following inversion, upright capture cannot be assured once inversion has occurred. (The scale of the graph is such that during the period of inversion, the performance cannot be plotted.)

If the bias rate had been 1.0 deg/sec instead of .8 deg/sec, a forward rate uncertainty of 1 deg/sec would have caused the vehicle to tumble (Figure 5). Had the uncertainty been negative, however, the vehicle would have captured (Figure 6). It should be noted in Figures 3 through 6, that the performance is not symmetrical as it is in Figures 1 and 2. This results because of the change in the bias rate, which was originally selected to provide symmetry.



If the bias rate is held to 0.8 deg/sec, and the vehicle does not capture because of a variation in a parameter other than bias rate, the "non-capture" will be more nearly symmetrical.

The marginal nature of the capture with a growth ratio of 49:1 led to evaluating a system with a higher growth ratio. Figure 7 is a capture run using a system with 150-foot rods. The moment of inertia of this configuration is more than 2.25 times that of the configuration with 100-foot rods. The improvement in performance is obvious even with the nominal separation conditions optimized for the 100-foot rod configuration (Figure 7 assumes a +1 deg/sec separation rate uncertainty).

### CONCLUSIONS

Several problems have manifested themselves during the course of the study. The particular problem is, of course, the marginal upright capture capability of ATS-A with 100-foot rods. As a part of the solution, the Agena booster must be biased both in position and rate at the time of separation. Thus, not only is the reliability of capture decreased, but the problem is complicated by the tolerance on the Agena maneuver. Further aggravating the situation is the request for a time delay between separation and rod deployment to decrease the probability of collision between the gravity gradient rods and the booster. This makes the system more sensitive to variations in initial rate, since the rate is integrated over the delay time.

With these limitations and restrictions, upright capture cannot be assured and several courses of action are recommended. These are:

1. Consider an ATS-A system with initial rod deployment to 150 feet.
2. Determine the need for a time delay and consider alternatives which do not require a time delay.
3. Investigate the tolerances on the booster to determine if the bias conditions can be met satisfactorily.

The first recommendation offers a steady state advantage as well as a capture advantage and should be given serious consideration. The second item is necessary to clarify the need for the delay time or at least to clarify the nature and magnitude of the problem. The third recommendation is self-explanatory.



Figure 1

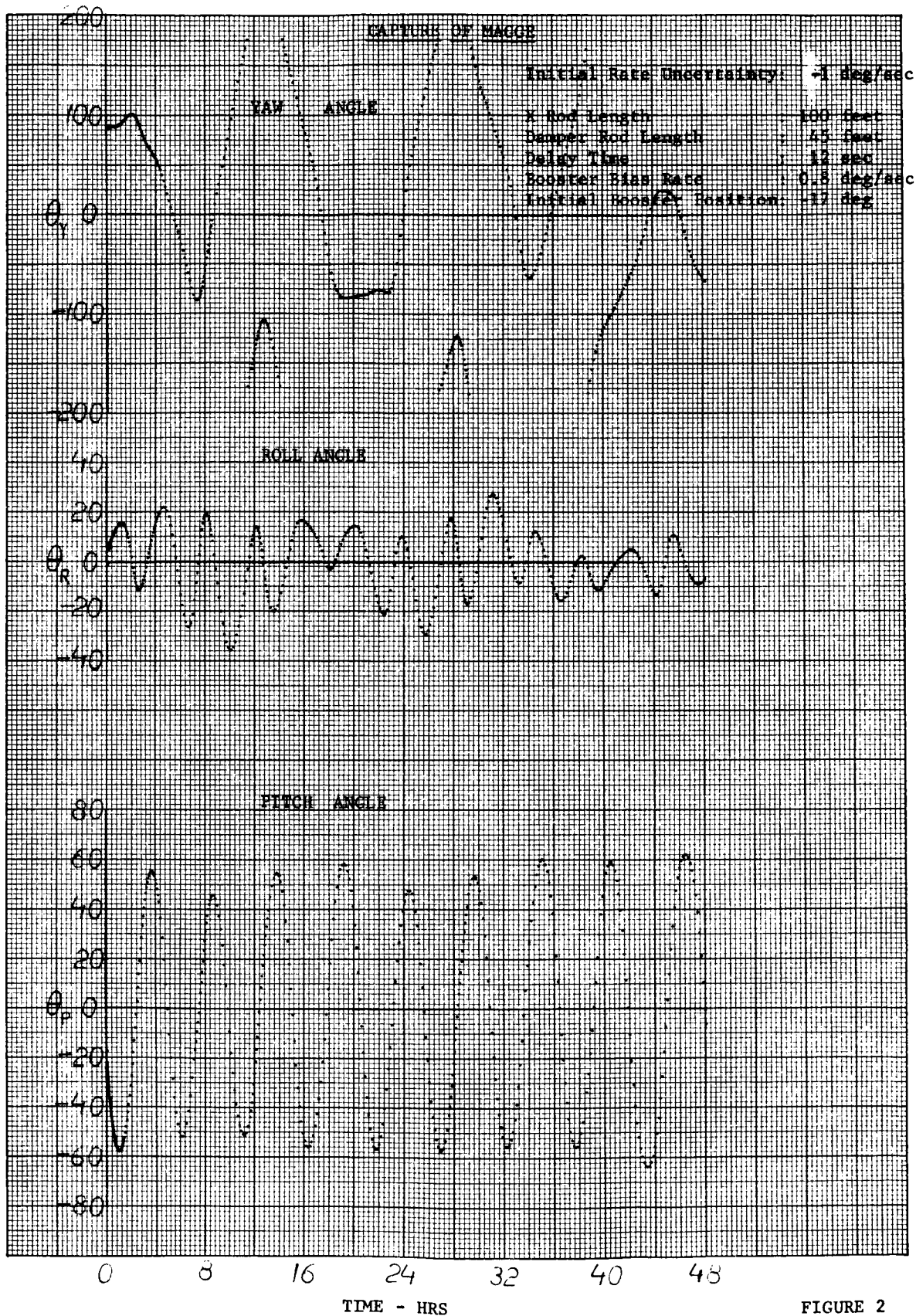


FIGURE 2

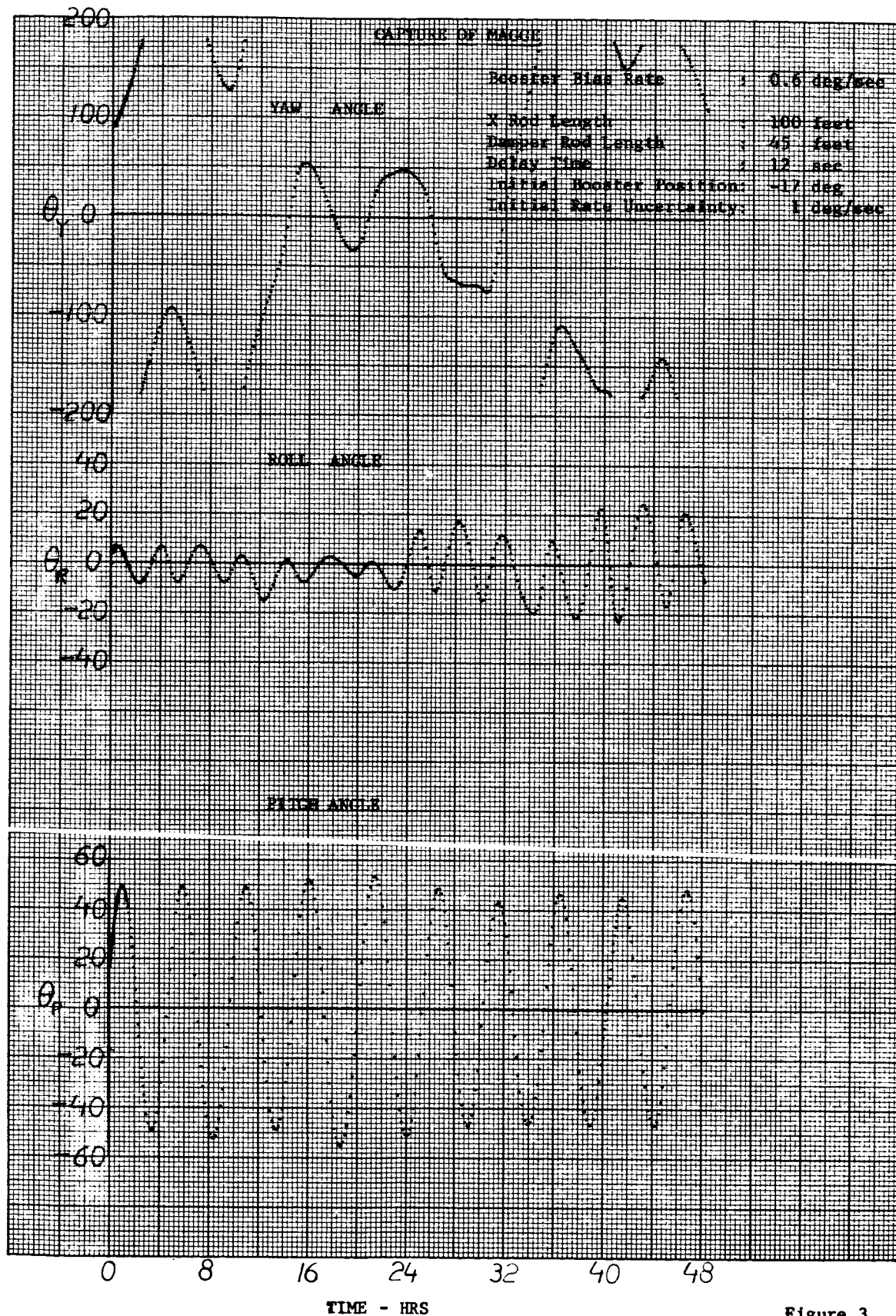


Figure 3



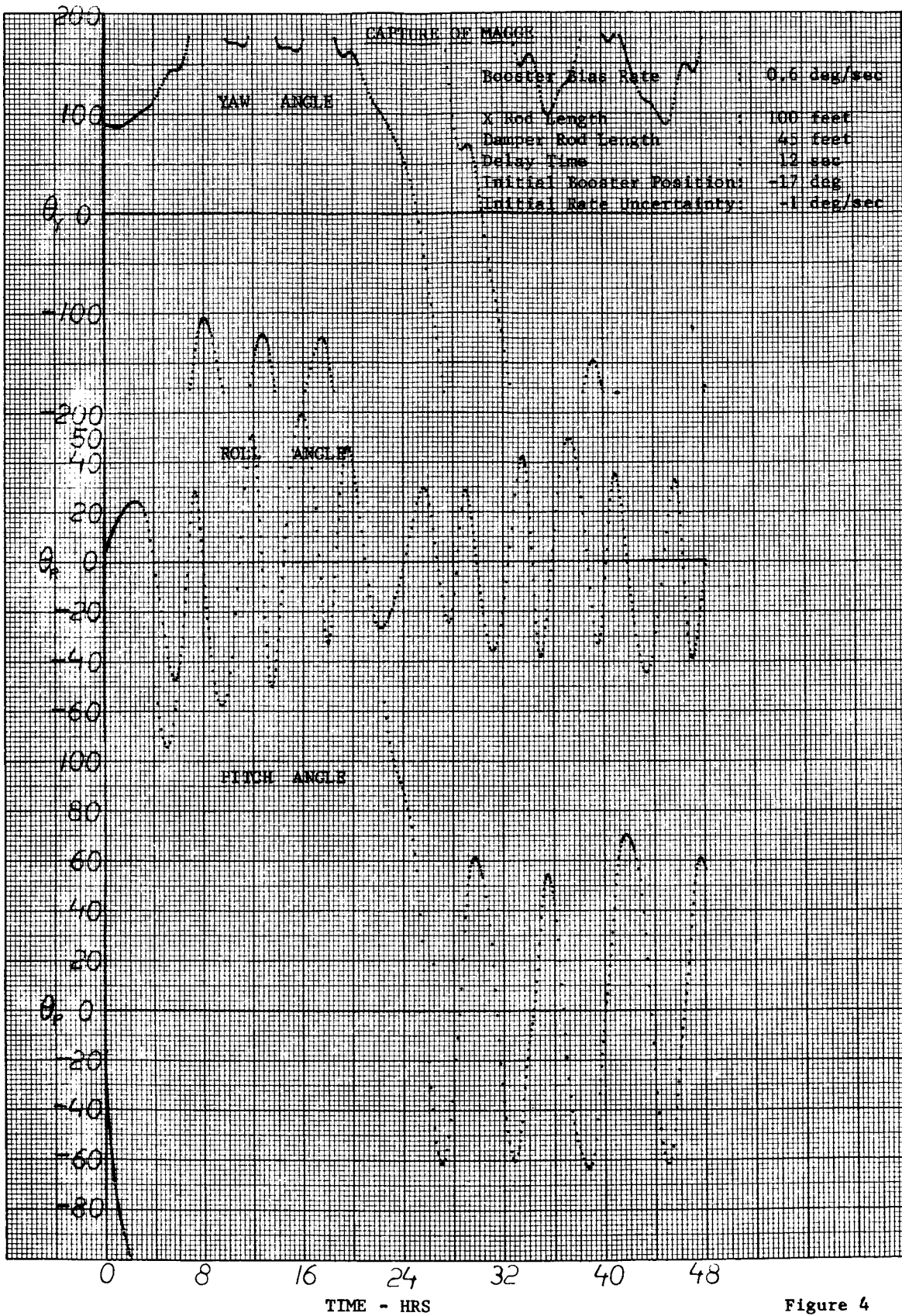


Figure 4

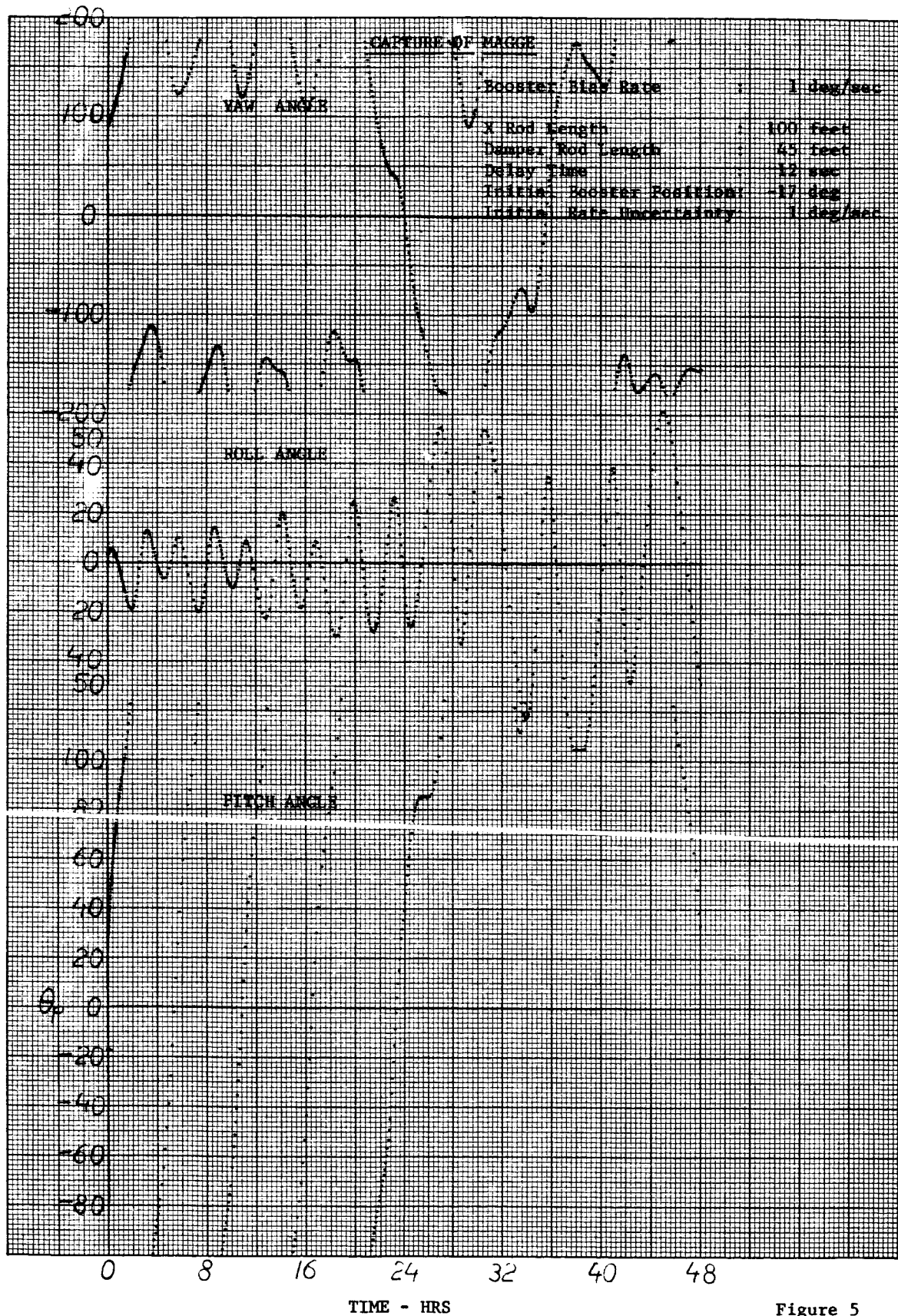


Figure 5

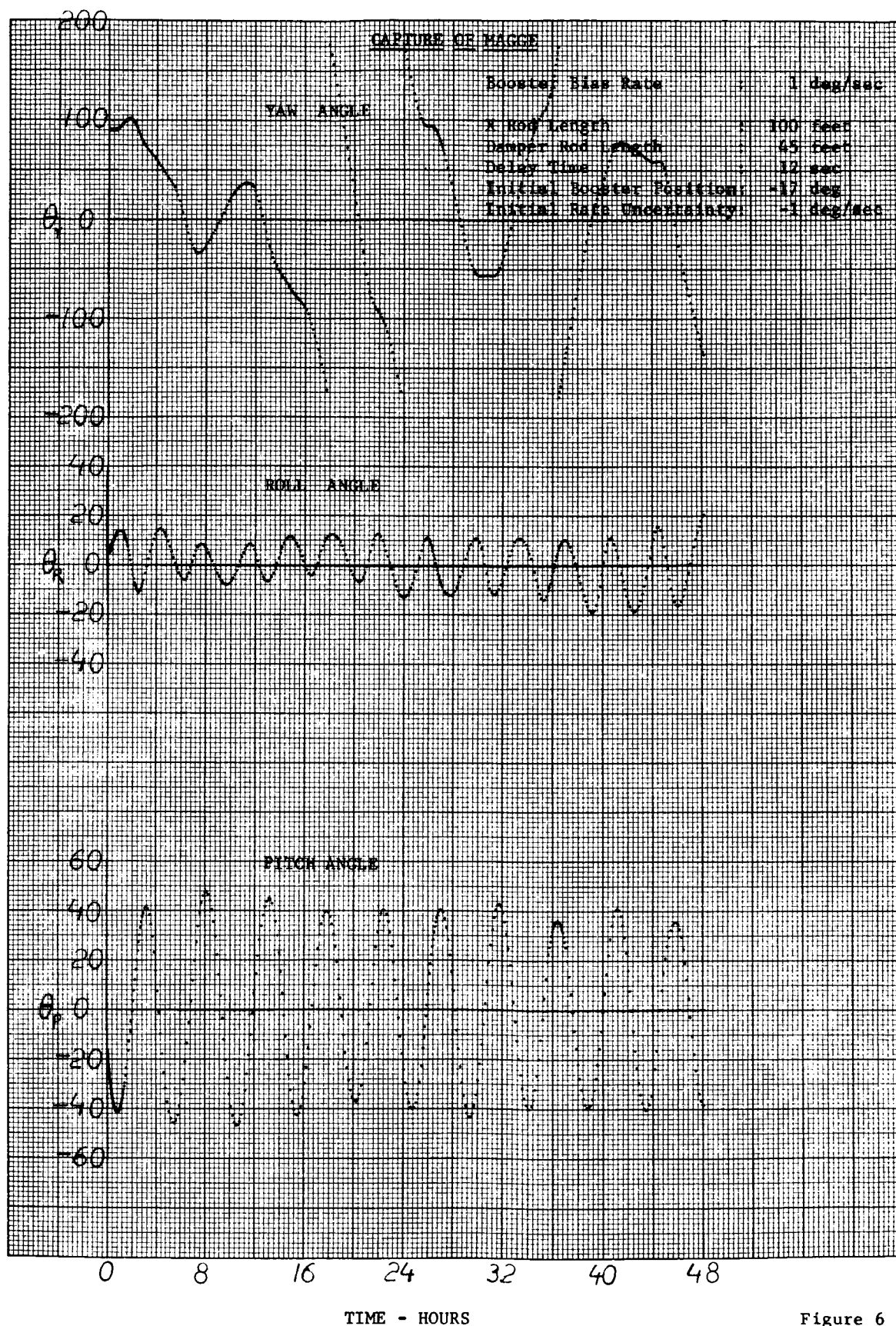


Figure 6



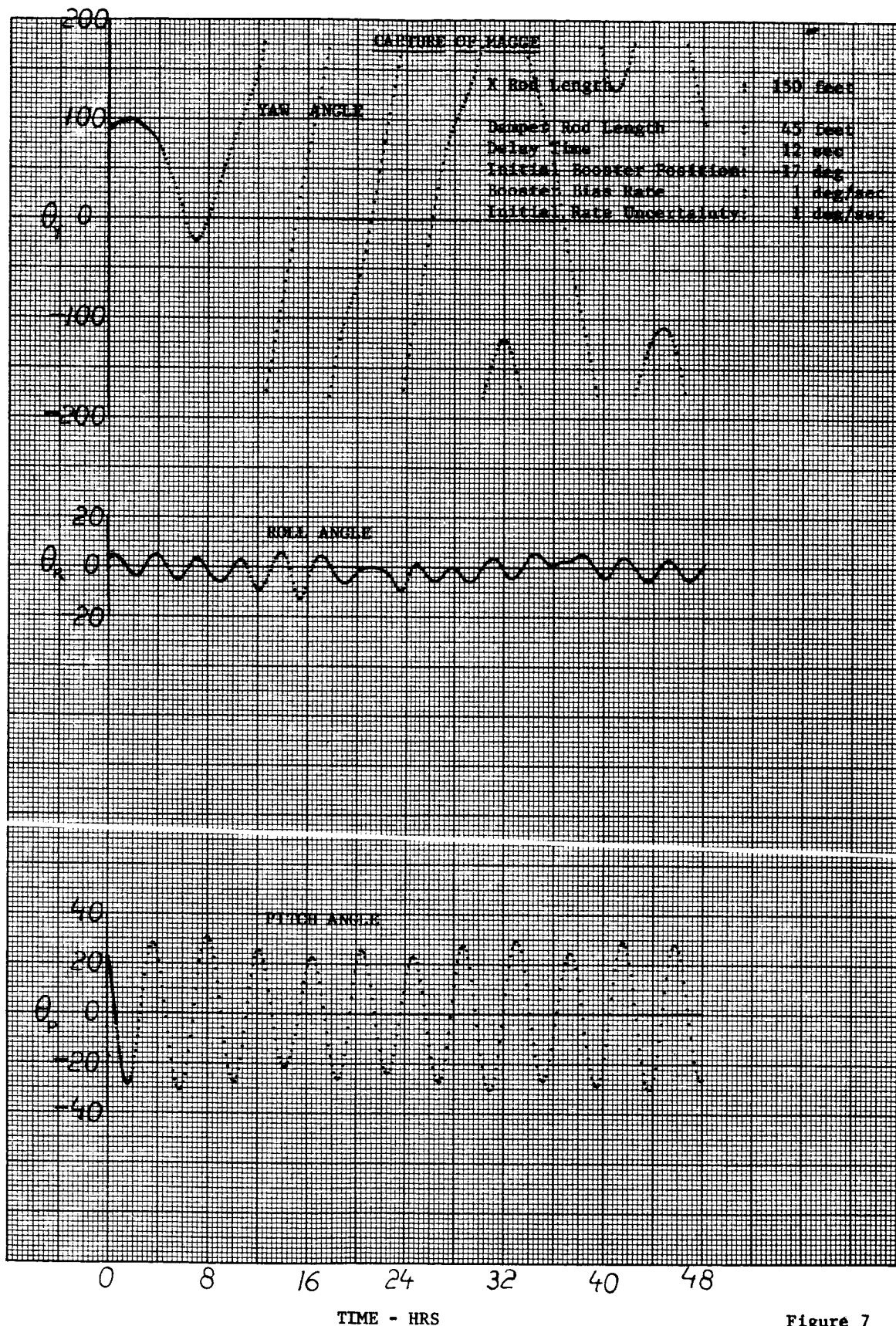


Figure 7

# APPENDIX D RESPONSE TO INTERNAL DISTURBANCE TORQUES

The response to finite impulse bits will be calculated by assuming that each axis of the satellite behaves separately and that its behavior can be represented by:

$$(1) \quad I\ddot{\theta} + \beta\dot{\theta} + k\theta = T$$

where:  $I$  = moment of inertia about the appropriate axis - slug-ft<sup>2</sup>

$\theta$  = position angle - radians

$k$  = restoring torque - ft lbs per rad.

$T$  = disturbing torque - ft lbs

$\beta$  = damping constant

To permit easier comparison with other facets of this program the time base will be based on orbits: I.E.  $\tau = \omega_0 t$

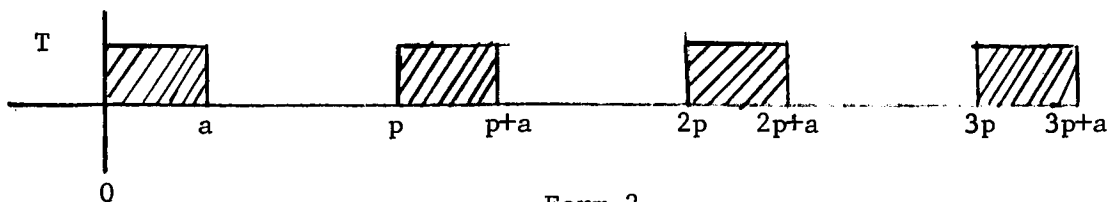
From this  $\frac{d}{dt} = \omega_0 \frac{d}{d\tau} \quad \frac{d^2}{dt^2} = \omega_0^2 \frac{d^2}{d\tau^2}$

Substituting these equivalents into equation (1) and simplifying yields.

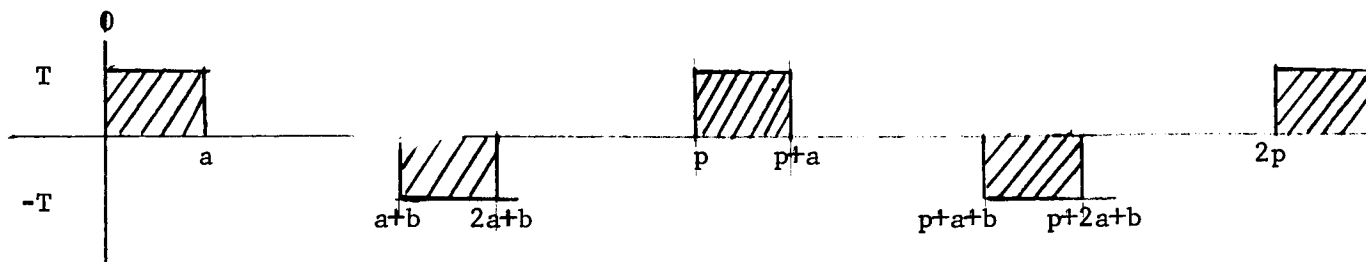
$$(2) \quad \ddot{\theta} + \frac{\beta\dot{\theta}}{I\omega_0} + \frac{k\theta}{I\omega_0^2} = \frac{T}{I\omega_0^2}$$

The disturbing torque  $T$  will be assumed to be repetitive, of constant period, of constant magnitude and of either of two forms. Form 1 is the type caused by a thruster and Form 2 is the type caused by internal rotating parts.

Form 1



Form 2



$p$  = period

$a$  = pulse duration

$b$  = separation between positive and negative pulses in Form 2.

The torquing function portrayed in Form 1 may be La Place transformed.

$$\begin{aligned}
 (3) \quad L \left\{ f_1(T) \right\} &= \int_0^p \frac{f(T) e^{-s\tau} d\tau}{(1 - e^{-ps})} \\
 &= \int_0^a T e^{-s\tau} d\tau + \int_a^p 0 \cdot e^{-s\tau} d\tau \cdot \frac{1}{1 - e^{-ps}}
 \end{aligned}$$

$$(4) \quad L \left\{ f(T) \right\} = \frac{T}{s} \cdot \left( \frac{1 - e^{-as}}{1 - e^{-ps}} \right)$$

dividing by  $I\omega_o^2$  so that (2) and (4) can be equated. Thence:

$$(5) \quad L \left\{ \ddot{\theta} + \frac{\beta \dot{\theta}}{I\omega_o} + \frac{k\theta}{I\omega_o^2} \right\} = \frac{T}{I\omega_o^2} \cdot \frac{1}{s} \left( \frac{1 - e^{-as}}{1 - e^{-ps}} \right)$$

If the assumptions that  $\theta(0^+) = 0 = \dot{\theta}(0^+)$  are made, (5) reduces to:

$$(6) \quad F_1(\theta) = \frac{T}{I\omega_o^2} \cdot \frac{1}{s} \left( \frac{1 - e^{-as}}{1 - e^{-ps}} \right) \left( \frac{1}{(s+r)^2 + q^2} \right)$$

where  $r = \frac{\beta}{2I\omega_o}$

$$q = \frac{\sqrt{4kI - \beta^2}}{2I\omega_o}$$

for Form 1.

The torquing function portrayed in Form 2 may also be La Place transformed.

$$(7) \quad L \{ f_2(T) \} = L \left\{ \int_0^a T e^{-sT} dT + \int_a^{a+b} 0 e^{-sT} dT + \int_{a+b}^{(2a+b)} (-T) e^{-sT} dT + \int_{2a+b}^p 0 e^{-sT} dT \right\} \left( \frac{1}{1 - e^{-ps}} \right)$$

$$= L \left\{ \int_0^a T e^{-sT} dT + \int_{b+a}^{2a+b} (-T) e^{-sT} dT \right\} \left( \frac{1}{1 - e^{-ps}} \right)$$

The first expression on the right is identically that for Form 1 and the integration of the second expression involves only different limits and a reversed sign. Therefore, the total expression for  $F_2(\theta)$  becomes

$$(8) \quad L \{ f_2(\theta) \} = \frac{T}{I\omega_o^2} \cdot \frac{1}{s} \left( \frac{1 - e^{-as}}{1 - e^{-ps}} \right) \left( \frac{1}{(s+r)^2 + q^2} \right)$$

$$\frac{-T}{I\omega_o^2} \cdot \frac{1}{s} \cdot \frac{1 - e^{-as}}{1 - e^{-ps}} \left( \frac{e^{-(a+b)s}}{(s+r)^2 + q^2} \right)$$

Which may be rearranged and compacted.

$$(9) \quad L \{ f_2(\theta) \} = \frac{T}{I\omega_o^2} \left( \frac{1 - e^{-as}}{1 - e^{-ps}} \right) \left( \frac{1 - e^{-(a+b)s}}{s((s+r)^2 + q^2)} \right)$$

## Inverse La Place Transforming

If (9) is rewritten with an expanded numerator:

$$(10) \quad L \left\{ f_2(\theta) \right\} = \frac{T}{I \omega_o^2} \left( \frac{1 - e^{-as} - e^{-(a+b)s} + e^{-(2a+b)s}}{(1 - e^{-ps}) \cdot s \cdot ((s+r)^2 + q^2)} \right)$$

and defining

$$(10A) \quad f(\theta) = L^{-1} \left( F(\theta) \right) = L^{-1} \left( \frac{1}{(1 - e^{-ps}) (s \cdot ((s+r)^2 + q^2))} \right)$$

and using the operational notation

$$L^{-1} (e^{-\alpha s} F(s)) = f(\tau - \alpha) u(\tau - \alpha)$$

it is very clear that:

$$(11) \quad L^{-1} F_2(\theta) = \frac{T}{I \omega_o^2} \left( f(\tau) - f(\tau - a) u(\tau - a) - f(\tau - (a+b)) u(\tau - (a+b)) + f(\tau - (2a+b)) u(\tau - (2a+b)) \right)$$

From expression (11) it is seen that the complete solutions are obtainable from the proper substitutions in  $f(\theta)$  (10A).

Solution of basic term

$$(10A) \quad F(\theta) = \frac{1}{s \cdot ((s+r)^2 + q^2)} \cdot \frac{1}{1 - e^{-ps}}$$

$$(12) \quad F(\theta) = \frac{1}{s \cdot ((s+r)^2 + q^2)} \left[ 1 + e^{-ps} + e^{-2ps} + e^{-3ps} + \dots + e^{-nps} + e^{-(n+1)ps} + \dots \right]$$

$$\text{Thus, if } \phi(s) = \frac{1}{s \cdot ((s+r)^2 + q^2)}$$

$$(13) \quad F(\theta) = \phi(s) + e^{-ps} \phi(s) + e^{-2ps} \phi(s) + e^{-3ps} \phi(s) + \dots$$

# Inverse Transforming

$$(14) \quad f(\theta) = f(\tau) + f(\tau-p) u(\tau-p) + f(\tau-2p) u(\tau-2p) + \text{etc} \dots$$

Therefore,  $f_A(\tau)$  becomes

$$(15) \quad f_A(\theta)_0 = \left[ \frac{1}{r^2 + q^2} - \frac{e^{-r\tau}}{(r^2 + q^2) q} (r \sin q \tau + q \cos q \tau) \right] u(\tau)$$

and

$$f_A(\theta)_1 = \left[ \frac{1}{r^2 + q^2} - \frac{e^{-r(\tau-p)}}{q (r^2 + q^2)} (r \sin q (\tau-p) + q \cos q (\tau-p)) \right] u(\tau-p)$$

or in general:

$$f_A(\theta)_n = \left[ \frac{1}{r^2 + q^2} - \frac{e^{-r(\tau-np)}}{q (r^2 + q^2)} (r \sin q (\tau-np) + q \cos q (\tau-np)) \right] u(\tau-np)$$

Therefore, the sum of the series over n terms becomes:

$$(16) \quad f_A(\theta)_{n \text{ th}} = \sum_{n=0}^{\infty} \left[ \frac{1}{r^2 + q^2} - \frac{e^{-r(\tau-np)}}{q (r^2 + q^2)} (r \sin q (\tau-np) + q \cos q (\tau-np)) \right] u(\tau-np)$$

By defining  $\phi = \tan^{-1} \frac{q}{-r}$  and making the corresponding changes (16) may be expressed as:

$$(17) \quad f_A(\theta)_{n \text{ th}} = \sum_{n=0}^{\infty} \left[ \frac{1}{r^2 + q^2} - \frac{e^{-r(\tau-np)}}{q (r^2 + q^2)^{\frac{1}{2}}} \sin [q (\tau-np) - \phi] \right] u(\tau-np)$$

The next term to be evaluated is:

$$(18) \quad \mathcal{F}_B(\theta) = - \frac{e^{-as}}{s((s+r)^2 + q^2)} \left[ 1 + e^{-ps} + e^{-2ps} + e^{-3ps} \dots \right]$$

$$(19) \quad = (-) \frac{1}{s((s+r)^2 + q^2)} \left[ e^{-as} + e^{-(a+p)s} + e^{-(a+2p)s} + e^{-(a+3p)s} + \dots \right]$$

Expressions (15) and (19) are similar, therefore

$$(20) \quad f_B(\theta)_0 = - \left[ \frac{1}{r^2 + q^2} - \frac{e^{-r(\tau-a)}}{q(r^2 + q^2)} (r \sin q(\tau-a) + q \cos q(\tau-a)) \right] u(\tau-a)$$

and, in general

$$f_B(\theta)_n = - \left[ \frac{1}{r^2 + q^2} - \frac{e^{-r(\tau-np-a)}}{q(r^2 + q^2)} (r \sin q(\tau-np-a) + q \cos q(\tau-np-a)) \right] * u(\tau-np-a)$$

The series sum of n terms is:

$$(21) \quad \mathcal{F}_B(\theta)_{n \text{ th}} = - \sum_{n=0}^{\infty} \left[ \frac{1}{r^2 + q^2} - \frac{e^{-r(\tau-np-a)}}{q(r^2 + q^2)} (r \sin q(\tau-np-a) + q \cos q(\tau-np-a)) \right] u(\tau-np-a)$$

In the form of (17)

$$(22) \quad \mathcal{F}_B(\theta)_{n \text{ th}} = - \sum_{n=0}^{\infty} \left[ \frac{1}{r^2 + q^2} + \frac{e^{-r(\tau-np-a)}}{q \sqrt{r^2 + q^2}} (\sin(q[t-np-a] - \phi)) \right] u(\tau-np-a)$$

By similar steps the third expression is:

$$(23) \quad F_C(\theta) = - \left[ \frac{1}{s((s+r)^2 + q^2)} (e^{-(a+b)s} + e^{-(a+b+p)s} + e^{-(a+b+2p)s} + \dots) \right]$$

Transforming yields:

$$(24) \quad \mathcal{F}_C(\theta)_{n \text{ th}} = - \sum_{n=0}^{\infty} \left[ \frac{1}{r^2 + q^2} - \frac{e^{-r(\tau-(a+b)-np)}}{q(r^2 + q^2)} \left( (r \sin q(\tau-np-(a+b)) + q \cos q(\tau-np-(a+b))) \right) \right] u(\tau-np-(a+b))$$

or, in form of (17)

$$(25) \quad \mathcal{F}_C(\theta)_{n \text{ th}} = - \sum_{n=0}^n \left[ \frac{1}{r^2 + q^2} + \frac{e^{-r(\tau - np - (a+b))}}{q \sqrt{r^2 + q^2}} \cdot \sin(q(\tau - np - (a+b)) - \phi) \right] \cdot u(\tau - np - (a+b))$$

Similarly, the final expression becomes:

$$(26) \quad \mathcal{F}_D(\theta) = + \frac{S((s \pm r))}{S((s+r)^2 + q^2)} \left[ e^{-(2a+b)s} + e^{-(2a+b+p)s} + e^{-(2a+b+2p)s} + \dots \right]$$

The corresponding transform is:

$$(27) \quad \mathcal{F}_D(\theta)_{n \text{ th}} = + \sum_{n=0}^n \left[ \frac{1}{r^2 + q^2} - \frac{e^{-r(\tau - np - (2a+b))}}{q(r^2 + q^2)} \left( r \sin q(\tau - np - (2a+b)) + q \cos q(\tau - np - (2a+b)) \right) \right] u(\tau - np - (2a+b))$$

or

$$(28) \quad \mathcal{F}_D(\theta)_{n \text{ th}} = \sum_{n=0}^n \left[ \frac{1}{r^2 + q^2} + \frac{e^{-r(\tau - np - (2a+b))}}{q \sqrt{r^2 + q^2}} \cdot \sin(q(\tau - np - (a+b)) - \phi) \right] \cdot u(\tau - np - (2a+b))$$

From the initial derivations it is seen that the disturbance function of Form 1 generates a response function defined by expressions (16) and (21) or by (17) and (22).

$$\text{i.e.} \quad \mathcal{F}_1(\theta) = \frac{T}{I\omega_c^2} [\mathcal{F}_A(\tau) + \mathcal{F}_B(\tau - a) u(\tau - a)]$$

or, in detail:

$$(29) \quad \mathcal{F}_1(\theta) = \frac{T}{I\omega_c^2} + \sum_{n=0}^{\infty} \left[ \frac{1}{r^2 + q^2} - \frac{e^{-r(\tau - np)}}{q(r^2 + q^2)} (r \sin q(\tau - np) + q \cos q(\tau - np)) \right] u(\tau - np) \\ - \sum_{n=0}^n \left[ \frac{1}{r^2 + q^2} - \frac{e^{-r(\tau - np - a)}}{q(r^2 + q^2)} (r \sin q(\tau - np - a) + q \cos q(\tau - np - a)) \right] u(\tau - np - a)$$

The corresponding alternate equation is:

$$(30) \quad \mathcal{F}_1(\theta) = \frac{T}{I\omega_c^2} \sum_{n=0}^n \left[ \frac{1}{r^2 + q^2} + \frac{e^{-r(\tau - np)}}{q \sqrt{r^2 + q^2}} \cdot \sin(q(\tau - np) - \phi) \right] u(\tau - np) \\ + \sum_{n=0}^n \left[ \frac{1}{r^2 + q^2} + \frac{e^{-r(\tau - np - a)}}{q \sqrt{r^2 + q^2}} \cdot \sin(q(\tau - np - a) - \phi) \right] u(\tau - np - a)$$



The disturbance function of Form 2 will generate a response which is defined by the expressions (16), (21), (24) and (27) or by expressions (17), (22), (25) and (28).

$$(i.e.) \quad \mathcal{F}_2(\theta) = \frac{T}{I\omega_o^2} \left[ \mathcal{F}_A(\tau) + \mathcal{F}_B(\tau-a) + \mathcal{F}_C(\tau-(a+b)) u(\tau-a-b) \right. \\ \left. + \mathcal{F}_D(\tau-2a-b) u(\tau-2a-b) \right]$$

$$(31) \quad \mathcal{F}_2(\theta) = \frac{T}{I\omega_o^2} \sum_{n=0}^n \left[ \frac{1}{r^2 + q^2} - \frac{e^{-r(\tau-np)}}{q(r^2 + q^2)} (r \sin q(\tau-np) \right. \\ \left. + q \cos q(\tau-np)) \right] u(\tau-np) \quad \text{unit step} \\ - \sum_{n=0}^n \left[ \frac{1}{r^2 + q^2} - \frac{e^{-r(\tau-np-a)}}{q(r^2 + q^2)} (r \sin q(\tau-np-a) \right. \\ \left. + q \cos q(\tau-np-a)) \right] u(\tau-np-a) \\ - \sum_{n=0}^n \left[ \frac{1}{r^2 + q^2} - \frac{e^{-r(\tau-np-(a+b))}}{q(r^2 + q^2)} (r \sin q(\tau-np-(a+b)) \right. \\ \left. + q \cos q(\tau-np-(a+b))) \right] u(\tau-np-(a+b)) \\ + \sum_{n=0}^n \left[ \frac{1}{r^2 + q^2} - \frac{e^{-r(\tau-np-(2a+b))}}{q(r^2 + q^2)} (r \sin q(\tau-np-(2a+b)) \right. \\ \left. + q \cos q(\tau-np-(2a+b))) \right] u(\tau-np-(2a+b))$$

The alternate expression is:

$$(32) \quad \mathcal{F}_2(\theta) = \sum_{n=0}^n \left[ \frac{1}{r^2 + q^2} + \frac{e^{-r(\tau-np)}}{q \sqrt{r^2 + q^2}} \cdot \sin |q(\tau-np) - \phi| \right] u(\tau-np) \\ - \sum_{n=0}^n \left[ \frac{1}{r^2 + q^2} + \frac{e^{-r(\tau-np-a)}}{q \sqrt{r^2 + q^2}} \cdot \sin |q(\tau-np-a) - \phi| \right] \\ u(\tau-np-a) \\ - \sum_{n=0}^n \left[ \frac{1}{r^2 + q^2} + \frac{e^{-r(\tau-np-(a+b))}}{q \sqrt{r^2 + q^2}} \cdot \sin |q(\tau-np-(a+b)) - \phi| \right] \\ \cdot u(\tau-np-(a+b)) \\ + \sum_{n=0}^n \left[ \frac{1}{r^2 + q^2} + \frac{e^{-r(\tau-np-(2a+b))}}{q \sqrt{r^2 + q^2}} \cdot \sin |q(\tau-np-(2a+b)) - \phi| \right] \\ \cdot u(\tau-np-(2a+b))$$

## APPENDIX E

### EFFECTS OF PRIMARY ROD EXTENSION RATE ON STRUCTURAL INTEGRITY

In order to change the spacecraft inertial properties, the length of the gravity gradient rods must be varied in part of the ATS mission. It is assumed that the fully extended length of the boom is 150 feet, and its minimum length, after initial deployment, is 50 feet. The same motor that deploys the primary boom initially is also used for the extension-retraction maneuvers. These boom movements are performed at the rate of 2 feet per second. The motor is stopped almost instantaneously at the end of the retraction sequence, and the kinetic energy associated with the moving rod and tip mass must be absorbed. Since the extended rods become unstable at very low compressive loads, the question arises as to the structural adequacy of the rod itself and the effect on overall spacecraft behavior.

An investigation was made to determine the effects of rod extension and retraction rates on the structural integrity of the primary booms. The investigation was based on the following simplifying assumptions:

1. Rods have no mass
2. Material is stressed below proportional limit
3. Small deflection theory
4. Spacecraft is undisturbed by shear and moment build-up at root of rod
5. Energy of the system is conserved
6. No lateral velocity of tip mass when system is stopped.

Using these assumptions, a set of equations was developed to express rod behavior and the problem was set up for computer solution. Results were obtained for rod stopped at the 50-foot length having tip weights of 10 and 2.6 pounds, retraction rates of 2 and 3 feet per second, and initial tip eccentricities of 0, 15 and 30 inches.

Preliminary results indicate that stopping the booms at 50 feet was more severe than stopping at greater lengths, and that the maximum bending moments varied inversely as the square

root of the length and directly as the velocity of retraction. The major results of the investigation indicate that the allowable bending moment will be exceeded with the 10-pound tip weight, and it is marginal with the 2.6-pound tip weight.

The behavior of the rods is illustrated in the sequence shown in Figure 1.

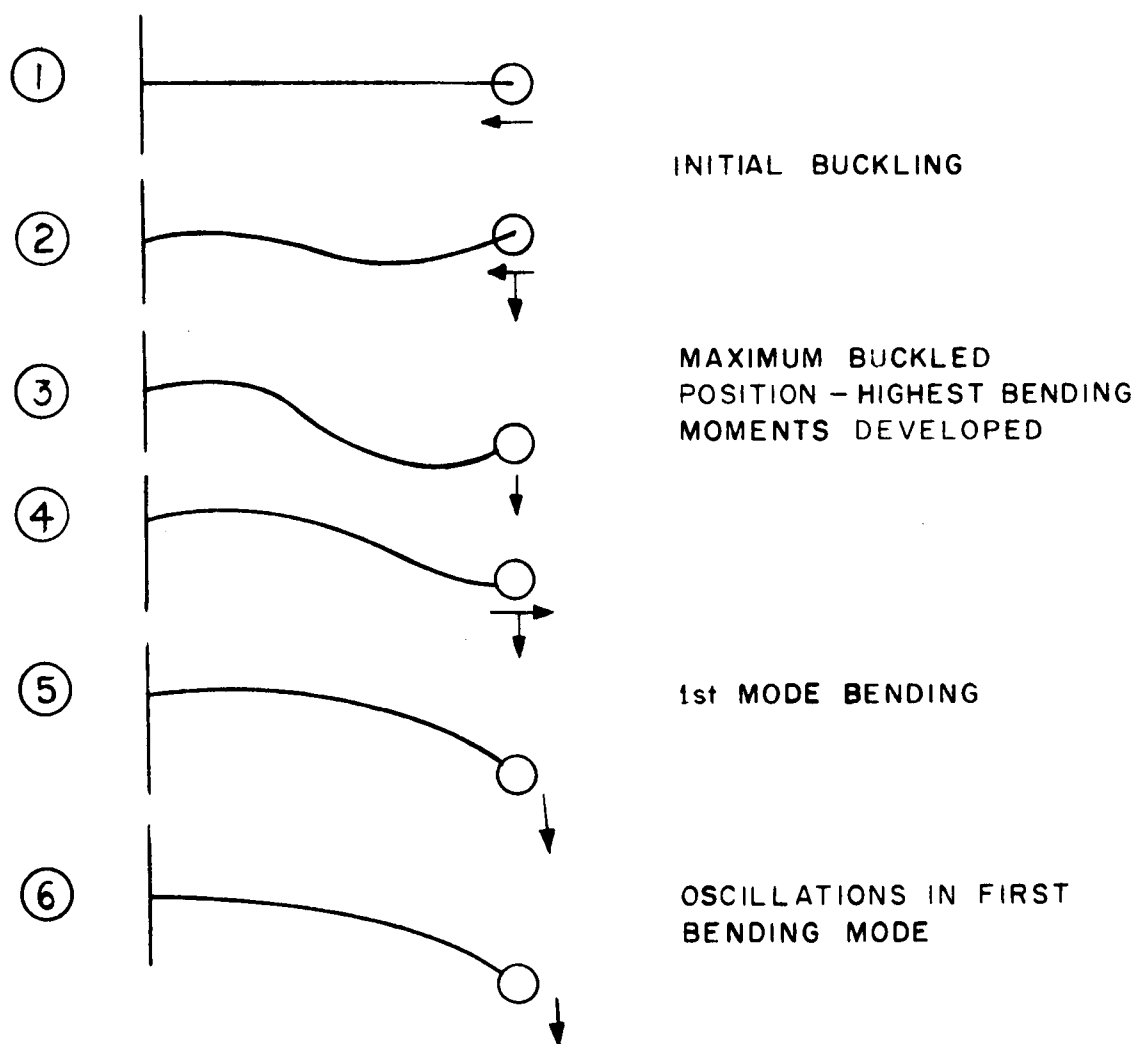


Figure 1. Rod Bending Moment Sequence

As the rod buckles under the critical load, a transverse force is developed on the tip mass which induces transverse tip displacements and velocities (2) and (3) . When the rod returns to the unbuckled position (4) , the tip mass has a residual transverse velocity and displacement which determine the amplitude of oscillations in the first bending mode of the rod (5) and (6) . The motion of the rod as described has been physically observed utilizing a simple model of the system. As can be seen from Figures 2 and 3, the bending moments during initial buckling are most severe; however, the amplitude of oscillations in the first mode may have some bearing on the overall spacecraft performance. The amplitudes and bending moments for the first bending mode (6) are shown in Table 1. The computer outputs shown in Tables 2 and 3, are the bending moments and transverse shear force developed on the rods while it is in the buckled position (1) through (4) . Column 102 (t) is the time after the rods have been stopped. Column 130 ( $\delta_o$ ) is the initial tip mass transverse eccentricity. This eccentricity is due to both thermal bending and manufacturing effects. Column 141 ( $V_o$ ) is the retraction velocity. Column 156 (Q) is the transverse tip force developed at time t. Column 166 ( $M_{\text{root}}$ ) is the bending moment at the rod spacecraft interface at time t. Column 173 ( $M_{\text{max}}$ ) is the maximum bending moment developed in the rod at time t. This occurs at a point approximately at 2/3 of the length of the rod. The last two numbers of the output data are the exponents of ten by which the data must be multiplied. The development of the equations of motion are given at the end of this appendix.

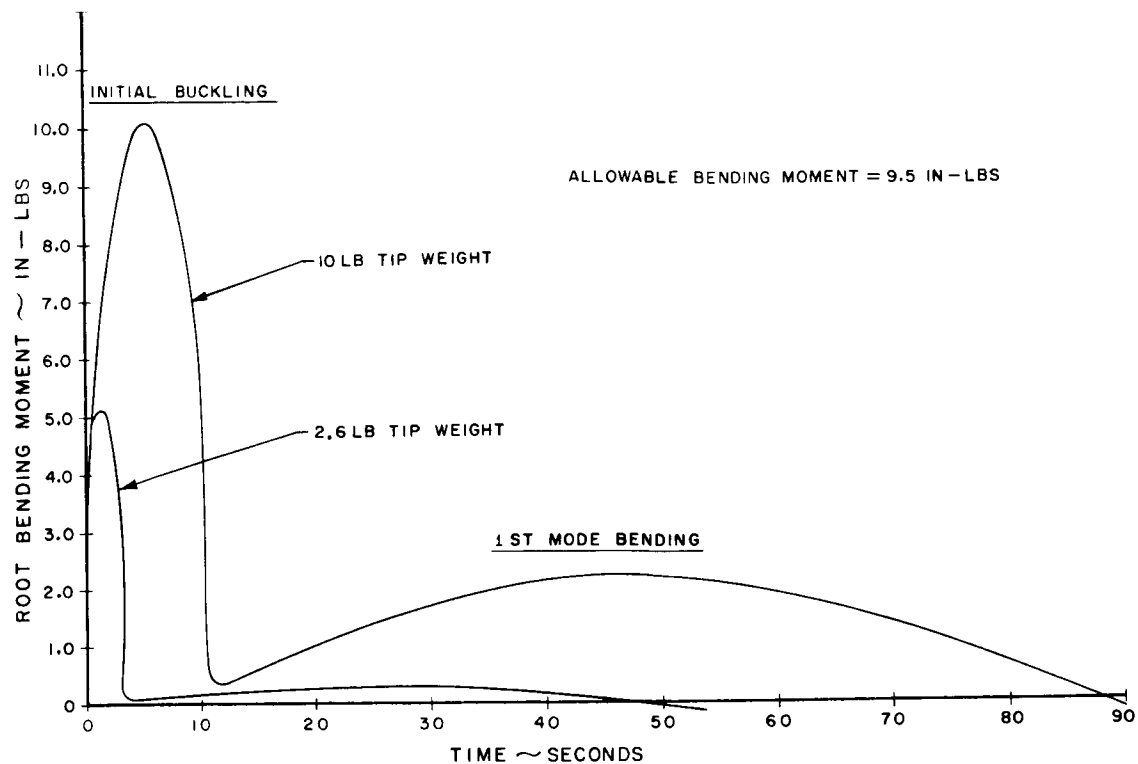


Figure 2. Root Bending Moment vs Time After Stopping at 50 Feet (Retraction Rate = 2 Ft/Sec)

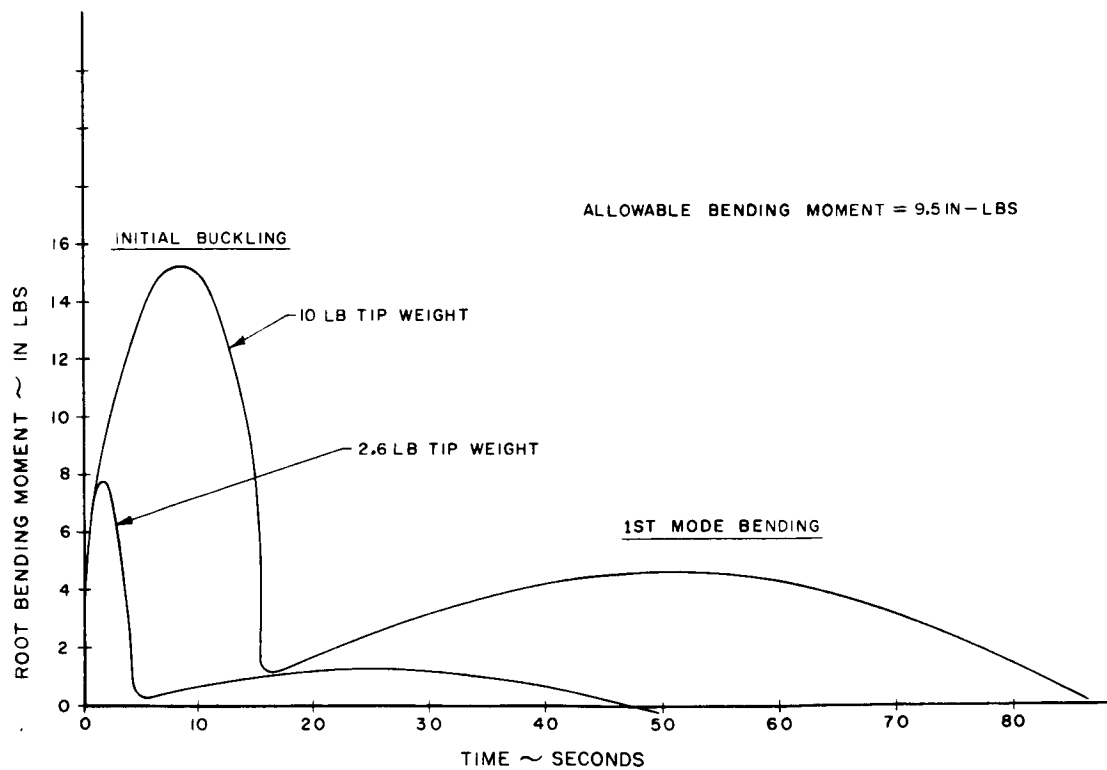


Figure 3. Root Bending Moment vs Time After Stopping at 50 Feet (Retraction Rate = 3 Ft/Sec)

TABLE 1. FIRST MODE BENDING MOMENTS AND AMPLITUDES

W	V	$\delta_o$	A	M	T
10	24	0	134	2.2	192
10	24	15	112	1.86	192
10	24	30	87	1.45	192
10	36	0	286	4.76	192
10	36	15	253	4.21	192
2.6	24	0	35	.58	98
2.6	24	15	23	.38	98
2.6	24	30	11	.18	98
2.6	36	0	79	1.3	98
2.6	36	15	61	1.01	98

W = Tip Weight, lbs.

V = Retraction Velocity, inches/sec.

$\delta_o$  = Initial Eccentricity, inches

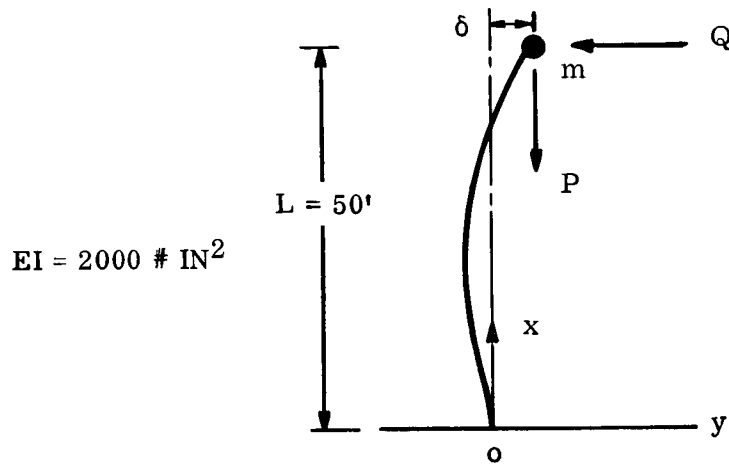
A = Amplitude, inches

T = Period, seconds

M = Moment, ft-lbs.

## Development of the Equations of Motion

Approach to problem will be conservation of energy using assumptions stated earlier.



$\delta$  is transverse tip deflection at any time

$V_x$  is longitudinal tip velocity

$V_y$  is transverse tip velocity

Conservation of energy

$$\frac{1}{2} m V_x^2 + \frac{1}{2} m V_y^2 + \xi = \frac{1}{2} m V^2 \quad (1)$$

where  $\xi$  is strain energy in bending. In order to evaluate  $\xi$ , the differential equation for rod bending moment can be written as:

$$EI \frac{d^2 y}{d^2 x} = P (\delta - y) + Q (l - x) \quad (2)$$

$$P = m\ddot{x} = P \text{ critical}$$

$$Q = m\ddot{y}$$

$$\frac{d^2 y}{dx^2} = \frac{P}{EI} (\delta - y) + \frac{Q}{EI} (1 - x)$$

$$\text{Let } p^2 = \frac{P}{EI}$$

then

$$\frac{d^2 y}{dx^2} + p^2 y = p^2 \frac{Q}{P} (1 - x)$$

The complete solution is

$$y = C_1 \cos px + C_2 \sin px + \delta + \frac{Q}{p} (1 - x)$$

invoking the following boundary conditions:

$$1) \quad y \Big|_{x=0} = 0$$

$$2) \quad y \Big|_{x=e} = \delta$$

$$3) \quad \frac{dy}{dx} \Big|_{x=0} = 0$$

$$y = \frac{Q}{P} \left\{ -1 \cos px + \frac{1}{p} \sin px + 1 - x \right\} + \delta (1 - \cos px) \quad (3)$$

where  $p = \frac{4.5}{l}$



The strain energy in bending can now be found using Equation 3.

$$\xi = 1/2 \frac{1}{EI} \int_0^l m^2 dx \quad (4)$$

$$m = EI \frac{d^2 y}{dx^2} \quad (5)$$

The following expression can be derived.

$$\xi = \frac{EI}{Z_p} \left[ A^2 (2.355) - .95 AB + B^2 (2.145) \right] \quad (6)$$

where:

$$A = \left( \frac{Q}{P} p^2 l + \delta p^2 \right)$$

$$B = \frac{Q}{P} p$$

$$P = EI p^2 = \frac{EI 4.5}{l^2} = \text{Period} = .112 \#$$

$$\delta = \delta_o + \int_0^t \int_0^t \frac{Q(t)}{M} dt dt$$

Initial computer runs indicated that  $Q(t) = Q \sin \frac{\pi}{T} t$

where T is total time that column remains in buckled shape

$$T = \frac{2 W V}{g (\text{Period})}$$

The transverse velocity at any time will be

$$V_y = \int_0^t \frac{Q}{M} dt = \frac{QT}{M\pi} \left( 1 - \cos \frac{\pi t}{T} \right) \quad (7)$$

and transverse displacement

$$\delta = \delta_0 + \int V dt = \delta_0 + \frac{QT}{M\pi} \left[ t - \frac{T}{\pi} \sin \frac{\pi t}{T} \right] \quad (8)$$

The velocity in the X direction is found by assuming the force, P, on the tip mass remains constant at P critical, i. e.,

$$V_x = V_0 - \frac{P}{M} t \quad (9)$$

Now substituting Equations 6, 7, 8, and 9 into 1, Equation 1 can be solved for Q. Knowing Q we substitute in Equations 3 and 5 for rod deflections and moments. These final steps were done by digital computer. These results are given in Tables 2 and 3.

Table 2. Bending Moments and Transverse Shear Force (10-Pound Tip Weight)

$t$ 10 <sup>3</sup> SECONDS	$\delta$ 130 INCHES	$V_0$ 141 INCHES/SEC	$Q$ 156 POUNDS	$M_{rest}$ 165 IN-LBS	$M_{max}$ 173 IN-LBS
1	.0000-01	0.	2.4000+01	4.4573-03	2.6894+00
2	.5000-01	0.	2.4000+01	7.2858-03	4.3876+00
3	1.0000+00	0.	2.4000+01	1.0019-02	6.0406+00
4	.5000+00	0.	2.4000+01	1.1905-02	7.1906+00
5	.2000+00	0.	2.4000+01	1.3300-02	8.0556+00
6	.7500+00	0.	2.4000+01	1.4346-02	8.7207+00
7	.3000+00	0.	2.4000+01	1.5110-02	9.2287+00
8	.3500+00	0.	2.4000+01	1.5632-02	9.6046+00
9	.4000+00	0.	2.4000+01	1.5933-02	9.8630+00
10	.4500+00	0.	2.4000+01	1.6025-02	1.0013+01
11	.5000+00	0.	2.4000+01	1.5892-02	1.0058+01
12	.5500+00	0.	2.4000+01	1.5593-02	1.0003+01
13	.6000+00	0.	2.4000+01	1.5057-02	9.8416+00
14	.6500+00	0.	2.4000+01	1.4291-02	9.5704+00
15	.7000+00	0.	2.4000+01	1.3273-02	9.1794+00
16	.7500+00	0.	2.4000+01	1.1971-02	8.6528+00
17	.8000+00	0.	2.4000+01	1.0344-02	7.9653+00
18	.8500+00	0.	2.4000+01	8.3390-03	7.0753+00
19	.9000+00	0.	2.4000+01	5.9030-03	5.9084+00
20	.9500+01	0.	2.4000+01	5.8919-06	4.0266-01
21	.0000-01	1.5000+01	2.4000+01	1.5745-03	2.6354+00
22	.5000-01	1.5000+01	2.4000+01	4.4015-03	4.3381+00
23	1.0000+00	1.5000+01	2.4000+01	7.1420-03	5.9933+00
24	.5000+00	1.5000+01	2.4000+01	9.0346-03	7.1446+00
25	.2000+00	1.5000+01	2.4000+01	1.0440-02	8.0108+00
26	.7500+00	1.5000+01	2.4000+01	1.1498-02	8.6771+00
27	.3000+00	1.5000+01	2.4000+01	1.2278-02	9.1866+00
28	.3500+00	1.5000+01	2.4000+01	1.2820-02	9.5642+00
29	.4000+00	1.5000+01	2.4000+01	1.3145-02	9.8248+00
30	.4500+00	1.5000+01	2.4000+01	1.3268-02	9.9775+00
31	.5000+00	1.5000+01	2.4000+01	1.3176-02	1.0026+01
32	.5500+00	1.5000+01	2.4000+01	1.2919-02	9.9748+00
33	.6000+00	1.5000+01	2.4000+01	1.2441-02	9.8192+00
34	.6500+00	1.5000+01	2.4000+01	1.1749-02	9.5555+00
35	.7000+00	1.5000+01	2.4000+01	1.0826-02	9.1746+00
36	.7500+00	1.5000+01	2.4000+01	9.6495-03	8.6621+00
37	.8000+00	1.5000+01	2.4000+01	8.1915-03	7.9751+00
38	.8500+00	1.5000+01	2.4000+01	6.4221-03	7.1364+00
39	.9000+00	1.5000+01	2.4000+01	4.3279-03	6.0193+00
40	.9500+01	1.5000+01	2.4000+01	-7.7999-06	1.1544+00

TABLE 2. BENDING MOMENTS AND TRANSVERSE SHEAR FORCE (10-POUND TIP WEIGHT)

Table 2 (Continued)


BY CK. DATE		REV.		GENERAL  ELECTRIC		PAGE 11 MODEL REPORT
10 POUND TIP WGT						
t 102	$\delta$ 130	$V$ 141	Q 156	$M_{root}$ 166	$M_{max}$ 173	
41	2.0000-01	3.0000+01	2.4000+01	-1.3568-03	2.5581+00	-2.5081+00
42	2.0000-01	3.0000+01	2.4000+01	1.4937-03	4.2745+00	-4.2605+00
43	1.1000+00	3.0000+01	2.4000+01	4.2474-03	5.9357+00	-5.9362+00
44	1.6500+00	3.0000+01	2.4000+01	6.1502-03	7.0899+00	-7.1241+00
45	2.2000+00	3.0000+01	2.4000+01	7.5670-03	7.9581+00	-8.0190+00
46	2.7500+00	3.0000+01	2.4000+01	8.6383-03	8.6261+00	-8.7011+00
47	3.3000+00	3.0000+01	2.4000+01	9.4347-03	9.1373+00	-9.2220+00
48	3.8500+00	3.0000+01	2.4000+01	9.9960-03	9.5167+00	-9.6080+00
49	4.4000+00	3.0000+01	2.4000+01	1.0346-02	9.7793+00	-9.8746+00
50	4.9500+00	3.0000+01	2.4000+01	1.0498-02	9.9344+00	-1.0031+01
51	5.5500+00	3.0000+01	2.4000+01	1.0446-02	9.9866+00	-1.0082+01
52	6.0500+00	3.0000+01	2.4000+01	1.0231-02	9.9383+00	-1.0030+01
53	6.6000+00	3.0000+01	2.4000+01	9.8108-03	9.7875+00	-9.8728+00
54	7.1500+00	3.0000+01	2.4000+01	9.1909-03	9.5298+00	-9.6062+00
55	7.7000+00	3.0000+01	2.4000+01	8.3606-03	9.1570+00	-9.2218+00
56	8.2500+00	3.0000+01	2.4000+01	7.3058-03	8.6555+00	-8.7056+00
57	8.8000+00	3.0000+01	2.4000+01	6.0116-03	8.0041+00	-8.0369+00
58	9.3500+00	3.0000+01	2.4000+01	4.4698-03	7.1674+00	-7.1800+00
59	9.9000+00	3.0000+01	2.4000+01	2.7046-03	6.0820+00	-6.0727+00
60	1.1100+01	3.0000+01	2.4000+01	-1.3058-05	2.4826+00	-2.4583+00
61	4.0000-01	0.	3.6000+01	7.7126-03	4.6439+00	-4.7406+00
62	1.6650+00	0.	3.6000+01	1.5058-02	9.0956+00	-9.2841+00
63	2.4930+00	0.	3.6000+01	1.7840-02	1.0822+01	-1.1045+01
64	3.3300+00	0.	3.6000+01	1.9848-02	1.2115+01	-1.2362+01
65	4.1620+00	0.	3.6000+01	2.1290-02	1.3104+01	-1.3368+01
66	4.9950+00	0.	3.6000+01	2.2270-02	1.3854+01	-1.4129+01
67	5.8280+00	0.	3.6000+01	2.2840-02	1.4401+01	-1.4681+01
68	6.6600+00	0.	3.6000+01	2.3034-02	1.4767+01	-1.5047+01
69	7.4930+00	0.	3.6000+01	2.2867-02	1.4966+01	-1.5241+01
70	8.3250+00	0.	3.6000+01	2.2349-02	1.5005+01	-1.5270+01
71	9.1600+00	0.	3.6000+01	2.1475-02	1.4885+01	-1.5135+01
72	9.9960+00	0.	3.6000+01	2.0241-02	1.4602+01	-1.4832+01
73	1.0400+01	0.	3.6000+01	1.9513-02	1.4405+01	-1.4623+01
74	1.0829+01	0.	3.6000+01	1.8646-02	1.4151+01	-1.4356+01
75	1.1660+01	0.	3.6000+01	1.6685-02	1.3519+01	-1.3094+01
76	1.2450+01	0.	3.6000+01	1.4476-02	1.2731+01	-1.2874+01
77	1.3350+01	0.	3.6000+01	1.1631-02	1.1603+01	-1.1704+01
78	1.4160+01	0.	3.6000+01	8.6217-03	1.0240+01	-1.0299+01
79	1.4990+01	0.	3.6000+01	5.4088-03	8.4804+00	-8.4975+00
80	1.6650+01	0.	3.6000+01	1.9329-05	6.6141-01	-6.5535-01

Table 2 (Continued)


BY CK. DATE		REV.		GENERAL  ELECTRIC		PAGE 12 MODEL REPORT
10 POUND TIP WGT						
t 102	$\delta_o$ 130	$V_o$ 141	Q 156	$M_{root}$ 166	$M_{max}$ 173	
1	4.0000-01	1.5000+01	3.6000+01	4.8284-03	4.5948+00	-4.6382+00
2	1.5450+00	1.5000+01	3.6000+01	1.2190-02	9.0506+00	-9.1202+00
3	1.4950+00	1.5000+01	3.6000+01	1.4907-02	1.0779+01	-1.0740+01
4	1.3300+00	1.5000+01	3.6000+01	1.7015-02	1.2074+01	-1.2207+01
5	4.1620+00	1.5000+01	3.6000+01	1.8485-02	1.3065+01	-1.3178+01
86	4.0050+00	1.5000+01	3.6000+01	1.9499-02	1.3818+01	-1.4042+01
87	5.8180+00	1.5000+01	3.6000+01	2.0112-02	1.4368+01	-1.4592+01
88	5.6400+00	1.5000+01	3.6000+01	2.0357-02	1.4739+01	-1.4970+01
89	5.4700+00	1.5000+01	3.6000+01	2.0254-02	1.4943+01	-1.5170+01
90	1.3250+00	1.5000+01	3.6000+01	1.9811-02	1.4988+01	-1.5207+01
91	5.1600+00	1.5000+01	3.6000+01	1.9028-02	1.4876+01	-1.5081+01
92	5.9960+00	1.5000+01	3.6000+01	1.7903-02	1.4602+01	-1.4790+01
93	1.0400+01	1.5000+01	3.6000+01	1.7236-02	1.4411+01	-1.4584+01
94	1.0320+01	1.5000+01	3.6000+01	1.6439-02	1.4163+01	-1.4328+01
95	1.1660+01	1.5000+01	3.6000+01	1.4636-02	1.3546+01	-1.3683+01
96	1.2450+01	1.5000+01	3.6000+01	1.2607-02	1.2775+01	-1.2883+01
97	1.3330+01	1.5000+01	3.6000+01	1.0007-02	1.1671+01	-1.1741+01
98	1.4160+01	1.5000+01	3.6000+01	7.2813-03	1.0336+01	-1.0360+01
99	1.4990+01	1.5000+01	3.6000+01	4.4154-03	8.6103+00	-8.6079+00
00	1.6630+01	1.5000+01	3.6000+01	-3.4361-05	5.1174-01	-5.0614-01

Table 3. Bending Moments and Transverse Shear Force (2.6 Pound Tip Weight)

	$t$ 102	$\delta_0$ 130	$V_0$ 141	$Q$ 156	$M_{root}$ 166	$M_{max}$ 173
1	1.4000-01	0.	2.4000+01	3.6788-03	2.2149+00	-2.2610+00
2	2.8000-01	0.	2.4000+01	5.0667-03	3.0513+00	-3.1148+00
3	4.2000-01	0.	2.4000+01	6.4332-03	3.6350+00	-3.7106+00
4	5.6000-01	0.	2.4000+01	6.7606-03	4.0761+00	-4.1607+00
5	7.0000-01	0.	2.4000+01	7.3200-03	4.4174+00	-4.5090+00
6	8.4000-01	0.	2.4000+01	7.7473-03	4.6807+00	-4.7777+00
7	9.8000-01	0.	2.4000+01	8.0631-03	4.8788+00	-4.9796+00
8	1.1200+00	0.	2.4000+01	8.2796-03	5.0192+00	-5.1226+00
9	1.2600+00	0.	2.4000+01	8.4042-03	5.1066+00	-5.2115+00
10	1.4000+00	0.	2.4000+01	8.4407-03	5.1438+00	-5.2490+00
11	1.5400+00	0.	2.4000+01	8.3899-03	5.1318+00	-5.2362+00
12	1.6800+00	0.	2.4000+01	8.2498-03	5.0700+00	-5.1724+00
13	1.8200+00	0.	2.4000+01	8.0157-03	4.9566+00	-5.0558+00
14	1.9600+00	0.	2.4000+01	7.6790-03	4.7875+00	-4.8822+00
15	2.1000+00	0.	2.4000+01	7.2258-03	4.5564+00	-4.6450+00
16	2.2400+00	0.	2.4000+01	6.6338-03	4.2525+00	-4.3332+00
17	2.3800+00	0.	2.4000+01	5.8659-03	3.8578+00	-3.9281+00
18	2.5200+00	0.	2.4000+01	4.8555-03	3.3382+00	-3.3951+00
19	2.6600+00	0.	2.4000+01	3.4670-03	2.6188+00	-2.6571+00
20	2.8000+00	0.	2.4000+01	1.4091-03	1.4748+00	-1.4863+00
21	1.4000-01	1.5000+01	2.4000+01	7.8214-04	2.1584+00	-2.1518+00
22	2.8000-01	1.5000+01	2.4000+01	2.1773-03	2.9987+00	-3.0096+00
23	4.2000-01	1.5000+01	2.4000+01	3.1480-03	3.5842+00	-3.6072+00
24	5.6000-01	1.5000+01	2.4000+01	3.8792-03	4.0263+00	-4.0585+00
25	7.0000-01	1.5000+01	2.4000+01	4.4426-03	4.3684+00	-4.4077+00
26	8.4000-01	1.5000+01	2.4000+01	4.8744-03	4.6325+00	-4.6771+00
27	9.8000-01	1.5000+01	2.4000+01	5.1955-03	4.8312+00	-4.8798+00
28	1.1200+00	1.5000+01	2.4000+01	5.4185-03	4.9723+00	-5.0236+00
29	1.2600+00	1.5000+01	2.4000+01	5.5511-03	5.0605+00	-5.1134+00
30	1.4000+00	1.5000+01	2.4000+01	5.5974-03	5.0986+00	-5.1520+00
31	1.5400+00	1.5000+01	2.4000+01	5.5589-03	5.0877+00	-5.1404+00
32	1.6800+00	1.5000+01	2.4000+01	5.4345-03	5.0273+00	-5.0784+00
33	1.8200+00	1.5000+01	2.4000+01	5.2209-03	4.9158+00	-4.9641+00
34	1.9600+00	1.5000+01	2.4000+01	4.9115-03	4.7496+00	-4.7938+00
35	2.1000+00	1.5000+01	2.4000+01	4.4961-03	4.5226+00	-4.5614+00
36	2.2400+00	1.5000+01	2.4000+01	3.9591-03	4.2254+00	-4.2572+00
37	2.3800+00	1.5000+01	2.4000+01	3.2765-03	3.8423+00	-3.8652+00
38	2.5200+00	1.5000+01	2.4000+01	2.4117-03	3.3456+00	-3.3575+00
39	2.6600+00	1.5000+01	2.4000+01	1.3131-03	2.6794+00	-2.6775+00
40	2.8000+00	1.5000+01	2.4000+01	-1.3442-05	1.6734+00	-1.6570+00

Table 3 (Continued)

BY CK. DATE		GENERAL ELECTRIC			PAGE 14 MODEL REPORT	
2.6 POUND TIP WGT						
	$t$ 102	$\delta_o$ 130°	$V_o$ 141	$Q$ 156	$M_{root}$ 166	$M_{max}$ 173
41	1.4000-01	3.0000+01	2.4000+01	-2.1618-03	2.0735+00	-2.0136+00
42	2.8000-01	3.0000+01	2.4000+01	-7.4617-04	2.9256+00	-2.8836+00
43	4.2000-01	3.0000+01	2.4000+01	2.3429-04	3.5162+00	-3.4864+00
44	5.6000-01	3.0000+01	2.4000+01	9.7232-04	3.9612+00	-3.9407+00
45	7.0000-01	3.0000+01	2.4000+01	1.5416-03	4.3053+00	-4.2918+00
46	8.4000-01	3.0000+01	2.4000+01	1.9792-03	4.5708+00	-4.5628+00
47	9.8000-01	3.0000+01	2.4000+01	2.3064-03	4.7706+00	-4.7667+00
48	1.1200+00	3.0000+01	2.4000+01	2.5363-03	4.9125+00	-4.9115+00
49	1.2600+00	3.0000+01	2.4000+01	2.6769-03	5.0016+00	-5.0023+00
50	1.4000+00	3.0000+01	2.4000+01	2.7329-03	5.0404+00	-5.0418+00
51	1.5400+00	3.0000+01	2.4000+01	2.7061-03	5.0302+00	-5.0312+00
52	1.6800+00	3.0000+01	2.4000+01	2.5966-03	4.9707+00	-4.9702+00
53	1.8200+00	3.0000+01	2.4000+01	2.4019-03	4.8602+00	-4.8572+00
54	1.9600+00	3.0000+01	2.4000+01	2.1175-03	4.6952+00	-4.6886+00
55	2.1000+00	3.0000+01	2.4000+01	1.7364-03	4.4699+00	-4.4584+00
56	2.2400+00	3.0000+01	2.4000+01	1.2480-03	4.1750+00	-4.1575+00
57	2.3800+00	3.0000+01	2.4000+01	6.3285-04	3.7951+00	-3.7701+00
58	2.5200+00	3.0000+01	2.4000+01	-1.0640-04	3.3018+00	-3.2679+00
59	2.6600+00	3.0000+01	2.4000+01	-9.9126-04	2.6262+00	-2.5826+00
60	2.8000+00	3.0000+01	2.4000+01	-2.0716-03	1.2068+00	-1.1571+00
61	2.1000-01	1.5000+01	3.6000+01	2.6290-03	3.2705+00	-3.2871+00
62	4.2000-01	1.5000+01	3.6000+01	4.7139-03	4.5276+00	-4.5703+00
63	6.3000-01	1.5000+01	3.6000+01	6.1623-03	5.4042+00	-5.4650+00
64	8.4000-01	1.5000+01	3.6000+01	7.2488-03	6.0662+00	-6.1405+00
65	1.0500+00	1.5000+01	3.6000+01	8.0799-03	6.5782+00	-6.6628+00
66	1.2600+00	1.5000+01	3.6000+01	8.7091-03	6.9730+00	-7.0654+00
67	1.4700+00	1.5000+01	3.6000+01	9.1671-03	7.2695+00	-7.3675+00
68	1.6800+00	1.5000+01	3.6000+01	9.4721-03	7.4794+00	-7.5809+00
69	1.8900+00	1.5000+01	3.6000+01	9.6348-03	7.6096+00	-7.7128+00
70	2.1000+00	1.5000+01	3.6000+01	9.6605-03	7.6642+00	-7.7674+00
71	2.3100+00	1.5000+01	3.6000+01	9.5505-03	7.6447+00	-7.7460+00
72	2.5200+00	1.5000+01	3.6000+01	9.3021-03	7.5504+00	-7.6481+00
73	2.7300+00	1.5000+01	3.6000+01	8.9086-03	7.3785+00	-7.4706+00
74	2.9400+00	1.5000+01	3.6000+01	8.3588-03	7.1234+00	-7.2079+00
75	3.1500+00	1.5000+01	3.6000+01	7.6360-03	6.7759+00	-6.8505+00
76	3.3600+00	1.5000+01	3.6000+01	6.7158-03	6.3212+00	-6.3833+00
77	3.5700+00	1.5000+01	3.6000+01	5.5646-03	5.7356+00	-5.7825+00
78	3.7800+00	1.5000+01	3.6000+01	4.1387-03	4.9779+00	-5.0058+00
79	3.9900+00	1.5000+01	3.6000+01	2.4026-03	3.9674+00	-3.9731+00
80	4.2000+00	1.5000+01	3.6000+01	4.9155-04	2.4826+00	-2.4675+00

Table 3 (Continued)

BY CK. REV.		GENERAL ELECTRIC		PAGE 15 MODEL REPORT		
2.6 POUND TIP WGT						
$t$ 102	$\delta_o$ 130	$V_o$ 141	$Q$ 156	$M_{root}$ 166	$M_{max}$ 173	
81	2.1000-01	0.	3.6000+01	5.5176-03	3.3223+00	-3.3914+00
82	4.2000-01	0.	3.6000+01	7.5962-03	4.5767+00	-4.6719+00
83	6.3000-01	0.	3.6000+01	9.0393-03	5.4519+00	-5.5651+00
84	8.4000-01	0.	3.6000+01	1.0120-02	6.1129+00	-6.2396+00
85	1.0500+00	0.	3.6000+01	1.0943-02	6.6240+00	-6.7608+00
86	1.2600+00	0.	3.6000+01	1.1564-02	7.0178+00	-7.1622+00
87	1.4700+00	0.	3.6000+01	1.2010-02	7.3133+00	-7.4630+00
88	1.6800+00	0.	3.6000+01	1.2301-02	7.5219+00	-7.6750+00
89	1.8900+00	0.	3.6000+01	1.2447-02	7.6506+00	-7.8051+00
90	2.1000+00	0.	3.6000+01	1.2451-02	7.7032+00	-7.8513+00
91	2.3100+00	0.	3.6000+01	1.2315-02	7.6812+00	-7.8330+00
92	2.5200+00	0.	3.6000+01	1.2032-02	7.5837+00	-7.7312+00
93	2.7300+00	0.	3.6000+01	1.1595-02	7.4074+00	-7.5487+00
94	2.9400+00	0.	3.6000+01	1.0989-02	7.1463+00	-7.2789+00
95	3.1500+00	0.	3.6000+01	1.0189-02	6.7899+00	-6.9113+00
96	3.3600+00	0.	3.6000+01	9.1627-03	6.3220+00	-6.4290+00
97	3.5700+00	0.	3.6000+01	7.8557-03	5.7149+00	-5.8038+00
98	3.7800+00	0.	3.6000+01	6.1879-03	4.9196+00	-4.9855+00
99	3.9900+00	0.	3.6000+01	4.0431-03	3.2366+00	-3.8737+00
100	4.2000+00	0.	3.6000+01	1.3655-03	2.2086+00	-2.2123+00



**APPENDIX F**  
**ANALYSIS OF SOLAR ASPECT SENSOR**  
**ELECTRICAL, MECHANICAL AND OPTICAL ERRORS**

The Adcole Corporation has supplied a detailed analysis of Solar Aspect Sensor errors including those from electrical, mechanical and optical sources. The analysis is reprinted in this appendix.

## SECTION I

IA.	Data Bit and AGC Amplifier	1
IB.	Worst Case $E_{agc}$ Drift Equations	5
IC.	General Drift Equations	6
ID.	Threshold Drift	8
IE.	Other Sources of Error in Electronic System Due to Threshold Drift	10
IF.	Total Threshold Drift	12
IG.	Angular Error Due to Threshold Drift	13
IH.	Angular Errors Due to Sensor Mechanics and Optics	15
IJ.	Probable System Errors Due to Threshold Drift	21
IK.	Total System Errors	23
IL.	Error in Eye Selection	25

IA. Data Bit and AGC Amplifier - See Figure 1

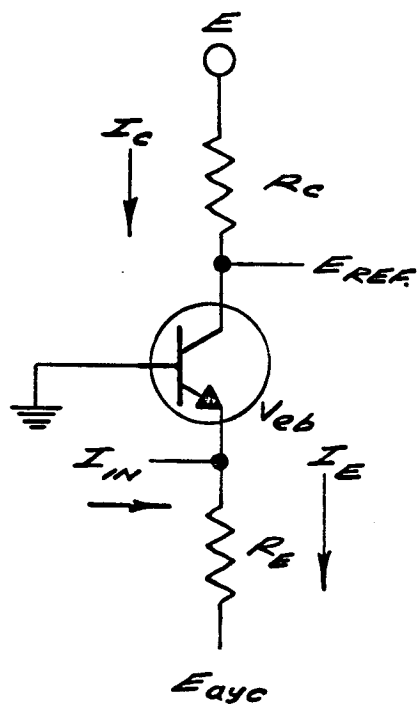


FIGURE NO. 1

At threshold point:

$$I_C = I_E - I_{in}$$

$$I_C R_C = E_{Rc}$$

Assume  $\alpha = 1$

$E = \text{constant}$

$$E - E_{ref} = K_o$$

At the threshold point

$$(1) (I_E - I_{in}) R_C = E_{Rc} = K_o$$

$$(2) I_E = \frac{E_{agc} - V_{eb}}{R_E}$$

For any particular input

current  $E_{agc} - V_{eb} =$   
constant for the data bit  
amplifiers.

$$(3) I_E = \frac{K_1}{R_E}$$

From (1)

$$\left(\frac{K_1}{R_E} - I_{in}\right)R_c = K_o$$

$$(4) \quad I_{in} = \frac{K_1}{R_E} - \frac{K_o}{R_c}$$

$I_{in}$  is the current required for the amplifier to reach the threshold level ( $E_{ref}$ ).

From (4) it can be seen that the worst case (maximum deviation from true input current threshold level) is:

$$(5) \quad I_{in+} = \frac{K_1}{R_{E-}} - \frac{K_o}{R_{c+}}$$

$$(6) \quad I_{in-} = \frac{K_1}{R_{E+}} - \frac{K_o}{R_{c-}}$$

where:

$$I_{in+} = \text{maximum input current}$$

$$I_{in-} = \text{minimum input current}$$

$$R_{E+} = R_E + \Delta R_E$$

$$R_{E-} = R_E - \Delta R_E$$

$$R_{c+} = R_c + \Delta R_c$$

$$R_{c-} = R_c - \Delta R_c$$

#### Amplifier Design

From 3 it can be seen that the term  $\frac{K_1}{R_E}$  is equal to  $I_E$ .  
For minimum deviation in  $I_{in}$  it is desirable to keep  $I_E$  small.

Since the solar cell electrically is a constant current source the best mode of operation is to have an input impedance of zero ohms. Since this is not practical an examination of the solar cell V - I curve shows the current output to be constant out to approximately 7K ohms at a given light level and room temperature.

The input impedance of a grounded base amplifier is given by:

$$(7) \quad Z_{in} = h_{ib} - \frac{h_{rb} h_{fb}}{h_{ob} + G_c}$$

for 2N930 (Texas Instruments)

Typical values at  $I_E = 20 \text{ ua}$

$$h_{rb} = 9 \times 10^{-3}$$

$$h_{ob} = .045 \text{ u mho}$$

$$h_{fb} \stackrel{a}{=} 1$$

$$h_{ib} = 1.5K$$

$$\text{Let } R_c = 500 K \text{ ohms}$$

$$\frac{h_{rb} h_{fb}}{h_{ob} + 1/R_c} = \frac{2 \times 10^{-4} (1)}{4.5 \times 10^{-8} + 2 \times 10^{-6}} = 100 \text{ ohms}$$

$$Z_{in} = 1.5K - .1K = 1.4K \text{ ohms}$$

Note that:

$$Z_{in} \stackrel{a}{=} h_{ib}$$

and

$$h_{ib} \propto I_E$$

i.e. at  $I_E = 40 \text{ ua}$

$$Z_{in} = 700 \text{ ohms}$$

$$\text{Let } E_{ref} = 6.7 \text{ volts} \quad I_E = 20 \text{ ua} \quad R_c = 500 \text{ K}$$

from (1)

$$(I_E - I_{in})R_c = K_o$$

$$I_{in} = 0 \text{ (dark)}$$

$$K_o = (20 \times 10^{-6}) 500 \times 10^3 = 10 \text{ volts}$$

$$\therefore E = 16.7 \text{ volts}$$

IB. Worst Case  $E_{agc}$  Drift Equations

From (1) at the threshold point

$$\left( \frac{E_{agc} - V_{eb}}{R_E} - I_{in} \right) R_c = K_o$$

$$(8) \quad E_{agc} = \frac{K_o R_E}{R_c} + V_{eb} + R_E I_{in}$$

The worst case drifts in  $E_{agc}$  due to  $R_E$  and  $R_c$  changes are:

$$(9) \quad E_{agc+} = \frac{K_o R_{E+}}{R_{c-}} + V_{eb} + (R_{E+}) I_{in}$$

$$(10) \quad E_{agc-} = \frac{K_o R_{E+}}{R_{c+}} + V_{eb} + (R_{E-}) I_{in}$$

# IC. General Drift Equations

- If the tolerances in the circuit become small ( < 6%)

the following equations will give an accurate drift figure (+5%).

From (8)

$$E_{agc} - V_{eb} = K_1 = \frac{K_o R_E}{R_c} + R_E I_{in}$$

$$dK_1 = \frac{\partial K_1}{\partial R_E} dR_E + \frac{\partial K_1}{\partial R_c} dR_c$$

$$dK_1 = \frac{K_o}{R_c} dR_E + I_{in} dR_E + K_o R_E (-R_c^{-2}) dR_c$$

$$(11) \quad \Delta K_1 = \frac{K_o}{R_c} \Delta R_E + I_{in} \Delta R_E - \frac{K_o R_E}{R_c^2} \Delta R_c$$

From (4)

$$I_{in} = \frac{K_1}{R_E} - \frac{K_o}{R_c}$$

$$dI_{in} = \frac{\partial I_{in}}{\partial R_E} dR_E + \frac{\partial I_{in}}{\partial K_1} dK_1 + \frac{\partial I_{in}}{\partial R_c} dR_c$$



$$(12) \quad \Delta I_{in} = \frac{\Delta K_1}{R_E} - \frac{K_1}{R_E^2} \Delta R_E + \frac{K_o}{R_c^2} \Delta R_c$$

ID. Threshold Drift

The drift due to  $\pm 1\%$  tolerances on  $R_E$  and  $R_c$  is:

$$\Delta R_E = 200K (\pm .01) = \pm 2K$$

$$\Delta R_c = 500K (\pm .01) = \pm 5K$$

$$K_o = 10 \text{ volts}$$

From (11)

$$\begin{aligned} \Delta K_1 &= \frac{K_o}{R_c} \Delta R_E + I_{in} \Delta R_E - \frac{K_o R_E}{R_c^2} \Delta R_c \\ &= \frac{10}{500K} (\pm 2K) + 10 \text{ ua} (\pm 2K) - \frac{10 (200K) (\pm 5K)}{(500K) (500K)} \\ &= \pm 0.04 \pm 0.02 \pm 0.04 \end{aligned}$$

$$\Delta K_1 = \pm 0.1 \text{ volts}$$

$$K_1 = \frac{K_o R_E}{R_c} + R_E I_{in}$$

$$K_1 = \frac{10 (200K)}{500K} + 200K (10) = 6 \text{ volts}$$

From (12)

$$\Delta I_{in} = \frac{\Delta K_1}{R_E} - \frac{K_1}{(R_E)^2} \Delta R_E + \frac{K_o}{(R_c)^2} \Delta R_c$$

$$\Delta I_{in} = \frac{+0.1}{200K} - \frac{6 (+2K)}{(200K)(200K)} + \frac{10 (+5K)}{(500K)(500K)}$$

$$= +0.5 \text{ ua } +0.3 \text{ ua } +0.2 \text{ ua}$$

$$\Delta I_{in} = \begin{matrix} +1 \\ -0 \end{matrix} \text{ ua } \quad \begin{matrix} +1\% \\ -1\% \end{matrix} R_E R_c$$

$$K_1 R_E R_c$$

$$\Delta I_{in} = \begin{matrix} -1 \\ +0 \end{matrix} \text{ ua } \quad \begin{matrix} +1\% \\ -1\% \end{matrix} R_E R_c$$

$$K_1 R_E R_c$$

Purchase tolerance of  $R_c$  and  $R_E$  is  $\pm 1/2\%$ .

IE. Other sources of error in Electronic System due to threshold drift.

a.  $V_{be}$

Variations in  $V_{be}$  of the data bit amplifiers with respect to the AGC amplifiers may be  $\pm 50$  mv. This could result in an error of:

From (12)

$$\frac{\Delta I_{in}}{V_{be}} = \frac{\Delta K_1}{R_E} = \frac{+0.05v}{200K} = \pm 0.25 \text{ ua}$$

b. Variations in diode forward voltage drop

$$\Delta V_d = \pm 0.1 \text{ volt}$$

$$\frac{\Delta I}{V_d} = \pm 0.1 \text{ volt} \times \frac{2 \text{ ua}}{\text{volt}} = \pm 0.2 \text{ ua}$$

c. Variation in AGC cell output with respect to the data bit cells ( $\pm 5\%$  match)

$$\frac{\Delta I}{\text{AGC cell}} = \pm 0.05 (10 \text{ ua}) = \pm 0.5 \text{ ua}$$

d. Leakage

1. Data bit amplifier transistor

$$\Delta I_t = +0.1 \text{ ua}$$

2. Diode leakage

$$\Delta I_d = \text{negligible at thresh point}$$

3. Capacitor leakage

$$\Delta I_c = -0.1 \text{ ua}$$

Note that  $\Delta I_t$  tend to cancel  $\Delta I_c$

e. Other

1. Dynamic on resistance of series and shunt switches.
2. Solar cell leakage
3. Stray capacities
4. AGC voltage errors

All of the above will contribut less than:

$$\Delta I = \underline{+0.1} \text{ ua}$$

Other

IF. Total Threshold Drift

$$\Delta I_{\text{thresh}} = \Delta I_{R_E R_c} + \Delta I_{V_{be}} + \Delta I_{V_d} + \Delta I_{\text{AGC cell}} + \Delta I_{\text{leakage}} + \Delta I_{\text{other}}$$

+1%

$$\Delta I_{\text{thresh}} = \pm 1.0 \pm 0.25 \pm 0.2 \pm 0.5 \pm 0.1 \pm 0.1 \text{ ua}$$

$$\Delta I_{\text{thresh}} = \pm 2.15 \text{ ua}$$

IG. Angular Error due to Threshold Drift

Experimental measurement and analysis of the output current from the least significant bit shows that this current is sinusoidal in form. See Figure 2.

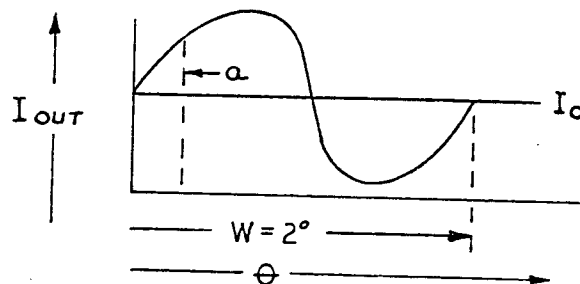


FIGURE 2

The general expression for the output waveform is given by:

$$(13) \quad I_{out} = CI_o \left[ 1 + m \sin 360 \left( \frac{a}{w} \right) \right]$$

where  $C$  is the multiplying factor and is determined by cell tolerance.

$I_o$  = D.C. component of the output and is the true threshold point.

$m$  = modulation factor experimentally determined to be 0.8.

W = periode for one cycle (2 degrees)

a = Angular displacement

The angular error due to the threshold drifts may be calculated by solving for a:

$$a = \frac{\sin^{-1} \left( \frac{1}{m} \right) \left[ \frac{I_{out}}{CI_0} - 1 \right]}{180}$$

$$C = 1 + \Delta C$$

cell tolerance

$$C = 1 \pm .05$$

For the least significant bit the angular error is:

$$a+ = \frac{\sin^{-1} \left( \frac{1}{.8} \right) \left[ \frac{12.15}{.95 (10)} - 1 \right]}{180}$$

$$a+ = \frac{\sin^{-1} (.350)}{180} = \frac{20.5}{180} = 0.1135 \text{ degree}$$

$$a- = \frac{\sin^{-1} \left( \frac{1}{.8} \right) \left[ \frac{7.85}{1.05 (10)} - 1 \right]}{180}$$

$$= \frac{\sin^{-1} (.318)}{180} = - \frac{18.5}{180} = -0.1025 \text{ degree}$$

$$a = \begin{matrix} +0.1135 \\ -0.1025 \end{matrix} \text{ degree}$$



IH. Angular Errors Due to Sensor Mechanics and Optics

1. Mechanical errors

- a) The slit position tolerance is set at  $\pm 1 \times 10^{-4}$  inches.

The scale factor is  $5.5 \times 10^{-3} \frac{\text{in}}{\text{deg}}$  (approximately)

The error due to slit position is:

$$E_{(a)} = \frac{\pm \text{S.P.}}{\text{S.F.}} = \frac{\pm 1 \times 10^{-4}}{5.5 \times 10^{-3}} = 0.018 \text{ degree}$$

- b) Pattern tolerance is set at  $\pm 1 \times 10^{-4}$  inches.

i.e. No pattern edge shall depart from the specified position by more than  $\pm 1 \times 10^{-4}$  inches.

The error due to pattern variations is:

$$E_{(b)} = \frac{\pm \text{P.P.}}{\text{S.F.}} = \frac{1 \times 10^{-4}}{5.5 \times 10^{-3}} = \pm 0.018 \text{ degree}$$

- c) Error due to reticle thickness

The tolerance on the thickness of the fused silica is specified to be  $\pm 2 \times 10^{-4}$  inches.

The nominal thickness of the silica is 0.4480 inches.

At 64 degree angle of incident light to the slit surface the slit image is displaced 0.3520 inches at the pattern surface.

Therefore

$$\frac{x}{3.52 \times 10^{-1}} \approx \frac{+2 \times 10^{-4}}{4.48 \times 10^{-1}}$$

$$x \approx +1.57 \times 10^{-4} \text{ inches}$$

Where x is the slit image position error.

The error due to variations in thickness

is:

$$E_{(c)} = \frac{+x}{\text{S.F.}} = \frac{+1.57 \times 10^{-4}}{5.5 \times 10^{-3}} \approx +0.029 \text{ degree}$$

d) Error due to reticle position

The tolerance in position of the reticle relative to the reference surface is set at

$+2 \times 10^{-4}$  inches. Since the width of the reticle seat is 0.750 inches the maximum angular error is:

$$E_{(d)} = \tan^{-1} \left[ \frac{2 \times 10^{-4}}{7.5 \times 10^{-1}} \right]$$

for small angles

$$E_{(d)} \approx \frac{2 \times 10^{-4}}{7.5 \times 10^{-1}} \times \frac{180 \text{ deg}}{\pi \text{ rad}} = 0.015 \text{ degree}$$

The total mechanical error ( $E_{(m)}$ ) is:

$$E_{(m)} \approx E_{(a)} + E_{(b)} + E_{(c)} + E_{(d)}$$

$$\approx \pm 0.018 \pm 0.018 \pm 0.029 \pm 0.015 \text{ degree}$$

$$E_{(m)} \approx \pm 0.080 \text{ degree}$$

## 2. Optical errors

Errors which might be called optical in nature arise from the manufacturing variations of fused silica, changes of the index of refraction of fused silica with temperature and wavelength.

Also errors will occur due to manufacturing variations and temperature which cause shifts in the spectral response of silicon solar cells.

- a) Variation in index of refraction due to manufacturing variations.

The index of refraction will not vary more than one part in  $10^4$  parts from sample to sample. Thus the maximum error at 64 degree angle of incidence is:

$$E_{o(a)} = \frac{64}{\pm 1 \times 10^4} = 0.0064 \text{ degree}$$

- b) Index of refraction change of fused silica with temperature.

This change will be approximately  $1.4 \times 10^{-5}$  parts per  $^{\circ}\text{C}$ . For a  $130^{\circ}\text{C}$  change in temperature this error is:

$$E_{o(b)} = \frac{64}{1.4 \times 10^{-5} (1.3 \times 10^2)} = -0.04 \text{ degree}$$

c) Spectral response of photo cells

The silicon photo cell spectral response shifts toward the red with increasing temperature. This is in the direction of a lower index of refraction for fused silica. This change in angle at 64 degrees light incidence and 130 degrees Centigrade change in temperature has been determined to be

$$E_{o(c)}^a = +0.04 \text{ degree}$$

d) Manufacturing tolerance on photo cell spectral response.

At 64 degree incident light:

$$E_{o(d)} = \pm 0.02 \text{ degree}$$

e) Total optical errors

$$E_o = E_{o(a)} + E_{o(b)} + E_{o(c)} + E_{o(d)}$$

Note that  $E_{o(b)}$  tends to cancel  $E_{o(c)}$

$$E_o^a = \pm 0.03 \text{ degree}$$

3. Total mechanical and optical errors:

$$E_{mo} = E_m + E_o$$

$$E_{mo} = \pm 0.08 \pm 0.03 = \pm 0.11 \text{ degree}$$

4. Total probable mechanical and optical errors:

$$E_{mo} \text{ Probable} = \pm \sqrt{(E_a)^2 + (E_b)^2 + (E_c)^2 + (E_d)^2 + (E_{oa})^2 + (E_{od})^2}$$

$$E_{\text{Probable}} = \pm 0.05 \text{ degree}$$

IJ. Probable System Errors Due to Threshold Drift

$$\Delta I_{\text{threshold probable}} = \pm \sqrt{(\Delta I_{R_E R_c})^2 + (\Delta I_{V_{be}})^2 + (\Delta I_{V_d})^2 + (\Delta I_{AGC})^2 + (\Delta I_{Leak})^2 + (\Delta I_{\text{other}})^2}$$

$$\begin{aligned} \Delta I_{\text{threshold probable}} &= \pm \sqrt{1.0 + .0625 + .04 + 0.25 + .01 + .01} \\ &= \pm \sqrt{1.37} \quad \text{ua} \end{aligned}$$

$$\begin{aligned} \Delta I &= \pm 1.17 \text{ ua} \\ \text{threshold} \\ \text{probable} \end{aligned}$$

The probable angular error due to threshold drifts is:

From (13)

$$a+_{\text{probable}} = \frac{\sin^{-1}(\frac{1}{.8}) \left[ \frac{11.17}{.95(10)} - 1 \right]}{180}$$

$$a+_{\text{probable}} = \frac{\sin^{-1}(.220)}{180} = \frac{12.7}{180} = 0.076 \text{ degree}$$

$$a-_{\text{probable}} = \frac{\sin^{-1}(\frac{1}{.8}) \left[ \frac{8.83}{1.05(10)} - 1 \right]}{180} = \frac{\sin^{-1}(-0.20)}{180}$$

$$\begin{array}{rcl} a- & = & \frac{11.5}{180} = 0.064 \text{ degree} \\ \text{probable} & & \end{array}$$

$$\begin{array}{rcl} a & = & +0.0760 \\ \text{probable} & = & -0.0640 \end{array} \text{ degree}$$



IK. Total System Errors

1. Total worst case errors

The total worst case errors due to electrical, mechanical and optical variations are:

$$E_{\text{total}} = a + E_{\text{mo}}$$

$$E_{\text{total}} = \begin{array}{l} +0.1135 \\ -0.1025 \end{array} \pm 0.110 \text{ degree}$$

$$E_{\text{total}} = \begin{array}{l} +0.2235 \\ -0.2125 \end{array} \text{ degree}$$

$E_{\text{total}}$  represents the angular variation about a true switching point. For a  $\pm 1/2$  degree resolution system  $E_{\text{total}}$  must be less than  $\pm 0.25$  degree. Hence the system readout will not be in error. (i.e: The order of bits will always be correct.)

Note also that the resolution would be preserved if  $E_{\text{total}}$  drifted only one way but less than 0.5 degree.

2. Total probable error

$$E_{\text{probable}} = \pm \sqrt{(a_{\text{probable}})^2 + (E_{\text{mo probable}})^2}$$

$$E_{\text{probable}} = \pm \sqrt{(0.076)^2 + (.05)^2} \text{ degree}$$

$$E_{\text{probable}} = \pm 0.091 \text{ degree}$$

This number is still worst case and exceeds the error expected during initial test.

## IL. Error in Eye Selection

The error in the threshold point in the AGC amplifier is a measure of the current required from any particular eye AGC solar cell to control the AGC loop and therefore be the selected eye. For  $\pm 3\%$  resistor tolerances on  $R_c$  and  $R_E$  the error will be:

$$I_{in} = 10 \text{ ua}$$

from (12)

$$\Delta I_{in} = \frac{\Delta K_1}{R_E} - \frac{K_1}{R_E^2} \Delta R_E + \frac{K_o}{R_c^2} \Delta R_c$$

$$\Delta K_1 = 0 \text{ in this case}$$

$$K_1 = 6 \text{ volts} \quad R_E = 200K (.03) = \pm 6K$$

$$K_o = 10 \text{ volts} \quad R_c = 500K (.03) = \pm 15K$$

$$\frac{\Delta I_{in}}{R_E R_c} = \pm .9 \pm .6 = \pm 1.5 \text{ ua}$$

Other causes of error are:

1. Error due to  $\pm 5\%$  solar cell mismatch.

$$\Delta I = 10 \text{ ua } (\pm .05) = \pm 0.5 \text{ ua}$$

S. C.

2.

Assume:

Control of AGC circuit requires that one cell produce 1 ua more than any other cell. (maximum)

$$\triangle I_{AGC} = \triangle I_{R_E R_c} + \triangle I_{S.C.}$$

$$= \pm 1.5 \quad \pm 0.5$$

$$\triangle I_{AGC} = \pm 2 \text{ ua} \quad \text{Drift due to } \pm 3\% \text{ change in } R_E, R_c$$

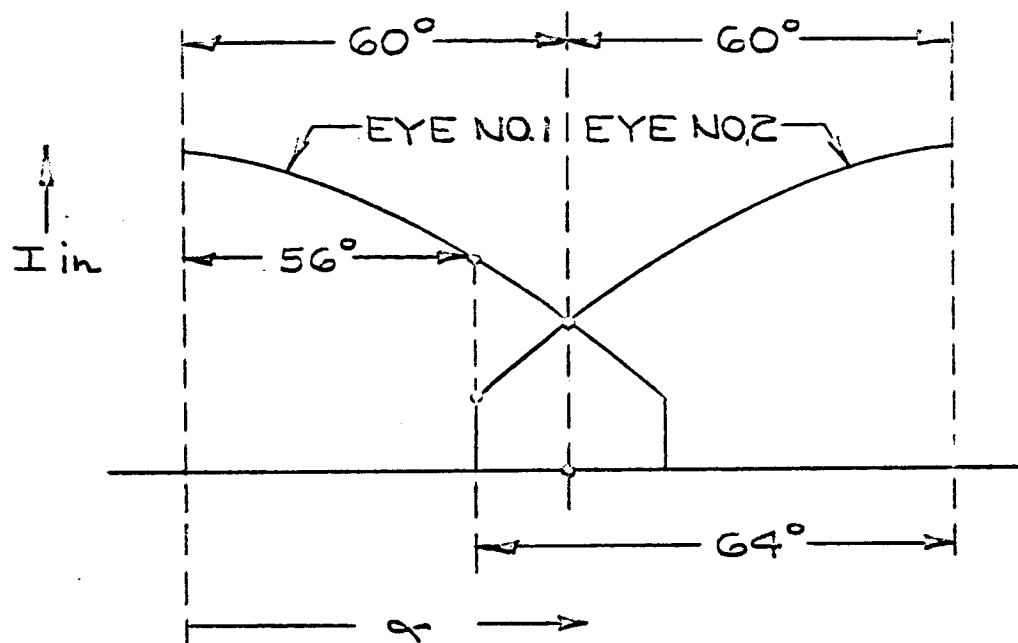
Figure 3 is a profile view of the AGC bit output current vs angle of light incidence for two overlapping eyes. From this figure it can be seen that an error could occur if eye #2 data bits were out of the field of view (dark) and the AGC bit was at the edge of the field of view but not dark (10 ua output) and eye #2 was selected by the electronics.

From curves of Figure 4 assume

$$I_{64}^o = 10 \text{ ua}$$

from curve

$$\frac{I_{56}^o}{.42} = \frac{10 \text{ ua}}{.28}$$



PROFILE OF AGC CURRENT OUTPUT  
OF TWO OVERLAPPING FIELD OF  
VIEW ASPECT EYES

FIGURE NO. 3

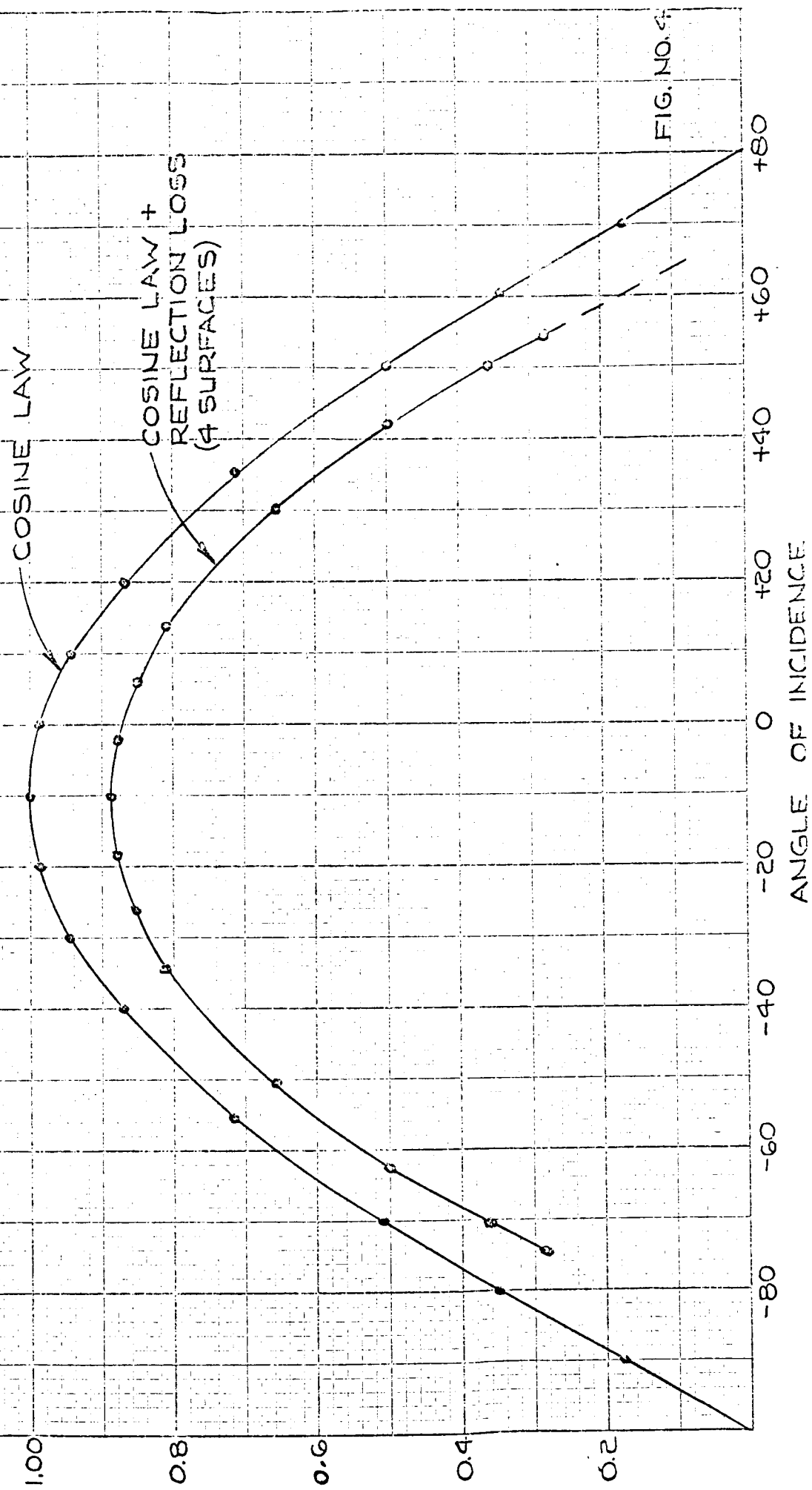


FIG. NO. 4

$$I_{56^\circ} = \frac{.42}{.28} (10) = 15 \text{ ua}$$

since:

$$\frac{\Delta I}{AGC} = \pm 2 \text{ ua}$$

Eye #1 AGC bit = 13 ua minimum

Eye #2 AGC bit = 12 ua maximum

Hence Eye #1 would be the selected eye and no error would occur. (See Figure 3)

Using  $\pm 1/2\%$  tolerances on  $R_E$  and  $R_C$  would considerably improve the maximum drift.